Université du Québec
INRS-ÉMT

Molecular modulation of surface electrical conduction in silicon

Par
Girjesh Dubey

Thèse présentée pour l'obtention du grade de Philosophiae doctor (Ph.D.) en Science de l'Énergie et des Matériaux

Jury d'évaluation

Président du jury	Prof. Mohamed Chaker
Examinateur interne	Prof. Mohamed Chaker
Examinateur externe	Prof. Richard Martel, Université de Montréal
Examinateur externe	Prof. Marta Cerruti, McGill
Directeur de recherche	Prof. Federico Rosei, INRS-ÉMT
Codirecteur de recherche	Dr. Gregory Lopinski, NRC-SIMS

Abstract

Adsorption of charged or polar species on semiconductor surfaces can modulate the electrical properties through long-range field effects. Hydrogen-terminated silicon-on-insulator (SOI-H) is an interesting model system for investigating this sensitivity to surface processes. Sheet resistance, Hall effect, and accumulation mode pseudo-MOSFET measurements have been used to probe molecular adsorption and reaction events on SOI-H.

The sheet resistance of SOI-H increases significantly with time in ambient air, due to depletion of majority carriers caused by oxidation. Physisorbed water further modulates the conductivity, inducing downward band bending and accumulation of majority carriers on *n*-doped films, without changing the carrier mobility significantly. Adsorption of water in a controlled vacuum system is found to strongly and reversibly increase the conductivity of both *n*-type and *p*-type SOI-H substrates. These conductivity changes can be attributed to water induced field effects that lead to accumulation of majority carriers on *n*-type and the formation of a minority carrier channel (inversion) on *p*-type substrates. The surface charge densities required to account for these effects are on the order of $\sim 10^{11}$ q·cm^{-2}.

Pyridine adsorption in the torr range gives rise to similar yet stronger reversible conductivity modulation effects as compared with water (several fold) on both *n*-type and *p*-type substrates, inducing positive surface charges of the order 10^{11}-10^{12} q·cm^{-2}. The ability of pyridine, water and other nitrogen containing molecules such as ammonia and triethylamine to reversibly bias *p*-type surfaces into inversion demonstrates a new type of molecular triggered electronic switch where adsorption is used to reversibly gate transport through the silicon substrate.

In addition to conductivity/Hall Effect observations, the current-voltage characteristics of SOI-H pseudo-MOSFET *n*-channel devices are also found to be sensitive to the environment. The accumulation threshold voltage, or flat-band voltage,

exhibits large reversible changes upon cycling between ambient atmosphere, high vacuum and exposure to water and pyridine vapour at pressures in the torr range. Both these adsorbates shift the flat band potential to more negative values, consistent with their ability to act as effective electron donors. The field-effect mobility is found to be comparatively less affected through these transitions. Adsorption of the well known electron acceptor tetracyanoethylene (TCNE) is shown to cause depletion, with ppm levels of TCNE vapour in ambient atmosphere found to rapidly decrease the saturation current by over two orders of magnitude. The effect is only partially reversible on the hydrogen terminated surface, due to the accumulation of strongly bound TCNE molecules on the surface. In addition, oxidation of the H-terminated surface is seen to result in irreversible shifts in both the flat-band voltage and field-effect mobility. In order to passivate the surface from these irreversible processes, a photochemical gas phase reaction with decene was used to form a decyl monolayer on the SOI(100)-H surface. Formation of this monolayer is found to result in a relatively small shift of threshold voltage and only a slight degradation of the field effect mobility. Decyl passivation only slightly decreases the response of the FET to TCNE adsorption while significantly improving the reversibility of the response. These results suggest that alkyl monolayer dielectrics formed by the gas phase photochemical method can function as good passivating dielectrics in field effect sensing applications.

Acknowledgements

I am very fortunate for having a unique experience at the National Research Council, and am indebted to my colleagues and staff members for years of support and expert advice.

I will always be grateful to Dr. Greg Lopinski, who has taught me so much; for training me personally from the very start to conduct scientific research with integrity and only of the highest quality; for allowing me to progress in his lab; for his patience; for his unequivocal support and confidence in me.

So much has been made possible because of Prof. Federico Rosei, who I have increasing grown to admire for his energy, inspiration, and positive power. He believed in me from the very beginning and proved to me anything is possible with persistence.

I will never be able to repay Irene for her unconditional love and support, for sharing this experience, for her unceasing patience and understanding. I am overjoyed that she will be staying by my side for the endeavors to come.

To

Ram Janam Dubey

“papa”

Contents

List of Figures

List of Tables

Notation

z	coordinate perpendicular to surface	[cm]
ρ	electrical resistivity	[Ω·cm]
Φ	electric potential	[V]
d	film thickness	[cm]
L_D	Debye length	[cm]
L_{dep}	depletion length	[cm]
n,p	electron, hole density	[cm^{-3}]
E_F	Fermi level	[eV]
$\mu_{n,p}$	electron, hole mobility	[$cm^2/V{\cdot}s$]
R_s	sheet resistance	[Ω/sq.]
R_a,R_b	pseudo-resistance a,b	[Ω]
$G_{s,b}$	surface,bulk conductance	[S]
V_H	Hall voltage	[V]
R_H	Hall coefficient	[cm^3/C]
B_z	magnetic field (z-component)	[G]
I_x	current perpendicular to Hall field	[A]
Q_s	surface charge density	[$q{\cdot}cm^{-2}$]
ΔN	excess/deficit surface electrons	[cm^{-2}]
ΔP	excess/deficit surface holes	[cm^{-2}]
$N_{A,D}$	acceptor, donor density	[cm^{-3}]
D_{it}	interface state density	[$cm^{-2}eV^{-1}$]
V_{FB}	flat-band voltage	[V]
V_D	drain voltage	[V]
V_G	substrate voltage	[V]
I_D	drain current	[A]
β	gain factor	[A/V^2]

Acronyms

SCR	space charge region
HREELS	high resolution electron energy loss spectroscopy
FTIR	Fourier transform infrared spectroscopy
SOI	silicon-on-insulator
BOX	buried oxide
DB	dangling bond
SIMOX	separation by implantation of oxygen
WB	wafer bonded
NW	nanowire
CB, VB	conduction band, valence band
SS	surface state
HV	high vacuum
UHV	ultra-high vacuum

Chapter 1

Introduction

1.1 Molecular Sensing on Silicon Films

Semiconductors are highly tunable electronic materials. Their electrical resistivities span several orders in magnitude 10^{-3} Ω·cm<ρ<10^{7} Ω·cm corresponding to a range of Debye screening lengths 10 nm<L_D<1 μm[1]. Surface electronic properties of semiconductors are influenced by a transverse electric field at the interface, inducing *band-bending* of the electronic energy levels and thus developing a *space-charge* region (SCR) in which charge redistribution results in a different concentration of free carrier(s) than in the bulk material [Kingston55a]. Depending on the depletion length L_{dep}, the full spatial extent of the SCR can be substantial, with the field penetrating up to several microns as it attenuates inside the crystal. Besides the application of an external bias, adsorption of charged or polar species on a semiconductor surface can also modulate the electrical properties via changes in electron affinity and through long-range field effects [Cohen97;Cohen99].

[1] This contrasts metals which completely screen electric fields within 1 Å below the first atomic layer. Their narrower range of resistivies10^{-6} Ω·cm<ρ<10^{-8} Ω·cm are also weakly dependent on T by comparison.

Electrical transport in semiconductors is generally insensitive to these surface processes because of parallel conduction paths through the bulk, with the exception of special cases under very strong band-bending or favorable conduction through surface state bands [Landsrass89;Jiang96;Lopinski05]. The simplest way to suppress bulk conduction and enhance the sensitivity to the SCR is to use a planar 2*d* thin film in which the thickness *d* has a similar magnitude to L_D, thus providing ideal sensitivity to the surface condition.

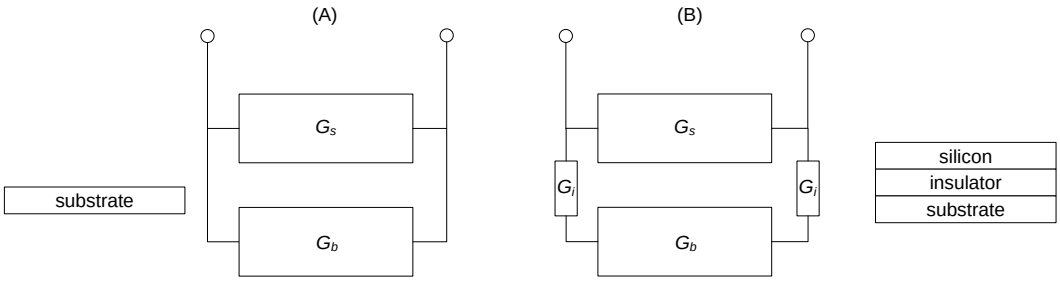

Figure 1.1: (A) Surface and bulk paths are parallel resistors $R_{s,b}=1/G_{s,b}$. The total conductance $G=G_s+G_b \sim G_s$ if $d \sim L_D$. (B) An SOI structure with $d \sim L_D$ isolates surface from bulk paths through an insulator $G_i \sim 0$.

An exciting, emerging use of thin film semiconductors is the electrically-based application of chemically passivated silicon-on-insulator substrates (SOI) to probe simple molecular adsorption and reaction events. This approach enables the study of molecule-semiconductor interactions from a basic viewpoint, but also supports exploration of the chemical sensing properties of silicon surfaces and possible control over their electronic properties from an applied perspective. The effects of ambient gases on the conductivity and surface potential of germanium surfaces were initially explored in the 1950s [Brattain53]. Recently the development of nanostructured semiconductor materials has led to renewed interest in adsorption induced effects. In particular, the conductivity of 1*d* silicon nanowires (SiNWs) has been shown to exhibit sensitive responses to a range of molecular adsorption events from small molecules in the gas phase [Zhou03;Talin06] to biomolecules (DNA, proteins) in solution [Cui01;Hahm04;Bunimovich06;Stern07]. A key property of these nanostructured materials is that one or more of the physical

dimensions are less than or comparable to L_D~100 nm, at doping levels of ~10^{15} cm^{-3}. Hence the conductivity of these structures is expected to be extremely sensitive to adsorption events that result in charge re-distribution at the surface. Compared to SiNWs, use of the planar SOI geometry facilitates a more direct interpretation of the effects of adsorption events as well as enabling the application of standard surface science techniques for characterization of the active interface [Lin98].

Silicon on insulator (SOI) substrates consist of a thin silicon layer (30-3000nm) separated from the bulk wafer by a buried oxide (BOX) layer. The presence of the BOX serves to isolate conducting paths to the bulk substrate, rendering the conductivity highly sensitive to surface processes. A substrate bias can be used to gate the conductivity of the device layer, activating a majority/minority channel at the 'back' Si/SiO_2 interface, which forms a simple device known as a pseudo-MOSFET [Cristoloveanu92]. Top gating effects of molecules can also modulate conduction in the pseudo-MOSFET [He06;He09]. Thin film resistors based on oxidized SOI-FETs operating in electrolyte solutions have been explored for biosensing applications [Nikolaides04;Lud06;Neff07].

Oxide-free, hydrogen terminated silicon-on-insulator (SOI-H) substrates are model systems for investigating the ability of adsorbed or covalently attached molecules to modulate the conductivity [He06]. Each surface atom is fully coordinated, and the low density of defect states D_{it}~10^{10} $cm^{-2}eV^{-1}$ results in nearly flat-bands [Yablonovich86;Oskam96a;Henrion02]. These substrates are stable enough to be handled in ambient atmosphere for several minutes without oxidizing significantly. They are suitable for electrical measurements in ambient as well as controlled experiments in vacuum.

This work aims to probe and understand the electrical properties of oxide-free, hydrogen terminated and chemically modified silicon using SOI to increase the sensitivity of the conductivity to surface processes that can give rise to field-effects. Four probe methods are used to measure the sheet resistance and Hall effect to determine the conductivity, carrier type and mobility. A two-probe pseudo-MOSFET geometry is used to measure the output characteristics, flat-band voltage, and monitor the drain current.

The recurring theme from our observations is that the gaseous chemical environment strongly influences the conduction. This enables systematic studies of molecular adsorption and reaction events in ambient atmosphere and in controlled vacuum environments by monitoring one or more electrical properties in the device layer as a function of time and exposure. The effects are quantified and discussed. Although these surfaces are found to exhibit highly sensitive electrical responses to a range of adsorbed molecular species and reactions, the development of practical sensors falls outside the scope of this work, but the outlook and prospects for potential applications are considered throughout.

1.2 Silicon

1.2.1 Properties of Silicon

Elemental silicon ^{14}Si(28amu) is a group IV intrinsic semiconductor occurring in a face-centered cubic lattice with a basis at (¼,¼,¼)·5.43 Å. Each sp^3 hybridized Si atom is covalently bonded to four nearest neighbours with Si-Si bond length of 2.3 Å in a bulk tetrahedral arrangement. Growth of device grade silicon, normally by the Czochralski (Cz) method [Czochralski18;Gomperz22] or floating-zone (Fz) method [Striplin49], in large single crystals is strictly required for manufacturing IC's. Si crystals are the highest purity materials available, containing impurity levels as low as one part per trillion (Fz). Si ingots cleave with a diamond saw to expose a facet, typically (100) or (111).

Table 1.1: Important electronic properties of silicon.

Property	Symbol	Value	Units
Dielectric constant	ε	11.9	$\varepsilon_0=8.9\times10^{-14}$ Fcm^{-1}
Valley Degeneracy	g_v	6	
Electron effective mass† (4 K)	$m_e=g_v^{2/3}(m_l m_t^2)^{1/3}$	1.08	$m_0=9.1\times10^{-31}$ kg
Hole effective mass† (4 K)	m_h	0.57	m_0
Bandgap (300 K)	E_g	1.12	eV
CB effective DOS (300 K)	$N_C=2(2\pi m_e kT/h^2)^{3/2}$	2.82	cm$^{-3}\times10^{19}$
VB effective DOS (300 K)	$N_V=2(2\pi m_h kT/h^2)^{3/2}$	1.83	cm$^{-3}\times10^{19}$
Intrinsic carrier density (300 K)	$n_i=(N_C N_V)^{1/2}exp(-E_g/2kT)$	10^{10}	cm^{-3}

† DOS average effective mass. Conductivity effective masses are $0.26m_0$ for electrons and $0.93m_0$ for holes.

1.2.2 Energy Bands of Silicon

The condensation of isolated atoms into a crystalline solid causes broadening of the discrete electronic energy levels into continuous bands [Ashcroft76]. Qualitatively, this arises from the mixing of spatially overlapping wavefunctions as the interatomic spacing decreases, while satisfying the Pauli Exclusion Principle so that each state contains at most two electrons. The band structure is the energy-momentum *E vs* ***k*** relationship, which is generally a complex surface in three dimensions. It is usually obtained by solving the Schrödinger equation as a one-electron problem for a periodic potential containing the periodicity of the lattice [Bloch28], but essentially treats the electron as a quasiparticle free from electron-electron interactions, within Landau Fermi-Liquid Theory [Landau57]. The simplified band structure *E vs* ***k*** of silicon is shown in Figure 1.2.

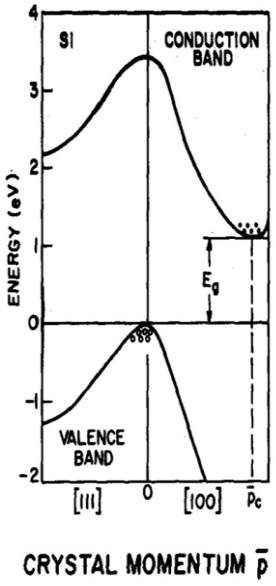

Figure 1.2: Simplified schematic band structure of silicon adapted from [Sze69].

There is a forbidden energy gap in which allowed states in the bulk material cannot exist[2]. The energy spacing between the upper, conduction band (CB) minimum E_C and lower, valence band (VB) maximum E_V defines the bandgap $E_g=E_C-E_V$. Silicon has an indirect gap since E_C and E_V do not coincide at the same point in $\boldsymbol{k}$; optical transitions also require a momentum change, assisted a phonon or other mechanism. There is a direct gap at 3.2eV. Current flow in silicon arises from the availability of unoccupied states in the CB or VB for electrons to move into in the presence of an external electric field.

[2] The DOS in the gap $E_v<E<E_C$ is $N(E)=0$. Near the band-edges $N(E)\approx 4\pi(2m_{e,h}/h^2)^{3/2}|E-E_{C,V}|^{1/2}$

1.2.3 Charge carriers at thermal equilibrium

1.2.3.1 Intrinsic carriers

At 0 K there are no free carriers, the VB states are occupied and CB states are empty. At finite *T*, electrons and holes, thermally generated in pairs, are free to conduct with intrinsic density n_i. Effective mass components of electron and hole quasiparticles takes into account the non-ideality of the Fermi-liquid, determined from the curvature of the bands. The Fermi level[3] E_F is at mid-gap E_i=½(E_C+E_V), where E_i is the intrinsic level.

1.2.3.2 Extrinsic carriers

Intentional doping of silicon with hypervalent donor impurities (e.g. pentavalent Group V "donors" phosphorus, arsenic, etc.) of density N_D, or hypovalent acceptor impurities (e.g. trivalent Group III "acceptors" boron etc.) of density N_A, increases the conductivity and alters the predominance of either electrons or holes as majority carriers, resulting in *n*-type and *p*-type material respectively. Impurities creating hydrogenic-like levels in the gap are ionized depending on their ionization level $E_{D,A}$ in relation to E_F and *kT*. Phosphorus and Boron have $E_{D,A}$=0.045 eV from E_C and E_V, respectively, more than 99.9% ionized above 100 K. The density of carriers in Maxwell-Boltzmann statistics[4]

$$n = N_c e^{-\frac{E_C - E_F}{kT}} = n_i e^{\frac{E_F - E_i}{kT}}, p = N_v e^{-\frac{E_F - E_V}{kT}}, \quad (1.1)$$

shows their product is a constant equal to n_i^2. If the dopants are fully ionized, e.g. on n-type $n \approx N_D = 10^{15}$ cm^{-3}, majority carriers are electrons, the donors are positively charged, and the minority hole density is $n_i^2/n = 10^5$ cm^{-3}. The position of E_F in relation to mid-gap is $E_F - E_i = kT \cdot \ln(n/n_i)$=0.304 eV.

[3] E_F represents the chemical potential where the Fermi-Dirac distribution $F(E)=(1+\exp((E-E_F)/kT)^{-1}$ is ½.
[4] From integrating the DOS×filling probability: $\int N(E)F(E)dE$ in each band, assuming $E_g >> kT$.

1.3 Band-Bending at Silicon Surfaces

1.3.1 Surface States

Many important properties of silicon arise because of surface and interface states, such as Fermi-level pinning [Allen62], 2*d* band structure [Wagner72; Himpsel83], surface state conduction [Jiang96;Yoo02], band-bending [Hiremath08;Jie08;Cooper11], and charge carrier recombination [Shockley52;Yaffe09;Seiffe11]. Surface states originate from the abrupt deviation of atoms in the bulk, terminating at a surface adjacent to vacuum or other junction; this modifies the electronic band structure at the surface to allow a density of states in the gap otherwise absent in the bulk [Tamm32;Maue35;Shockley39]. In atomically cleaved reconstructions of silicon, unsaturated Si orbitals create intrinsic surface states (dangling bond states) near mid-gap [Palmer61], which give rise to a 2*d* surface-state band structure of the topmost atomic layer [Wagner72]. The large density of electrically active DB's~10^{15} $cm^{-2}eV^{-1}$ buffer the local potential, pinning the Fermi level at the surface[5] on *p*-type to E_i-E_F≈0.25 eV and E_i-E_F≈0.15 eV on *n*-type, irrespective of bulk doping [Heiland59;Allen62;Fischer68]. Chemical passivation of silicon dangling bonds e.g. with hydrogen [Ibach74], oxygen [Wagner72] or other species [Avasthi10] can electronically passivate (destroy) the intrinsic states thereby un-pinning the Fermi-level. New extrinsic surface state bands can be created by low coverage adsorption of alkali adatoms Cs, K, and other metals Ag, Au, moving E_F away from mid-gap, closer to the CB or VB [Fischer67;Mönch70;Jiang96]. Discussed further in section 1.8.3, extrinsic states on chemically/electronically passivated silicon can arise at defects [Henrion02;Oskam96a], from chemical modification, surface reactions and oxidation [Mischki06;Bin08;Scott09] and by adsorption of charged species [Cohen97;Grupp98].

[5] E_F pinning may also result under MS junctions; decaying wavefunctions from the metal's continuum into the semiconductor create extrinsic surface states. Deviation in apparent barrier heights expected from the Mott-Schottky rule result from pinning [Bardeen47;Heine65;Sze69].

Whether intrinsic or extrinsic in origin, surface and interface states have either donor or acceptor type character; they are neutral or charged depending on their position from E_F and the density of interface states $D_{it}(E)$ in the gap [Monch95]. For instance, in *n*-type material acceptor levels below E_F are easily occupied with majority carriers, leading to a negative surface charge Q_{ss}. Overall charge neutrality requires there be equal and opposite positive charge Q_{SCR}=-Q_{ss} below the surface [Bardeen47], accomplished by the formation of a space-charge region (SCR) in which carriers are gradually re-distributed over a finite width. Similarly, donor states above E_F on *p*-type material become positively charged leading to a negatively charged SCR. States outside the gap do not contribute to an SCR.

1.3.2 Band-bending

Charge from adsorbed species or in surface states creates an electric field at the surface. The 2*d* surface charge acts as a repulsive barrier or attractive well, drawing majority carriers toward or away from the SCR. To accommodate an SCR all the electronic band levels must shift their positions relative to the bulk Fermi level. By convention, simplified 1*d* band-diagrams draw the CB/VB edges $E_C(z)$, $E_V(z)$ as a function of distance *z* into the crystal as shown in Figure 1.3. The band-bending also increases/decreases the spatial density charge carriers $n(z)$, $p(z)$ according to Eqn. 1.1 compared with their bulk concentrations n_b, p_b. Often the terms band-bending, charge-redistribution, and space-charge region are used interchangeably as they describe the same principle. In *n*-type material, the field of a positive surface charge lowers the potential energy electrons (attractive) causing downward band-bending and resulting in an accumulation layer in excess of electrons at the surface. A negative surface charge on *p*-type induces an accumulation layer of holes. Similarly in *n*-type material, the field from a negative surface charge raises the potential of the electron (repulsive) causing upward band-bending and resulting in a depletion layer with a deficit of majority electrons in the SCR. A positive surface charge on *p*-type causes depletion of holes.

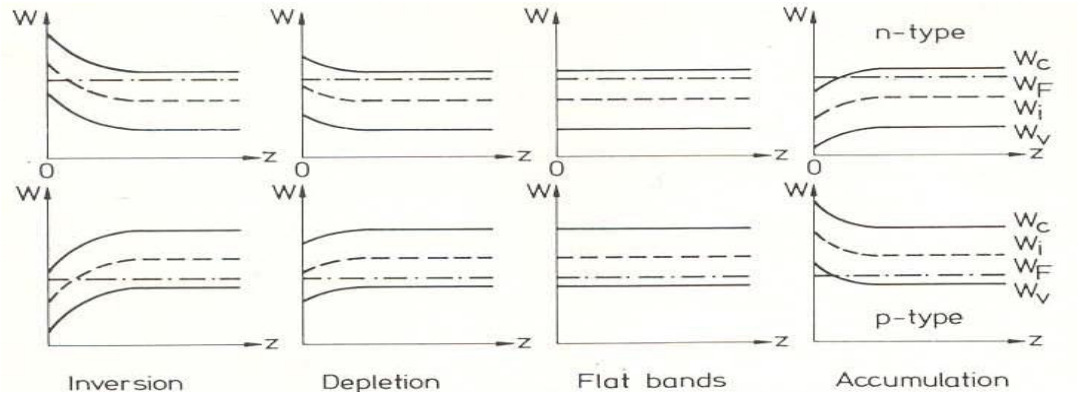

Figure 1.3: Schematic depiction of the possible band-bending conditions and terminology on *n*-type and *p*-type semiconductors adapted from [Monch95].

A repulsive field to majority carriers is attractive to minority carriers. An interesting case arises in depletion when the band-bending exceeds the built in-potential $|E_F\text{-}E_i|$. The band-edge with minority carriers becomes closest to E_F resulting in an inversion of carrier type at the surface containing more minority than majority carriers in the SCR. Strong inversion occurs when the band-bending exceeds twice the built-in potential, resulting in a larger minority carrier density at the surface than majority carrier density in the bulk[6]. Inversion channels are interesting because their conduction is quantized and restricted to the surface [Stern67]. They behave as 2*d* free-particle gases electrically isolated from the bulk since they are confined to a narrow width <100 Å by vacuum barrier on one side and a depletion layer on the other side [Ando82].

1.3.3 Causes of Band-bending

Band-bending and the formation of an SCR arise in three distinct situations [Hasegawa99]. Cause 1: External electric fields due to a gate bias or adsorption of

[6] In MOSFET operation, a voltage applied through a gate insulator is used to form a minority N-channel (NMOS) between source/drain n^+ contacts implanted on a *p*-Si substrate or a P-channel (PMOS) contacted between p^+ regions on an n-type Si [Sze69].

foreign charge. Cause 2: Contact potential difference, in which dissimilar work functions at *p-n* or M-S junctions etc. transfer charge to equilibrate the chemical potential, causing band-bending in the semiconductor(s) Cause 3: Occupation of surface states as discussed in section 1.3.1.

1.4 Silicon-on-Insulator Material

1.4.1 Overview

The aim is to use SOI to study surface processes on chemically/electronically passivated silicon. This approach makes conductivity measurements more sensitive to band-bending induced by adsorption and reaction events as discussed in section 1.3.[7] The motivation to develop SOI technology was for the improved performance over conventional silicon MOSFET circuits, exhibiting radiation hardness, smaller parasitic capacitances, immunity to latch-up, and reduced short channel and floating body effects [Colinge88].

The present SOI concept originates from the 1960's variant SOS: silicon-on-sapphire [Heiman66;Dumin68], formed by epitaxially grown silicon onto an insulating Al_2O_3 substrate for circuits requiring resistance to damage from radiation (hardness) in military and aerospace settings [Schlesier76], and radiation detection [Smith81]. The insulating substrate on SOS prevents transient parasitic currents generated by e.g. alpha particles from spreading to adjacent devices, whereas circuits from single silicon wafers do not.

Advantages of SOI circuits arise due to isolation of device layers from each other as well from the substrate [Colinge89;Colinge98]. Most of the current in a MOSFET flows within 200 nm from the surface and 99.9% of the silicon does not conduct [Sze69]. Parasitic internal capacitances are present between the silicon and depletion regions under the source and drain contacts; charging and discharging in these parallel

[7] Depending on the specs/manufacturer, SOI is several times more costly per unit area than Si wafers.

capacitances increases the overall switching time, reducing speed and increasing dynamic power consumption. The presence of the BOX in SOI eliminates the depletion region extending into the substrate, thereby reducing the internal parasitic capacitance [Balestra83]. Source and drain regions in SOI are also smaller, forming vertical contacts extending up to the BOX, whose lateral sides are used in conduction [Cristoloveanu95]. Smaller contact areas reduce overlap and depletion parasitic capacitances. The net result is faster circuits which consume less power. CMOS transistors in SOI circuits consist of millions of single-device islands dielectrically isolated from each other by the supporting BOX which prevents unintentional activation of adjacent devices known as latch-up [Colinge88;Cristoloveanu01]. In addition to CMOS devices SOI applications extend to bipolar devices [Colinge87], radiation-hardened circuits [Schwank99], high-voltage [Kobayashi98;Udrea00], high-temperature [Korec95] and low-power devices [Kuge96]. SOI CMOS processes emerged in communications devices driven by NTT and Motorola [Alls98], and presently contend with silicon microelectronics [Ortiz-Conde07], used in IBM's PowerPC™ [Irom02], AMD's 65 nm multi-core microprocessors [Horstmann05], Nintendo Wii [Sweda06] and likely in Intel's 22 nm nodes [LaPedus10].

1.4.2 Fabrication and Electrical Properties

Methods of forming SOI wafers are wide-ranging [Celler03] including zone melt recrystallization (ZMR), epitaxial lateral overgrowth (ELO), solid phase epitaxy (SPE), epitaxial layer transfer (ELTRAN), silicon-on-nothing (SON), Smart-Cut™, separation by implantation of oxygen (SIMOX), and Wafer bonding/etch-back (WB). Our studies used SIMOX purchased from Ibis[8] and WB SOI from Tracit, exclusively.

SIMOX: A buried oxide (BOX) is synthesized *in-situ* by implanting oxygen into a wafer [Cristoloveanu95]. Although somewhat destructive, device grade SOI with reasonably high quality/uniformity is achieved. Ibis implanters produce large-diameter SIMOX in

[8] Ibis no longer manufactures wafers [LaPedus04].

hours/batch. A deep, high-dose implantation (1.8×10^{18} O^+/cm^2) with high energy (190 keV) at 650 ^oC oxidizes the Si underneath. Post-implantation high temperature annealing (HTA) sharpens the boundaries at the interfaces and recovers the crystallinity of the top Si film. Ibis film/BOX thicknesses are typically 200 nm/380 nm respectively. The top silicon film is stress free. Oxygen is a source of electrical contamination in the form of thermal donors (TD) and new donors (ND), known to overcompensate *p*-type films into n-type[9]. Silicon "pipes" in the BOX may lead to ohmic leakage paths into the bulk. The upper buried oxide interfaces are sharp and uniform with density of traps/fixed charges in the range of $0.5\text{-}2\times10^{11}$ $cm^{-2}eV^{-1}$. Gate oxide interface state densities are the same as for silicon~10^{10} cm^{-2}/eV.

Wafer Bonding: Two bulk wafer oxides become one SOI wafer. The WB process produces undamaged crystalline films and thermal BOX quality [Cristoloveanu95]. Thermal oxides of a passive base wafer and an active wafer are mated together in a micro-clean room, requiring hydrophilic, flat, clean surfaces, with no air/ bubbles/dust particles at the bonding interface. Van der Waals and hydrogen bonding forces between adsorbed water multilayers initiate the bonding at RT, strengthened above 800 ^oC. The active wafer is thinned down to 10-100 μm by mechanical grinding/polishing. Additional thinning to 2-3 μm can be achieved by selective etching up to an implanted etch-stop, in a process called bonding and etch-back (BESOI)[10]. A shortfall of WB is thicker and less uniform films compared to SIMOX. Advantages over SIMOX include a non-destructive process, BOX quality, and absence of silicon pipe leakage paths through the BOX. The interface state density at the buried interfaces is also lower than SIMOX and symmetric.

The highest quality SOI uses the SmartCut^{TM} processes developed by Soitec (France), offering the most versatile thickness control of the silicon and BOX (5 nm-μm) [Celler03]. A seed wafer is thermally oxidized and implanted with hydrogen ions at doses $>5\times10^{16}$ cm^{-2}, then wafer bonded to a passive handle wafer. Microcavities in the silicon

[9] SIMOX dopant overcompensation was observed in our samples, reviewed in Ch3 (section 3.3.2.2).
[10] A p^+ boron etch-stop is typically implanted into the active wafer. The low doped region is etched up to the etch-stop by one etchant. The p^+ layer is then removed by another selective etchant.

establish a fracture plane; heating to 400-500 ^{o}C fills H_2 bubbles in the microcavities, cleaving the implanted plane to produce one SOI wafer and re-usable seed wafer.

1.4.3 Other Applications of SOI

SOI integration with microelectro-mechanical systems (SOI-MEMS), has developed [Usenko99] and applied in transducers, including *mechanical sensors*: pressure sensors, cantilevers, resonators and *optical sensors:* interferometers, micro-mirrors and waveguides. Electrically based chemical and biosensing on planar SOI and nanowires fabricated on SOI is also developing. A growing body of research confirms SOI substrates are model platforms for studying surface processes such as adsorption and reactions, outlined in the subsequent sections of this chapter.

The remaining sections review current efforts, molecular sensing on oxides, and the electrical properties of oxide-free silicon/SOI surfaces.

1.5 Early Semiconductor Studies

Shortly after the invention of the germanium transistor several basic studies of semiconductor surface electronic properties exposed to various gases emerged, mainly in the 1950's. In subsequent decades these effects were less pertinent as silicon transistors in devices were encapsulated specifically to protect them from the influence of the external gaseous environment. However due to renewed interests in oxide-free silicon, SOI, SiNWs and other bare electronic materials, the often significant effects of ambient gases have re-emerged in the present literature and are becoming increasingly important in the interpretation of electrical measurements.

Early studies began with W. Brattain and J. Bardeen who were first to apply the Kelvin Probe technique to measure the contact potential in the dark and the change in contact potential under illumination using a platinum electrode to estimate the dipole and

band-bending on several Germanium surfaces, providing direct evidence of the existence of a space-charge region under the surface [Brattain53]. In this pioneering work, the contact potential was cycled between two extremes nearly 0.5 V apart upon changing the gaseous ambient; vapours of ozone or peroxide were found to shift the work function and band-bending in the opposite direction to that of vapours containing OH radicals. These surprisingly large effects inspired more studies on germanium throughout the decade. Shortly thereafter W. Brown reported the existence of a positive charge on the etched surfaces of *p*-type Germanium in *n*-*p*-*n* transistors, inducing an *n*-type surface conductivity (in the *p*-type base region) easily permitting conduction from one *n*-region to another which he called the "channel effect" [Brown53]. Brown proposed this *n*-channel could be formed by either the accumulation of positive ions over the base due to the lateral field between the *n*-junctions or the possible ionization of neutral impurities. Kingston showed this effect is facilitated by water vapour present in the ambient atmosphere [Kingston54] since the *n*-channels formed in milliseconds using un-encapsulated structures measured at 100% humidity as opposed to minutes/hours in Brown's work with encapsulated structures. Kingston later suggested the inversion layer is caused by ionization of surface impurities rather than the migration of ions [Kingston55]. The precise origin of this effect continued to evolve throughout the decade with some authors suggesting the presence of surface ions [Hutson56] and others concluding that water induces donor-like states at the surface [Statz56;Statz58]. These mechanisms and other possibilities are considered in Ch3 in our discussion of the effect of water on SOI-H surfaces.

In this chapter, recent electrical measurements on silicon surfaces, SOI and related nanostructures have investigated surface properties, surface modification, and molecular sensing. Progress on oxides and electronically passivated oxide-free silicon is reviewed.

1.6 Surface Conductivity

1.6.1 Separating surface from bulk conductivity

Macroscopic conduction is insensitive to surface conditions unless the surface conductance G_s is on the order of the bulk conductance G_b. In strong accumulation or inversion, most of the current flows through a narrow conduction channel. However in mild depletion $G_s << G_b$, bulk conducting paths generally suppress the surface contribution. In the few special cases outlined below, the surface contribution could be measured distinctly on the bulk material.

Intrinsic diamond is expected to be electrically insulating since E_g=5.5 eV, yet undoped hydrogenated diamond (HD) exhibits a measurable *p*-type surface conductance $10<G_s<100$ μS with hole density $p_s \sim 10^{13}$ cm^{-2} as revealed by resistance and Hall effect measurements [Hayashi97]. This unusual property is observable in air on micron-thick films formed by chemical-vapor-deposition (CVD) of CH_4/H_2 mixtures. Landstrass and Ravi first reported the low resistivity (for an insulator) $\rho \sim 10^6$ Ω·cm of ~3 μm CVD HD increases by six orders after heating to 350 ^oC for 30 min., due to dehydrogenation in the film [Landstrass89]. Hydrogen de-passivation of defect states leaves a large trap density $\sim 10^{15}$ cm^{-2} pinning the surface Fermi level, thereby strongly depleting the film of carriers and increasing the resistivity. However the initially low resistivity was poorly understood until Maier et al. showed HD is insulating when prepared and measured in UHV, with the resistivity decreasing ten orders, to typically reported values, upon exposure to air [Maier00]. They proposed a slightly acidic adsorbed water layer from ambient accepts electrons via a redox couple between H_3O^+ and HD, inducing the upward-band bending responsible for an observed *p*-type conductance[11]. This effect has been applied to study the gas sensing properties of HD via resistivity changes upon exposure to NH_3 and NO_2

[11] Supporting DFT calculations show an electron transfer process from an H-terminated diamond (100)-2×1 surface to an adsorbed water layer is favorable [Larsson05].

gases, which modify the water layer *p*H, and accordingly the degree of electron transfer and band-banding [Helwig07a].

The influence of Au and Ag adlayers on the surface conduction in atomically ordered Si(111)-7×7 in UHV has been measured using bulk silicon [Hasegawa92;Jiang96]. Jiang et al. deposited 1 ML of Ag and 0.4 ML of Au in distinct regions between point contacts on a single Si(111)-7×7 wafer and measured the conductivities separately. The superstructures in these regions Ag-$\sqrt{3}\times\sqrt{3}$ and Au-5×2 are inherently more conductive than the starting Si(111)-7×7 surface by 12 μS and 5 μS respectively. Since the bulk contribution for all three surfaces is the same, the increased conductivity under the metal adlayers is explained by a higher surface contribution relative to the bare surface $G_{s,7x7}<G_{s,\text{Au-5}\times2}<G_{s,\text{Ag-}\sqrt{3}\times\sqrt{3}}$. These observations are explained by un-pinning of the surface Fermi level, initially near mid-gap, to below the bulk E_F of the *p*-doped wafer, causing accumulation of holes at the surface. The larger conduction of the Ag superstructure is consistent with a new surface state band in addition to un-pinning.

Surface modification of H-terminated silicon to form Cl-terminated silicon has been studied with conductivity of bulk wafers. A recent experiment on low-doped 10 Ω·cm $<\rho<$1000 Ω·cm *n*-type Si(111)-H observed that chlorine termination leads to an enhancement in conductance [Lopinski05]. Gas phase chlorination can be assisted with UV [Terry97;Luo97] or occurs spontaneously in the dark with molecular chlorine (2% Cl_2/Ar) at RT [Lopinski05]. The surface conductance of Si(111)-Cl is ~10 μS higher than Si(111)-H. A reduction in Hall voltage (Hall effect) and increased free carrier plasmon energy (HREELS) is also observed. The large electronegativity of Cl, together with these observations, is consistent with the formation of an inversion layer with hole density $p_s\sim4\times10^{11}$ cm^{-2} and mobility $\mu_p\sim100$ cm^2/Vs. The 2*d* hole gas arises from a surface charge $Q_s=-6\times10^{11}$ q·cm^{-2} or 1e per 1280 Cl causing 0.68 eV of upward band-bending. DFT calculations have explored the influence of defects and Cl impurities as alternative sources of the hole gas [Blomquist06], but the precise origin of the enhanced conductance remains open.

1.6.2 SOI surface conductivity

Electrical conduction on SOI wafers is more sensitive to surface effects due to the absence of bulk conducting paths. The increased sensitivity of SOI was initially exploited to measure surface state conduction on clean Si(100)-2×1. Yoo and Weitering measured the metallic-like surface state conductance on ultrathin 90 nm SOI(100) between 120-300 K, by measuring the conductivity before and after passivating with~5000 L O_2, which destroys the surface-state bands, eliminating their contribution[12] [Yoo01a]. Note the surface conductance change is positive through surface state bands but negative in the SCR because surface Fermi level pinning near mid-gap leads to depletion of free carriers. The resistance thereby increases after exposure to oxygen. Decreasing surface-state conductance with increasing *T* is attributed to scattering and more disorder as the frozen buckled dimer c(4×2) superstructure becomes the time-averaged Si(100)-2×1 structure. A characteristic signature of the c(4×2)→2×1 order-disorder transition of buckled Si dimers at 200 K is observable in the surface conductance. They further classify the conductance to be that of a bad metal as it falls below the universal quantum of conductance. Metallic-like properties of the SOI(111)-7×7 surface state bands have also been measured from 120-280 K [Yoo01b;Yoo02].[13]

[12] Surface-state conduction also explains why STM imaging of ultrathin 20 nm SOI(100)-2×1 is possible [Zhang06a;Zhang06b], since the film would otherwise be too resistive to expect tunneling.

[13] In addition to conductivity measurements, the influence of roughness and quantum confinement on the electronic band structure of silicon has been studied on ultrathin SOI(100) and SOI(110) surfaces [Chen09].

1.7 Molecular Sensing on Oxides

In parallel with studies using 2*d* SOI wafers, other 1*d* nanostructures have emerged [Xia03;Ramgir10], with metal oxides [Comini02;Carrico07;Kolmakov04;Fan05], carbon nanotubes [Li03;Qi03;Cao09] and silicon nanowires [Engel10;Vu10;Chen11] spurring considerable interests for bio and chemical sensing applications. 3*d* micro-porous silicon films are similarly studied for electrically based chemical sensing [Ozdemir07]. In particular, silicon nanowire (SiNW) fabrication has developed quickly, producing high density 1*d*-FETs capable of sensing small molecules in the gas phase [Talin06] and label-free biomolecules in solution [Gao11;Peng11]. Their high surface to volume ratio enables electrical detection of charged proteins and DNA with comparable sensitivity to conventional microfabricated silicon FETs [Fritz02]. SiNW's are also pursued for photovoltaic applications such as solar energy conversion [Peng11].

1.7.1.1 Bottom-up silicon nanowires

Promising results from Lieber's group [Cui01] have stimulated many ensuing studies. Cui et al. synthesized B-doped SiNWs {l~3 μm;r~15 nm} aligned onto an oxidized silicon substrate, serving to gate the FETs into accumulation. The conductance changed linearly over $2<pH<10$ on -NH_2 and –OH terminations according to the degree of protonation on the NW's. Real time current measurements were sensitive to the irreversible protein binding of 25 pM streptavidin (K_d~10^{-15} M) and reversible binding of m-antibiotin (K_d~10^{-9} M) onto biotin-modified SiNW's, and similar data found SiNW's modified with calmodulin receptors specifically responded to added calcium ions (K_d~10^{-5} M). The authors later applied their SiNW FETs to array-based multiplexed electrical detection of cancer markers such as prostate specific antigen [Zheng05]. Hahm and Lieber also formed two-terminal devices with no-back gating to monitor the raw conductance of SiNWs functionalized with peptide nucleic acid probes to distinguish the wild-type oligonucleotide sequence from a mutant sequence in the cystic fibrosis

transmembrane receptor gene at DNA concentrations ranging from 10 fM to 300 fM [Hahm04]. Negatively charged complementary oligonucleotide binding causes hole accumulation, increasing the raw conductance of the *p*-SiNWs significantly more than the mismatched sequence.

1.7.1.2 SOI based nanowires

Alternatively, top-down NW's do not require transfer and positioning, offer more straightforward integration with signal processing circuits, reproducible ohmic contacts and increased feasibility for high-density applications. SOI-based nanowire[14] features are typically fabricated by thermal oxidation and lithography, combined with either reactive ion etching (RIE) [Li04], wet chemical etching [Stern07], and more recently with simple gas-phase etching [Naumova10].

The Williams group patterned SiNWs using EBL/RIE from commercially available 60 nm SOI (SEH) creating rectangular nanostructures {w=50 nm;h=60 nm;l=20 μm}, immobilizing 12-mer DNA onto 3 nm thermal oxide [Li04]. A 46% increase in conductance was monitored in real time upon hybridization with 25 pM complementary target in pure water for the *p*-type NWs and a 12% decrease for the *n*-type NWs, and no change was observed when the NW's were exposed to a single base mismatch. The group later fabricated a biocompatible, minimally invasive, micro-needle cantilever from SOI (Soitec, France) using photolithography/focused-ion-beam machining (FIB) to make the microneedle; serpentine-shaped SiNW sensor areas were defined at the tip of the needle, which was electrochemically passivated using parylene-N for potential in-vitro cellular biochemical sensing [Park07]. Real time *p*H detection on oxide surfaces (linear response 80 nS/*p*H from 2<*p*H<12) has been demonstrated in sodium phosphate/phosphoric acid buffers with a sensitivity of 0.2 *p*H units [Park10].

[14] Applications of free standing SOI nanowires have emerged recently, such as piezoresistive NEMS and Quantum dot's [Ritz10].

A different approach to the William's EBL patterned high density SiNW's that does not require RIE-induced device degradation, but maintains CMOS compatibility, is the wet-chemical etching of SOI(100) using TMAH, first demonstrated by Reed's group [Stern07] and currently adopted for SiNW-biosensing in Ingebrandt's group [Vu09] and elsewhere [Chen09]. Anisotropic etching with TMAH under an oxide mask produces trapezoidal NW's {w=300 nm;h=25 nm;l=1 μm} while exposing the ideal (111) plane for surface chemistry. Stern et al. used 200 nm degenerately doped contacts to form the source and drain and applied a negative voltage to the SOI substrate to activate a *p*-accumulation mode pseudo-MOSFET. The wide geometry enabled the first six-point Hall-bar structure on a single nanowire which was used to measure the Hall mobility μ_p~100 cm^2/Vs for holes at RT (bulk 450 cm^2/Vs). On biotin modified SiNW's, 1 nM-10 fM streptavidin/avidin increased/decreased the drain current due to the negative/positive charge of the protein, while streptavidin already quenched with biotin or streptavidin exposed to a PEG modified gave no response. In a recent application of these NWs, the authors have quantitatively detected cancer biomarker antigens from 10 μL of whole blood within 20 min. [Stern10].

Chemical sensing in gas phase and non-aqueous media is another area of interest. Nanoimprint lithography of 10-20 Ω·cm B-doped 100 nm SOI (Silicon Quest Inc.) has been used to fabricate large area SiNW arrays spaced 200 nm apart; individually addressable, parallel interdigitated Al electrodes {l=180 μm;w=1 μm} each contacting 900 NWs are used to vary the effective NW length L [Talin06]. At V_G=-18 V the resistance 25 kΩ<R<150 kΩ is linear in length 1 μm<L<60 μm, confirming diffusive conduction through the NWs. Exposure of ammonia vapor to oxidized silicon shifts the I_{SD}-V_G characteristics to the left, increasing the threshold voltage in accumulation to more negative values by 5.4 V on the nanowires but only shifts unpatterned SOI by 0.2 V. The enhanced sensitivity of the NW array is attributed to a decreased capacitance (×0.5) and larger surface to volume ratio compared to SOI, possibly enhanced by RIE. Nitrobenzene and phenol were also pipetted onto the NWs in cyclohexane solutions (1 mM-0.25 M). Corresponding threshold voltages shifted by 8.5 V/M for electron withdrawing

nitrobenzene and by -4.5 V/M for electron donating phenol. These observations indicate the threshold voltage shift is both linear in analyte concentration and also proportional to the Hammet parameter of the analyte; σ_p=0.78 for nitrobenzene and -0.4 for phenol.

1.7.2 SOI Thin film Resistors

Thin film resistors based on oxidized SOI substrates have been explored for biosensing applications extensively by the Bausch group. Their measurements demonstrate that two-dimensional SOI structures are highly sensitive platforms for chemical and biomolecular sensing applications, offering an interesting approach to one-dimensional silicon nanowires. Since planar two-dimensional systems are easier to fabricate and characterize, they serve as a useful starting point for understanding the behavior of nanowire systems, particularly with regard to investigating the effects of surface chemical modification. The Bausch group used B-doped, 10^{16} cm^{-3}, 30 nm ELTRAN SOI (Canon) to fabricate a hallbar-like structure 240 μm×80 μm at the center of a 1×1 mm^2 chip for four-point conductivity measurements using lithography and wet chemical HF/H_2NO_3 mesa-etching, with thermally evaporated/annealed Al contacts at the edges of the chip far from the solution flow chamber.

Ionic strength dependence at constant surface charge and pH: The sheet resistance response 60 kΩ <R_s<75 kΩ on the native oxide corresponding to 0.01 mM-1 M KCl in 10 mM phosphate buffer at *p*H 6.4 is calibrated to a 50 mV change in surface potential[15] which gives consistency with the Grahame equation with reasonable fitting parameters for surface charge density ~2.3×10^{13} cm^{-2} and dissociation of divalent phosphate~30% [Nikolaides03] A positive substrate voltage V_G=16 V was chosen to prevent alkali ion diffusion into the oxide and maximize the response dR/dV_G, gating the back interface into an electron inversion layer.

[15] R_s was calibrated to surface potential beforehand by stepping the potential of a Ag/AgCl reference electrode from -150-150mV.

Surface charge dependence at constant ionic strength: Injection of 0.1 nM poly-L-lysine (PLL) in 490 nM KCl has no effect on R_s. At 1 nM PLL, R_s decreases irreversibly by 100 Ω, corresponding to a 2.2 mV change in surface potential and charge density 2.5e per 100 nm^2. These observations demonstrate that planar devices are capable of detecting small charge variations at sub-monolayer coverage.

pH dependence: The sheet resistance of their devices increases linearly by 2.6 kΩ/*p*H from 5<*p*H<9, equivalent to 50 mV/*p*H in agreement with the site-binding model for SiO_2 [Nikolaides04]. The authors further demonstrated spincoating of 25 nm PMMA suppresses the *p*H response 2-5 fold and by dissolving the polymer in acetone the original sensor is recovered.

Biosensing: Their simplest example is the electrostatic adsorption of a positively charged PLL monolayer onto the negatively charged oxide in 50 mM NaCl Tris buffer (*p*H=7.4), raising the surface potential by 20 mV and lowering R_s by 30 kΩ [Neff07]. Injection of the peptidase enzyme trypsin from 10^{-4} mg/mL to 1 mg/mL cleaves the PLL covered sensor into unbound lysine fragments, reversing the signal in $R_s(t)$ at an initial velocity that quantitatively fits to Michaelis-Menten kinetics with K_m=400 nM and v_{max}=~0.3 mV/s. The inhibition of trypsin with PMSF suppresses the reversal in $R_s(t)$, and in another control test, exposure of the PLL surface to a much less specific protease chymotrypsin, resulting in much slower reversal kinetics. A quantitative capacitor model has been proposed to account for the sensor's surface potential response [Neff06a].

1.8 Oxide-Free Silicon

There are many choices available with respect to the passivation of silicon, each providing distinct opportunities as well challenges depending on their scope and application [Waltenburg95;Buriak02;Onclin05]. For instance, clean silicon surfaces terminated with dangling bonds enable controlled adsorption studies at low coverage [Wolkow99; Lopinski08], although are limited to UHV because of their high reactivity [Schlier59]. In solution based molecular sensing, the customary passivation starts with a

native, chemical, or thermal oxide, normally requiring silanization [Sagiv80;Allara95] of the Si-OH groups for additional modification, as described in section 1.7. An intermediate approach is the complete removal of the silicon oxide layer and subsequent chemical passivation of every surface atom with covalent bonds. The simplest oxide-free implementation is terminating with monovalent hydrogen atoms.

1.8.1 Hydrogen termination

Hydrogen termination is the most common atomic passivation of silicon, especially as a starting point for organic modification [Wayner02;Hamers08;Ciampi10], although halogenation with iodine, bromine and chlorine are also used [Bansal96;Cai02;Eves05]. H-terminated silicon is an attractive passivation for surface studies for several reasons. Firstly, these surfaces are easily prepared and reasonably stable in air [Niwano94;Morita90;Houston95], can withstand brief water rinsing without significant oxidation [Higashi91] and exhibit low reactivity toward a range of solvents including toluene [Bateman98], acetonitrile [Cleland95], hexane [Boukherroub99] and mesitylene [Sieval99;Sieval01]. Because hydrogen passivation saturates the valence of every surface atom, the stability of Si-H is high compared to that of a dangling bond, yet the surface retains a moderate degree of reactivity which is desired in subsequent reactions with alkenes [Linford93;Linford95], alkynes [Terry97;Cicero00], Grignard reagents [Boukherroub99], alcohols [Cleland95] and diazonium reagents [Fidelis00], towards the formation of molecular monolayers.

1.8.2 Etching

The oxide on any silicon facet can be etched in aqueous HF solution, chemically modifying the surface to be atomically passivated by hydrogen [Grudner86], but the final morphology depends strongly on *p*H and initial orientation [Higashi90]. Dilute HF (DHF) in water 1%<HF:H_2O<10% is acidic 1<*p*H<2 and known to produce microscopically

rough Si(100) and Si(111) surfaces containing a mixture of monohydride (SiH), dihydride (SiH_2), and trihydride (SiH_3) species [Burrows88;Chabal89;Higashi90]. In these early studies, Chabal and co-workers used IR absorption in a multiple internal reflection absorption geometry (MIRAS) to resolve the SiH_x stretch vibrations near 2100 cm^{-1}. A larger number of "defect" dihydrides were observed with concentrated 49% HF. These observations implied the buried morphology of the underlying Si/SiO_2 interface is exposed by etching in acidic DHF [Jakop91] and that HF itself does not etch silicon once the H-termination is complete.

Higashi and co-workers [Higashi90] elucidated the role of hydroxide (OH^-) in the etching of Si(111) and Si(100), using ammonium fluoride as a buffering agent[16] to maintain constant *p*H levels in the HF solution, then raised or lowered the *p*H by addition of ammonium hydroxide $5<pH<12$ or HCl $0<pH<5$. Although heterogeneous terminations were always obtained at low *p*H, to their surprise, etching Si(111) in high *p*H solutions resulted in an IR spectrum dominated by one sharp line at 2083.7 cm^{-1} (FWHM=0.95 cm^{-1}) in the *p*-polarized, perpendicular stretch component. These observations demonstrated the first ideally monohydride termination of silicon, oriented perpendicular to the surface. The comparatively minor *s*-polarization intensity was integrated to quantify the parallel stretch 'defect density' at 0.5 %, which is consistent with the presence of dihydrides at step edges and reasonable given the wafer miscut of 0.5^o. Since the spectra of the initially heterogeneous rough surface and the monohydride terminated surface could be reversibly attained by alternately etching in DHF/BOE, the authors attributed the etching of silicon itself to another species rather than HF. This notion was confirmed by immersing a rough DHF-etched Si(111) wafer in pure water (*p*H~7) for 5 min. and observing the complete loss of dihydrides, to reveal a spectrum similar to that after BOE etching[17]. Chabal and co-workers concluded that the $OH^-(aq)$ concentration plays an important role in the etching of silicon, similar to that of KOH, which is known to preferentially etch the (100) plane. BOE is an anisotropic etchant that

[16] Etching in HF buffered by ammonium fluoride (NH_4) is also called a buffered-oxide-etch (BOE).
[17] Around the same time, the formation of atomically flat, oxide-free Si(111)-H surfaces by immersing DHF -etched surfaces in boiling water was also reported [Watanabe91;Watanabe95].

results in (111) planes due to their slow etch rate compared to all other planes. Shortly after Higashi et al. reported the ideal passivation of Si(111), atomically resolved images of Si(111)-H were obtained in electrochemical STM [Itaya92].

In contrast, Si(100) is always atomically rough, yielding strong equal intensity of Si-H stretch in *s* and *p*-polarization. A DHF-etched Si(100) sample that is then etched in BOE increases the intensity of monohydride modes, indicating the formation of small (111) microfacets [Yau95]. Formation of ideally terminated Si(100)-H by wet chemical methods continues to be prove challenging; one study used highly acidic etching conditions, *p*H<1, with a solution of HF:HCl=1:20 to suppress hydroxide attack, forming an atomically flat dihydride terminated surface that could be imaged in STM [Morita95].[18]

Although it is now understood that fluorine is only a minority species on chemically etched H-terminated silicon [Dumas91;Schlaf99;Bollani00], it was erroneously believed for many years that HF-etching resulted in F-termination [Weinberger86;Weinberger85] from observations of F contamination in XPS, which does not provide chemical sensitivity to hydrogen. Evidence for complete hydrogen passivation was elucidated by vibrational spectroscopies which predominantly measured the SiH stretch using IR and HREELS [Grudner86; Takahagi88]. From thermodynamic considerations alone, this outcome might seem counter-intuitive since the 6 eV SiF bond [Ricca98] is one of the strongest covalent bonds known in chemistry, considerably stronger than the ~3.5 eV SiH bond [Gupta88], which suggests the termination is dominated instead by reaction kinetics. The presently accepted explanation [Kolasinski09] follows that F–terminated silicon is kinetically unstable in HF [Ubara84] because SiF bonds are simply too polar [Gerischer88]; an Si-F_x species, where x=1,2,3 increasingly polarizes the Si-Si backbonds which are vulnerable to attack by dipolar HF, sequentially flourinating the surface species until x=4 and SiF_4 (*aq*) is released into solution, leaving behind Si-H. Ab initio molecular orbital calculations of reactions on

[18] Note that atomically flat monohydride Si(100) can be prepared by exposing clean reconstructed Si(100)-2×1 to atomic hydrogen at 300 ^{o}C [Boland92] and chemisorption of H to Si(111)-7×7 leads to a complex heterogeneous termination [Kobayashi83].

model transition states using model silicon compounds suggests each of these fluorination steps have a similar low activation barrier of ~1 eV and are exothermic by ~2 eV [Trucks90]. Once H-terminated, improved kinetic stability results because the activation barrier to the reaction of SiH directly with HF increases to ~1.6 eV. Furthermore, the small electronegativity difference of the Si-H bond only weakly polarizes the Si-Si backbonds, thereby inhibiting further bond cleavage with HF. In the absence of OH^-, only the first atomic layer of silicon layer is removed once the initial oxide is dissolved by HF, explaining why the final morphology of DHF-etched silicon only depends on the underlying structure of the Si/SiO_2 interface[19].

1.8.3 Electrical Properties

Studies on the influence of chemical treatments and ambient atmospheres on the surface electrical properties of HF-etched silicon began early [Buck58] and have since continued progressively [Colman69;Heilig79;Heilig84;Angermann95;Angermann08]. As the dimensions of device features continue to decrease, awareness on the relationships between surface electronic properties and common treatments such as wafer cleaning, surface preparation or HF immersion has increased [Grunthaner86;Kern90;Weldon03].

Renewed interest in H-terminated silicon is largely due to the excellent electronic passivation. In contrast to clean reconstructions of silicon in which the surface E_F is pinned near mid-gap by a large trap density $D_{it}(E)\sim10^{15}$ $cm^{-2}eV^{-1}$, chemical passivation with hydrogen shifts the surface state bands out of the gap into the VB and CB, resulting in relatively inactive surfaces, electrically. In an important study, Yablonovich et al. first reported that HF etching leads to termination by ~1 ML of SiH bonds rather than SiF (MIRAS), and that the resulting surface exhibits a remarkably low interface state density in HF, $D_{it}(E)<10^{10}$ $cm^{-2}eV^{-1}$, determined from surface recombination velocity (SRV) measurements [Yablonovich86]. Their SRV setup generates EHP's in float-zone Si(111)

[19]A recent study reported reversible submonolayer F-termination (<0.3 ML) is possible at isolated methoxy sites (0.3 ML) patterned on a Si(111)-H surface (0.7 ML SiH), via cycles of immersion in HF or methanol; this suggests a complete mechanism of HF etching of silicon is still lacking [Michalak10].

immersed in HF, n=p=4×10^{14} cm^{-3}, using a strobe lamp inductively coupled to an r.f. bridge and an oscilloscope to determine the excess carrier lifetime decay time constant τ. Measurements of τ~{20,10,7} msec. at corresponding thicknesses d~{250,60,35} μm are used to extract the bulk recombination time τ_b and surface recombination velocity S from a linear plot of $1/\tau$ *vs* $1/d$, using the relation $1/\tau=1/\tau_b-2S/d$. This particularly good FZ-batch gave τ_b=35 msec., which was 10^3 times better than that of silicon used in IC's. The surface contribution S=0.22 cm/sec. was the lowest SRV ever reported at the time, an order of magnitude below that of the highest quality thermal oxide interfaces. They measure S to be almost invariant at doping levels from 10^{14}-10^{17} cm^{-3} on n-type and p-type Si.[20]

The significance of a low SRV in HF is either a low density of interface states, which act as electron-hole recombination centers, or the presence of a surface charge inducing band-bending (qV_{bb}). The authors argue against the latter case; since band-bending tends to lower S by the factor exp(-qV_{bb}/kT), and V_{bb} decreases at higher doping, they would have observed a dependence in S on carrier density. A strict upper limit on the surface charge present in HF given these measurements is Q~10^8 cm^{-2}. Applying the relationship $S=\sigma \cdot v_{th} \cdot N_R$, where σ~10^{-15} cm^{-2} is a typical recombination cross section, v_{th}~10^7 cm/s is the carrier thermal velocity, the density of recombination centers is found to be N_R~3×10^7 cm^{-2}, on the order of ~1 per 10^8 surface atoms!

Immersing the H-terminated surface in concentrated acids (1 mM-10 M) HF, HCl, H_2SO_4, H_3PO_4 retained good SRV's 10 cm/s<S<0.2 cm/s, exhibiting the same, decreasing dependence on molarity, irrespective of acid. This reversible dependence suggests that recombination centers, in the form of strained silicon bonds, behave as Lewis bases which are energetically inactivated (neutralized) with respect to recombination after complexation with acid molecules in solution. This hypothesis was used to simulate their observations by such an acid-base equilibrium model with N_R~10^9 cm^{-2}.

[20] Recombination was found to be two-fold faster on Si(111)-H than Si(100)-H in HF, which is interesting since the trend is reversed on their respective thermal oxides.

Oskam et al. also studied electrically active surface states (SS) in the dark and recombination centers under illumination by in-situ impedance spectroscopy of low doped~10^{13} cm^{-3} *n*-type Si(111) immersed in *p*H adjusted NH_4F solutions [Oskam96a;Oskam96b]. The authors measured the frequency and band-bending dependence of the SS capacitance by subtracting the parallel space charge capacitance from the measured capacitance. Observation of a capacitance peak at low frequencies <5 kHz can be modeled to quantify four parameters; they extracted a SS energy of 0.38 eV below the CB, SS filling rate constant of 2×10^{-9} cm3/s, an emptying rate constant of 2×10^{4} /s and SS capture cross section of 10^{-16} cm^{-2}. The H-terminated surface is stable at low *p*H with nearly constant SS density $N_{ss}=2\times10^{10}$ cm^{-2} from 3<*p*H<6. Evidence for oxidation is observed in more basic solutions; at *p*H=7, N_{ss} increases sharply to $N_{ss}\sim2\times10^{11}$ cm^{-2} and from 8<*p*H<11 stabilizes to $N_{ss}\sim10^{12}$ cm^{-2}, although the surface state energy remains *p*H independent, suggesting these states are physically the same for oxidized and H-terminated surfaces.

In addition to the surface state capacitance peak present in the dark, a second frequency dependent peak is observed under varying illumination intensity, characteristic of a recombination process at centers physically different than surface states. By varying the photocurrent density from 1-9 $\mu A/cm^2$ at *p*H=9, a recombination density is measured in the range 5×10^{11} $cm^{-2}<N_R<5\times10^{12}$ cm^{-2}. A markedly slow electron-hole recombination rate constant $k_n=3\times10^{-10}$ $cm^{-3}s^{-1}$ is determined on H-terminated silicon, e.g., four orders in magnitude smaller than that reported for *n*-GaAs[21].

Combined electrical, optical and spectroscopic properties of hydrogen terminated silicon surfaces using multiple complementary techniques have been studied extensively by Angermann and co-workers [Angermann96;Henrion99;Angermann00].[22] In a study of native oxidation in 50% R.H. clean room air, they monitored the interface state distribution $D_{it}(E)$ by field modulated surface photovoltage, the native oxide thickness d_{ox} and roughness d_r by UV-Vis spectroscopic ellipsometry (SE), and the Si-H coverage by

[21] Microwave reflectivity measurements of H-terminated silicon in fluoride solution has also been applied to determine the band-bending at the semiconductor/solution interface [Natarajan98].
[22] Applications in solar cell are under recent investigation [Angermann04;Angermann08;Angermann09].

FTIR-SE [Henrion02]. $D_{it}(E)$ of *p*-type Si(111)-H is shown to be U-shaped with minimum near mid-gap $D_{it,min}<2\times10^{10}$ $cm^{-2}eV^{-1}$ at t=0 (100% Si-H, d_{ox}=0 Å), increasing to $D_{it,min}\sim8\times10^{10}$ $cm^{-2}eV^{-1}$ after t=24 h (50% Si-H, d_{ox}=1 Å), then increasing at a faster rate to $D_{it,min}\sim2\times10^{12}$ $cm^{-2}eV^{-1}$ at t_{1ML}=48 h (<5% Si-H, d_{ox}=3 Å) corresponding to the first monolayer of oxide. Changes in the distribution $D_{it}(E)$ were attributed to oxidation induced broken bonds or defects in the form of dangling bond at the silicon surface as well as the back Si/SiO_2 interface.

In contrast to the slow oxidation of atomically smooth Si(111) surface (d_r=1 Å), rougher surfaces exhibited faster oxidation rates during the initial monolayer phase of oxide growth, directly correlated to the initial surface microroughness. For instance, t_{1ML} was only 3.5 h on a thin film microcrystalline CVD hydrogenated Si-H surface. In addition to the oxidation rate, increasing initial roughness of Si(111)-H surfaces re-etched in HF for various times was shown to be directly correlated to increasing initial interface state densities $D_{it,min}$. The authors propose that oxidation initiates at Si-Si backbonds preferentially at steps, edges and HF-induced defects which increasingly polarize the backbonds and assist further nucleophillic attack. Formation of 2*d* islands that eventually extend into a monolayer of oxide are expected to be completed more rapidly on rougher surfaces, comprising of a larger number of nucleation sites.

Interesting electronic properties of H-terminated silicon on new and creative structures continue to be studied. The fabrication and low temperature transport properties of a hydrogen passivated field-effect transistor gated through a vacuum cavity has been reported [Eng05;Eng07]. A *p*-type Si(111) wafer with four n^+ source and drain contacts for Hall effect and Van der Pauw measurements is used to form the 2DEG inversion channel, and the substrate of an SOI wafer acts as a remote gate under a 760 nm deep cavity formed by RIE through the BOX. An encapsulated vacuum cavity between the mated wafers in HV preserves the ideal electrical properties and eliminates ambient sensitivity. The electron density is linear in gate voltage above threshold (10 V) but because of breakdown in the oxide (100 V), the peak inversion density is only $n_s\sim7\times10^{11}$ cm^{-2}. A this 100 V peak, a high mobility $\mu_e\sim8000$ cm^2/Vs is observed, more than three

fold higher than reported on Si(111)-MOSFETs, which reflects the high quality of the atomically flat, electronically passivated surface. More recently, a very high mobility μ_e=110,000 cm^2/Vs has been observed at 70 mK [McFarland09].

1.8.4 Molecular Sensing on Oxide-Free Silicon

In parallel to widespread studies on oxide surfaces discussed in section 1.7, similar applications of H-terminated silicon structures demonstrate their utility for highly sensitive electrically based detection of molecular species. Some examples are provided.

H-Terminated Nanowires: Gas-phase chemical sensing using with H-terminated nanowires has been demonstrated recently [Zhou03]. The resistance between two Ag glued contacts on HF-etched SiNW bundles (oxide-assisted growth) pressed onto glass substrates has been used to detect the reversible effects of water or ammonia vapors in a large 70 L vacuum chamber. Under a 10 mTorr rough vacuum, venting the chamber to 760 Torr air at 60% R.H decreases R_{2p} by 3 orders from 5×10^{12} Ω (V_s=10 V;I_{meas}=2 pA) to 5×10^{9}Ω (V=10 V;I=2 nA). This effect is attributed mainly to the water component of air since dehumidifying the surrounding atmosphere to 40% R.H. opposes the effect, increasing the resistance to 5×10^{10} Ω. By comparison N_2 exposure only reduced R several fold. Upon exposure to 760 Torr 0.1% NH_3:N_2 the resistance decreases by four orders from 10^{13} Ω to 10^{9} Ω. These effects were found to reverse upon evacuating the chamber. The authors concluded SiNWs are promising for use as chemical sensors, noting the mechanism of sensing in their bundles must take into account the conductivity of individual wires as well as changes in nanowire junction resistance, since hundreds of NW contacts are expected to form with 1-10 μm long wires between electrodes 5 mm apart.

Amine-Terminated Nanowires: H-terminated silicon can be organically modified with amine functionality for subsequent molecular attachment. In a recent study, amine

functionalized alkene and alkenyl monolayers formed on H-terminated (111) SiNW's fabricated from SOI have been used for subsequent biotinylation and attachment of streptavidin [Masood10].

Heath's group demonstrated that electrical detection of DNA immobilization and hybridization on amine functionalized nanowires formed on H-termination silicon is more sensitive than using the common oxide/silane route [Bunimovich06]. In this top-down approach, nanowires fabricated out of 35 nm SOI (Ibis) were processed by EBL/RIE/FGA and used to make arrays {w=20 nm;h=35 nm;l=30 μm}. Amine terminated *p*-type devices are protonated (positive charge) near neutral *p*H (pK_a~9), causing depletion of holes and hence increases the resistance *R*. Electrostatic adsorption of negatively charged 16 mer probe followed by complementary target DNA successively reduces *R*. Since the DNA is most likely 'lying-flat' rather than 'standing up', the detection is quite sensitive at physiologically relevant electrolyte concentrations (0.14 M) in which L_D~1 nm in solution. Over the same sensor response range $0<R/R_0<12\%$ a larger range in target concentration is detected (100 nM-10 pM) on non-oxidized NWs, compared to using an oxidized/silane route (100 nM-1 nM), attributed to higher dielectric screening and higher interface state density on the chemical oxide.

Hydrogenated Amorphous Films: An interesting alternative to wet chemically etched crystalline silicon, amorphous hydrogenated thin silicon films (a-SiH) can be formed directly by a 250 ^oC plasma deposition of silane (SiH_4) onto glass substrates, although at the cost of reduced electrical quality. These systems have long been known exhibit electrical response to adsorption of various gases [Tanielian78]. In a recent study, reversible modulation of the resistance of undoped 200 nm a-SiH at 250 ^oC was reported, decreasing $R_{2p}(t)$ in the range ~10-75% in response to various exposure levels (100-5000 ppm) of H_2O, NH_3, NO_2 gases, and found to be rather insensitive to H_2, CO, and C_2H_2 [Helwig07b]. The authors tentatively attributed the increased conductivity to strongly ionically adsorbed species, i.e. H_3O^+ or NH_4^+ ions.

1.8.5 SOI-H Substrates

Having reviewed previous experimental studies in the field we arrive at SOI-H surfaces, completing this chapter with an overview of recent contributions. Much of the work presented hereafter and related literature concentrates on electrical properties of SOI-H which will be expanded upon in upcoming chapters 3-6. Hydrogen passivated silicon surfaces present interesting model systems for surface conductivity studies, in particular with respect to surface modification on thin SOI films. Their increased sensitivity to band-bending has been applied to monitor the sheet resistance of SOI-H, shown to be a sensitive probe of ambient oxidation and humidity [Dubey07]. The strong influence of humidity on the conductivity of SOI-H has been confirmed in a separate study which further suggests HF-induces band-structure modification in ultrathin films [Scott09]. Controlled adsorption of water, pyridine and other amines in vacuum are found to strongly modulate the sheet resistance and Hall effect, forming electron accumulation and inversion layers on *n*-type or *p*-type surfaces [Dubey10]. Using the substrate as a gate in a pseudo-MOSFET geometry [Cristoloveanu92], reversible conductivity modulation of an electron channel at the back Si/SiO_2 interface is shown to be consistent with the previous surface conductivity studies, confirming water or pyridine adsorb as positively charged species, lowering the accumulation threshold voltage [Dubey11a]. Because of their simplicity, pseudo-MOSFETs on oxide-free silicon have become increasingly popular for characterization of charge transfer studies. Electron donor/acceptor molecules covalently grafted onto H-terminated SOI have been shown to controllably modulate the threshold voltage, attributed to a top-gating effect induced by charge transfer between the molecule and the silicon [He06;He09]. In related work, direct adsorption of electron acceptors such as TCNE [Dubey11b] and TNT on SOI-H pseudo-MOSFETS has been shown to decrease the conductivity of the back-gated accumulation channel, thereby raising the flat-band voltage as a result of the negatively charged species. Chapters 3-6 present our results and discuss these effects in more detail. The central experimental techniques and methods employed are given in Ch2.

1.9 Research Environment

This project was executed in Ottawa at the National Research Council's Steacie Institute for Molecular Sciences (NRC-SIMS). The work performed here involves experimental physical research at molecule/semiconductor interfaces which is aligned with but distinct from ongoing NRC-supported research. This work is specifically aligned with a SIMS project initially entitled "Molecular Sensing at Chemically Modified Semiconductor Surfaces" which aims to explore the potential use of chemically modified Si surfaces for sensor applications. The group dynamic associated to this project area at SIMS is highly multidisciplinary; members originate from diverse educational backgrounds comprising mostly of organic chemists, physical chemists, electrochemists, surface scientists and physicists. The labs are equipped with sample preparation fumehoods, impedance analyzers, electronic test equipment, probestations, and UHV surface science characterization tools STM and HREELS.

1.10 Dissertation Structure

The dissertation structure is organized into seven chapters outlined as follows: Chapter One contains a statement of the research problem, an introduction to silicon, energy bands, surface states, band-bending, and an overview of SOI material and literature review. Core experimental techniques are described in Chapter Two. Chapter Three studies native oxidation of SOI-H and reports the influence of physisorbed water from ambient or controlled adsorption in vacuum to reversibly enhance the conductivity of *n*-type and *p*-type SOI-H. Chapter Four explores similar effects of other gases pyridine, ammonia, triethylamine, and methanol, as well as milder species nitrogen, oxygen, thiophene and toluene. Conductivity modulation effects observed in Ch3 and Ch4 are re-investigated in Chapter Five using SOI-H pseudo-MOSFETs, expressed through

reversible modulation of the flat-band voltage instead. A gas-phase photochemical reaction used to form a SOI-**C10** alkyl monolayer is also characterized. In Chapter Six, the pseudo-MOSFET is applied to study the highly sensitive response to vapors of the electron accepter tetracyanoethylene on SOI-H and SOI-**C10** in ambient. Chapter Seven summarizes and attempts to reconcile our observations and offer perspectives to the field.

Chapter 2

Methods

2.1 Introduction

Core experimental techniques, materials and equipment are discussed briefly. Four probe methods are applied in Ch3 and Ch4 to measure the sheet resistance R_s, Hall coefficient R_H, and carrier mobility $\mu_{n,p}$ of SOI samples. In Ch5 and Ch6 the pseudo-MOSFET technique is used to extract the flat-band voltage V_{FB} from the current-voltage $I_D(V_D,V_G)$ output characteristics.

2.2 Four Probe Methods

2.2.1 Two probes

Two probe measurements (2*p*) are generally afflicted by the parasitic contribution of the electrical contacts. When a constant current I_0 flows between two electrical contacts with resistances R_C in series with a sample under test with resistance R^*, voltage drops across

the sample as well as the contacts $V=I_0R^*+2I_0R_C$ leading to a two probe resistance V/I_0:

$$R_{2p} = R^* + 2R_C. \tag{2.1}$$

From Eqn. 2.1 it is clear this measurement is only acceptable when $R^* >> R_C$ which applies to most insulators. For instance a commercial resistor R^*=1 MΩ with metallic leads can be measured accurately using an inexpensive voltmeter (input impedance ~100 MΩ) since R_C is on the order of 1 Ω, whereas a 2 Ω resistor cannot be determined with good accuracy in this case. On semiconductors implantation of heavily doped contact regions (~10^{19} cm^{-3}) can be used to suppress contact resistance as with the conductance studies of SiNW's discussed in Ch1. However for most metals and semiconductors the contact resistance is either unknown, comparable to or larger than the resistance of the sample under test, requiring the use of four probe methods in place of two probes.

2.2.2 Four probes

Four probe techniques (4*p*) employ two contact pairs (2×2*p*); one contact pair sources a current/voltage and the other contact pair measures a current/voltage. For sheet resistance measurements determined in-line (2.2.4) or in the Van der Pauw geometry (2.2.5) a constant current is sourced between two probes and a voltage drop is sensed with high impedance between another pair of probes. The contact resistance of the current sourcing pair is not needed in the determination of R_s. Because the voltage drop across the sensing pair is measured passively using a small sense current (pA) in a high impedance circuit (>100 GΩ), the influence of parasitic contact resistance is eliminated in a four probe measurement. A schematic circuit is shown in Figure 2.1.

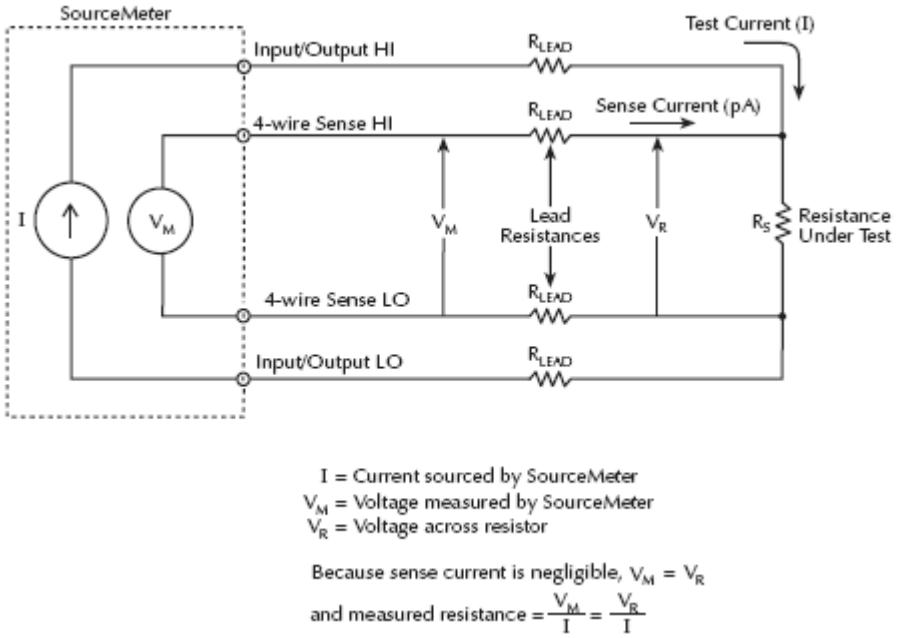

Figure 2.1: A four probe measurement minimizes/eliminates the effects of contact resistance (lead resistance) by measuring the voltage across the resistor under test with a second set of test leads. Because of the high input impedance of the SourceMeter voltmeter, the current through the sense leads is negligible, and the measured voltage is essentially the same as the voltage across the resistor under test, adapted from the Keithley 2400 Series SourceMeter® User's Manual.

2.2.3 Sheet Resistance

The electrical resistance R of thin films with uniform thickness d is commonly expressed in terms of their sheet resistance R_s which is a quantity independent of aspect ratio and can be measured directly by four probe methods. For a slab with length L and width W as shown in Figure 2.2 the resistance is related to the electrical resistivity ρ using Ohm's Law:

$$R = \rho L / A = (\rho / d) \cdot (L / W) = R_s (L / W). \tag{2.2}$$

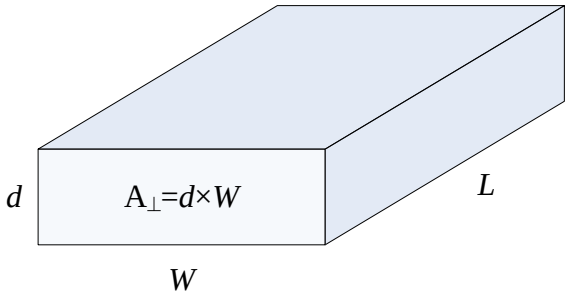

Figure 2.2: Thin film slab with thickness *d*, width *W* and length *L*.

Which gives the definition $\rho=R_s d=1/\sigma$, where $\sigma=nq\mu_n$ is the electrical conductivity for one type of carrier with carrier density *n* and mobility μ_n. R_s differs from *R* by dividing out the aspect ratio *L*/*W*. Although both *R* and R_s have units of Ω, R_s is distinguished from *R* by the notation {ohms/square; Ω/sq.; Ω/□} since a square sample with *L*=*W* will have the same resistance as its sheet resistance $R=R_s$.

2.2.4 In-line Geometry

In-line geometry uses four equidistant co-linear probes [Sze69]. The outer pair sources constant current *I* and the inner pair sense a voltage drop Δ*V*. The sheet resistance is determined by Ohm's Law [Smits58]:

$$R_s = (\Delta V / I) \cdot C, \tag{2.3}$$

where $1<C<4.5$ is a correction factor that arises due to the spreading of current lines around the sample depending on the probe spacing and sample aspect ratio, listed in Table 2.1 [Smits57]. Changing the direction of the current and averaging two readings improves the accuracy of the measurement by eliminating parasitic DC offset voltages, although in most cases these were not observed to be significant.

Table 2.1: In-line geometry correction factors as a function of aspect ratio L/W and width W to probe spacing s as shown schematically at the right, adapted from [Smits57].

W/s	L/W=1	L/W=2	L/W=3	$L/W\geq$4
1.0			0.9988	0.9994
1.25			1.2467	1.2248
1.5		1.4788	1.4893	1.4893
1.75		1.7196	1.7238	1.7238
2.0		1.9454	1.9475	1.9475
2.5		2.3532	2.3541	2.3541
3.0	2.4575	2.7000	2.7005	2.7005
4.0	3.1137	3.2246	3.2248	3.2348
5.0	3.5098	3.5748	3.6750	3.5750
7.5	4.0095	4.0361	4.0362	4.0362
10.0	4.2209	4.2357	4.2357	4.2357
15.0	4.3882	4.3947	4.3947	4.3947
20.0	4.4516	4.4553	4.4553	4.4553
40.0	4.5120	4.5129	4.5129	4.5129
∞	4.5324	4.5324	4.5325	4.5324

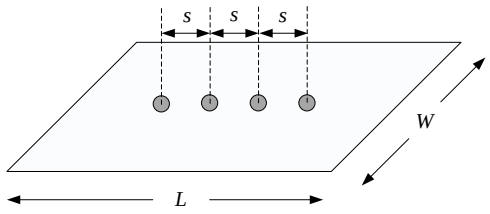

From Table 2.1 it can be seen the correction factor depends strongly on the width to probe spacing for a given aspect ratio, approaching $\pi/\ln 2 \sim 4.532$ when the probe spacing is much smaller than the sample dimensions. For most in-line studies the SOI samples were cut to L~2 cm; W~1 cm (L/W=2) and the probe spacing was s~0.5 cm (W/s=2) which yielded C~2. The sample dimensions and were always measured after cutting to determine the precise factor from Table 2.1.

2.2.5 Van der Pauw Geometry

The Van der Pauw method for measuring sheet resistance is based on a theorem which applies to flat samples of arbitrary shape with sufficiently small contacts located at the circumference of the sample [van der Pauw57; van der Pauw58]. Samples are assumed to be singly connected i.e. they should not have isolated holes. Unlike the in-line method there are no geometric correction factors. In this configuration a pair of sequential contacts sources a constant current and the opposite pair sense a voltage drop, corresponding to a pseudo-resistance R_a. This process is repeated after incrementing the

index of the contact pairs by one unit corresponding to a second pseudo-resistance R_b, as shown schematically for a rectangular film in Figure 2.3.

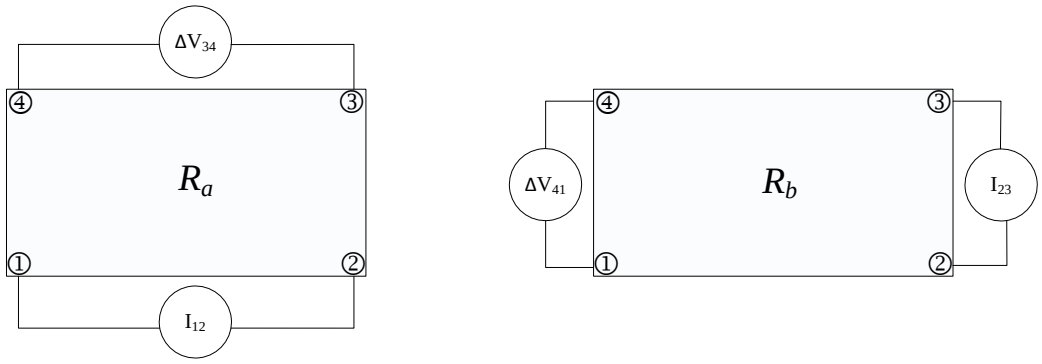

Figure 2.3: Schematic of the Van der Pauw geometry pseudo-resistances R_a and R_b used to solve for R_s. Both directions of current are used and the current/voltage pairs are also interchanged requiring four voltage readings to be averaged for each pseudo-resistance.

The sheet resistance is obtained by solving

$$\exp(-\pi R_a / R_s) + \exp(-\pi R_b / R_s) = 1. \qquad (2.4)$$

Eqn 2.4 can be solved exactly by numerical methods. The custom written program used in our measurements applies the Newton Raphson method to calculate R_s. For each pseudo-resistance both directions of current are used and the current-source and voltage-measure contact pairs are also interchanged; in total four voltage readings are averaged in the calculation of $R_a = \langle \Delta V^{(4)} \rangle / I$ and similarly four readings for R_b.

2.2.5 Hall Effect

The Hall effect can be used to determine the sign and density of carriers in a conductor [Kittel96]. When a longitudinal current density J_x (current I_x) flows across a transverse magnetic field B_z moving charges flow to one side due to the Lorentz force. An electric field E_y (Hall field) develops in opposition to the magnetic force which leads to a measurable Hall voltage V_H, shown schematically for a Hall Bar geometry ($L>W$) in Figure 2.4.

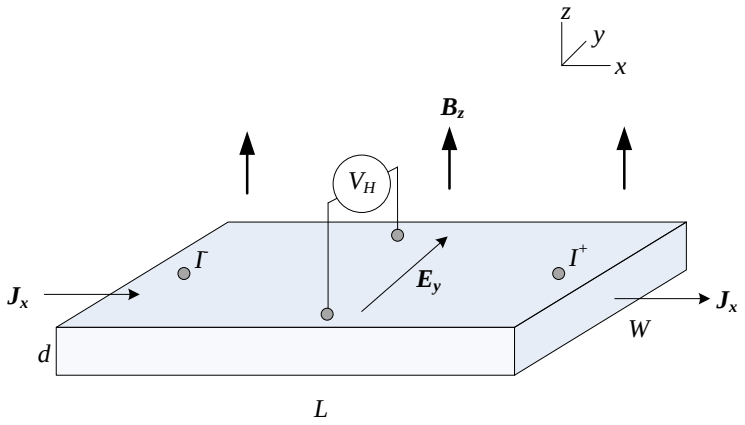

Figure 2.4: Schematic illustration of the Hall Effect in a Hall Bar geometry ($L>W$).

Although square geometries $L=W$ have also been employed (Ch3), an aspect ratio of two or more (Hall Bar geometry) is preferred experimentally to maximize the component of the Hall field perpendicular to the current density and minimize offset voltages. On *p*-type material $q>0$ the Hall voltage is positive and for *n*-type $q<0$ the sign of V_H is negative. A quantity independent of the magnetic field and current defined as the Hall coefficient $R_H=E_y/J_xB_z$ is commonly reported in place of the Hall voltage itself. When one type of carrier is predominant carrier density is inversely proportional to the Hall voltage:

$$n = \frac{1}{d}\int_0^d n(z)dz = \frac{I_x B_z}{V_H q d} = \frac{1}{R_H q}. \tag{2.5}$$

The Hall voltage and sheet resistance can be used to extract the carrier mobility:

$$\mu_n = \frac{V_H}{I_x R_s B_z}. \tag{2.6}$$

Rare earth permanent magnets were used to source the magnetic field. The direction of the magnetic field was always reversed by rotating the permanent magnets 180^o around the sample; the difference between these readings ($2V_H$) effectively eliminated parasitic offset voltages. The field strength at the sample was determined via calibration measurements using silicon wafers with known doping concentrations.

2.3 Pseudo-MOSFET Technique

This three-terminal measurement uses two point contacts on the device layer of a SOI wafer to form the source and drain regions and a third contact to the substrate which acts as a gate [Cristoloveanu92]. The measurement configuration is analogous to that of a conventional MOSFET [Sze69]. A separate chapter (Ch5) has been dedicated to this technique, describing the basic operation in detail, including specific examples of the experimental conditions used and parameter extraction.

2.4 Electrical Contacts and Electronic Test Equipment

Contact to the top silicon film was made via 2.5 μm diameter tungsten probes touching small EGaIn drops (work function 4.1 eV) applied directly onto the H-terminated samples. The eutectic made ohmic contact to *n*-type samples and slightly rectified on *p*-type. Keithley 2400 source-measure units were used in all electrical measurements. Computer interfacing was done by GPIB using Labview software.

2.5 Measurement Systems

This section is intended as a reference to define and clarify the measurement systems and chambers used in various experiments reported throughout this thesis.

2.5.1 Ambient Probestation

All electrical measurements in ambient were conducted in a vibration-isolated commercial probe-station equipped with micropositioners for probing the SOI samples.

2.5.2 Gen0, Gen1, Gen2 vacuum systems

Throughout the course of this research a small vacuum system backed by a turbo-molecular pump was adapted to perform specific combinations of the electrical measurements as described in the previous sections. These systems are referred to as Gen0, Gen1 and Gen2, and their primary functions are sketched in Figure 2.5.

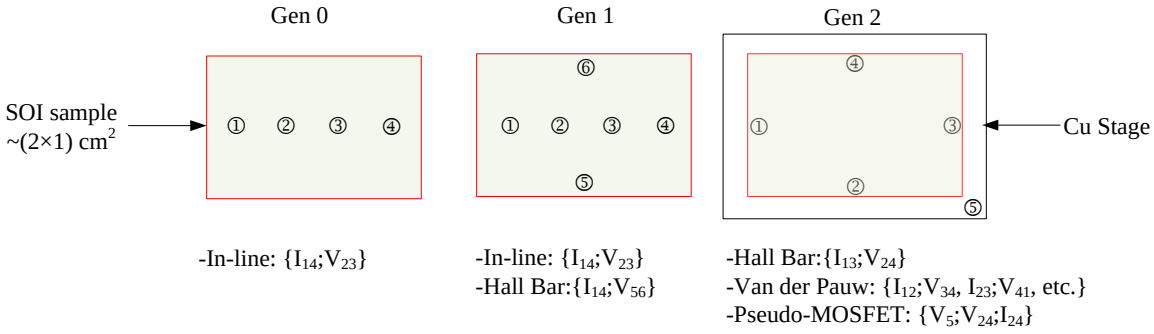

Figure 2.5: Schematics of the Gen0, Gen1 and Gen2 electrical configurations and their primary functions.

The Gen0 and Gen1 configurations were used exclusively in Ch3 and Ch4. The Gen2 system was used in Ch5. All wiring in vacuum was insulated with Teflon or Kapton. Samples were mounted on stages that fit inside a 2.75” flange fitting.

Chapter 3

Influence of Water Adsorption

3.1 Introduction

The adsorption of charged or polar species on a semiconductor surface can modulate the electrical properties of the substrate through long-range field effects, resulting in charge redistribution and changes in surface conductivity [Kingston55a;Cohen97;Cahen05]. As described in Ch1, adsorbate induced changes in conductivity were first noted in pioneering experiments in the 1950's, leading to considerable debate as to the precise origin of these effects [Brattain53;Brown53;Kingston54;Kingston55b]. These early experiments, carried out on germanium surfaces covered by thin native oxide layers, indicated that relative humidity can have a strong influence on the surface potential. The effect of water vapour was seen to be large enough to drive *p*-type substrates into inversion, creating a minority (*n*-type) channel at the surface [Kingston55b].

Recently, the development of thin film semiconductors and nanostructures with dimensions that are comparable to the materials' Debye field screening length L_D has understandably led to renewed interests in adsorption and reaction events on their

surfaces. As described in Ch1, the motivation in the present studies is to use oxide-free, silicon-on-insulator (SOI) material for probing molecular adsorption and reaction events; they exhibit increased sensitivity to field effects as the top layer thickness d is generally less than or equal to the depletion length L_{dep}. Note that at moderate doping levels of 10^{15} cm^{-3}, L_D is on the order of 100 nm and L_{dep} is on the order of 1 μm. This implies film thicknesses less than 1 μm will have relatively small bulk contribution, as with our wafer bonded SOI (where $d \sim L_{dep}$ is 1 μm or 3 μm), although the sensitivity to surface field effects is enhanced on thinner films as with our SIMOX material (where $d \sim L_D$ is 150 nm or 200 nm).

Compared to silicon nanowires (SiNWs), planar SOI geometry is simple and facilitates a more direct interpretation of the effects of adsorption events. Furthermore, in many cases, SOI wafer material is just as compatible with the application of surface science and characterization techniques as is bulk silicon [Lin98;Zhang06a;Zhang06b]. For instance, Weitering and co-workers [Lin98] prepared Si(100)-2×1 from 35 nm ultrathin SIMOX SOI (UTSOI), and demonstrated using Auger electron spectroscopy (AES), low energy electron diffraction (LEED) and scanning tunneling microscopy (STM) that the surfaces are of similar quality as bulk Si(100). Lagally and co-workers have also carried out STM characterization studies of UTSOI over a range of thicknesses 10 nm<d<200 nm [Zhang06a;Zhang06b]. In addition to traditional surface science techniques, SOI material has been used recently in Casimir force measurements [Anthony08], surface plasmon enhanced solar cells [Pillai07], and selective oxide-free sensor geometries [Seitz11].

Hydrogen passivated silicon surfaces present interesting model systems for surface conductivity studies. Obtained by etching in HF or ammonium fluoride [Higashi90], these surfaces exhibit a low density of electrically active defects [Yablonivich86;Oskam96a;Henrion02] and have recently been used to form high mobility 2d electron gases [Eng05;Eng07] as described in some detail in Ch1. Oxide-free, hydrogen terminated silicon-on-insulator (SOI-H) substrates are ideal for investigating the ability of adsorbed or covalently attached molecules to modulate the conductivity.

These substrates are stable enough to be handled in ambient atmosphere for several minutes without oxidizing significantly [Niwano94], and have extended lifetimes once in high vacuum environments ($<10^{-5}$ Torr) in which surface reactions with water and oxygen are limited [Morita90;MacLaren02].

This chapter reports the results of conductivity measurements performed both in ambient atmosphere (3.2) and in a turbo-pumped high vacuum system with base pressure of 1×10^{-7} Torr (section 3.3). In section 3.2, the sheet resistance of hydrogen terminated silicon-on-insulator (SOI-H) is shown to increase significantly with time in air due to depletion of free carriers, attributed to the growth of electrically active defects as the surface oxidizes. Surprisingly, physisorbed water causes an increase in the conductivity via adsorption from ambient or controlled exposure in vacuum. This effect is largely reversible when the water layer is displaced by inert gas purging, heating, or pumping. The observed conductivity changes in ambient purge experiments are correlated with Hall voltage changes, suggesting that the adsorbed water layer induces accumulation of majority carriers on *n*-doped substrates. Reported in section 3.3, simultaneous sheet resistance and Hall effect measurements on moderately doped $N_{A,D}<10^{16}$ cm^{-3} *n*-type and *p*-type SOI-H samples mounted in a home-built vacuum system are used to monitor the effect of water exposure in the Torr range on the electrical transport properties of these substrates. Minority channels on *p*-type and majority channels on *n*-type silicon are formed upon controlled exposure to pure 10^{18} Ω·cm water vapour. These observations can be explained by a simple classical band-bending model which considers the adsorbates as the source of a uniform surface charge on the order of $+10^{11}$ q·cm^{-2}, described in some detail in section 3.4. The submonolayer coverage of water on a Si-H surface and a discussion of the possible and implausible mechanisms are presented in section 3.5. The observation that adsorbed water can induce significant band bending and surface conductivity modulation has implications for the interpretation of electrical measurements on Si surfaces and nanowires in ambient or aqueous solutions. These results demonstrate the utility of DC transport measurements of SOI platforms for studies of molecular adsorption and charge transfer effects at semiconductor surfaces.

3.2 Characterization of WB-SOI and SIMOX

The sheet resistance of H-terminated SOI is observed to increase significantly with time in ambient air due to depletion of free carriers, attributed to the growth of electrically active defects as the surface oxidizes. In addition, water adsorption (either from the ambient humidity in air or controlled dosing in vacuum) is seen to cause additional reversible changes in the conductivity due to accumulation of majority carriers.

3.2.1 Preparation and Surface Characterization

Lightly doped *n*-type 1 μm SOI(111)-H and SIMOX 200 nm SOI(100)-H substrates have been employed. SOI(111) samples made via wafer bonding (Tracit, 1 μm buried oxide layer, 3 μm active layer) were thinned down by successive thermal oxidation and etching cycles to obtain a top layer thickness of d=1 μm. We thank D. Landheer (IMS-NRC) for providing the thinned SOI wafers. Hydrogen terminated samples were prepared by cleaning in piranha solution followed by etching in 2% HF in the case of SOI(100) or etching in degassed ammonium fluoride for 15 min followed by a brief water rinse in the case of SOI(111). STM imaging revealed that SOI(111)-H surfaces were atomically flat and of similar quality to that achieved on conventional Si(111) wafers. High resolution electron energy loss spectroscopy (HREELS) confirmed the resulting surfaces were monohydride terminated with minimal oxidation (Si-O-Si) and hydrocarbon (C-H) modes. The low energy, low current density incident beam (6 eV) effectively probes surface vibrational modes without causing observable desorption or defect formation. Surface vibrational modes of WB SOI(111)-H and SIMOX SOI(100)-H are shown below in the HREELS spectra in Figure 3.1. The dominant features are the Si-H stretch and bend modes. Assignment of peaks in Figure 3.1 is listed in Table 3.1 and based on previously reported vibrational studies [Dumas91;Dumas92]. On SIMOX SOI(100)-H substrates a strong Si-H_2 scissor mode is observed, as expected for these surfaces which are known to exhibit a mixture of mono and dihydride species.

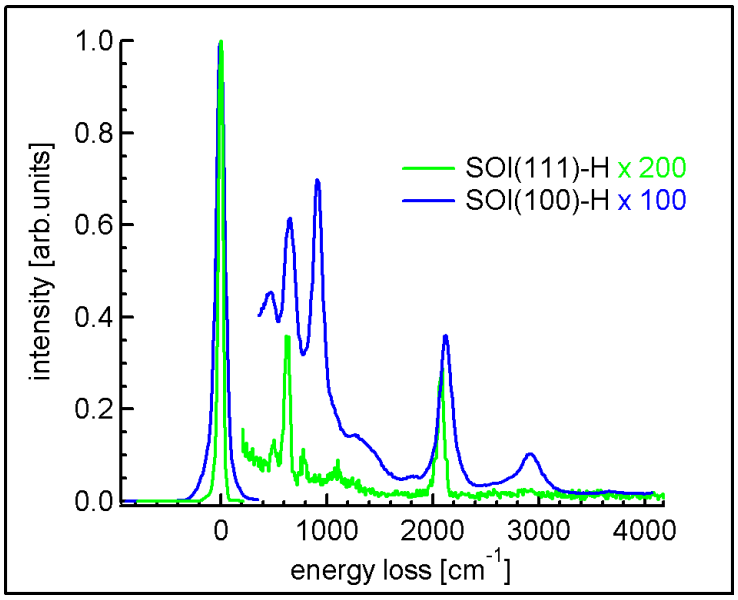

Figure 3.1: HREELS spectra of HF etched SOI(100)-H (blue) and buffered oxide etched SOI(111)-H (green) normalized to their elastic peaks. Measurements are taken in specular geometry at 60^{o} with respect the surface normal at incident beam energy of 6 eV and nominal resolution of 32 cm^{-1}.

Table 3.1: Dominant vibrational modes observed in HREELS of (100) and (111) SOI-H based on the spectra presented in Figure 3.1.

Mode Assignment	SOI(100)-H [cm^{-1}]	SOI(111)-H [cm^{-1}]
Si substrate phonon	464	505
Si-H bend	655	630
Si-H_2 scissor	912	-
Si-H_x stretch	2117	2087
Phonon-bend resonance	-	779
Si-O-Si	-	1102
CH stretch	2917	-

3.2.2 Monitoring ambient Oxidation with Surface Conductivity on SOI(111)-H

Sheet resistance in ambient was measured using four probe measurements in the van der Pauw geometry using Keithley 2400 source meters. Contact to the top silicon layer was made via tungsten probes touching small EGaIn eutectic drops. Figure 3.2a shows the sheet resistance $R_s(t)$ of two distinct *n*-type SOI(111)-H surfaces as a function of time in similar ambient conditions. In an alternate representation, the associated sheet conductance change $G_s(t)$-G_0 is plotted in Figure 3.2b as a fraction of the initial conductance G_0 for Sample 1.

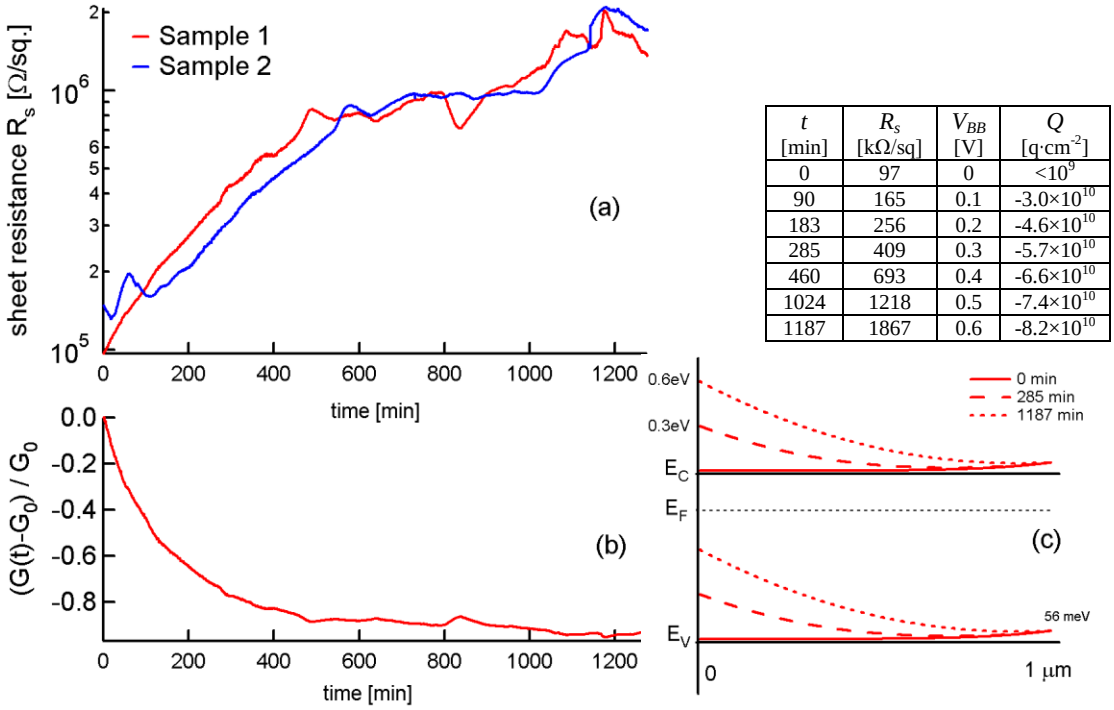

t [min]	R_s [kΩ/sq]	V_{BB} [V]	Q [q·cm^{-2}]
0	97	0	$<10^9$
90	165	0.1	-3.0×10^{10}
183	256	0.2	-4.6×10^{10}
285	409	0.3	-5.7×10^{10}
460	693	0.4	-6.6×10^{10}
1024	1218	0.5	-7.4×10^{10}
1187	1867	0.6	-8.2×10^{10}

Figure 3.2: Air-oxidation of *n*-type 1 μm thick SOI(111)-H observed by increasing sheet resistance $R_s(t)$ of (a) Samples 1 and 2. (b) Relative surface conductance change $\Delta G_s(t)/G_0$ for Sample 1. The table inset (top-right) relates R_s to a surface charge density $Q(t)$ and surface band-bending $V_{BB}(t)$, using the parameters N_D=9.2×10^{14} cm^{-3}, μ_n=900 cm^2/Vs, BOX charge densities of ~10^{10} q·cm^{-2}, and assuming Q_0<10^9 q·cm^{-2}. The corresponding band-diagrams are illustrated in (c) at t_0~0 h, t~5 h, and t~20 h.

The initial measured resistance corresponds to a resistivity of ~10 Ω·cm, close to that expected based on the doping level on the order of 10^{15}cm^{-3}, consistent with the low density of electrically active defects expected of H-passivated silicon surfaces [Yablonovich86;Oskam96a;Henrion02]. However, this resistance increases immediately upon commencing measurements, increasing by ~20 times after 12–18 h. As demonstrated by the two traces in Fig. 3.2a, while small deviations in the behavior are observed from run to run the overall rate of increase is highly reproducible. The increase in resistance is attributed to the growth of electrically active defects which trap majority carriers (electrons) resulting in upward band bending and depletion of free carriers.

The upper-right table lists R_s of Sample 1 at various times and simulates the measurements to an equivalent surface charge density $Q(t)$ and surface band-bending $V_{BB}(t)$; the upward band-bending causing depletion is illustrated in Figure 3.2c at three time-points: 0 h, 5 h and 20 h. In this simulation (details in 3.4), the parameter for doping density was N_D=9.2×10^{14} cm^{-3}, similar to the quoted bulk doping, and the electron mobility was μ_n=900 cm^2/Vs based on Hall Effect measurements. Upper and lower BOX charge densities of ~10^{10} q·cm^{-2} are reasonable for thermal oxide quality WB-SOI [Cristoloveanu95]. An unknown in this simulation was the initial surface charge Q_0. Surface photovoltage measurements in the same lab taken with a Kelvin probe of bulk *n*-type Si at similar doping, show the H-terminated surface does not exhibit significant band-bending and normally ranges from 20 mV<V_{BB}<-20 mV. Based on these observations it is assumed the bands are initially flat and the initial surface charge is negligible Q_0<10^9 q·cm^{-2}.

3.2.3 Monitoring ambient Oxidation with Surface Conductivity 200nm SOI(100)-H

Analogous to the observations on 1 μm WB-SOI in 3.2.2, the sheet resistance increase of *n*-type 200 nm SIMOX samples confirm that ambient atmosphere degrades the initial conductivity significantly with time in air as illustrated in Figures 3.3a, 3.3b, 3.3 c and the upper right table inset.

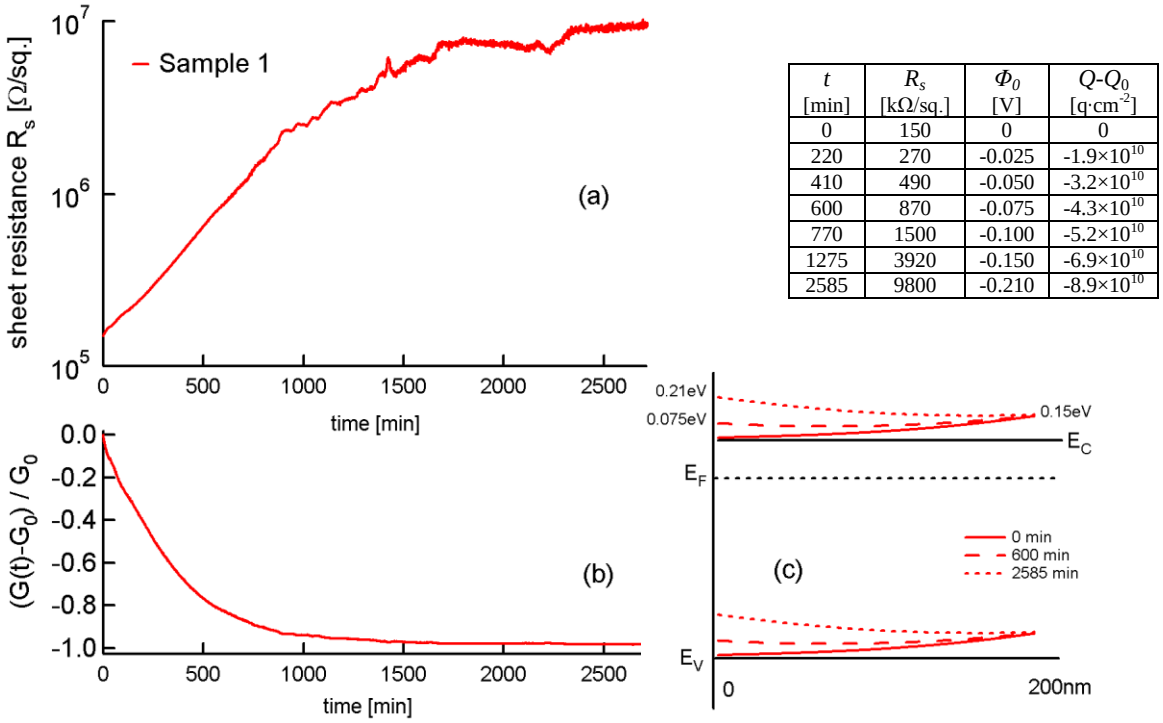

t [min]	R_s [kΩ/sq.]	Φ_0 [V]	Q-Q_0 [q·cm^{-2}]
0	150	0	0
220	270	-0.025	-1.9×10^{10}
410	490	-0.050	-3.2×10^{10}
600	870	-0.075	-4.3×10^{10}
770	1500	-0.100	-5.2×10^{10}
1275	3920	-0.150	-6.9×10^{10}
2585	9800	-0.210	-8.9×10^{10}

Figure 3.3: Air-oxidation of *n*-type 200 nm thick SOI(100)-H observed by increasing (a) sheet resistance $R_s(t)$. (b) Relative surface conductance change $\Delta G_s(t)/G_0$. The table inset (top-right) relates R_s to a surface charge density $Q(t)$ relative to Q_0, and surface potential $\Phi_0(t)$, using the parameters $N_D=4.7\times10^{15}$ cm^{-3} and BOX charge densities of ~10^{11} q·cm^{-2}. The corresponding band-diagrams are illustrated in (c) at t_0~0 h, t~10 h, and t~43 h.

For similar levels of surface charge, the sheet resistance in Figure 3.3 spans two orders in magnitude on 200 nm SOI compared to one order on 1 μm SOI in 3.2.2, confirming that the sensitivity improves when d~L_D. The donor density and BOX interface charges were

chosen based on typical values known for SIMOX samples fabricated from Ibis [Cristoloveanu95]. Since the potential does not go to zero throughout the film, the upper right table lists the surface potential as Φ_0 rather than using the notation V_{BB} as was used on 1 μm SOI. Note that we published the results of Figure 3.2 [Dubey07], but decided not to include Figure 3.3. However, the Lagally group has published $R_s(t)$ of 200 nm HF-etched SOI (100) and observed a similar degradation in conductivity as illustrated in Figure 3.3 [Scott09]. The authors also attribute their observations to the growth of electrically active defects and reference our work.

3.2.4 Discussion of Native oxidation

The precise rate of oxidation is influenced by numerous environmental parameters [Morita90] and since the conditions were not well controlled in our studies it is suspected that R_s evolves distinctly in each run (e.g. Figure 3.2) due to these differences. The growth of electrically active defect states on H-terminated surfaces in ambient environments is presumably due to oxidation as the initial resistance value is recovered by re-etching the oxidized surface in HF. The increase in R_s with t can be attributed to the initial stages of oxide reconstruction: as O atom insertion builds strain in the silicon lattice, creation and occupation of electrically active charge trap states develops an interface charge, causing depletion [Henrion02].

Fluctuations in R_s observed in Figures 3.2 and 3.3 are not entirely understood, they may be related to time-dependent stress mechanisms, adsorption from ambient and variations in lab conditions over time. When ambient oxidation was monitored in a closed sealed chamber filled with air to simulate a more constant environment, many of these irregularities disappeared and R_s increased monotonically. This suggests the fluctuations arise from the external conditions rather than the oxide growth process.

Native oxide growth on H-terminated silicon is complicated to model [Cerofolini06;Kovalgin05]. It is distinct from thermal oxide growth (>700^{o}C), described by Deals-Grove kinetics [Deal65], which by extrapolation to RT would predict little

oxidation (<1 Å), contrary to experiment (~10 Å). The adsorption and diffusion of many contributing species is involved [Sakata00;Zaborovskiy04] as well as the possibility of photochemical reactions in the presence of UV [Mitchell03]. IR studies of initial oxidation of Si(111)-H shows the H-termination is largely preserved at the initial stages with oxygen insertion appearing in the Si-Si backbonds [Ogawa96;Zhang01].

One distinct feature of native oxidation is the requirement for the coexistence of both oxygen and water [Morita90]. Morita et al used ellipsometry and XPS to follow oxidation in clean room air at room temperature. When no efforts were made to reduce humidity the oxide thickness after one week was ~7 Å. However in pure N_2 (<0.1 ppm H_2O) or a mixture of dry N_2/O_2 (<0.1 ppm H_2O) the oxide growth was suppressed to <2 Å. These observations are listed below in Figure 3.4 (left). Alternatively, native oxide growth of H-Terminated silicon immersed in water was also suppressed when efforts were made to deoxygenate the water, shown in Figure 3.4 (right). These experiments indicate that room temperature oxidation of silicon is negligible in pure water or pure oxygen, but and accelerated when both species coexist.

Ambient	H_2O concentration	Oxide thickness (Å)
Air	1.2%	6.7
O_2/N_2	<0.1 ppm	1.7
N_2	<0.1 ppm	1.9

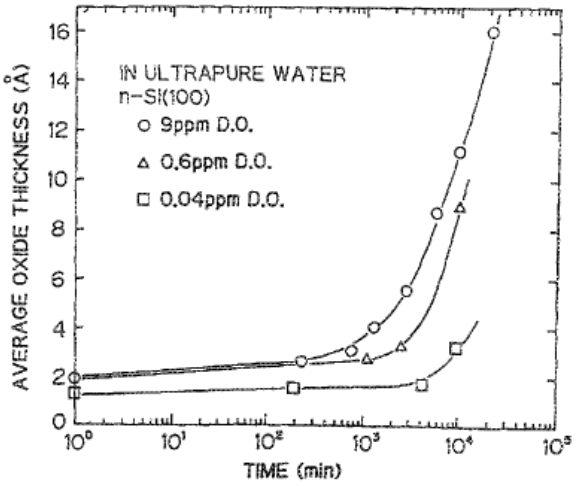

Figure 3.4: (left) tabulation of the growth of native oxide at various H_2O concentrations over one week, adapted from [Morita90]. (right) oxide thickness *vs* immersion time in pure water at RT different dissolved oxygen concentrations.

A direct relation between native oxide growth time and the resulting electrical properties is difficult to model quantitatively and is outside the scope of this work. Empirical

observation of oxide thickness and interface state growth is more straightforward and has been studied extensively by the Angermann group. The authors correlate surface state distribution changes during native oxidation in clean room air with increasing oxide thickness [Henrion02;Angermann94] as described in some detail in Ch1.

3.2.5 Ambient Purge Experiments

Although the probestation humidity was not controlled in these experiments, efforts were made to suppress the influence of adsorbed water on the electrical degradation of SOI-H. To reduce the rate of oxidation (and hence the resistance increase), 1 μm SOI(111)-H samples were purged with dry inert gases (Ar or N_2). The home-built setup is shown below in Figure 3.5 for schematic purposes.

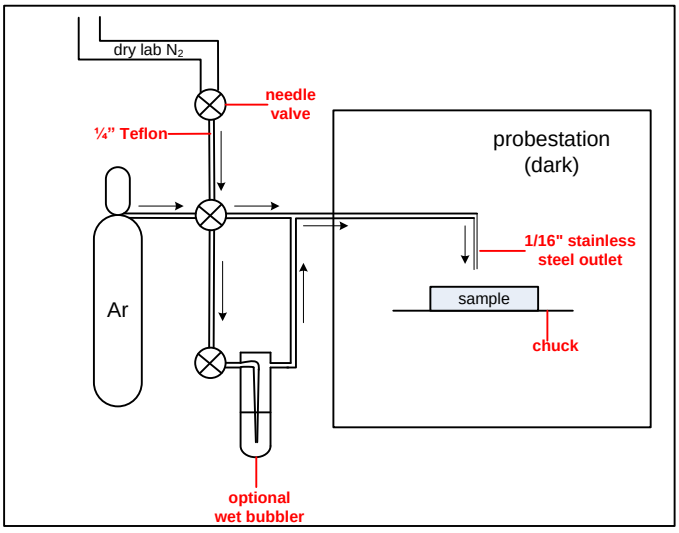

Figure 3.5: Schematic of the ambient purge experiments reported in this section. The SOI-H surface was purged with nitrogen or argon during conductivity measurements.

Although the slope of $R_s(t)$ decreases under gas purging as expected, the surprising observation is that initiating the flow of purge gas over the sample causes a sharp increase in the sheet resistance, as shown in Figure 3.6 and quantified in Table 3.2.

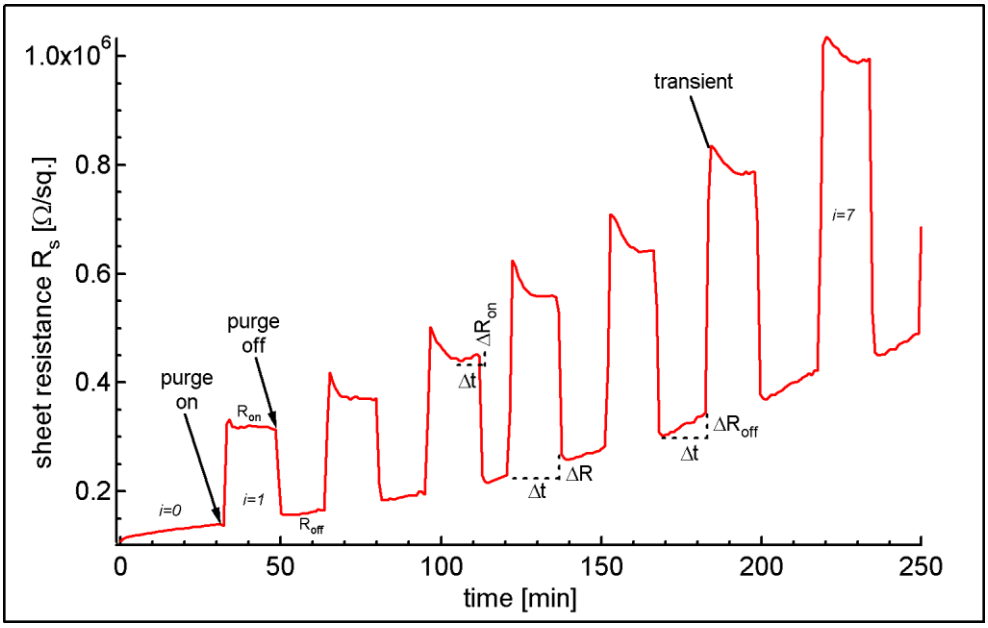

Figure 3.6: Air-oxidation of *n*-type 1 μm thick SOI(111)-H observed by increasing sheet resistance $R_s(t)$. Purging with dry Ar results in reversible changes in the sheet resistance.

Table 3.2: Quantitative summary of the purge experiments in Figure 3.6 per iteration *i*. Purging increases the resistance approximately two-fold as shown in the column R_{on}/R_{off}. The rate of increase during purging $\Delta R_{on}/dt$ is at least five-fold smaller than when the purge is off $\Delta R_{off}/dt$, measured between any two on states. The rate of increase $\Delta R/dt$, before and after each purge is at least three-fold smaller than $\Delta R_{off}/dt$, indicating the intermittent oxidation rate per purge is smaller compared to no purging.

iteration *i*	R_{on}/R_{off}	$\Delta R_{off}/dt$ [Ω/min]	$\Delta R_{on}/dt$ [Ω/min]	$\Delta R/dt$ [Ω/min]
0	-	811±29	-	-
1	1.99	680±110	180±150	934
2	2.03	1230±140	90±374	1025
3	2.08	2430±70	190±460	1240
4	2.15	1970±100	110±190	1445
5	2.09	3150±150	160±335	1057
6	2.12	3310±100	670±410	1475
7	2.21	3570±140	550±440	1524

The sheet resistance is largely reversible upon stopping the purge, although increases each iteration, attributed to the level of intermittent oxidation when the purge is on. When the purge is initiated, occasionally large transients are observed with long time-constants before the measurements equilibrate and the resistance increases noticeably again. The origin of these transients is not entirely understood, and occasionally they are not observed at all. One possibility is the local humidity above the sample takes a long time to reach equilibrium or the purging rate in our setup is non-uniform, decaying slightly with time.

Ambient purge experiments were also carried out on 200 nm *n*-type SIMOX SOI(100)-H. As with the 1 μm surface in Figure 3.6, the sheet resistance increases upon purging. The effect is largely reversible with the resistance decreasing upon stopping the gas flow. At elevated substrate temperatures (80 °C), the sensitivity of the resistance to gas purging decreases two-fold, suggesting that the reversible resistance changes upon inert gas purging are due to the displacement of physisorbed water molecules likely present on the H-terminated silicon surface in ambient. The temperature dependent signals are summarized below in Table 3.3.

Table 3.3: Quantitative summary of the purge experiments at different substrate temperatures on *n*-type 200 nm SIMOX SOI(100)-H. The magnitude of the 'signal' R_{on}/R_{off} decreases two-fold upon increasing T from 25 ^{o}C to 85 ^{o}C.

T [^{o}C]	R_{on} [kΩ]	R_{off} [kΩ]	$(R_{on}-R_{off})/R_{off}$
25	292	108	1.70
45	227	92	1.46
85	89	65	0.37

Since purging reduces the humidity above the SOI-H samples, the reversible modulation in sheet resistance in Figure 3.6 suggests that adsorbed water from ambient induces a measurable conductivity enhancement. The presence of a water layer can alter the observed conductivity either directly by introducing an additional conducting path

through the water layer itself or indirectly by modifying the substrate conductivity via field effects. To account for the observed conductivity changes in Figure 3.6 via direct conduction through the water layer, this layer would need to exhibit a surface conductance of ~10^{-5} S, approximately ten orders of magnitude higher than previously reported for ambient water layers on Teflon and quartz surfaces [Awakuni72]. To definitively attribute the observed conductivity changes to a field effect, the observed resistance changes during the ambient purge experiments were correlated with intermittent Hall voltage measurements, which represent the sign and density of free carriers. Figure 3.7 shows that the increase in resistance associated with inert gas purging and desorption of the water layer is accompanied by a decrease in the carrier density.

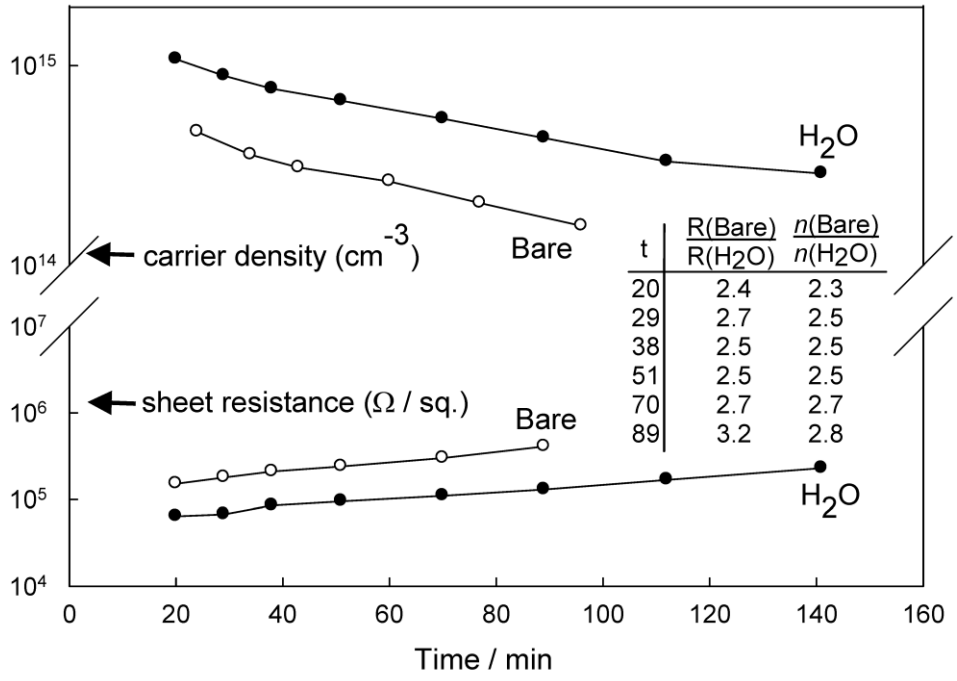

t	R(Bare) / R(H_2O)	n(Bare) / n(H_2O)
20	2.4	2.3
29	2.7	2.5
38	2.5	2.5
51	2.5	2.5
70	2.7	2.7
89	3.2	2.8

Figure 3.7: The sheet resistance as well as free carrier densities extracted from the Hall voltage (BZ=540 G) as 1 μm n-type SOI(111)-H is cycled between bare (purge on) and "H2O-covered" (purge off) states as a function of time. The table demonstrates that the ratio of sheet resistances (R) and carrier densities (n) in the two states scale together with time as the surface oxidizes and goes into depletion.

The field strength at the sample (for ambient measurements) was determined to be B_z=540 G via calibration measurements using silicon wafers with known doping concentrations. The carrier density n was extracted from the expression $n=(I_x \cdot B_z)/(V_H \cdot q \cdot d)$ where I_x is the source current. Both the sheet resistance and carrier densities in Figure 3.7 were taken in the van der Pauw geometry on square samples. Measurement of the Hall voltage during purging was technically challenging since the permanent magnet covered a large area above the sample, requiring the purge tubing to be positioned at an angle in between the magnet and the sample, making it difficult to hold the fixture in place. We note that these experiments only show there is a correlation between R_s and n in the presence/absence of the purge, although we are attributing these effects to humidity changes. In section 3.3 more conclusive evidence is provided upon controlled adsorption in vacuum that is consistent with the present hypothesis.

Although the carrier density decreases with time in Figure 3.7 due to the oxidation of the H-terminated surface, at any given time the carrier density is always lower on a sample under dry gas purge than when adsorbed water is present. As seen in the inset table in Figure 3.7, the ratios of resistances for bare (purge on) and water covered (purge off) surfaces correlate with the ratio of the carrier densities in purge on/off states, indicating that the mobility remains constant. These observations suggest the effect of the adsorbed water layer is to cause downward band-bending, leading to accumulation of majority carriers on *n*-type SOI-H.

The combined Hall effect and resistance measurements also facilitate estimation of the degree of band bending induced by the adsorbed water layer. The initial measurements in Figure 3.7 (obtained 20 min after preparation of the H-terminated surface) indicate that the sheet resistance and carrier density are 64 kΩ and 1.1×10^{15} cm^{-3} with the adsorbed water layer present (purge off) and change to 152 kΩ and 4.7×10^{14} cm^{-3} upon purging to at least partially displace the layer. This indicates that the adsorbed water layer has increased the surface conductance by +9 μS relative to the purged sample, which requires 86 mV of band bending into accumulation.

In hindsight, purging experiments in Figure 3.6 and Figure 3.7 show that interpretation of the sheet resistance increase of SOI-H in ambient air described in sections 3.2.2 and 3.2.3 and Figures 3.2 and 3.3 is generally complex to simulate. While water is a necessary species for native oxidation [Morita90] which gradually causes irreversible depletion, its adsorption induces the opposite effect, reversibly driving *n*-type SOI-H into accumulation. Since both of these competing processes occur simultaneously and their changes may be interdependent over time, it is difficult to convert a single measurement of $R_s(t)$ into the charge component due water and the charge due to surface states.

3.3 Controlled adsorption of water in vacuum

3.3.1 Conductivity of *n*-type 1 μm SOI(111)-H

To conclusively attribute the effects observed in the ambient purge experiments (3.2.5) to the displacement of adsorbed water layers, conductivity measurements were repeated in the more controlled environment of a high vacuum system. Four probe in-line measurements were carried out in a home-built vacuum system (Gen 0) consisting of four 28-guage tungsten wires pressed onto EGaIn contacts, shown schematically in Ch2 Figure 2.5. As seen below in Figure 3.8, pumping on a 1 μm thick *n*-type SOI(111)-H surface exposed to ambient air causes a large increase in the resistance.

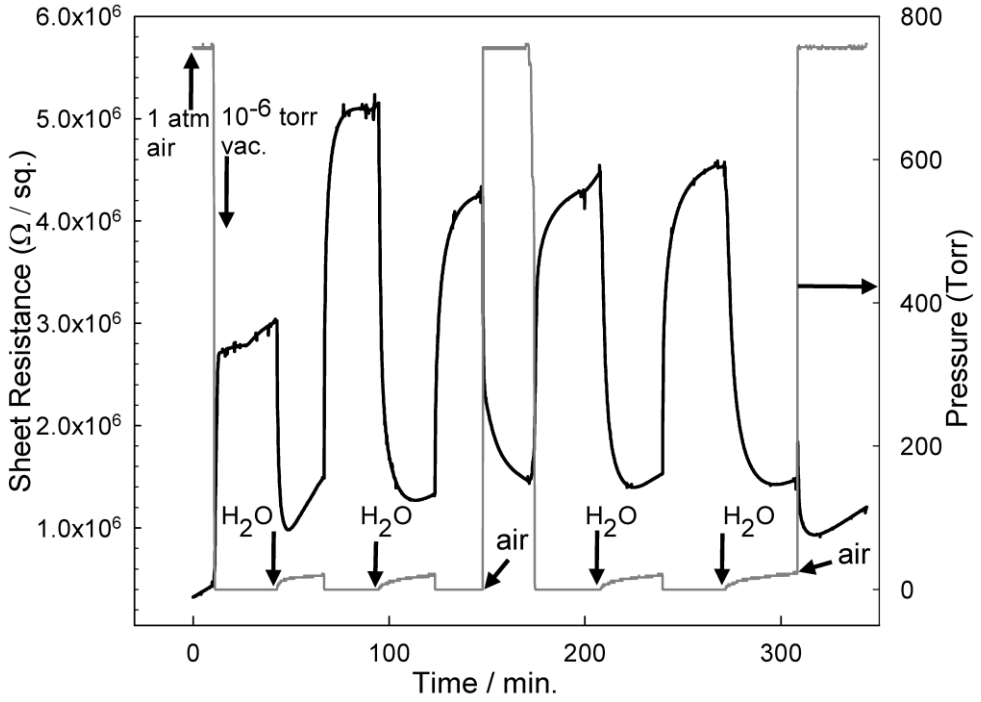

Figure 3.8: Effect of water on the resistance of n-type SOI(111)-H in vacuum. Pumping down a sample from ambient increases the resistance while exposure to 15 Torr of water vapor causes a decrease similar to that observed upon venting to laboratory air. Venting a

sample with water already present on the surface causes only a small change in the resistance.

This is similar to the effect of inert gas purging although the magnitude of the change induced by pumping is larger. This is presumably due to the greater efficiency of pumping as compared with purging in removing the adsorbed water layer. Milli-Q water was freeze-pump-thawed with liquid N_2 before exposure of the vapor into the chamber. Exposure of the surface to water vapor at pressures of 10–15 Torr reversibly lowers the resistance, analogous to the effect of stopping the gas flow in Figure 3.6.

The ability of adsorbed water to cause significant conductivity changes on the Si–H surface could arise either from a charge transfer interaction of the water molecules with the substrate or as a result of the field of a partially oriented layer of molecular dipoles. On the basis of the electrical data presented here, these mechanisms are indistinguishable; only the effective charge at the surface can be inferred. Further discussions on the origin and mechanism are presented in section 3.5. From the amount of band-bending required to account for the observed conductivity changes in Figure 3.8, the field at the surface is ~50 kV/cm and can be ascribed to a positive surface charge of 6.3×10^{10} cm^{-2}. In terms of a charge transfer picture, this requires a low coverage ~0.0001 ML of integrally charged water molecules or equivalently, a complete monolayer of water carrying a fractional charge of ~0.0001 q/H_2O molecule.

3.3.2 Combined Hall Effect and Conductivity measurements

In the previous sections it was shown that ambient humidity (3.2.5) or adsorption of water vapour under vacuum conditions (3.3.1) enhances the conductivity of *n*-type 1 µm-thick SOI-H substrates, an effect recently confirmed by others [Scott09]. Lagally and co-workers reported pumping their SOI samples under rough vacuum caused a large “jump” in their van der Pauw measurements, attributing these changes to water desorption and referenced our previous studies [Dubey07]. Because of the significant influence of water, the authors made efforts to control the humidity in their ambient experiments.

Here we show that controlled exposure of water to *n*-type and *p*-type SOI-H substrates significantly modulates the conductivity in a reversible manner using a home-built chamber (Gen1) to accommodate sheet resistance as well as Hall effect measurements, shown schematically in Ch2 Figure 2.5. Combining four probe resistance and Hall voltage measurements allows the observed conductivity changes to be correlated with changes in carrier density and effects due to majority and minority carriers to be distinguished. While water adsorption on *n*-type SOI-H is confirmed to induce accumulation of majority carriers, adsorption of this molecule on *p*-type SOI-H is seen to lead to minority carrier dominated conduction (inversion), as observed in the early studies on germanium [Brown53;Kingston54]. These observations demonstrate the utility of transport measurements on SOI-H substrates for studies of adsorption events at silicon surfaces and suggest potential applications in chemical sensing.

Phosphorous or boron doped SIMOX SOI(100) samples from Ibis with 380 nm BOX and150 nm top Si film, and boron doped WB SOI(111) *p*-type from Tracit with 1 μm BOX and 3 μm top Si layer were used. Samples cut to ~20 mm×7 mm were mounted in the Gen1 turbo-pumped high vacuum system with a base pressure of 1×10^{-7} Torr. The substrate was grounded in these measurements; the sheet resistances remained largely unchanged whether the substrate was grounded or allowed to float. Complementary Hall voltages were measured in the four probe Hall-bar geometry using two additional probes perpendicular to the current density, along the sample width as shown in Figure 2.5.

3.3.2.1 Water vapor on n-type SOI-H surfaces

Figure 3.9 illustrates the response of the sheet resistance $R_s(t)$ of an *n*-type 150 nm SIMOX SOI(100)-H substrate to pure water vapour under vacuum conditions. Under a pressure of 11 Torr of water the sheet resistance is found to be constant at 40 kΩ. Upon pumping away the water vapour the sheet resistance increases nearly twenty-fold to 762 kΩ. This is consistent with our previous observations in section 3.3.1 Figure 3.8, although the magnitude of the resistance change is much greater due to the fact the SOI is

considerably thinner than the 1 μm samples employed previously. In addition here we have also monitored the Hall voltage associated with changes in the sheet resistance.

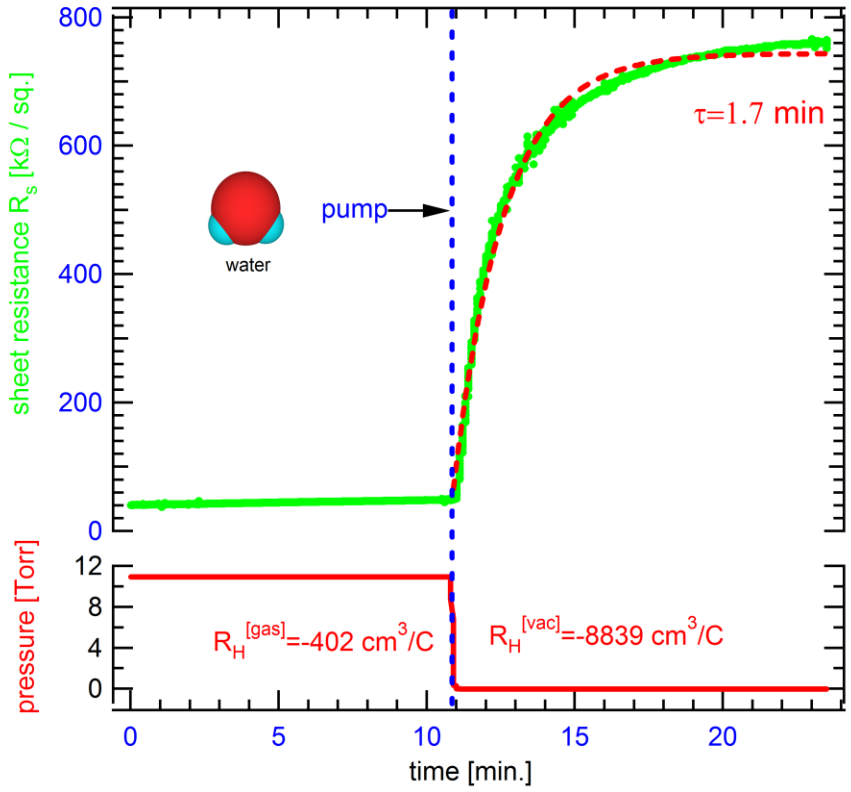

Figure 3.9: Monitoring the rise in sheet resistance of an *n*-type 150 nm SOI(100)-H film as 11 Torr of H_2O is pumped from the vacuum system. Pressure is shown in red. Both the Hall coefficient (calculated from the measured Hall voltage at I_x=100 nA, B_z = 280 G) and resistance increase 20 fold in vacuum, indicating that conductivity enhancement in water occurs via a field effect increasing mainly the carrier density rather than mobility. The dashed curve represents a fit to an exponential rise to maximum with a time constant of 1.7 min.

The measured Hall coefficient increases from -400 cm^3/C to -8840 cm^3/C, proportional to the increase in sheet resistance. The Hall coefficient (R_H) and sheet resistance measurements can be used to extract the free carrier density and mobility from the standard expressions for one type of carrier using Eqn 2.5 and Eqn 2.6. The scaling of the Hall coefficient with resistance indicates that the conductivity changes are associated primarily with changes in carrier density induced by a field effect rather than changes in

mobility. The increase in resistivity and Hall voltage as water desorbs from the surface indicates that the presence of water on the surface acts to increase the carrier density (i.e. induce accumulation of majority carriers).

Upon pumping away the water, the sheet resistance follows an exponential rise back to its initial value with a time constant of 1.7 minutes, significantly longer than the 20 s required for the pressure to be reduced to below ~10^{-4} Torr. If the relaxation of the conductivity reflects desorption of water, the observed time constant corresponds to a binding energy of 0.86 eV, assuming first order desorption kinetics and using a prefactor of 10^{13} s^{-1}, which is considerably higher than expected for physisorbed water molecules. To account for the formation of the accumulation layer indicated by the observations in Figure 3.9 requires an induced surface charge density of Q_s=+2.2×10^{11} q·cm^{-2}. Details of this calculation are provided in section 3.4, addressing the experiment of Figure 3.9 as a specific example. The band-bending changes corresponding to Figure 3.9 are shown below in Figure 3.10.

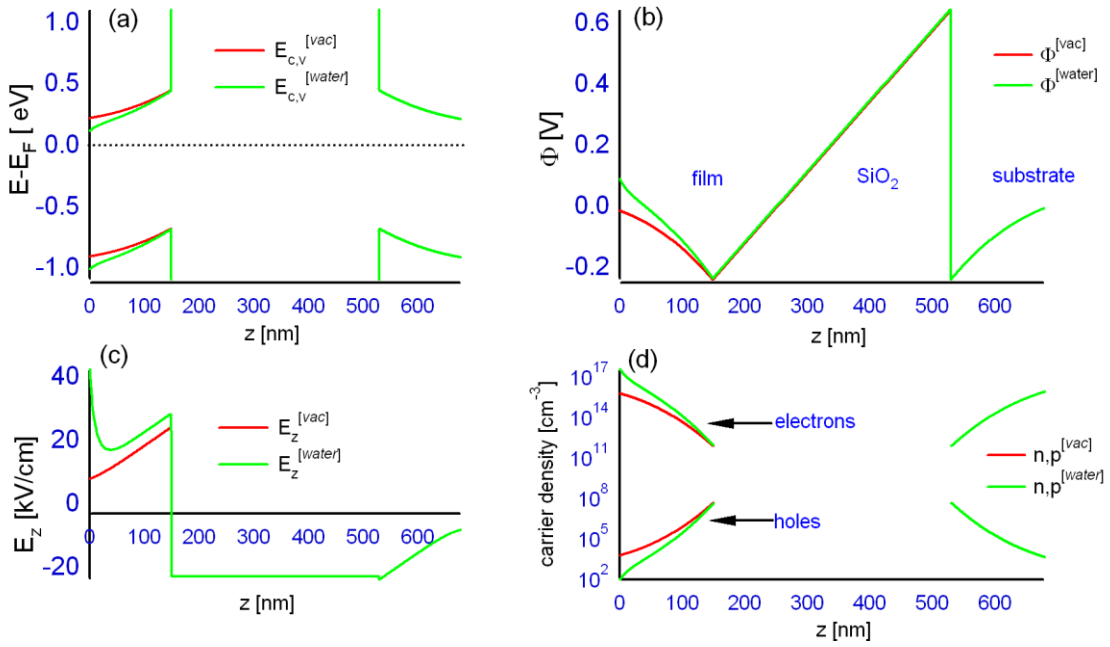

Figure 3.10: Electrostatic-consistent depiction of the H_2O adsorption experiment in Figure 3.9, corresponding to initial (vacuum, red) and final (gas, green) sheet resistances. The (a) band-bending, (b) electrostatic potential, (c) electric field, (d) electron and hole densities are shown across the SOI structure.

One possibility is that this surface charge originates from a small amount of strongly bound water which undergoes charge transfer and adsorbs as a positive species. This requires a spectroscopically undetectable coverage of ~0.03% or one integrally charged H_2O molecule for every 3000 Si atoms. This ionosorbed component will have a higher activation to desorption than the surrounding physisorbed water, which is expected to desorb rapidly (~10 μs for an activation energy of 0.4 eV). Another possibility is that the timescale for the changes in sheet resistance is not determined by desorption but by electronic processes such as de-trapping from charged donor states at the surface.

3.3.2.2 Water vapour on *p*-type 3 μm SOI-H surfaces

Hall effect measurements on thin (<200 nm) boron doped nominally *p*-type SIMOX samples indicated *n*-type conduction in the top silicon layer, even though the substrate below the BOX remained *p*-type. This well established effect for SIMOX samples [Cristoloveanu91a;Ionescu96;Cristoloveanu00;Ichimura02;Shibata04] has been attributed to the introduction of unintentional donors leading to dopant overcompensation during the implantation and annealing steps. The change in carrier type renders the influence of physisorbed water on the conductivity of either *n*-type or overcompensated *p*-type H-terminated SIMOX the same, causing electrons to accumulate on both surfaces. To investigate the effects of water adsorption on *p*-type SOI we used 3 μm thick boron doped samples formed by the Unibond method. In these samples the Hall voltages from the top silicon layer are consistent with lightly doped *p*-type conduction. However, since the thickness of the top silicon layer is larger than the depletion length, reduced sensitivity to field effects is expected. Attempts to thin these samples to 1 μm by repeated thermal oxidation and etching cycles resulted in increased sensitivity to adsorption events but also resulted in Hall effect measurements indicating *n*-type conduction, likely due to the oxygen donor mechanism discussed above.

The sheet resistance response to water exposure cycles for 3 μm *p*-type SOI-H is shown in Figure 3.11. On exposure to 11 Torr of H_2O, the resistance is seen to decrease from an initial value $R_s^{[vac]}$=88 kΩ down to $R_s^{[gas]}$=64.8 kΩ. As on *n*-type substrates this effect is observed to be reversible upon pumping the water vapor from the chamber. However, in contrast with the resistance decrease seen in Figure 3.9, in this case the Hall voltage is observed to change sign. This change in sign of the Hall voltage implies that the increase in surface conductivity on the *p*-type substrates is due to the formation of a minority carrier channel at the surface (i.e. inversion). Another difference from the behavior of *n*-type substrates is the fact that the resistance change with water exposure is not monotonic. On *p*-type SOI-H, the resistance is found to increase slightly before decreasing. This initial change is expanded in the inset of Figure 3.11.

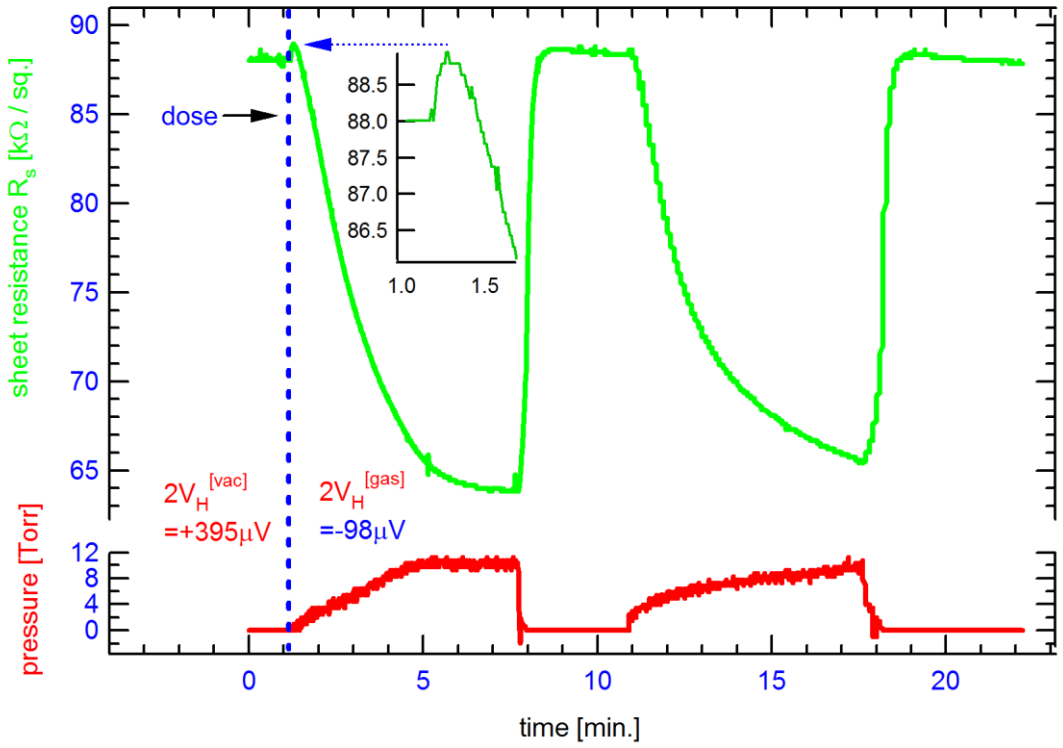

Figure 3.11: Sheet resistance changes to water adsorption and desorption cycles on *p*-type 3 μm thick SOI(111)-H. The surface becomes inverted in 11 Torr H_2O, indicated by a change in sign of the Hall voltage from its value in vacuum (measured at I_x=1 μA, B_z= 560 G). The transition from depletion into inversion is weakly visible for this thickness and adsorption rate, shown in the inset. The Hall coefficient in vacuum (+10,580 cm^3/C) remains the same before dosing and after pumping away the water.

We attribute this behavior in $R_s(t)$ to the initial depletion of majority carriers (holes) which increases the resistance before additional adsorption leads to inversion (decreased resistance, negative Hall voltage). Due to the large thickness of the top silicon layer the initial increase in resistance is small, in contrast to films where the thickness is smaller than the depletion length. The rate of adsorption and time-resolution of the measurements will also affect the shape of this transition. A positive surface charge of ~$1x10^{11}$ $q \cdot cm^{-2}$ is sufficient to account for the observations in Figure 3.11. The band-bending changes are shown in Figure 3.12. A discussion of the Hall voltage measurements in inversion is given in section 3.4.

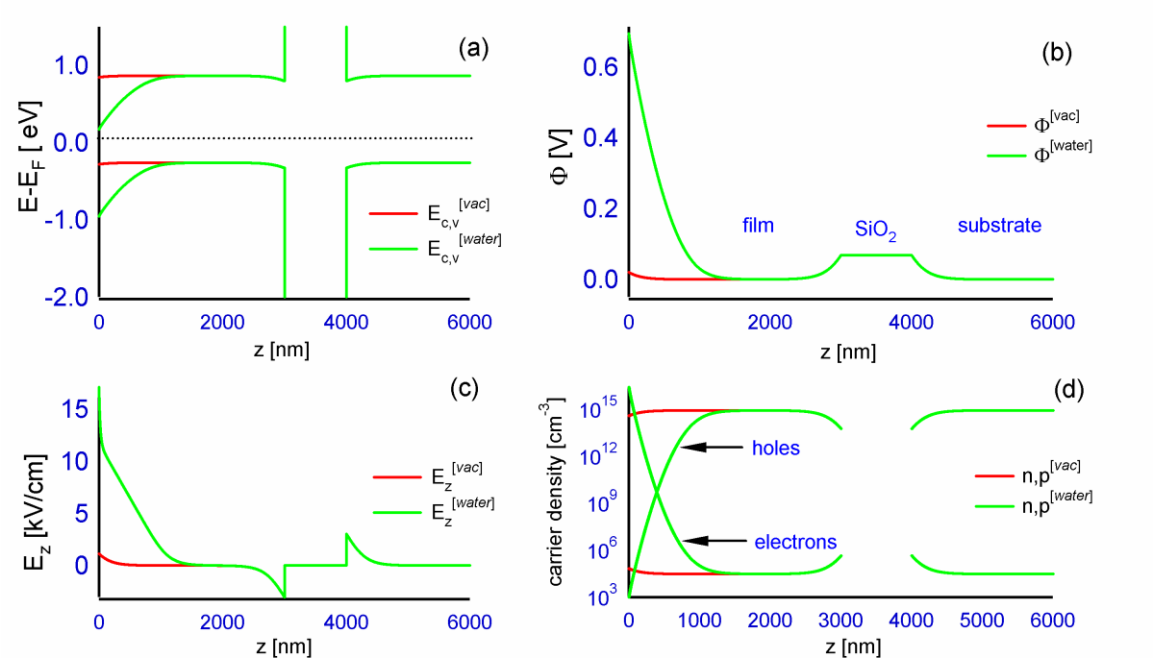

Figure 3.12: Electrostatic-consistent depiction of the H_2O adsorption experiment in Figure 3.11, corresponding to initial (vacuum, red) and final (gas, green) sheet resistances. The (a) band-bending, (b) electrostatic potential, (c) electric field, (d) electron and hole densities are shown across the SOI structure.

3.4 Modeling of the Transport Measurements

3.4.1 Summary of electrical parameters on n-type and p-type SOI-H

The band-bending diagrams in section 3.3.2, Figure 3.10 and Figure 3.12 were computed in Matlab in order to simulate the measured sheet resistance $R^{[gas]}$, $R^{[vac]}$ and mobility $\mu^{[vac]}$, $\mu^{[gas]}$ in the presence of water or in HV, assuming a given set of interface state charge densities. An outline of these simulations is given in section 3.4.2. Listed below in Table 3.4 is a summary of the numerically extracted parameters from Figure 3.9 and Figure 3.11.

Table 3.4: Summary of numerically extracted electrical parameters from Figure 3.9 and Figure 3.11

Fig. #, *Type*, Thickness, Pressure, Gas Status	$\mu^{[vac]}$ $\mu^{[gas]}$ /cm^{2}V^{-1}s^{-1} ±10%	$q^{[0]}$ /cm^{-3} ±10%	$q^{[vac]}$ $q^{[gas]}$ /cm^{-3} ±10%	$\Delta N^{[vac]}$ $\Delta N^{[gas]}$ /cm^{-2} ±10%	$\Delta P^{[vac]}$ $\Delta P^{[gas]}$ /cm^{-2} ±10%	$G_s^{[vac]}$ $G_s^{[gas]}$ /µS ±10%	Q_s /cm^{-2} ±10%	$\Phi(0)^{[vac]}$ $\Phi(d)^{[vac]}$ /mV ±10%	$\Phi(0)^{[gas]}$ $\Phi(d)^{[gas]}$ /mV ±10%
3.9 *n-type* 150 nm 11 Torr H_2O Accumulation	774 670	7.85×10^{15}	7.12×10^{14} 1.57×10^{16}	-1.07×10^{11} 1.17×10^{11}	- -	-13.3 12.5	$+2.20\times10^{11}$	-17.5 -240	87.5 -240
3.11 *p-type* 3 µm 11 Torr H_2O Inversion	400 -	6.83×10^{14}	5.9×10^{14} N.A.	- 3.78×10^{10}	-2.75×10^{10} -9.69×10^{10}	-1.76 2.34	$+1.10\times10^{11}$	20 68	694 68

In table 3.4, the figure number, original carrier type, thickness d, water vapour pressure, and band-bending status in the presence of water are labeled in the first left-hand column. Additional list the extracted electrical parameters in both [vac] and [gas] states. From left to right the columns indicate the mobility μ, background doping density $q^{[0]}$, excess/deficit surface carriers ΔN (electrons), ΔP (holes), surface conductance G_s, net surface charge induced by the gas Q_s, and the electric potentials $\Phi(0)$, $\Phi(d)$ at the boundaries of the top Si film. Although the standard notation $\{N_{A,D}, n, p\}$ for doping, density of electron and holes could have been applied, we have used a generic notation $\{q^{[0]}, q^{[vac]}, q^{[gas]}\}$ to represent the initial doping level of the film $q^{[0]}$ before considering surface states, and the measured *average* majority carrier densities in the film $q^{[vac]}$, $q^{[gas]}$, which take into account surface states and band-bending.

As seen in Table 3.4, hole mobilities on *p*-type 3 μm WB-SOI(111)-H were measured to be the same as bulk substrates $\mu_{p,bulk}$~400 cm^2/Vs. Note that electron mobilities on *n*-type SIMOX wafers are smaller compared to measurements on bulk wafers $\mu_{n,bulk}$~1300 cm^2/Vs, but values in the range <1000 cm^2/Vs are common in SIMOX films [Cristoloveanu95]. Since unintentional doping, or autodoping occurs during SIMOX synthesis [Cristoloveanu95], the dopant density in the top Si film can be much higher than the manufacturer's specifications, which only quote the dopant density (and carrier type) of the starting substrate wafer. Rather than using the bulk doping value, the background doping in the film $q^{[0]}$ was estimated based on commonly reported autodoping levels in Ibis manufactured SIMOX 2×10^{15} $cm^{-3}<q^{[0]}<8\times10^{15}$ cm^{-3} [Cristoloveanu95] and using reasonable estimates for the interface charges in the BOX, which give consistency with the measured carrier densities However in 3 μm WB-SOI, both the top film and substrate were found to have similar doping $q^{[0]}\approx q^{[vac]}\sim1\times10^{15}$ cm^{-3}. We also note that the BOX charge densities in SIMOX (~$2x10^{11}cm^{-2}$) are much higher than in WB-SOI (~$2\times10^{10}cm^{-2}$), which is reflected as a relatively larger amount of deficit carriers $\Delta N^{[vac]}$ (Figure 3.9) compared to $\Delta P^{[vac]}$ (Figure 3.11) in Table 3.4. Despite this offset, the surface charge Q_s induced by water was essentially the same on either type of SOI (Table 3.4).

3.4.2.1 Band-bending simulations

The band-bending changes induced by H_2O adsorption on *n*-type SOI(100)-H based on Figure 3.9 corresponding the first row of Table 3.4 is outlined as a specific example. To relate the observed conductivity changes to band-bending, it is necessary to construct a model, including effects of intrinsic defects present in SIMOX systems. These defects cause depletion of carriers. The film has a background doping density $q^{[0]}$ but because of intrinsic states, the measured carrier density is lowered to $q^{[vac]}$. In this example we have assumed surface charge densities $Q_{ss}(0)=1\times10^{10}$ cm^{-2} (H-terminated surface), $Q_{ss}(d)=2\times10^{11}$ cm^{-2} (upper BOX interface), and $Q_{ss}(d+d_{BOX})=1\times10^{11}$ cm^{-2} (lower BOX interface). The surface charge is inherent to the H-termination itself [Yablonovich86] and the BOX charges result from the Si/SiO_2 interface created by O^+ implantation. Upper and lower BOX charge asymmetry is representative of the damage levels induced by implantation at both oxide interfaces [Cristoloveanu95].

Sheet resistance R_s and Hall voltage $2V_H$ are the only measured quantities; in the simulations, we require their (equilibrium) values in the [vac] and [gas] states to be consistent with an appropriate potential distribution $\Phi(z)$ in the top silicon film. The distribution depends on the background doping density $q^{[0]}$, the surface charge, (intrinsic as well as that induced by the gas), and the amount of charge at the buried interfaces, which is the same before and after adsorption. The substrate is grounded. Carrier densities $q^{[vac]}$, $q^{[gas]}$ and mobilities $\mu^{[vac]}$, $\mu^{[gas]}$ are obtained explicitly from the measurements using Eqn. 3.1 and Eqn. 3.2, respectively.

To obtain $q^{[0]}$, Poisson's equation is solved on $0<z<d$ in iterations using the set of intrinsic surface charges $Q_{ss}(0)$, $Q_{ss}(d)$, $Q_{ss}(d+d_{BOX})$ and a trial estimate for $q^{[0]}$. The estimate is varied until the integrated carrier density over the film matches $R_s^{[vac]}$, e.g. on *n*-type when:

$$1\Big/ R_s^{[vac]} = q\mu^{[vac]} \int_0^d q^{[0]} e^{\frac{q\Phi}{kT}}\, dz. \qquad (3.1)$$

In this example it was found that $q^{[0]}$=7.85x10^{15}cm^{-3}, and the potentials in the silicon film at the surface and upper BOX interface to be $\Phi^{[vac]}(0)$=-17.5 mV and $\Phi^{[vac]}(d)$=-240 mV. Numerical solutions to Poisson's equation are discussed briefly in section 3.4.2.2.

Similarly to obtain consistency with the measurements in the [gas] state, Poisson's equation is solved again in iterations with a trial estimate for the surface potential, same set of intrinsic surface charges, and value of bulk doping solved for previously, $q^{[0]}$. The surface potential estimate is varied until the integrated carrier density over the film matches $R_s^{[gas]}$. In this example the potentials at the surface and upper BOX interface were found to be $\Phi^{[gas]}(0)$=87.5 mV and $\Phi^{[gas]}(d)$=-240 mV. Hence the appropriate distribution in the top silicon film has been found for each state. The potential in the substrate below the lower BOX interface is also determined analogously but is not relevant to the measurements and therefore omitted from Table 3.4.

Then net band-bending induced at the surface by water adsorption is $\Phi_s^{[gas]}(0)$-$\Phi_s^{[vac]}(0)$=105 mV. The net surface charge density Q_s induced by the gas is obtained from the change in electric field -Φ'(z) at the surface (not the change in Φ):

$$Q_s = \varepsilon_0 \varepsilon_r \left[\Phi^{[vac]\prime}(0) - \Phi^{[gas]\prime}(0) \right] , \tag{3.2}$$

=2.2×10^{11} cm^{-2}, with relative permittivity ε_r=11.9.

An alternate way to get the surface charge is to track changes in excess (deficit) surface carriers, e.g. for electrons (with respect to no interface states):

$$\Delta N^{[vac]} = \int_0^d (q^{[vac]}(z) - q^{[0]}) dz, \tag{3.3}$$

and so on for $\Delta P^{[vac]}$, $\Delta N^{[gas]}$, $\Delta P^{[gas]}$.

The excess electron density at the surface is changed by the gas by an amount

$$\Delta N^{[vac]\to[gas]} = \Delta N^{[gas]} - \Delta N^{[vac]} = \int_0^d (q^{[gas]}(z) - q^{[vac]}(z))dz, \qquad (3.4)$$

$=2.2\times10^{11}$ cm^{-2} and similarly for holes, which is negligible in the present case, and the net surface charge density is alternatively expressed as

$$Q_s / q = \Delta N^{[vac]\to[gas]} - \Delta P^{[vac]\to[gas]}. \qquad (3.5)$$

The surface conductance change in vacuum caused by the interface charges is:

$$G_s^{[vac]} = q(\mu_n^{[vac]}\Delta N^{[vac]} + \mu_p^{[vac]}\Delta P^{[vac]}), \qquad (3.6)$$

$=$-13.8μS and using a similar expression, $G_s^{[gas]}$=13.8 μS, which includes the contribution of the water as well as the interface charges. The net surface conductance change induced by the water only, relative the bare H-terminated surface is:

$$G_s^{[vac]\to[gas]} = G_s^{[gas]} - G_s^{[vac]}\ , \qquad (3.7)$$

=25.8 μS. As a final check, this net conductance change must also agree with the conductivity measurements, determined explicitly from the sheet resistance:

$$G_s^{[vac]\to[gas]} = (\frac{1}{R_s^{[gas]}} - \frac{1}{R_s^{[vac]}})\ , \qquad (3.8)$$

=25.8 μS.

3.4.2.2 Numerical solutions to the 1D Poisson Equation

This section gives a description of the steps taken to actually calculate $\Phi(z)$, which provides all of the information needed to generate the electrical parameters in section 3.4.2.1 and Table 3.4. Assuming Boltzmann statistics for electrons and holes, the 1*d* Poisson equation is:

$$\frac{d^2\Phi}{dz^2} = \frac{q}{\varepsilon_0\varepsilon_r}\left(n_b(e^{\frac{q\Phi}{kT}} - 1) + p_b(1 - e^{-\frac{q\Phi}{kT}}) \right), \tag{3.9}$$

where n_b and p_b represent bulk carriers q[0]. Eqn 3.9 is discretized over a uniform mesh with 1 nm spacing and the potential Φ(z) is solved numerically in Matlab using the method of finite differences. The matrix representation has the form A$\mathbf{\Phi}$=$\boldsymbol{b}$ where A is a tridiagonal matrix, $\boldsymbol{b}$ a column vector representing the right hand side of Eqn 3.9 and $\mathbf{\Phi}$ a column vector obtained by sparse matrix division $\mathbf{\Phi}$=A\$\boldsymbol{b}$.

In the simulations, an initial surface potential Φ_0 is specified, which is modified slightly by the superimposed initial potential profile from the back interface at $z=d$ and vice versa. The upper and lower BOX charges are specified, which gives the electric field E_z at the back film interface in the silicon from Gauss's law:

$$E_z(d^-) = -\Phi'(d) = \frac{q}{2\varepsilon_0\varepsilon_{Si}}(Q_{ss}(d) + Q_{ss}(d + d_{box})) = \frac{kT}{qL_D}F\left(\frac{E_F - E_i}{kT}, \frac{q\Phi_d}{kT} \right), \tag{3.10}$$

where F is the space charge function, E_F the Fermi level, E_i the intrinsic level and L_D the extrinsic Debye Length. The field in the oxide is determined by

$$E_z(d^+) = \frac{q}{2\varepsilon_0\varepsilon_{ox}}(Q_{ss}(d) - Q_{ss}(d + d_{box})). \tag{3.11}$$

The factor of 2 in Eqn. 3.10 and Eqn. 3.11 arises here because we have assumed the BOX charges are free charges and influence the field at each silicon boundary. From these expressions it can be verified that the change in electric displacement $D=\varepsilon\cdot\varepsilon_0\cdot E$ across the

Si/BOX and BOX/Si boundaries is thereby satisfied to equal to $Q_{ss}(d)$ and $Q_{ss}(d+d_{BOX})$ respectively.

The right hand side of Eqn. 3.10 is solved numerically to give the initial band-bending at the back-interface Φ_d. A trial solution is then constructed as follows:

$$\Phi^{(i=0)} = \Phi_0 e^{-z/L_D} + \Phi_d e^{-(d-z)/L_D}, \tag{3.12}$$

which superimposes the potential profiles from both the surface and back interface and is used to initiate the iteration process. The trial function approaches the analytic solution for small band-bending $q\Phi<<kT$ and large separation $d>>L_d$ between interfaces. The trial solution also slightly modifies the input surface potential Φ_0 and initial band-bending at the back-interface Φ_d due to the 'mixing' of the superimposed potentials. It sets the final values of the potential on the boundaries to be:

$$\Phi(0) = \Phi_0 + \Phi_d e^{-d/L_D} \ ; \tag{3.13}$$

$$\Phi(d) = \Phi_d + \Phi_0 e^{-d/L_D}. \tag{3.14}$$

For each iteration i, the right hand column vector $\boldsymbol{b}^{(i)}$ is formed and used to generate the next solution on the left hand side $\boldsymbol{\Phi}^{(i+1)}=\boldsymbol{\Phi}^{(i)}\pm\delta\cdot|\mathrm{A}\backslash\boldsymbol{b}^{(i)}-\boldsymbol{\Phi}^{(i)}|$, which shifts each solution by the residual, using a damping factor of $\delta=10^{-4}\sim10^{-7}$. The process is repeated until a convergence criterion, i.e., residual $<10^{-6}$ is obtained. The converged solution $\boldsymbol{\Phi}$ is re-inserted into the left and right hand sides of Poisson's equation (Eqn. 3.9) to verify consistency. Results obtained using this approach gives the same answers as to those obtained from available Poisson solvers.

3.4.2.3: Comment on the Hall voltage in inversion

On moderately doped 3 μm *p*-type SOI-H the positive charge induced by water adsorption caused an increase in conductivity and change in sign of Hall voltage indicating *n*-type conduction as shown in Figure 3.9. Since the mobility of the electron inversion layer is unknown, it is not possible to accurately model the results; the system is under-determined. Despite this drawback a semi-quantitative estimation of the Hall voltage for this inversion layer is outlined which at the most explains, why the sign should change.

To account for the sign and magnitude of $V_H^{[\mathrm{gas}]}$ in Figure 3.11 requires contributions from electrons in the surface N channel, both electrons and holes in the adjacent space-charge region and majority holes in the adjacent bulk. The density of carriers $n(z)$ and $p(z)$ in these three regions can be identified in Figure 3.12d. The spatial electron/hole concentrations in these three regions are partitioned into three sheet resistors possessing the average carrier density of each segment. The inversion layer width d_{inv}=66 nm is determined by the depth at which the surface potential exceeds more than twice the built-in potential φ_b=0.304 eV (Figure 3.12a). The built-in potential also determines the width of the adjacent depletion layer d_{dep}=700 nm and remaining bulk segment d_b=2234 nm. By imposing that the equivalent parallel sheet resistance be the same as $R_s^{[\mathrm{gas}]}$=64.8 kΩ, the resistances of these layers are found to be R_{inv}=122 kΩ, R_{dep}=2675 kΩ and R_b=145 kΩ. Using the current dividing rule, the source current I_x=1 μA partitions into I_{inv}=530 nA, I_{dep}=24 nA and I_b=446 nA, giving rise to individual Hall contributions $2V_{inv}$=-1041 μV, $2V_{dep}$=-1053 μV and $2V_b$=+290 μV. The measured Hall voltage can be estimated if the series resistance between adjacent layers and circulating currents are neglected. Currents and Hall voltages are in parallel and the resulting open-circuit potential is [Petritz58]

$$2V_H^{[gas]} = R_s^{[gas]}\left(\frac{2V_{inv}}{R_{inv}} + \frac{2V_{dep}}{R_{dep}} + \frac{2V_b}{R_b}\right), \tag{3.15}$$

=-448 μV. While this calculated Hall voltage is somewhat larger than the measured signal of -98 μV, it illustrates why V_H is expected to change sign in inversion. This outline has assumed bulk mobilities for electrons in the inversion layer and holes in the depletion layer. Because of these unknowns and other assumptions, we reiterate it is not possible to accurately model the transport measurements in inversion beyond these simple estimates.

3.5 Discussion of Water Adsorption and Band-bending

The data presented in Figure 3.9 through Figure 3.12 and Table 3.4 clearly demonstrates that water induces accumulation on *n*-type and inversion on *p*-type H-terminated substrates. This is consistent with downward band-bending in both cases. This is not particularly surprising since charge-transfer and orientation of H_2O molecules on the H-Si surface is expected to be independent of doping type. A surface charge of the order of $\sim 10^{11}$ q·cm^{-2} is required to account for the observations on both substrates. This example illustrates the importance of measuring changes in both R_s and V_H to distinguish between accumulation or inversion, since both scenarios result in an increased surface conductance.

Lagally and co-workers have recently reported surface conductivity and Hall effect measurements on moderately doped *p*-type SOI etched in 12% HF followed by 5 min water rinsing [Scott09]. Measurements in ambient air or rough vacuum (Torr range) at thicknesses from 27-220 nm indicate their surfaces exhibit *n*-type conduction which they attribute to the influence of the chemical modification with HF, inducing band-structure changes in the silicon. They also consider the influence of residual fluorine species to be responsible for this inversion layer: The authors recently showed H-terminated SOI prepared in vacuum (silane in H2 exposed to SOI-2×1) has a lower conductivity than that of HF-etched SOI [Zhao11]. However in this study they did not confirm with Hall measurements or comment on whether the *n*-type conduction is absent in the vacuum prepared samples. While these considerations are interesting our

measurements (Figure 3.11) show that the presence of water in the Torr range is sufficient to induce the inversion layer observed. The *n*-type conduction should disappear if the pressure is reduced from the Torr range to high vacuum range (HV)~10^{-5} Torr. This is clearly observed in Figure 3.11: The Hall voltage is positive in HV and changes in sign only when water is leaked into the chamber.

It is interesting to note that although two different surface orientations and etching procedures have been used here (the *n*-type SIMOX samples are HF etched (100) and *p*-type WB samples are ammonium fluoride etched (111)), the effective surface charges induced by water adsorption are similar. In section 3.3.1 similar positive charge densities were reported for water on *n*-type ammonium fluoride etched SOI(111) substrates. Taken together these observations indicate that despite the differences in morphology and structure of these two types of H-terminated SOI surfaces, the field effects induced by water adsorption are quite similar.

Although the pressure of water in the chamber has been maintained constant in these adsorption experiments at P=11 Torr, an important unknown is the coverage θ. Knowledge of the coverage could be of significance in understanding the origins of the field-effects of water on Si-H surfaces. The coverage of water on the surface may be too small to be measured by conventional spectroscopic means: Supposing the low surface charge densities measured $Q_s=10^{11}$ q cm^{-2} can be ascribed to a molecular density of 10^{11} H_2O cm^{-2}, then the coverage of $\theta=(10^{11}$ H_2O cm$^{-2}/10^{15}$ Si cm$^{-2})=10^{-4}$ is two orders in magnitude smaller than the detection limit $\theta=10^{-2}$ of most surface characterization techniques such as FITR, HREELS and XPS. This suggests very accurate measurements of coverage could be difficult. In our efforts to shed light on the problem, we determined an upper bound on the coverage of water to be $\theta<1$, as described in section 3.5.1.

3.5.1 Evidence for submonolayer coverage

To the best of our knowledge, the desorption energy of water molecules on hydrogen passivated silicon surfaces have not been measured experimentally and its coverage in the

Torr range <1 Torr<*P*<20 Torr remains unknown on these surfaces. Although RT multilayer condensation of water is known to form on hydroxylated SiO_2 surfaces [Sneh96], which are hydrophilic (water contact angle $<10^o$), hydrogen terminated Si surfaces are comparatively hydrophobic (water contact angle $\sim 86^o$), suggesting significantly smaller coverage under similar adsorption conditions.

The opportunity to perform highly surface sensitive experiments in Chalk River using neutron reflectometry (NR) proved useful in confirming that contrary to oxides, multilayers of water do not form on H-terminated silicon surfaces, placing an upper bound on the coverage to be on the order of 1 ML. These experiments were performed in collaboration with Dr. J. Katsaras, Dr. Helmut Fritzsche and Dr. Norbert Kucera.

The NR technique was applied for its high sensitivity to D_2O adsorbed on silicon. Based on simulations and previous experience, it was expected that this technique should easily detect 1 ML of D_2O with very high sensitivity, corresponding to a ~ 5 Å thick layer. This prediction was tested with the following experiments. All chemicals were transported from SIMS in Ottawa to the facility. A 4" diameter Si(100) wafer was cleaned in nitric acid then H-terminated by carefully pipetting 2% HF over the entire wafer. The sample was then quickly transferred to a gas-cell in the NR setup which was purged in Argon to both dehumidify and preserve the Si(100)-H surface. Results of the NR experiments are shown below as reflectivity curves in Figure 3.13.

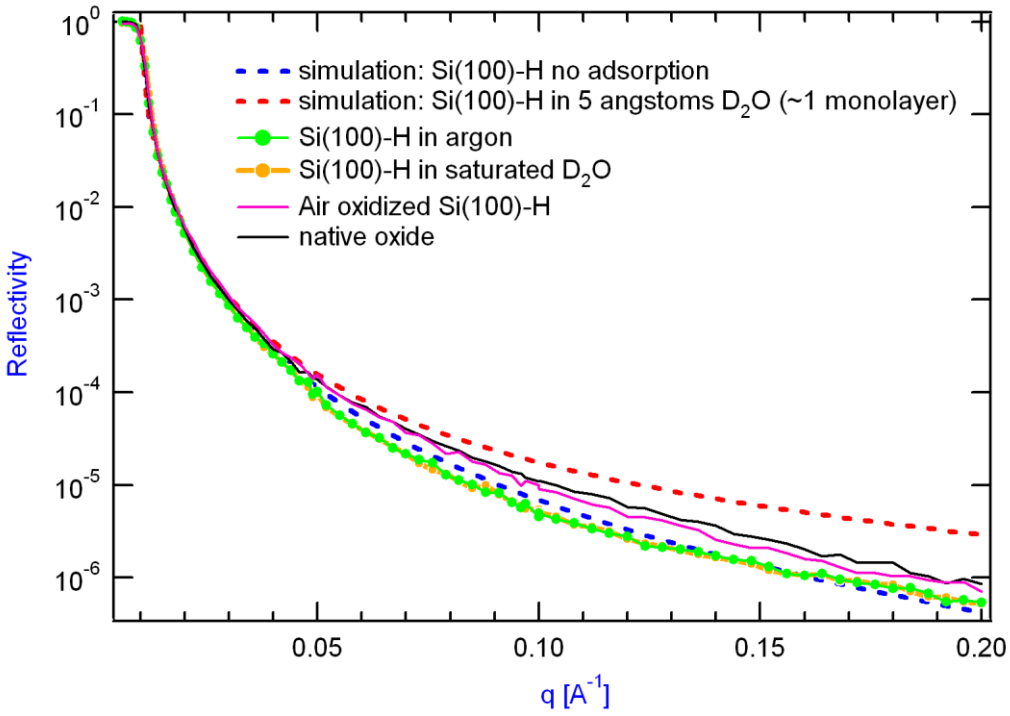

Figure 3.13: Results of the neutron reflectometry experiments. Reflectivity curves of Argon purged (green) or D_2O saturated (orange) Si(100)-H are the same and can be fit to a simulation for a bare surface (dashed blue), indicating very little water is adsorbed. The expected result for a 5 Å D_2O film is shown (dashed red). After 4 h air oxidation at 50 ^oC the curves shift upward (mangenta) corresponding a D_2O thickness under 5 Å. By comparison an untreated native oxide has a similar D_2O layer thickness of less than 5 Å.

As seen in Figure 3.13 the reflectivity curves in the presence of Argon purging or in saturated D_2O are nearly identical, indicating the D_2O thickness on a Si(100)-H surface is well below 5 Å; both curves correspond well to the fit of a bare silicon surface. However, upon air oxidation at 50 ^oC for four hours, the reflectivity curves in saturated D_2O shift upward as expected for a reduced hydrophobicity, which corresponds a D_2O thickness of just below 5 Å. By comparison an untreated native oxide has a similar D_2O layer thickness of less than 5 Å.

The results of the NR experiments provide strong evidence that the large conductivity modulation observed by water adsorption in Figure 3.9 and Figure 3.11 is due to a submonolayer coverage of H_2O. Knowledge of the binding energy E_d of water on

hydrogen terminated silicon should enable one to determine the precise coverage at different pressures.

3.5.2 Mechanisms

Because water molecules are always present in real environments, it is of practical importance to understand its adsorption properties on various electronic materials and the resulting interactions. Many interesting electronic effects involving water have been studied recently e.g. on diamond [Maier00], carbon nanotubes [Kim03;Na05], graphene [Schedin07;Wehling08] and metal oxides [Batzill06;Hernandez-Ramirez07]. Here we discuss the microscopic mechanisms on H-terminated silicon that could give rise to the observed conductivity changes.

3.5.2.1 Conduction through the water layer

The electrical conductivity of ultrapure water at 25 ^{o}C is 0.055 μS/cm (resistivity 18.2 MΩ·cm) which arises solely from the specific conduction of OH^- and H_3O^+ ions generated by its auto-dissociation [Light05]. Supposing a 5 Å layer has similar bulk resistivity, its conductance of 3×10^{-15} S (resistance 4×10^{14} Ω) would represent an insignificant contribution to the total surface conductance increase (typically on the order of 10 μS) measured on moderately doped SOI-H (Table 3.4) upon adsorption of water. This estimate is consistent with surface conductivity measurements of Teflon (10^{-17} S) and quartz (10^{-15} S) corresponding to 1 ML of H_2O adsorbed on their surfaces [Awakuni72]. In addition to these simple considerations, it is argued from our observations that electrical conduction through an adsorbed water layer on the hydrogen terminated surface is highly unlikely for the following reasons. Empirically it was shown in Figure 3.9 adsorption/desorption of water on *n*-type surfaces induces changes in conductivity of the underlying silicon since the changes in Hall coefficient and sheet resistance scale by the same ratio. If the enhanced conduction was due to conduction

through the water layer, the Hall coefficient would not change in proportion to R_s. Secondly the submonolayer coverage of water on Si(100)-H evidenced by the NR results in section 3.5.1 suggests there is no such contiguous path for conduction. Rather the water responsible for the conductivity change is likely adsorbed at isolated sites disconnected from each other. Thirdly in a test experiment using deuterated water vapor, the surface conductance increase of *n*-type SOI-H exposed to D_2O was measured to be the same (~10 μS) as that induced by H_2O at a similar pressure in the Torr range; since the specific conductivity of OH^- and H_3O^+ ions in H_2O is different from OD^- and D_3O^+ ions in D_2O [Light05], the observation that H_2O and D_2O adsorption on the SOI-H surface induces the same conductivity enhancement is inconsistent with conduction through a water ion channel.

3.5.2.2 Surface molecular dipoles

Water has a gas phase dipole moment of 1.85 D. The electric field of a 2*d* molecular surface dipole layer is an interesting possibility which can be argued paradoxically to have either a minimal or significant impact on the band-bending induced; the electrostatics depend strongly on the geometric arrangement, spatial extent and ideality of the dipole layer [Natan07;Deutsch07]. Surface dipoles largely influence the work function of semiconductors [Mönch95] but need not induce significant field-effects inside the material. The small field is rationalized from the definition that a dipole results from charge separation but remains electrically neutral as a whole; the field of an isolated dipole $\sim r^{-3}$ thereby decays more rapidly with distance than that of a charged electric monopole $\sim r^{-1}$. Furthermore, applying Gauss' Law to a 2*d* dipole layer modeled as an infinite parallel plate capacitor (continuous charge distribution) would result in identically zero electric field outside the oppositely charged plates.

Kronik and co-workers have expanded on the continuous charge parallel plate capacitor model by considering a dipole array comprising of discrete identical dipoles spaced by a distance *a* apart [Natan07]. By summing over the individual dipoles, the

electric field of a 2*d* perfectly ideal infinite dipole layer decays with height *z* below the layer as ~exp(-z^3/a^3). This sharply decaying field suggests that a perfectly infinite, partially ordered water layer adsorbed at isolated sites on a H-terminated surface should not induce substantial band-bending. However the authors argue that the ideal case is rarely encountered in real systems; non-ideal polar monolayers comprising of finite domain boundaries can induce substantial fields at the edges of the domains at strengths comparable to that of monopoles!

Cahen and co-workers have recently pointed out co-operative molecular field effects are possible when polar monolayers are present at a surface [Cahen05]. A simple calculation demonstrates a 2 nm thick 0.5 ML molecular monolayer with perpendicular dipole component of 1 D and ε=4 is inherently unstable since the field across the monolayer ~3 MV/cm is on the order of the breakdown field for such a thin film. In order to reduce the repulsive dipole-dipole interactions without changing the conformation of the close-packed layer, a small degree of charge transfer with the substrate, on the order of 0.01 e per molecule is sufficient enough to stabilize the system. Such a co-operative effect applied to polar water molecules densely packed on the hydrogen terminated silicon is also possible. Assuming the coverage of water is high enough (1 ML) to warrant a cooperative depolarization effect, this would require each water molecule to transfer charge of the order 10^{-4} e with the silicon (Q_s~10^{11} q/cm^2). Direct charge transfer is discussed in 3.5.2.4. Since we only know the upper bound on the coverage is 1 ML but do not know the precise coverage, structure and spacing of the water molecules, these dipole effects remain a possibility physically different from adsorbed monopolar surface charges, although the conductivity measurements do not explicitly enable this distinction.

3.5.2.3 Ionizable impurities

As mentioned in Ch1, observation of water induced field effects on *p*-doped surfaces dates back to the 1950's. In early studies on germanium NPN bipolar junction transistors, humid nitrogen gas was shown to lead to the formation of an inversion layer in the base

[Brown53;Kingston55] The appearance of donor like states induced by water adsorption was used to explain the origin of this inversion layer. For instance, Brown [Brown53] suggested that neutral donor impurities are ionized by water adsorption. Given the low density of surface charge Q_s~1×10^{11} q·cm^{-2} required to induce the effects observed here, it is difficult to rule out the presence of ionizable impurities at this level originating from the etching procedures. However, the observation that surfaces etched in both HF (Figure 3.9) and ammonium fluoride (Figure 3.11) exhibit similar effective charge densities in the presence of water perhaps argues against this explanation as different residual impurities are expected on these surfaces. Future studies on H-terminated SOI hydrogenated in ultrahigh vacuum may provide further insight into the possible role of impurities.

3.5.2.4 Charge transfer

The other possibility is that water itself acts as a donor, undergoing a charge transfer interaction with the substrate. An electrochemical charge transfer process involving transfer of electrons to a weakly acidic (H_3O^+ containing) water layer has been proposed previously to account for the observation of water induced *p*-type surface (upward band-bending) conductivity on hydrogen terminated diamond surfaces [Maier00;Larsson05]. However, this type of mechanism cannot account for the current observations as the surface conductivity observed on Si-H surfaces is of the opposite character (*n*-type), requiring the water layer to act as an electron donor (downward band-bending)[23].

The charge transfer may be intrinsic to the water-silicon interface or facilitated by a surface state in the gap inherent to the H-terminated surface. Theoretical calculations of the interaction of water on H-terminated silicon are required to further substantiate these possibilities.

[23] Water has been reported to induce *n*-doping on back-gated Si/SiO_2/graphene transistors [Levesque11] from observing negative shifts in the neutrality point; this process could have a similar origin to the effects observed on silicon (however, when oxygen is present a O_2/H_2O redox couple shifts the neutrality point to positive values, resulting in *p*-doping, as for H-terminated diamond).

3.6 Conclusions

We have shown that SOI-H substrates are interesting model platforms which enable the use of conductivity measurements to probe physical processes such as surface reactions and molecular adsorption/desorption events. The resistance of H-terminated SOI substrates was found to increase significantly with time in ambient air, due to depletion of majority carriers caused by oxidation. Physisorbed water was found to further modulate the conductivity, inducing downward band bending and accumulation of majority carriers. In addition to monitoring the sheet resistance, complementary information can be obtained from Hall voltage measurements. This facilitates distinguishing between accumulated, depleted and inverted states. Using this approach, adsorption of water in a controlled vacuum system is found to strongly and reversibly increase the conductivity of both *n*-type and *p*-type SOI-H substrates. These conductivity changes can be attributed to water induced field effects that lead to accumulation of majority carriers on *n*-type and formation of a minority carrier channel (inversion) on *p*-type substrates. The surface charge densities required to account for these effects are on the order of $\sim 10^{11}$ $q \cdot cm^{-2}$. This ability of adsorbed water to induce band bending is clearly a significant effect on oxide-free systems and should be accounted for, or at least considered in the interpretation of electrical transport measurements on silicon surfaces in ambient or aqueous solutions.

Chapter 4

Other Gases

4.1 Introduction

As demonstrated in Ch3 the influence of water from ambient or its controlled adsorption in vacuum induces significant modulation of the conductivity on SOI-H surfaces. By changing the pressure from HV to 10 Torr H_2O the response $R^{[vac]}/R^{[gas]}$ changes by an order of magnitude on moderately doped 200 nm SIMOX *n*-type samples. This response is ascribed to a surface charge density of $Q_s=10^{11}$ q cm^{-2} or one part in 10^4. Note that for a doping level of 10^{15} cm^{-3} a 100 nm thick film corresponds to a surface density of dopant atoms of order 10^{10} cm^{-2} and therefore the surface conductivity response should ultimately be sensitive to surface charge coverage as low as one part in 10^5. The highly sensitive response of H-terminated surfaces to water vapour suggests the electrical signals could be correlated to several known pressures to generate a response curve which in turn could be used to estimate the pressure of water above an SOI-H surface based on an electronic readout. The surprisingly large effects induced by water suggests

that oxide free chemically passivated surfaces offer the *potential* to operate as sensors via molecular modulation of the conductivity. In broadest terms a sensor is defined as a device that receives and responds to a signal or stimulus [Fraden96]; based on this definition the results presented in Ch3 qualify SOI-H substrates as sensors of humidity, but so too is a hair follicle that changes its conformation in response to hydration.

Since almost any system exhibits a stimulus-response or input-output relationship possessing some sensory qualities, what is more important is the classification of a sensor by listing and quantifying all of its attributes. The specifications of a real sensor include its sensitivity, stimulus range (span), stability (short and long term), resolution, accuracy, selectivity, response time (speed), hysteresis, operating life, size, weight and cost [Fraden96]. From this partial list, it can be verified that oxide free H-passivated thin film silicon surfaces are clearly worth exploration for their sensing properties, but fall short of practical use in real devices.

Evidently, SOI-H substrates rank highly with respect to their sensitivity to surface charge and stimulus range specifications. This desirable quality is sharply contrasted with their poor long term stability in ambient air as the surface oxidizes (Figure 3.2), causing interface state growth and thereby resulting in the depletion of free carriers (3.2.2). Although the long term stability in air remains a challenge, H-terminated films are still suitable at short times as model proof-of-concept charge detectors and if necessary their lifetimes can be extended in high vacuum in more controlled studies. Efforts to electronically stabilize oxide-free surfaces in ambient by additional passivation of Si-H with e.g. molecular monolayers is a promising avenue for improving the long term stability [Mischki06;Bin08]. In addition to low stability, based on the response times to water adsorption/desorption (minutes), SOI-H substrates would qualify as relatively slow sensors of humidity. These substrates do exhibit some inherent degree of cross-selectivity upon exposure to a range of molecular adsorbates, described in this chapter (section 4.3.1). Note that control over the specificity is a more formidable task; one approach involves passivation with functional monolayers (functionalization) to chemically tailor the surface for a desired receptor-target interaction [Mitchell02].

Based on the observations in Ch3 that SOI-H substrates are highly sensitive to water vapour in the Torr range, other gases have been studied to further explore the effects of band-bending and charge transfer on silicon surfaces. In this chapter, the adsorption of a range of molecular species (pyridine, ammonia, triethylamine, diaminopropane, methanol) is found to reversibly modulate the conductivity of hydrogen terminated silicon-on-insulator (SOI-H) substrates. Simultaneous sheet resistance and Hall effect measurements on moderately doped *n*-type and *p*-type SOI-H samples mounted in a vacuum system (Gen1) are used to monitor the effect of gas exposures in the Torr range on the electrical transport properties of these substrates. Reversible physisorption of "hole-trapping" species, such as pyridine (C_5H_5N) and ammonia (NH_3) produces highly conductive minority carrier channels (inversion) on *p*-type substrates, mimicking the action of a metallic gate in a field effect transistor. The adsorption of these same molecules on *n*-type SOI induces strong electron accumulation layers.

Pyridine (section 4.2) is found to give rise to similar but larger effects than water, inducing strong accumulation and inversion layers on *n*-type and *p*-type SOI-H, respectively. Similar electron donors (ammonia, triethylamine) are found to behave like pyridine (section 4.3) while certain aromatic molecules such as toluene and thiophene have minimal effects on the conductivity. As with the water adsorption studies, the electrical measurements presented here can be explained by a classical band-bending model which considers the adsorbates as the source of a uniform surface charge ranging from $+10^{11}$ q cm^{-2} to $+10^{12}$ q cm^{-2}. These observations demonstrate the utility of transport measurements on SOI-H substrates for studies of adsorption events at silicon surfaces and suggest potential applications in chemical sensing.

4.2 Pyridine

The strong influence of physisorbed water on the conductivity of SOI-H (Table 3.4) suggests exploration of the effects of other molecular species. Pyridine (Azine, Azabenzene) C_5H_5N is an interesting candidate as a polar molecule with a dipole moment

of 2.2 D [Middleton 38] and an active electron lone-pair [Pettinger78]. It is a well known weak base [Johnson65], making it susceptible to 'hole capture' or equivalently, to 'electron donation'. Recently the structure and adsorption geometries of pyridine on copper [Lee01], germanium [Cho03], platinum [Kliewer10] and silicon [Miwa08;Coustel11] have been investigated. Adsorption of pyridine at clean dimers of Si(100)-2×1 occurs initially in an aromatic, dative bonding configuration then over several minutes converts to a more stable non-aromatic, bridged configuration [Miwa05] as observed by in-situ STM dosing experiments. From experiments on partially H-terminated Si(100)-2×1surfaces, this dative bonding is seen to occur preferentially at isolated dimers (4e, 2DB) rather than isolated dangling bonds (3e, 1DB). The electronic interaction of pyridine with electronically passivated, hydrogen terminated silicon films has not been investigated aside from the results presented here. Some physical properties of pyridine are listed below in Table 4.1.

Table 4.1: Some physical properties of pyridine

Property	Value	Notes	Reference
Synthesis		Chichibabin synthesis	[Tschitschibabin24]
Number of π-electrons	6	$4n+2$ rule	[Bordwell91]
pK_b (300 K)	8.8	pK_a=5.2 for $[C_5H_5N]^+$	[Pearson53]
Dipole moment (300 K)	2.2 D	1 D=3.3×10^{-30} C·m	[Middleton38]
Vapour pressure (298 K)	20 Torr	P=45 Torr at 40°C	[Herington53]
Molecular diameter	0.5 nm	4.9 Å $\parallel$ C_{2v} axis; 5.5 Å $\perp$ C_{2v}	[Herber81]

4.2.1 Pyridine vapour on n-type SOI-H surfaces

Figure 4.1a shows the result of pyridine exposure on an *n*-type SIMOX substrate with film thickness *d*=148.7 nm. Within minutes of leaking pyridine into the chamber, the conductivity of the sample increases by almost two orders of magnitude as the pressure is allowed to increase continuously to 13 Torr. Pyridine (from Sigma Aldrich) was purified by several freeze-pump-thaw cycles. Note that the pressure of pyridine in the chamber was generally less than the equilibrium vapor pressure expected at RT (20 Torr), attributed to its adsorption on the chamber and gas-line walls. Hall voltage measurements prior to and after adsorption are found to scale with sheet resistance changes.

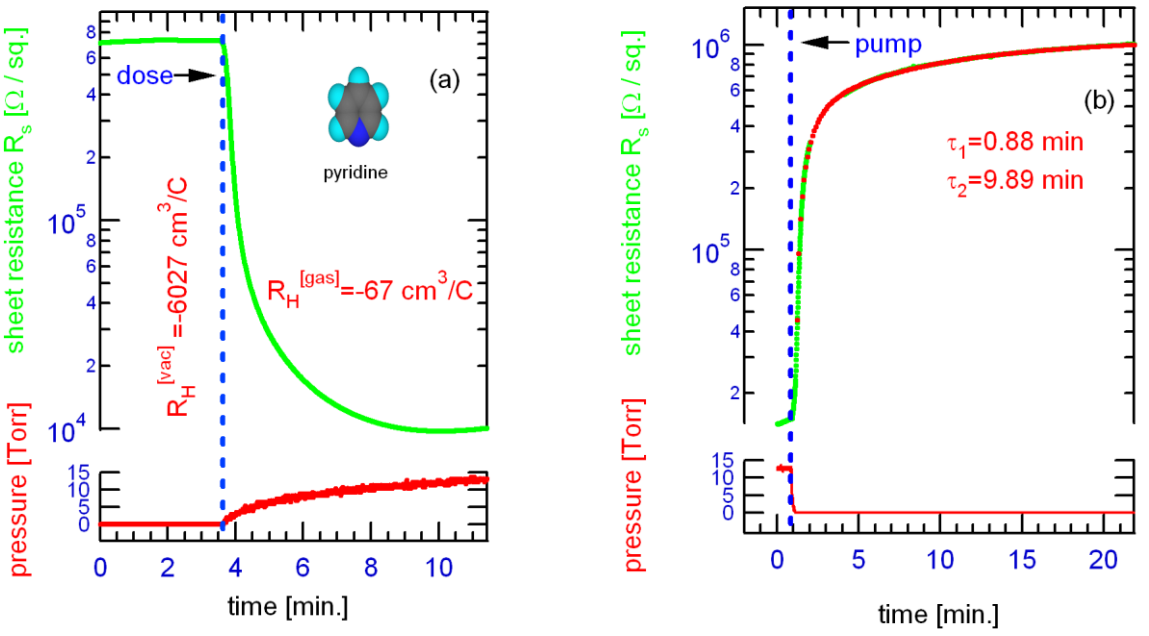

Figure 4.1 (a): Adsorption of pyridine vapor on an *n*-type 150 nm SOI(100)-H film from vacuum. The conductivity as well as Hall coefficient (taken at I_x=100 nA, B_z=560 G) increases by almost two orders in magnitude on exposure. (b). Evacuation of pyridine eliminates the accumulation layer and the resistance and Hall coefficients return to values comparable to what was measured initially.

The scaling of the Hall coefficient with resistance indicates that the conductivity changes are associated primarily with changes in carrier density induced by a field effect rather than changes in mobility. As with water adsorption on *n*-type Si, this observation shows that pyridine gives rise to strong accumulation of the majority carriers (electrons). Simulations as discussed in section 3.4 indicate that ~172 mV of downward band-bending is required to account for the observed sheet resistance changes, requiring an external charge of order ~+10^{12} q·cm^{-2}, nearly six times greater than that induced by water at a similar pressure (Table 3.4). A summary of electrical parameters presented for the case of pyridine on *n*-type (4.2.1) and *p*-type (4.2.2) SOI-H is shown in Table 4.2 for reference and comparison. The band-bending changes corresponding to Figure 4.1 are shown below in Figure 4.2.

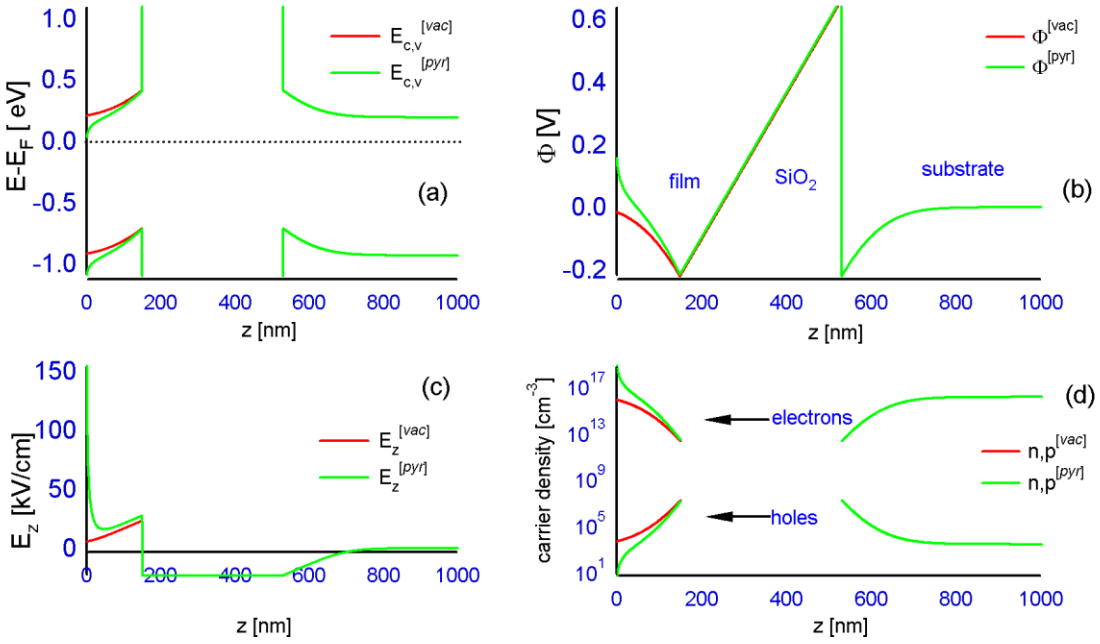

Figure 4.2: Electrostatic-consistent depiction of the pyridine adsorption experiment in Figure 4.1, corresponding to initial (vacuum, red) and final (gas, green) sheet resistances. The (a) band-bending, (b) electrostatic potential, (c) electric field, (d) electron and hole densities are shown across the SOI structure. Upper and lower BOX charges are assumed to be 2×10^{11} q cm^{-2} and 1×10^{11} q cm^{-2} respectively.

Evacuation of the pyridine confirms the reversibility of most of this effect upon desorption as illustrated in Figure 4.1b. A double asymptotic exponential rise in Figure 4.1b can be fit with a fast time constant (τ_1~0.9 min.) with an overall slow tail (τ_2~9.9 min.). The slower time constant suggests that at least some pyridine binds more strongly to the hydrogen terminated surface than water (Figure 3.9). The final sheet resistance in vacuum was approximately 30% higher than its initial value, suggesting some degradation of the H-terminated surface may have occurred.

The combined effect of pyridine with another impurity in the chamber or gas-line is the most probable cause. For instance, water combined with pyridine is known to accelerate oxidation of H-terminated porous silicon (PS) [Mattei02] In this study, the authors electrochemically prepared 700 nm thick mesoporous PS, which was then stored in a chamber containing air saturated with water (30% relative humidity) or air saturated with pyridine vapour at room temperature. The PS samples were studied by ex-situ FTIR reflection spectroscopy at discrete time-points over 12 days to monitor the intensities of the Si-H_x stretch vibration decrease, and increases in Si-O-Si, Si-OH and O_ySi-H_x intensities for the cases of humid oxidation (no pyridine) and humid oxidation in the presence of pyridine. The rate of oxidation in the presence of pyridine was much faster, but did not affect the final degree of oxidation as shown below in Figure 4.3. These observations suggest water is the main oxidizing reagent in the processes and pyridine acts to catalyze the native oxide growth. The authors interpret the accelerated oxidation due to pyridine in humid air as a result of the attractive interaction between the nitrogen lone pair and the Si-Hx species, causing weakening of the silicon-hydrogen bond. This interaction would give credence to the electron donor properties observed in our measurements in Figure 4.1.

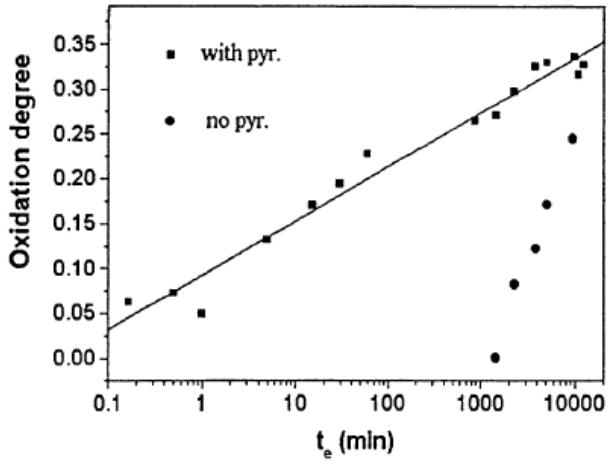

Figure 4.3: Degree of oxidation (based on the IR spectra) for two parts of the same PS sample exposed to air saturated with water vapour (circles) and humid air saturated with pyridine vapour (squares) at RT as a function of time over 12 days, adapted from [Mattei02].

4.2.2 Pyridine vapour on *p*-type SOI-H surfaces

Pyridine exposure to Unibond *p*-type 3 µm SOI is shown in Figure 4.4a. As with water, the same peak features (shown in the inset) show that R_s evolves from an initially depleted state to a stable inverted state, supported by a change in sign of Hall voltage. The reverse process is illustrated in Figure 4.4b. The resistance quickly increases to a maximum as the *n*-channel vanishes, but as residual pyridine continues to desorb, the surface slowly comes out of depletion and the resistance decays back to its initial value shown on the dotted line. The Hall voltage is also restored to its original positive value in vacuum.

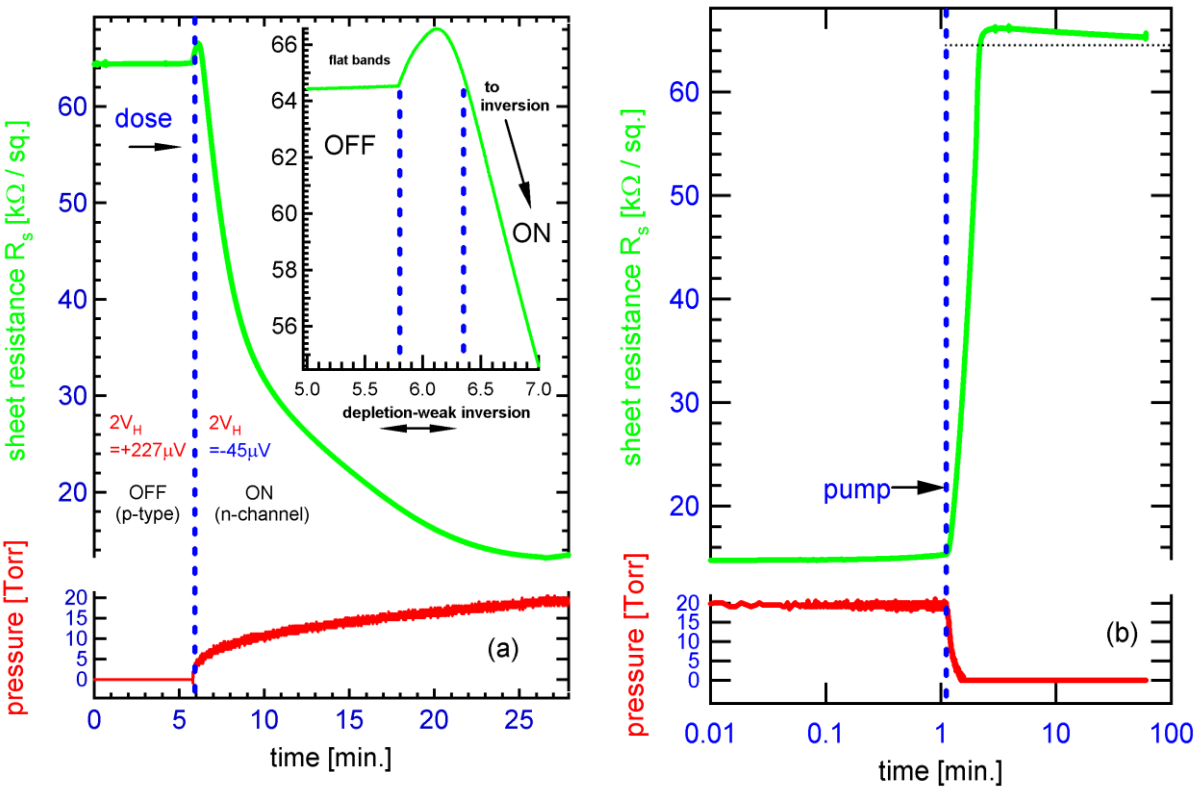

Figure 4.4: (a) Sheet resistance changes to adsorption of pyridine vapor on *p*-type 3 μm thick SOI(111)-H. A change in sign of the Hall voltage on exposure indicates the surface becomes inverted by pyridine adsorption. (b). The corresponding desorption isotherm shows this effect is reversible. The disappearance of the inversion layer occurs more rapidly than the reversal of the depletion layer to its initial flat-band value.

The surface charge required to account for the changes observed in Figure 4.4 is ~3.7×10^{11} q·cm^{-2}, more than a factor of 3 times greater than that induced by the presence of water. This can be attributed to the donor-like nature of the nitrogen lone pair which can trap holes from the surface, resulting in $(C_6H_5N)^+$. The band-bending changes corresponding to Figure 4.4 are illustrated in Figure 4.5 and a summary of electrical parameters presented for the case of pyridine on *n*-type (4.2.1 Figure 4.1) and *p*-type (4.2.2 Figure 4.4) SOI-H is shown in Table 4.2 for reference and comparison.

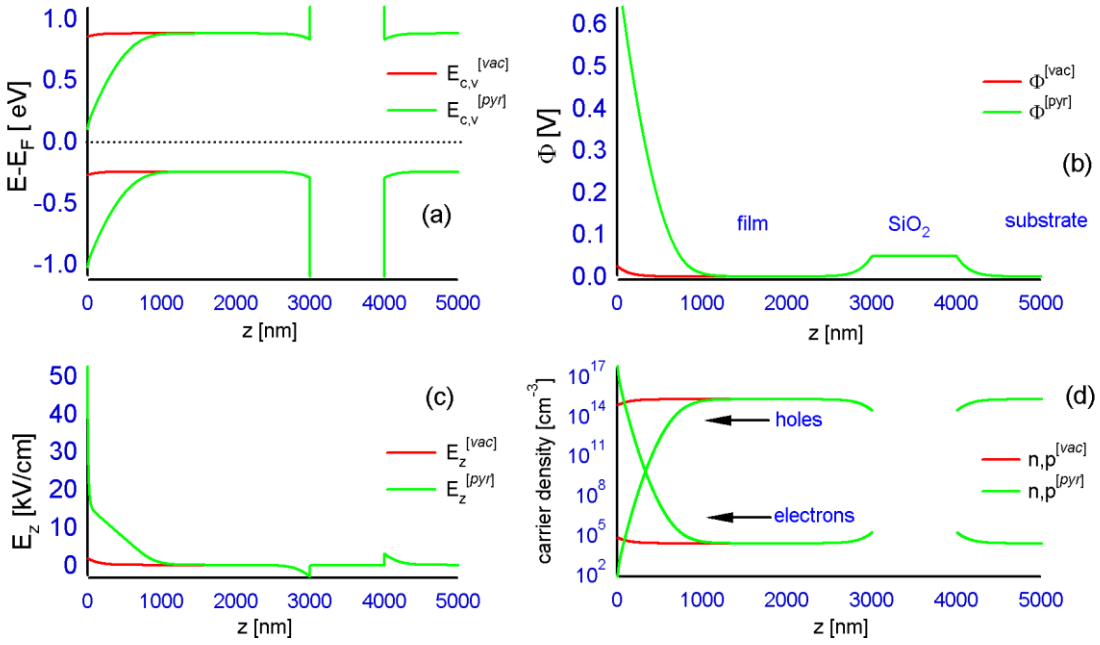

Figure 4.5: Electrostatic-consistent depiction of the pyridine adsorption experiment in Figure 4.4, corresponding to initial (vacuum, red) and final (gas, green) sheet resistances. The (a) band-bending, (b) electrostatic potential, (c) electric field, (d) electron and hole densities are shown across the SOI structure. Upper and lower BOX charges are assumed to be equal with value 2×10^{10} q cm^{-2}.

Table 4.2: Summary of numerically extracted electrical parameters from Figure 4.1 and Figure 4.4

Fig. #, *Type*, Thickness, Pressure, Gas Status	$\mu^{[vac]}$ $\mu^{[gas]}$ /cm^{2}V^{-1}s^{-1} ±10%	$q^{[0]}$ /cm^{-3} ±10%	$q^{[vac]}$ $q^{[gas]}$ /cm^{-3} ±10%	$\Delta N^{[vac]}$ $\Delta N^{[gas]}$ /cm^{-2} ±10%	$\Delta P^{[vac]}$ $\Delta P^{[gas]}$ /cm^{-2} ±10%	$G_s^{[vac]}$ $G_s^{[gas]}$ /µS ±10%	Q_s /cm^{-2} ±10%	$\Phi(0)^{[vac]}$ $\Phi(d)^{[vac]}$ /mV ±10%	$\Phi(0)^{[gas]}$ $\Phi(d)^{[gas]}$ /mV ±10%
#4.1. *n-type* 150 nm 15 Torr C_5H_5N Accumulation	566 443	8.80×10^{15}	1.05×10^{15} 9.41×10^{16}	-1.16×10^{11} 1.27×10^{12}	- -	-10.6 90.4	$+1.15\times10^{12}$	-15.1 -220	156.9 -215
#4.4 *p-type* 3 µm 19 Torr C_5H_5N Inversion	315 -	1.13×10^{15}	1.03×10^{15} N.A.	- 2.8×10^{11}	-3.17×10^{10} -1.23×10^{11}	-1.60 57.1	$+3.70\times10^{11}$	25 49	779 49

4.2.3 Discussion of the effects of pyridine

Similar to the possible mechanisms discussed for the case of water in section 3.5, although surface molecular dipoles and ionizable impurities cannot be ruled out completely, the electrical measurements summarized in Table 4.2 are consistent with a simple charge transfer interaction between pyridine molecules and the hydrogen terminated surface. This interaction is suspected to occur via the active lone pair at the nitrogen end, as suggested in previous experiments on hydrogenated porous silicon [Mattei02].

This mechanism is also consistent with vacuum in-situ IR transmission studies of pyridine adsorption in highly doped *p*-type porous, nano-crystalline silicon [Osminkina05]. The authors prepared a 30 μm porous film to make ~20 nm crystals with pore sizes <10 nm (porosity >50%) and determined the concentration of free holes based on the transmission spectra and a scattering model dependent on doping, porosity and optical constants of their silicon nanocrystals. It was found that pyridine adsorption at low pressures 0.1 Torr <*P*<1 Torr decreased the concentration of free holes by more than one order of magnitude from 2×10^{19} cm^{-3} in HV at 10^{-5} Torr to 10^{18} cm^{-3} (100 mTorr-1 Torr). This effect has been attributed to hole capture into surface states of adsorbed pyridine represented by the process:

$$h^{+}+C_5H_5N\rightarrow(C_5H_5N)^{+}.$$

However the main distinction is that our measurements in Figure 4.1b and Figure 4.3b are reversible upon pumping away the pyridine, whereas the hole trapping effects observed by Osminkina et al are not. This suggests the mechanism of charge transfer in highly doped porous silicon is different from that of our results on planar SOI (reversible), which is not entirely understood. Rather, at higher pressures (> 1 Torr) the authors observe a hole-detrapping effect attributed to the condensation of pyridine inside the pores which they attribute to an increase in the effective dielectric constant and therefore

activation energy of the boron impurities. Since the in-situ IR spectra did not show evidence of covalent bonds forming on the H-terminated surface, the irreversibility is attributed to strongly physisorbed charge center complexes. Since our electrical measurements are reversible on a timescale of 1 h, this suggests the pyridine adsorption is weaker on planar SOI than porous material.

Similar to the case of water, the binding energy and hence coverage of pyridine on the surface are unknown and so the precise microscopic mechanisms are underdetermined from the present measurements. The relative strength of the effect compared to water (3-6 fold) are thereby empirical and could simply be related to a larger coverage but similar charge transfer efficiency. The presence of multilayers on the H-terminated surface is also conceivable.

4.3 Additional Species

4.3.1 Selectivity

The selectivity of the gating effect to certain classes of molecules is demonstrated in Figure 4.6 where a *p*-type SOI-H substrate is exposed sequentially to three different types of molecules. To minimize cross-contamination between doses, the common gas-line is gently baked for several minutes when changing to a new molecule. The vacuum resistance of this sample is 65.7 kΩ while the Hall voltage is measured to be +224 μV (@ 1 μA and 560 G). There is a negligible change when 15 Torr of toluene ($C_6H_5CH_3$) is leaked into the chamber and then pumped away. The insets in Figure 4.6 display the measurements on a smaller scale to illustrate how little the conductivity changes at the point of dosing. Like pyridine, toluene is a hexacyclic aromatic molecule, except it is non-polar and does not have lone pairs that can participate in charge donation. Similar null responses were observed using benzene (C_6H_6) not shown in Figure 4.6. The lack of an observed response for this molecule supports the hole-trapping mechanism suggested for the pyridine observations [Osminkina05;Dubey10]. Again there is a negligible change

(<1%) when 20 Torr of thiophene (C_5H_4S) is introduced or evacuated. Thiophene is slightly polar with a dipole moment of 0.5 D at 298K [Lien70], which is considerably smaller than that of water or pyridine. Although this difference in polarity may be significant, the lone pair electrons in thiophene are also heavily incorporated into its aromaticity (as opposed to pyridine) rendering its overall activity similar to that of toluene or benzene. These observations also suggest the charge transfer observed for water molecules could involve its lone pair electrons. When ~10 Torr pyridine is introduced the familiar depletion-inversion peak feature is observed; there is a brief rise in resistance to 65.9 kΩ, followed by a significant decrease to 24.4 kΩ along with an inversion of the Hall reading to -58 μV. After pumping away the pyridine, the resistance returned back to 65.7 kΩ and Hall voltage was restored to its previous value of +224 μV (@ 1 μA and 560 G).

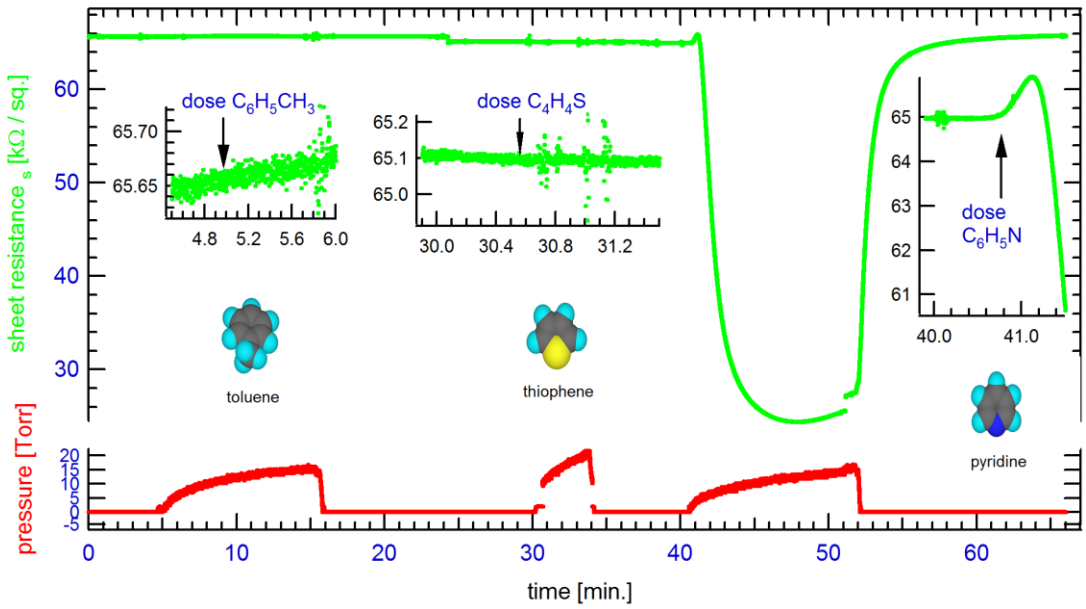

Figure 4.6: Monitoring the effect on the sheet resistance when toluene, thiophene, and pyridine are sequentially exposed to *p*-type 3 μm SOI(111)-H, respectively. The conductivity is unaltered upon exposure to toluene or thiophene. Exposure to pyridine induces the large resistance change observed previously.

4.3.2 Other donors on *p*-type 3 μm SOI-H

The ability of a few other gases to modulate the conductivity of SOI-H surfaces has also been investigated on *p*-type 3 μm SOI-H substrates. The results are summarized in Table 4.3. Dry oxygen or nitrogen gas did not significantly affect R_s over a pressure range of 1 Torr<P<1000 Torr. However, the vapours of amines induced strong modulation of the conductivity. We recall from section 1.7.1.2 that ammonia has been reported to induce significant changes in the response of oxidized silicon nanowire transistors [Talin06], shifting the threshold voltage to more negative values by 5.4 V, but only slightly changes that of a planar oxidized SOI wafer by only 200 mV. Yet in contrast to this small shift, the large response of an oxide-free SOI-H sample exposed to ammonia (Table 4.3) shows that the surface preparation/modification is also important, in addition to the device geometry. The increased sensitivity to ammonia when no intervening oxide is present likely results because the molecules can directly transfer charge with the silicon, thereby able to induce larger band-bending effects compared to that of an oxidized nanowire.

Ammonia (NH_3) and triethylamine ($N(C_2H_5)_3$) induced similar effects as pyridine causing the resistance of 3 μm *p*-type SOI(111)-H to decrease from ~56 kΩ to the ~6 kΩ range and inverted the surface conduction from *p*-type to *n*-type as evidenced by the change in sign of the Hall voltage. These effects are reversible with the conductivity and bulk carrier type restored upon pumping away the gases. Analogous to pyridine, ammonia and triethylamine are polar and have a basic lone pair that can abstract holes from the surface. Ammonia and triethylamine also inverted the surface conduction at much lower pressures (~mTorr range) than observed for pyridine or water (Torr range) and decreased R_s in a much shorter time such that the depletion-inversion peak feature was not (always) resolved.

Table 4.3: Summary of conductivity modulation induced by gaseous exposure to *p*-type 3 μm SOI-H.

Gas	P [Torr]	$(R^{[gas]}-R^{[vac]})/R^{[vac]}$
Pyridine	19	-0.80
Triethylamine	20	-0.83
Ammonia	85	-0.77
Ethanol	10	-0.05
Oxygen	9	<0.01
Nitrogen	1000	<0.01

Pressure-resistance measurements over a wide pressure range may provide useful contrast between these species. The relative strengths are difficult to compare at this point due to unknown differences in coverage.

4.3.3 Methanol

Controlled exposure of freeze-pump thawed 99.9 % anhydrous methanol (Sigma Aldrich) vapour (5 Torr) to 200 nm SIMOX SOI-H is also found to induce reversible enhancement of the conductivity by lowering the vacuum resistance from $R^{[vac]}$=120 kΩ to $R^{[gas]}$=40 kΩ. Several dose/pump cycles show this effect is highly reversible with a desorption time constant of ~1 min. As the magnitude of this effect is several fold smaller and than water in Figure 3.9 (20×) and reverses on a faster time scale (1.7 min for water), this difference would enable discrimination between the two species in a blind test even though gases behave as electron donors. Similarly the distinction between methanol and other alcohols could be studied and parameterized in two dimensions by recording the conductance change and reversibility times. These observations also suggest oxide-free SOI films have the potential to be used in alcohol vapor detection, in addition to humidity. However, cross-adsorption studies discussed briefly in 4.3.4 in relevant gas mixtures need be implored before leaping at alcohol breath-analyzers.

4.3.4 Co-adsorption

The majority of this work focuses on the band-bending effects induced by singly adsorbed molecular species from a basic perspective and to demonstrate the utility of SOI-H for potential sensing applications. However in real (practical) cases, interacting gaseous mixtures may induce very different responses than that of the individual species measured separately. For instance in Ch3, Figure 3.6, it was seen that although water specifically reduces the sheet resistance in a reversible manner, the combined effect of water and oxygen in ambient air results in an irreversible increase in R_s due to oxidation.

In a controlled study in vacuum (Gen 1) a surprising effect due to co-adsorption of 1,3-diaminopropane $NH_2(CH_2)_3NH_2$ and oxygen (Torr range) has also been observed. Exposed separately to an *n*-type 200 nm SIMOX SOI-H substrate, O_2 does not induce large changes in conductivity, but diaminopropane significantly modulates R_s, reversibly inducing accumulation of electrons similar to the effect of pyridine shown already in Figure 4.1a. However when both species are present at a total pressure of 5 Torr the sample becomes fully depleted of carriers in minutes as the resistance increases by two orders in magnitude from ~1×10^5 Ω ($2V_H$=-0.060 mV @ 100 nA, 560 G) to ~2×10^7 Ω (2V=-1.7 mV@ 10 nA, 560 G), and reverses in minutes when the mixture is pumped away. Depletion is consistent with a negative charge on the surface (presumably due to O_2^-) which can arise from a charge transfer interaction between the oxygen electron acceptor and donor diaminopropane molecules [Mitchell02]. This effect was observed accidentally when exposing diaminopropane to the surface in the presence of a small leak of O_2 in the gas-line and warrants further investigation for publication. The oxygen anion could be a general consequence of co-adsorption with any amine gas. These observations demonstrate the study of co-adsorption with multiple species is clearly an area worth exploration. Oxide-free SOI electronic noses or cross-reactive arrays would be ideally suited for systematic adsorption experiments on a large scale.

4.4 Conclusions

We have shown that SOI-H substrates are interesting model platforms which enable the use of conductivity measurements to probe molecular adsorption/desorption events. In addition to monitoring the sheet resistance, complementary information can be obtained from Hall voltage measurements. This facilitates distinguishing between accumulated, depleted and inverted states. Pyridine adsorption gives rise to similar yet even stronger reversible conductivity modulation effects as compared with water on both *n*-type and *p*-type substrates. Adsorption of pyridine in the Torr range gives rise to positive surface charges of 4×10^{11} q·cm^{-2} (*p*-type) and 1×10^{12} q·cm^{-2} (*n*-type), resulting in a surface electric field 3-6 fold higher than that caused by water adsorbed on the same surface. The ability of nitrogen containing molecules such as pyridine, ammonia and triethylamine to reversibly bias *p*-type surfaces into inversion demonstrates a new type of molecular triggered electronic switch where adsorption is used to reversibly gate transport through the silicon substrate.

Chapter 5

Pseudo-MOSFET Measurements

5.1 Introduction

As we have seen to up to this point, transport properties of oxide-free silicon surfaces are dramatically altered by adsorption and reaction events. Hydrogen-terminated silicon-on-insulator (SOI-H) has been shown to be an interesting model system for investigating this sensitivity to surface processes. Carrier transport studies via four-probe sheet resistance and Hall Effect measurements described in Ch3 and Ch4 were used to monitor the electrical conductivity, carrier density and carrier mobility of the top silicon film (device layer). Electrical characterization using these techniques was shown to be useful in correlating changes in carrier density with conductivity (accumulation or depletion) in addition to identifying changes in carrier type (inversion) induced by adsorption of several gaseous species. In these measurements the substrate was grounded and was not considered to influence the electrical properties of the device layer. However by applying a potential to the substrate with respect to one of the top contacts, band-bending in the device layer at the Si/BOX interface can substantially influence the conductivity,

analogous to the application of a bias to a metal through a top-gate oxide in a MOSFET [Sze69]. In thin SOI films this conductive layer can be accessed easily with two-probes on the surface in a simple three-terminal device.

The architecture of SOI substrates facilitates the formation of a pseudo-MOS transistor (Ψ-MOSFET) simply by making point contacts to the top silicon layer and using the silicon substrate as a gate. It was first described by S. Cristoloveanu and S. Williams [Cristoloveanu92] as a method for in-situ characterization of as-grown SIMOX wafers, a concept originating from Schottky-barrier SOI MOSFETs [Liu90]. Their key observations are that any two-probe system can be used to form the source and drain contacts i.e. low-pressure probes and that both accumulation and inversion channels can be probed simultaneously on the same wafer. As this allows recording of FET-like characteristics with minimal need for additional fabrication, the Ψ-MOSFET has become a mainstream tool for rapid and non-destructive characterization of SOI wafers [Cristoloveanu00;Hollt07;Rao08]. Application of this approach to monitor surface processes is still in its infancy.

Control over the inversion threshold voltage $V_{TH,inv}$ of FETs formed on SOI substrates was demonstrated initially for molecularly adsorbed layers formed on oxidized silicon by Gust and co-workers [Laws02;Yang02;Laws03]. In these studies the native oxide of 40 nm *p*-type SIMOX SOI was back-gated as a buried *n*-channel pseudo-MOSFET contacted by phosphorous spin-on-dopants at the surface. Drop-casting a series of acidic molecules (pK_a<6.8) containing carboxylic acid groups was shown to protonate the comparatively less acidic SiO_2 surface (pK_a~6.8) with positive charge, thereby inducing negative shifts in $V_{TH,inv}$. The series of molecules studied includes spiropyran {pK_a~4.9;ΔV=-4 V}, 4-nitrobenzoic acid {pK_a~3.4;ΔV=-1.7 V} and 4-dimethylaminobenzoic acid {pK_a~6.0;ΔV=-1.5 V}. A limited number of studies have investigated oxide-free systems, which are expected to be more sensitive to adsorbed surface charge. Recently in the Tour group, the covalent grafting of aromatic molecular layers to SOI-H (as $Si^{(sp3)}$-$C^{(sp2)}$ aryl-silicon bonds created by the reduction and loss of their diazonium salts) with a range of *para*-moiety substituents has been used to

demonstrate threshold shifts with respect to the H-terminated surface, in accordance with the electron donor/acceptor character of the aryl substituent (R-group) [He06]. The authors fabricated SOI device arrays on a chip to form hole accumulation channel pseudo-MOSFETs using nearly intrinsic *p*-type (>2000 Ω·cm) 450 nm SOI(100) with active area ~110×110 μm^2 contacted to 80×80 μm^2 p^{++} boron-implant source and drain electrodes. A controlled series of molecules ranging from π-donors {R=dimethylamino;Δ*V*=-1.9 V},{R=amino Δ*V*=-1.5 V} to π-acceptors {R=nitro;Δ*V*=-1.0 V}, {R=polymolybdate;Δ*V*=+0.6 V} results in accumulation threshold voltage shifts Δ*V* becoming more negative (hole current decreases) compared to SOI-H with increasing relative electron donor ability of the grafted molecules. These observations cannot be explained solely by the different dipole moments of the molecules; the authors argue differences in Δ*V* arise largely from charge transfer between the electron rich ring to the silicon device layer (acting as donor molecules), or from the silicon to the electron deficient ring (acting as acceptor molecules). Note that the π-acceptor molecule with nitro substituent (acceptor with respect to the ring) behaves as an electron donor to the silicon in this case because it is electron rich with respect to the low doped p-type SOI-H surface; the same molecule is shown to behave as an electron acceptor [He09] when the pseudo-MOSFET is biased into an electron rich inversion *n*-channel. The Tour group has also demonstrated reversible modulation in threshold voltage of *n* and *p* channel devices grafted with both photochromic spiropyran, and non-photoresponsive molecules, including the substituted-aryl species listed above and a C12 alkyl monolayer [He08]. Upon alternately switching between irradiation for prolonged periods with UV (electron withdrawing effect) and visible light (electron donating effect), the reversible shifts are found to differ slightly for each grafted molecule, and even the SOI-H control samples are observed to respond in a similar manner. The origin of this effect is not well understood; the authors suggest that UV-light induces new states at the molecule/Si interface which can be eliminated after exposure to visible light [He08]. Although these studies used H-terminated silicon as the starting point for forming molecular layers, the device properties of this surface in ambient atmosphere or its sensitivity to adsorption

events was not investigated, as the electrical measurements were carried out exclusively in a high vacuum chamber at $P<5\times10^{-6}$ Torr. The influence of monolayer formation on the resulting electrical quality i.e. interface states was not characterized either. The results described here build upon these previous studies by systematically demonstrating that modulation of the device properties of SOI-H due to reversible effects of physisorption and irreversible effects of chemisorption is alone very significant. These observations could be useful in advancing the studies of grafted donor/acceptor monolayers on silicon [He06;He09] since they show that further modulation would be expected by small molecules adsorbed onto such complexes.

In this chapter we employ the point contact Ψ-MOSFET technique to SOI(100)-H substrates and report significant modulation of the electrical properties caused by simply changing the gaseous environment. The scope of the present measurements has been limited to water and pyridine molecules, although other donor species studied by transport measurements in Ch4 (methanol, triethylamine, diaminopropane, ammonia) are expected to induce analogous effects. Moderately doped (~10^{15} cm^{-3}) *n*-type samples with film thickness d=150-200 nm are used. Current-voltage characteristics of the Ψ-MOSFETs are used to extract the "threshold voltage" to activate an accumulation *n*-channel ($V_{TH,acc}$) at the device layer/buried oxide interface, which we designate interchangeably as the "flat-band voltage" (V_{FB}). An important parameter in the characterization of FETs, this is the gate voltage required to flatten the bands in the device layer and the threshold point where a large onset in current is measured as the bands are driven further into accumulation. Changes in V_{FB} are observed upon operation in ambient, high vacuum and under controlled exposure to pure H_2O. Adsorption of water is found to shift V_{FB} to more negative values, corresponding to an increase in current at a fixed gate voltage and suggesting that the water induces a positive surface charge. Even larger effects are induced by exposure to pyridine (C_5H_5N), analogous to the transport measurements described in Ch3 and Ch4. The Ψ-MOSFET was also used to observe irreversible changes associated with ambient oxidation of the H-terminated surface in agreement with the increases in $R_s(t)$ discussed in Ch3. Passivation of the H-terminated

surface via molecular monolayer formation has also been investigated. A recently developed gas-phase photochemical method is found to be a simple and compatible means for covalent attachment of alkyl chains to the Si(100)-H surface. This process is found to maintain the low density of electrically active defects typical of the H-terminated surface, suggesting that alkyl monolayers formed in this highly practical way could be useful as ultrathin dielectrics for sensing applications.

5.2 Experimental Aspects

Separation by implantation of oxygen (SIMOX) substrates from IBIS with buried oxide (BOX) thickness d_{box}=377 nm and active Si(100) layer thicknesses d=150 nm (*n*-type film/ *p*-type substrate) and d=200 nm (*n*-type film/*n*-type substrate) cut to ~20 mm × 10 mm were used. On the 150 nm nominally *p*-doped SOI substrates Hall effect measurements indicated *n*-type conduction in the top silicon layer, a common occurrence for *p*-type SIMOX wafers known to arise from the formation of oxygen related donors at the BOX interface (dopant overcompensation) discussed already in section 3.3.2.2. The average carrier density in the top Si film was of the order of n_b=1×10^{15} cm^{-3}, determined from Hall effect and sheet resistance measurements. The native oxide was cleaned in piranha solution (3:1 H_2SO_4:H_2O_2) at 120 ^{o}C for 20 min., rinsed in milliQ water (18 MΩ·cm) then etched in dilute HF (2%) for 2 minutes. *Hazards*: Piranha solution should be handled with caution using the appropriate protective garments and kept isolated from other organic substances. Protective measures and caution should be exercised handling HF solutions. Tungsten probes were used to make electrical contact to ~1 mm sized Eutectic Gallium Indium (EGaIn) drops which were used to form the source and drain contacts to the H-terminated surface. Contacts were separated by <5 mm. The substrate back-contact was also formed by applying EGaIn to the HF etched surface. The source was the signal ground. A drain-to-source voltage (V_D) and gate-to-source voltage (V_G) were applied and the drain current (I_D) and leakage from gate-to-source (I_{GS}) were monitored as a function of time and gate bias using two Keithley 2400 source-measure

units. When large gate leakage currents were encountered the samples were discarded. Sidewall leakage from the Si film edge to the substrate was suspected. The sample was mounted in a newly built "Gen 2" small turbo-pumped high vacuum system with base pressure up to 10^{-7} Torr designed for carrying out electrical measurements during controlled exposure to various gases, as described in Ch2.

Decyl monolayers were formed via a recently reported gas phase photochemical route [Eves06]. H-terminated samples were quickly transferred to a small home-built vacuum chamber backed by a sorption pump with base pressure $<10^{-4}$ Torr. The chamber was equipped with a UV transparent sapphire port allowing 60% transmission at 190 nm as measured by a spectrophotometer. Freeze-pump thawed 1-decene vapour (~1 Torr) was leaked into the chamber and irradiated with a Hg-Ne spectral calibration lamp (Oriel 6035) for 10 minutes. Attenuated Total Reflection Fourier Transform Infrared Spectroscopy (ATR-FTIR) was used to confirm monolayer formation. FTIR spectra were obtained on Si(100) ATR elements (25mm long, 1mm thick with 45° bevels obtained from Harrick Scientific). Spectra were acquired using an N_2-purged Nicolet MAGNA-IR spectrometer equipped with a HgCdTe detector. The resolution was set to 4 cm^{-1}. Piranha cleaned chemical oxide (SiO_2) was taken as the background spectrum for the Si(100)-H surface whereas the Si(100)-H spectrum was used as the background to obtain the spectrum of the decyl modified Si(100)-**C10** surface.

5.3 Results and Discussion

5.3.1 Physisorption modulates V_{FB} reversibly

The output characteristics $I_D(V_D,V_G)$ of a SOI-H *n*-channel Ψ-MOSFET operating in accumulation mode, measured under vacuum and during exposure to water vapour are shown in Figure 5.1a.

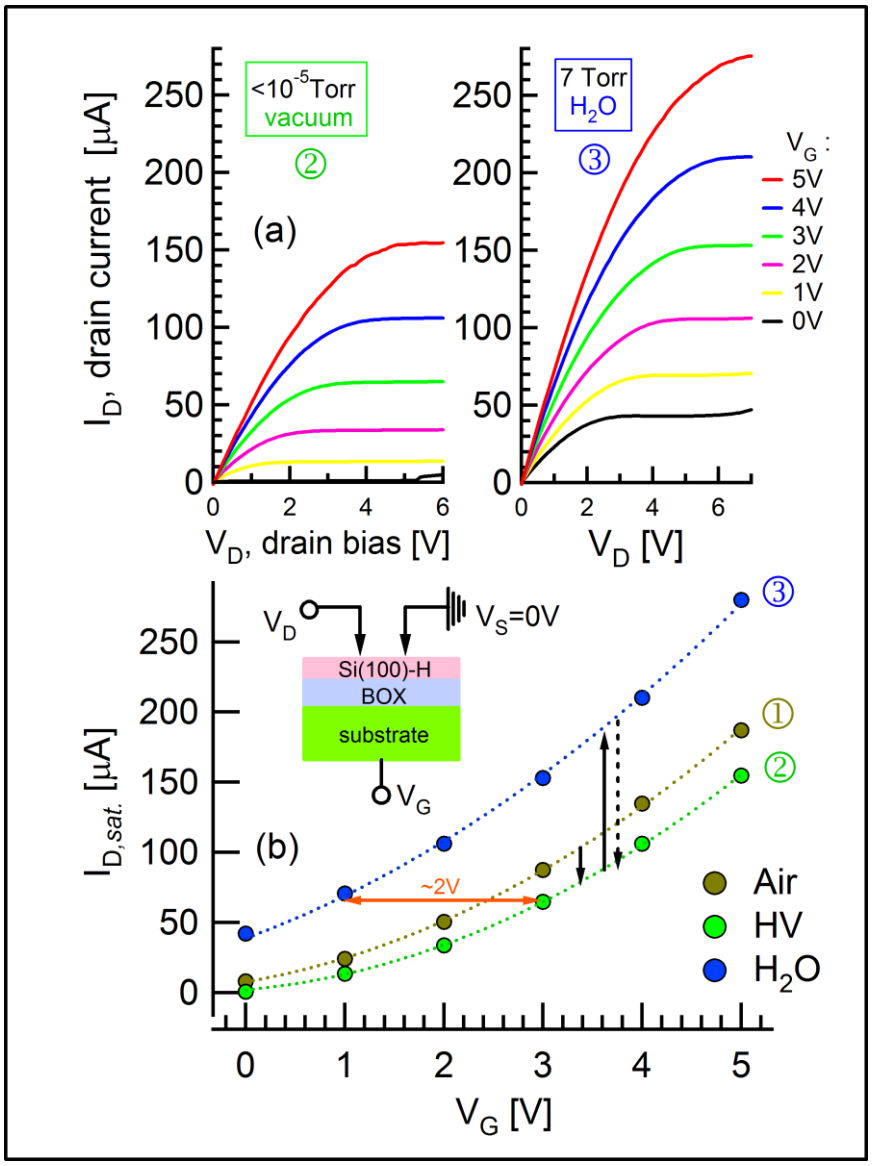

Figure 5.1 (a) Comparison of drain current (I_D) *vs* drain voltage (V_D) of 150 nm thick *n*-type (100) H-Terminated SIMOX operating in accumulation mode, under high vacuum (<10^{-5} Torr) and 7 Torr H_2O (g) environments. (b) I_D in saturation *vs* V_G from ambient initially (**1**), to <10^{-5} Torr high-vacuum (**2**), to 7 Torr water exposure (**3**), shows the stretch factor β_{sat}, which is proportional to a mobility-capacitance product $\mu_{sat}C_{box}$, is practically unchanged between transitions. However the relative change in V_{FB} is extremely sensitive to H_2O coverage, spanning ~2 V. Dotted lines are parabolic fits used for parameter extraction. A schematic of the pseudo-MOSFET is shown in the inset.

Exposure to water vapour is seen to have a significant effect on the FET characteristics, increasing the current at a given gate voltage. This can be seen clearly by comparing the characteristics at V_G=0 V as the device is "off" under vacuum while significant current is seen when the device is exposed to water vapour. This is further apparent from Figure 5.1b where the drain current in saturation ($I_{D,sat}$) is plotted versus gate voltage V_G for the SOI-H Ψ-MOSFET in three different environments: ambient (**1**), vacuum (**2**) and under 7 Torr of water vapour (**3**).

Before a formal analysis, it is already evident that the flat-band shifts are large enough to be estimated by visual inspection of the data in Figure 5.1. For instance, a ~2 V difference between vacuum *vs* water exposure is clearly observable by comparing adjacent sets of *I-V* traces in Figure 5.1a, and also apparent from the separation of saturation curves along the V_G-axis shown in Figure 5.1b. Analytically, the Ψ-MOSFET characteristics in saturation and linear (triode) modes of operations are analogous to the standard MOS transistor [Cristoloveanu00]. In the saturation regime $V_D>V_G-V_{FB}$ the drain current is properly described by $I_{D,sat}=½\beta_{sat}\cdot(V_G-V_{FB})^2$ as plotted in Figure 5.1b. Plots of this type can be fit with a two-parameter parabolic equation to determine V_{FB} and the gain factor $\beta_{sat}=f_g\cdot\mu_{sat}C_{box}$. This stretch factor incorporates a geometric coefficient f_g representing the actual aspect ratio of the channel formed, which was not measured in this study. Importantly, β_{sat} directly relates to a mobility-capacitance product $\mu_{sat}C_{box}$. The buried oxide capacitance per unit area is $C_{box}=\varepsilon_0\varepsilon_{box}/d_{box}$=9.2 nF/cm^2 using a relative permittivity ε_{box}=3.9 and thickness d_{box}=377 nm. It should be noted that in this model the high-field effective electron mobility μ_{sat} is in general influenced by many factors, including the series resistance of the contacts, as well as the lateral and vertical fields applied by the drain and gate biases, which cause mobility-attenuation [Cristoloveanu00].

The set of parabolas in Figure 5.1b are observed to have similar shapes; they can be practically superimposed onto one another by simple horizontal translations (corresponding to flat-band shifts) parallel to the V_G-axis. This is quantified by extracting similar stretch factors in the three environments β_{sat}(**1**)=9.6±0.2 μA/V^2, β_{sat}(**2**)=9.7±0.2 μA/V^2 and β_{sat}(**3**)=8.7±0.3 μA/V^2, corresponding to an average $<\beta_{sat}>$=9.3±0.6 μA/V^2.

This indicates that the product $\mu_{sat}C_{box}$ remains essentially constant in the three environments, and hence μ_{sat} itself is largely unaffected between transitions, as C_{box} is not expected to change. Based on comparing their *I-V* characteristics with four-probe measurements the geometric coefficient has been reported to be f_g=0.75 for a range of probe separations <5 mm [Cristoloveanu00], similar to that used here. Using this value of f_g yields an estimated apparent mobility of $<\mu_{sat}>\approx 1360\pm80$ cm^2/V·s.

In contrast to the stretching factor, the flat-band voltage is highly sensitive to the chemical environment: V_{FB}(**1**)=-1.3±0.05 V, V_{FB}(**2**)=-0.7±0.04 V and V_{FB}(**3**)=-3.0±0.1 V. Furthermore, the sample can be cycled between vacuum and water-exposed states reversibly (**2**)↔(**3**), reproducing the same values for V_{FB} and β_{sat} each cycle. This indicates that water adsorption on the H-terminated surface is a reversible process that does not itself degrade the electronic properties, consistent with previous studies (3.2.4) [Morita90;MacLaren02] and with the conductivity measurements presented in Ch3. Further confirmation of the low reactivity is evidenced by surface characterization with High Resolution Energy Loss Spectroscopy (HREELS) spectra of H-Terminated samples which show no evidence of oxidation after 7 h. exposure to H_2O under similar pressure conditions as in the electrical measurements (Figure 5.1). The observations of a relatively small change in mobility compared to the large change in flat-band voltage mirrors the measurements presented in Ch3, which found that adsorption of water induced changes in sheet resistance primarily due to changes in carrier density (band-bending) as opposed to changes in charge carrier mobility (scattering).

The surprisingly large effects induced by water are exceeded by other donor-type gases. Pyridine exposure at similar pressures to water (7 Torr) increased the channel conductivity significantly enough to suppress saturation at the same bias conditions used for water as in Figure 5.1a. However the relative gating strength could still be compared in the linear mode of operation as shown in Figure 5.2a,b and resulted in similar parameter extraction and the same trends between species computed for the quadratic regime in Figure 5.1b.

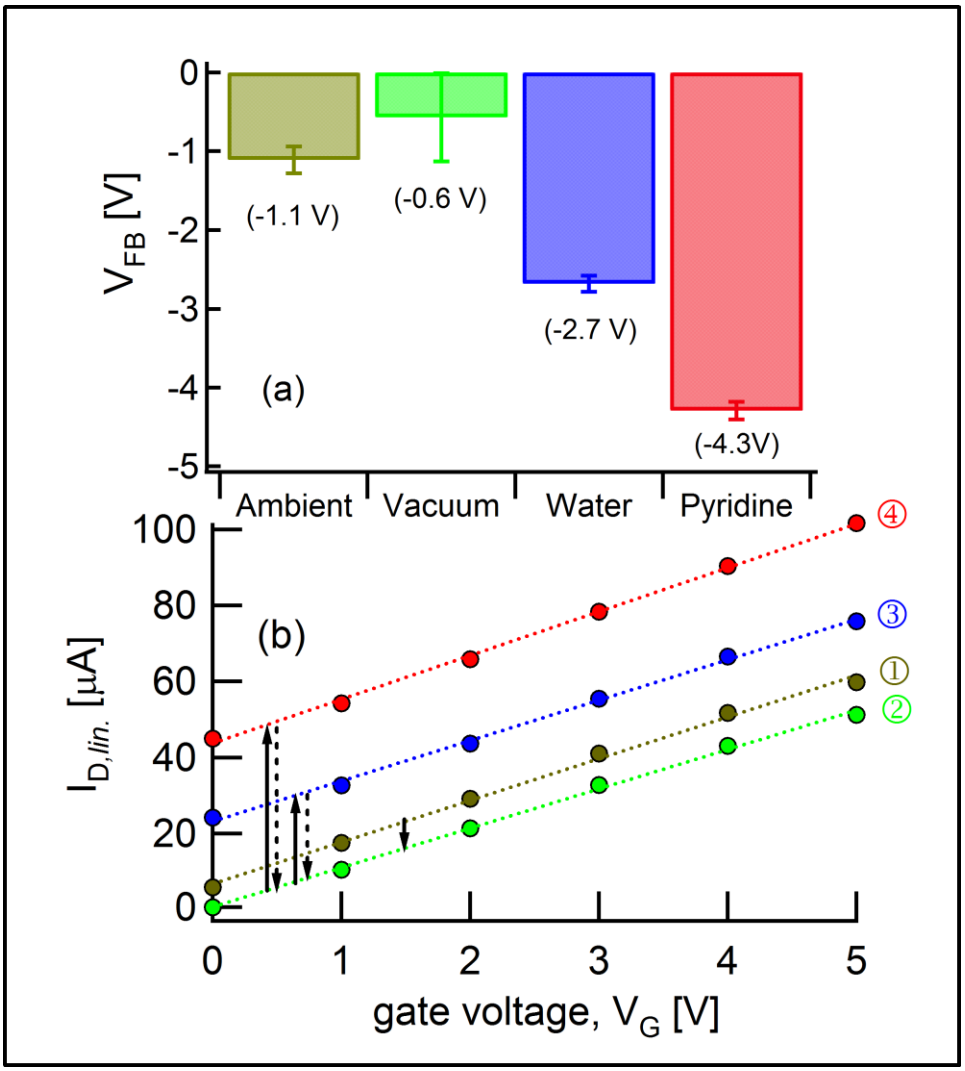

Figure 5.2: SOI(100)-H (a) flat-band voltages (V_{FB}) extracted in linear operation across ambient (**1**), <10^{-5} Torr vacuum (**2**), 7 Torr water (**3**) and 7 Torr pyridine (**4**) saturated environments. (b) Corresponding $I_{D,lin}$ *vs* V_G traces at V_D=1 V clearly shows the large shifts between transitions, indicated by solid arrows. The constant slopes but changing intercept implies only V_{FB} is affected by the medium. V_{FB} and $\mu_{lin}C_{box}$ were reproduced in vacuum after desorbing the molecules, confirming the effects arise from physisorption and are reversible, as indicated by the dashed arrows.

Comparison of the flat-band voltages extracted in the linear region is illustrated in Figure 5.2a at each of the stages; ambient (**1**), vacuum (**2**), water (**3**), and pyridine (**4**) and the corresponding I_D-V_G relationships are provided below in Figure 5.2b.

In the triode regime the dependence of the drain current ($I_{D,lin}$) is linear in gate voltage, described by $I_{D,lin}=a\cdot V_G+b$, with slope $a=\beta_{lin}V_D$ and intercept $b=\beta_{lin}V_D(V_{FB}+½V_D)$. Analogous to the case for saturation, $\beta_{lin}=f_g\cdot\mu_{lin}C_{box}$ is proportional to a mobility-capacitance product where μ_{lin} is the low-field effective electron mobility, also dependent on gate bias and contact resistance [Cristoloveanu00]. The slopes and intercepts from Figure 5.2b are used to determine $\beta_{lin}=a/V_D$ and $V_{FB}=-½V_D-b/a$. Immediately observable in Figure 5.2b, all four lines are parallel but vary significantly in intercept, which results in quite different values for V_{FB} (Figure 5.2a) depending on the chemical state, as was the case in saturation. At V_D=1 V the slope determination gives: β_{lin}(**1**)=11.00±0.03 μA/V^2, β_{lin}(**2**)=10.40±0.02 μA/V^2, β_{lin}(**3**)=10.60±0.02 μA/V^2 and β_{lin}(**4**)=11.50±0.02 μA/V^2 corresponding to an average $<\beta_{lin}>$=10.90±0.5 μA/V^2. This result is ~17% larger than $<\beta_{sat}>$ presented earlier, which can be understood by the lateral-field reduction of mobility μ_{sat} compared to the low-field limit μ_{lin} [Cristoloveanu00].

Analogous to the similar gain factors obtained in saturation, the constant slopes in the triode regime shows that the Ψ-MOSFET is primarily responding by changing V_{FB} instead of the field-effect mobility. After pyridine exposure and evacuation the original characteristics were recovered in vacuum indicating that the molecule does not induce irreversible changes to the H-terminated surface, namely (**2**)↔(**4**) is a reversible process (Ch4), as was similarly shown for water, (**2**)↔(**3**) (Ch3). The large -3.7 V shift in V_{FB} upon exposure to pyridine is similar to changes observed on silicon nanowire based FETs exposed to NH_3 vapour [Talin06].

5.3.2 Estimating the adsorption induced surface charge

The change in V_{FB} induced by water and pyridine vapours is consistent with the adsorbates inducing positive charge densities at the surface as observed previously with conductivity measurements in Ch3 and Ch4. Downward band-bending induced by this positive charge draws electron density toward the surface, resulting in the threshold for accumulation (*n*-channel) shifting to more negative values. These changes are further understood in terms of the field penetration depth in silicon. With n_b~10^{15} cm^{-3}, the device layer thickness d=150 nm is of the order of the Debye length L_D=130 nm in the material. Therefore adsorption-induced charges at the top film/vac interface produce fields capable of reaching the buried channel, modulating the conduction.

The absolute flat-band voltage is dependent on several parameters including the work function difference between the substrate gate material and Si film (φ_{MS}), the fixed/trapped and mobile charges in the buried oxide (Q_{box}) at the film/BOX interface, the capacitances of the film (C_{Si}) and buried oxide (C_{box}), the surface charge (Q_s) and interface state density (D_{it2}) at the top film/vac interface [Hovel03], expressed by Eqn. 5.1:

$$V_{FB} = \varphi_{MS} - \frac{C_{Si}}{C_{box}(C_{Si} + qD_{it2})} Q_s - \frac{Q_{box}}{C_{box}}. \qquad (5.1)$$

With respect to shifts in flat-band voltage, most of these parameters are essentially unchanged during adsorption except for the surface charge. Small variations, if any, in φ_{MS}, C_{Si}, C_{box}, Q_{box}, upon adsorption will contribute relatively less to V_{FB} compared to changes in Q_s and D_{it2}. Moreover, we have already confirmed that the top interface state density D_{it2} of SOI-H is unchanged by adsorption of water or pyridine, since the measurements are reversible after the gases are desorbed. Hence, if only Q_s changes and all other terms in the right hand side of Eqn. 5.1 are constant, then the shifts in flat-band voltage (ΔV_{FB}) are proportional to the relative surface charge induced (ΔQ_s) by Eqn. 5.2:

$$\Delta V_{FB} \approx -\alpha \cdot \Delta Q_s, \tag{5.2}$$

where $\alpha = C_{Si}/C_{box}(qD_{it2}+C_{Si})$. The device layer capacitance is $C_{Si}=\varepsilon_0\varepsilon_{Si}/d$ with relative permittivity ε_{Si}=11.9. We have taken $D_{it2}=1\times10^{10}$ $eV^{-1}cm^{-2}$ for the H-terminated surface. Applying this approximation (Eq. 2) to the data in Figure 5.2 yields the following; $\Delta V_{2\leftrightarrow3}=|V_{FB,(3)}-V_{FB,(2)}|$=2.1 V corresponds to $\Delta Q_{s,2\leftrightarrow3}=1.2\times10^{11}$ cm^{-2} between vacuum and water, and $\Delta V_{2\leftrightarrow4}$=3.7 V corresponds to $\Delta Q_{s,2\leftrightarrow4}=2.2\times10^{11}$ cm^{-2} between vacuum and pyridine. These changes in surface charge density are comparable with those induced by pyridine and water adsorption derived from four probe surface conductivity and Hall effect measurements in Ch3 (Table 3.4) and Ch4 (Table 4.2).

5.3.3 Ambient oxidation changes V_{FB} irreversibly

In contrast to the reversible modulation demonstrated by water and pyridine adsorption, reactions on H-terminated Si can induce permanent surface states which cause depletion of majority carriers and thereby irreversibly degrade device performance. Hydrogen terminated surfaces are known to oxidize slowly (over several days) in ambient atmosphere [Graf90;Houston95]. Figure 5.3 illustrates the changes in $I_{D,sat}$-V_G characteristics (Figure 5.3a) and corresponding changes in V_{FB} and β_{sat} (Figure 5.3b) of an SOI-H sample kept in ambient as a function of time. Insets in Figure 5.3b schematically depict the state of the surface termination initially and that expected after significant oxidation in air. As with the previous studies in Ch3, the measurements were carried out in a probestation in the dark with chuck temperature fixed to T=298 K, but the ambient conditions such as humidity were not controlled. The increase in flat-band voltage with time is consistent with previous measurements in Figure 3.2 and Figure 3.3 in which the sheet resistance $R_s(t)$ increases significantly (over similar time scales) as majority carriers become depleted in the device layer.

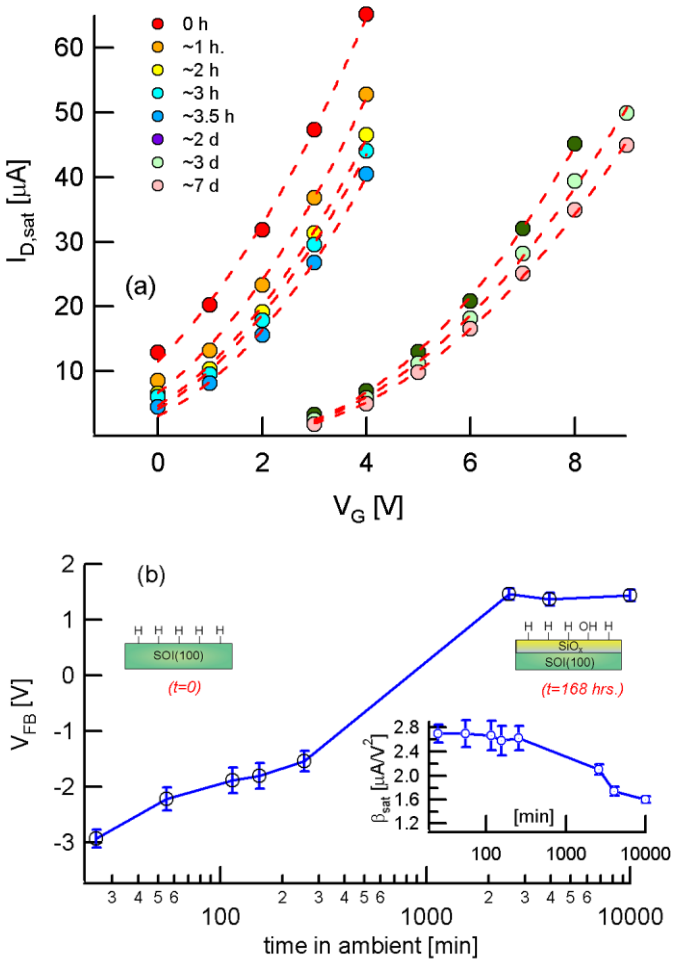

Figure 5.3: Oxidation of 200 nm SOI(100)-H (*n*-doped film/substrate) probed by pseudo-MOSFET measurements over seven days in ambient. (a) $I_{D,sat}$-V_G traces (circles) and parabolic fits (dashed lines) used for parameter extraction. (b) Evolution of V_{FB} for a Ψ-MOSFET. Corresponding changes in the gain factor β_{sat} are shown in the inset. As the surface incorporates oxygen, creation of interface states significantly raises the flat-band voltage and decreases the effective electron mobility.

Drift in the *I*-*V* traces is observable immediately after H-termination. Initially negative, V_{FB} is seen to change fairly rapidly, increasing by ~1 V in the first two hours. For longer exposures the flat-band voltage continues to increase, crossing over from negative to positive values up to ~36 h at which point it remains relatively constant. Quantitative interpretation of this shift is complicated since both the interface state density (due to

oxidation) and surface charge density (induced by water) change as the native oxide forms. Both processes affect the flat-band voltage and cannot be separated from one another in the present experiments.

Furthermore, the shapes of the $I_{D,sat}$-V_G parabolas slowly change during this process, resulting in an overall reduction in β_{sat} by 40% as shown in the inset of Figure 5.3. Lowering of β_{sat} can be attributed to interface roughening as the surface incorporates oxygen with time, causing degradation of the effective mobility. The apparent mobility is initially found to be 390±25 $cm^2/V{\cdot}s$, assuming f_g=0.75. Similar decreases in mobility associated with surface roughness have been noted for methyl terminated SOI(111)-CH_3 surfaces [Green08]. Increasing contact resistance could additionally contribute to the observed mobility lowering. A useful feature of the Ψ-MOSFET configuration is the ability to monitor and separate changes in V_{FB} and β_{sat} at all times. Previously in Ch3 section 3.2.5 (ambient purge experiments) we combined sheet resistance and Hall effect measurements during the early stages of oxidation to separate the carrier density (decreasing with time) from the conductivity mobility (essentially constant) on 1 μm thick SOI-H (Figure 3.7). However at later stages of ambient oxidation the samples became increasingly resistive and do not produce good Hall effect measurements, whereas the pseudo-MOSFET (Figure 5.3) can still be biased into accumulation suitably for parameter extraction. The observations in Figure 5.3 are in agreement with previous experience in section 3.2.5, confirming that degradation of the mobility is mostly observed at the later stages of oxidation (>8 h).

5.3.4 Alkylation

5.3.4.1 Molecular monolayers on silicon

In the past two decades, increasing attention has shifted toward surface modification of silicon to produce high quality interfaces with a focus to passivate and/or functionalize the surface [Wayner02]. Surface modification also has the ability to significantly alter

and/or tailor the chemical and electrical properties at a surface [Cohen97;Lopinski05]. Subsequent modification after H-termination usually involves reactions with molecules containing reactive groups or unsaturated regions e.g. diazonium radicals, alkenes, etc., which graft covalently to the surface to form adlayers called molecular monolayers. Monolayers may already have functionality embedded into their terminal groups e.g. acids, esters, amines, etc. or these may be incorporated afterward in subsequent steps. Silicon is of particular interest for its extensive use in the microelectronics industry, which has enabled single crystal wafers of high purity to be commercially available and fairly inexpensive. There are at least two short term incentives for studying the electronic properties of surface modified silicon. The first is in the area of molecular electronics, in which the transport properties, e.g. current-voltage characteristics through the molecules serves as the active component of transduction for signal amplification [Salomon05]. Although beyond the scope of this work, one can envision molecular electronics on silicon to involve incorporating adlayers of either photo- or electro- switchable molecules onto Si surfaces which interface with conventional CMOS based amplifiers for producing hybrid high density memory or logic [Lopinski06]. The second concept, more relevant to this work, views electrical current carried by the semiconductor as the active component of transduction, in which molecular binding events act to gate electronic transport in the underlying Si, as has been demonstrated already on H-terminated surfaces. This type of field effect is essentially analogous to application of a gate voltage in a conventional CMOS transistor. Such gating effects are not only unique to semiconductors, but could potentially be used in the area of molecular diagnostics, which includes chemical sensors and biosensing applications.

Since the first reports of the formation of covalently attached molecular monolayers on hydrogen-terminated Si(111) [Linford93;Linford95] by solution phase processes, there has already been significant progress in preparation and methods for optimizing monolayer formation and incorporating functionality [Wayner02]. In addition to surface characterization, the resulting electrical properties of these monolayers are beginning to receive increasing attention [Sieval03;Mischki06;Miramond04]. Interface

states arising from oxidation or chemical modification as well as subsequent adsorption and reaction events are expected to have a significant impact on the band-bending and resulting space-charge region. Surface transport measurement by conductivity and/or pseudo-MOSFET geometry offers a systematic means to facilitate these studies.

5.3.4.2 Gas phase alkylation of SOI(100)-H

In order to slow down the degradation of SOI-H caused by ambient oxidation demonstrated in section 5.3.3, the surface can be passivated by molecular monolayers consisting of covalently attached alkyl chains. Most commonly, solution-based methods involving thermal or photochemical reaction of alkenes with H-terminated silicon are used to form these monolayers, rendering the surface more resistant to oxidation [Linford95;Boukherroub99;Popoff10]. In order to use the Ψ-MOSFET technique to probe changes induced by alkyl monolayer formation we have chosen to employ a recently developed gas-phase photochemical alkylation process [Eves06]. In this process, absorption of 185 nm UV photons in the primary alkene $CH_3(CH_2)_kCH=CH_2(g)$ induces photolysis, forming the reactive radical fragments needed to generate dangling bonds on the H-terminated surface (initiation). A radical chain reaction involving the alkene itself directly reacting with these dangling bonds can then propagate on the surface, forming the methyl terminated monolayer $Si\text{-}(CH_2)_{k+2}CH_3$. This approach is found to be ideally suited for forming monolayers on our SOI(100)-H pseudo-MOSFETs. Particularly useful with respect to these measurements is that this process is compatible with prior EGaIn contact placement onto the freshly H-terminated SOI.

Since the previous report of alkyl monolayer formation using the gas phase photochemical route involved the use of atomically flat Si(111)-H substrates, it was necessary to fully characterize monolayers formed on Si(100)-H surfaces using this process. Shown in Figure 5.4 are ATR-FTIR spectra of the freshly etched Si(100)-H surface before and after gas phase photochemical reaction with decene to form a Si-**C10** surface.

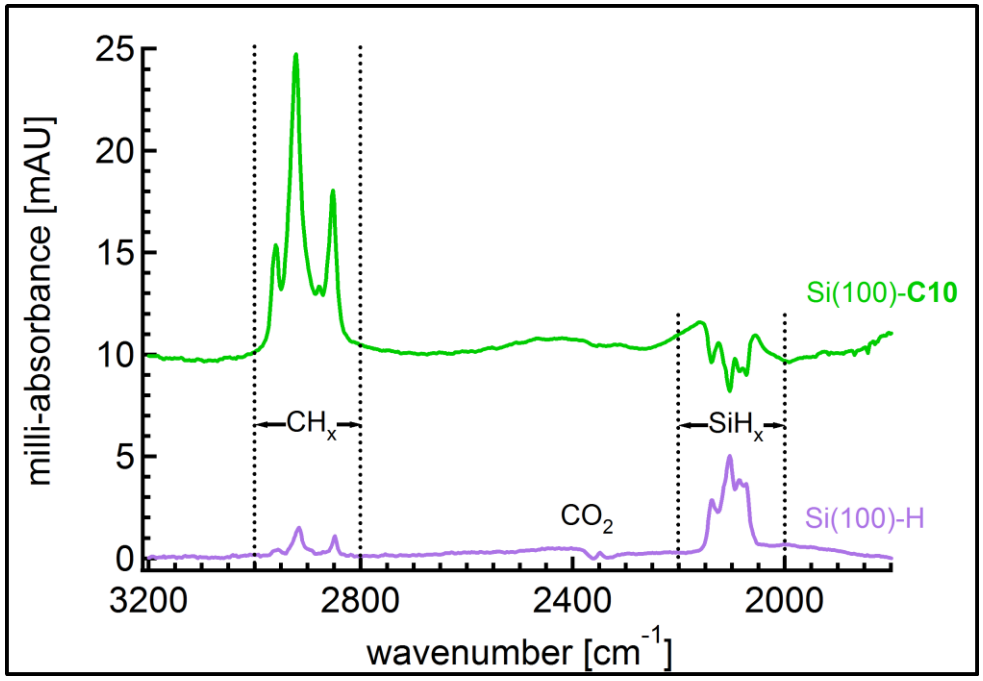

Figure 5.4: ATR-FTIR characterization of monolayer formation using the gas phase photochemical method of Eves *et al*. [Eves06]. Spectra correspond to the initial HF-etched Si(100)-H surface (bottom) and the alkylated Si-**C10** surface (top) formed by a radical chain reaction at 185 nm with 1-decene vapour.

The spectrum of the initial H-terminated surface is dominated by multiple silicon-hydrogen stretch modes. The integrated absorbance from 2070-2130 cm^{-1} is $\int A(\omega) - A_0(\omega)\, d\omega$ =0.25 cm^{-1}±2%, an area routinely obtained after H-termination. An uncertainty level of 2% reflects the variability in area resulting from inspecting several different baselines A_0. There is a small degree of hydrocarbon contamination in the CH_x stretch region, 3000-2800 cm^{-1}, with an integrated absorbance area of 0.058 cm^{-1}±2%. Five distinct modes are visible at $\upsilon_{as}(SiH_3)$=2138 cm^{-1}, $\upsilon_{as}(SiH_2)$=2115 cm^{-1}, $\upsilon_{s}(SiH_2)$=2104 cm^{-1}, $\upsilon_{as}(SiH)$=2086 cm^{-1} and $\upsilon_{s}(SiH)$=2073 cm^{-1}. The first in this series corresponds to the trihydride, the second pair to the asymmetric and symmetric dihydride, whereas the latter two are attributed to the asymmetric and symmetric coupled monohydride stretch modes in rows [Dumas92].

Upon reaction with 1-decene (top spectrum) these SiH_x modes appear as absorbance losses. This reflects the loss of hydrogen from the surface as a result of the reaction (since the H-terminated surface was used as the background). Quantitatively this loss corresponds to an integrated absorbance of -0.14 cm^{-1}±2% or approximately half of the initial hydrogen signal. There is significant absorbance gain in the CH_x region corresponding to an integrated area of 0.76 cm^{-1}±5%. The **C10** monolayer exhibits four modes at $\upsilon_{as}(CH_3)$=2959 cm^{-1}, $\upsilon_{as}(CH_2)$=2922 cm^{-1}, $\upsilon_s(CH_3)$=2878 cm^{-1}, and $\upsilon_s(CH_2)$=2852 cm^{-1} corresponding to methyl and methylene stretch vibrations of asymmetric and symmetric types [Porter87]. The position of the asymmetric methylene stretch at 2922 cm^{-1} indicates the chains are reasonably well packed [Linford95] and of similar quality to monolayers formed using wet chemical methods with 1-decene on Si(111)-H [Linford95;Boukherroub99]. An absorbance maximum of 15.2 mAU (1 mAU≡1 milli-absorbance unit) is measured at this frequency. Correcting for the number of internal reflections (25) and number of methylene units (9), this amounts to a contribution of 0.068 mAU/methylene, which is similar to values reported on Si(111)-H surfaces using solution phase methods. [Boukherroub99,Mischki09].

Additional surface characterization of Si-**C10** monolayers formed on moderately *n*-doped Si(100) wafer samples yielded ellipsometric thicknesses of 12±1Å and static water contact angles of 100±1^o, similar to typical values reported for decyl monolayers on Si(100) [Faber05]. Most importantly these monolayers were observed to have a small degree of band-bending into depletion, 50±15 mV, as measured by their surface photovoltage with an ambient Kelvin probe. For the carrier densities of the wafers used here (n_b~1×10^{15} cm^{-3}) this corresponds to a net surface charge density of Q_s=2×10^{10} cm^{-2}, demonstrating the gas-phase created monolayers produce electrically well-passivated interfaces.

Effects of forming a decyl monolayer on the SOI-H surface via the gas phase route have been studied using the pseudo-MOSFET as shown in Figure 5.5. Good FET output characteristics are obtained for the **C10** passivated surface, although the current at the same gate voltage is clearly reduced with respect to the SOI-H surface. From the

parabolic fits in Figure 5.5b, the decyl termination is found to increase V_{FB} by ~1.9 V and decrease β_{sat} by 15%. The initial mobility on SOI-H was μ_{sat}=1020±60 cm^2/V·s.

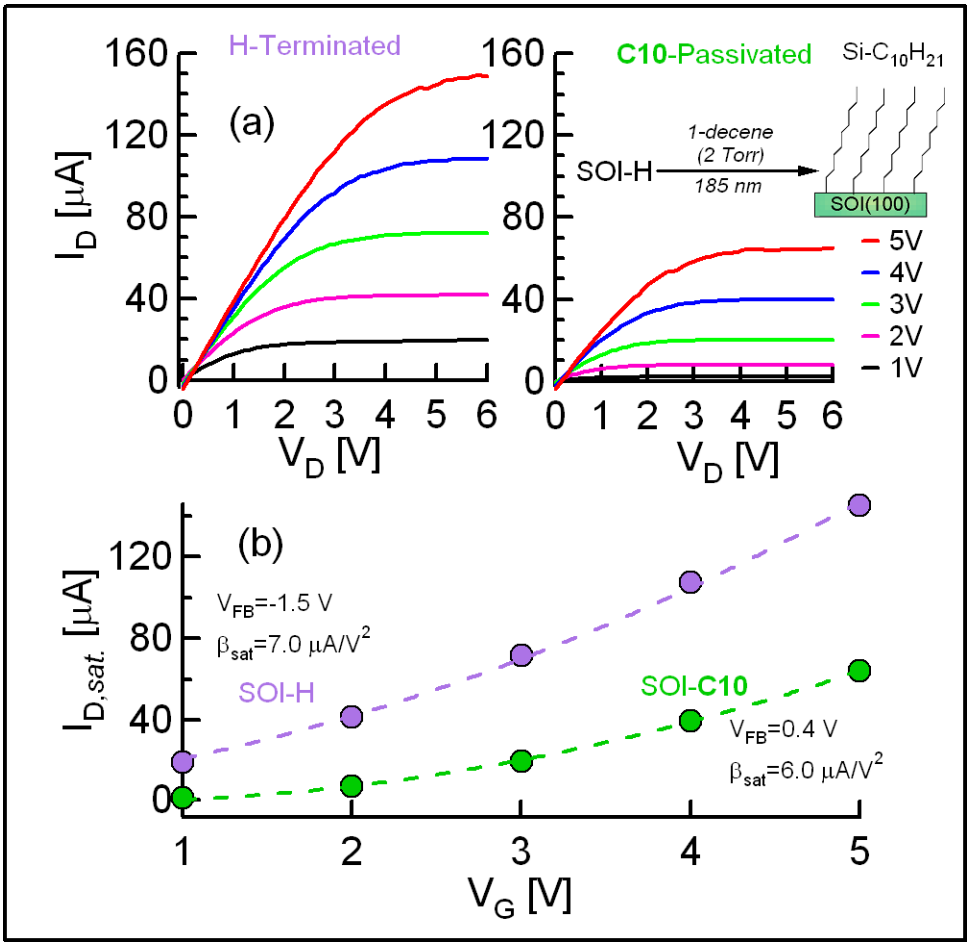

Figure 5.5: Effect of covalent modification of 150 nm SOI(100)-H on the Ψ-MOSFET characteristics. (a) I_D-V_D characteristics taken in ambient on the initial H-terminated surface and after formation of a decyl monolayer SOI-**C10** via a photochemical gas-phase reaction. (b) Corresponding $I_{D,sat}$-V_G curves along with the parameters extracted from the parabolic fits, indicating changes in V_{FB} and β_{sat}.

Part of the observed shift in V_{FB} may be attributed to the creation of electrically active defect states associated with the reaction. The shift in V_{FB} and the small decrease in mobility is consistent with a slight degree of oxidation. However, formation of the

hydrophobic monolayer is also expected to reduce the coverage of adsorbed H_2O at the interface relative to SOI-H, which was shown in section 5.3.1 to have a non-negligible impact on the flat-band voltage determination. Therefore some portion of the increase in V_{FB} is likely caused by (partial) displacement of water by the monolayer. The maximum contribution due to this displacement can be estimated by recalling from Figures 5.1 and 5.2 that V_{FB} increases by ~0.5 V upon pumping SOI-H from ambient to vacuum, corresponding to complete removal of surface bound H_2O. Consistency with the Eq. 5.2 and the observed shifts in V_{FB} from -1.5±0.1 V to 0.4±0.1 V can be obtained by imposing reasonable estimates for D_{it2} from 1.0×10^{10} $cm^{-2}eV^{-1}$ to 3.0×10^{10} $cm^{-2}eV^{-1}$ and Q_s from 1.2×10^{11} cm^{-2} to 1.0×10^{10} cm^{-2}. The cause and nature of interface state formation during this gas-phase process have not been characterized. These may be related to impurities in the decene solution or oxygen present in the background pressure of the chamber, in which case the process could be optimized. They may also originate from the generation of a small density of uncapped dangling bonds (mid-gap states) during the chain reaction. A moderate shift in device characteristics associated with the modification reaction indicates that these monolayers largely preserve the low density of electrically active defects observed on the H-terminated surface and suggests that they should form good passivating layers for molecular sensing applications.

Finally, we note that the gas phase photochemical process for alkyl monolayer formation used in the current work has a number of advantages compared to traditional solution-based methods. These include shorter reaction times (minutes *vs* hours), more efficient use of reagent, more systematic deoxygenating (freeze-pump-thawing *vs* rigorous bubbling in Ar), and no need for rinsing procedures which consume additional organic solvents. General drawbacks of this approach include its limited scope to alkenes with sufficiently high vapour pressure (Torr range), although this can be overcome by elevating the reaction temperature. While the method works well for alkenes with an unreactive terminal group (such as the methyl terminated layers studied here), formation of functional monolayers with reactive groups suitable for subsequent attachment reactions remains a challenge. This is in part because functional terminal groups such as

acid-COOH or amine-NH_2 etc. may also react directly with the H-terminated surface in a photochemical reaction, creating heterogeneous monolayers terminated with both the alkene end and the functional end.

5.4 Conclusions

Accumulation mode pseudo-MOSFETs formed on hydrogen terminated silicon-on-insulator (SOI-H) were used to probe molecular adsorption and reaction events. Current-voltage characteristics of such *n*-channel devices are found to be sensitive to the environment, with the accumulation threshold voltage, or flat-band voltage (V_{FB}), exhibiting large reversible changes upon cycling between ambient atmosphere, high vacuum ($<10^{-5}$ Torr) and exposure to water and pyridine vapour at pressures in the Torr range. The field-effect mobility is found to be comparatively less affected through these transitions. Oxidation of the H-terminated surface in ambient leads to irreversible shifts in both the flat-band voltage and field-effect mobility. A photochemical gas phase reaction with decene is used to form a decyl monolayer (**C10**) on the SOI(100)-H surface. Formation of this monolayer is found to result in a relatively small shift of threshold voltage and only a slight degradation of the field effect mobility, suggesting that alkyl monolayer dielectrics formed in this way could function as good passivating dielectrics in field effect sensing applications.

In summary, the characteristics of the SOI-H Ψ-MOSFET have been shown to be highly sensitive to molecular adsorption and reaction events, and can be used to distinguish between reversible adsorption induced modulation as opposed to irreversible reaction induced changes. Appreciable top-gating action of molecular adsorbates water and pyridine is shown to be highly reversible at room temperature and thus consistent with an adsorption induced charge transfer interaction. Such large shifts in flat-band voltage caused by charge transfer from donor type molecules is consistent with our previous studies in Ch3 and Ch4 and invites further experimental and theoretical investigations. Additionally, the influence of chemical modification can be probed

systematically by use of a controlled gas-phase alkylation process to form high quality ultra-thin organic dielectrics on SOI(100)-H. The passivation properties of these monolayers against oxidation and their response to adsorption of molecular species warrant further investigation. These studies demonstrate the utility of the Ψ-MOSFET as a fast and simple approach for probing molecule-surface interactions on chemically modified silicon surfaces.

Chapter 6

Sensitivity to Electron Acceptors

6.1 Introduction

A common feature throughout these studies is that adsorption events can lead to charge re-distribution on silicon surfaces which significantly alters the substrate conductivity through long-range electric field-effects. This principle suggests a strategy for molecular sensing is possible using oxide-free SOI platforms to enhance the sensitivity. Thus far the electrical response of SOI substrates has been used to monitor a range of surface processes including surface state conduction on clean surfaces in ultrahigh vacuum [Yoo01b;Zhang06a], biomolecule [Nikolaides04;Neff07] and gas adsorption [Takulapalli10] on oxidized surfaces, and covalent modification of hydrogen terminated surfaces by polar molecules [He06;He09], indicating the motivation for their use in real applications already exists and is progressing.

In the preceding chapters we have discussed our own work and that of others which has shown lightly doped (~10^{15} cm^{-3}) hydrogen terminated silicon-on-insulator (SOI-H) to be a highly sensitive platform for electrical monitoring of molecular

adsorption. Adsorbed gases including water (Ch3), pyridine, alcohols and other amines (Ch4) are all found to behave as positively charged species on H-terminated silicon, inducing accumulation of majority carriers on *n*-type and depletion-inversion on *p*-type surfaces with varying strengths (surface charge in the range $+10^{11}$ to $+10^{12}$ $q \cdot cm^{-2}$). As a result these species modulate the conductivity of the device layer through field-effects causing downward band-bending, as confirmed by transport measurements via four-probe sheet resistance/Hall Effect (Ch3,4) as well as two-probe pseudo-MOSFET measurements (Ch5). We refer to these molecules collectively as electron donors. In contrast to donors, molecules that behave as electron acceptors on silicon are expected to induce the opposite surface charge (negative) and band-bending (upward) thereby depleting *n*-type surfaces of majority electrons or accumulating majority holes at *p*-type surfaces. In this chapter we explore the effects of some electron acceptors which were found to substantially modulate the electrical properties of oxide-free SOI-H. In particular we focus on the electron acceptor TCNE.

Adsorption of tetracyanoethylene (TCNE) onto a hydrogen terminated silicon-on-insulator (SOI) surface is shown to strongly modulate the conductivity, inducing significant depletion of majority carriers on *n*-type SOI (section 6.2). Employing a pseudo-MOS transistor, ppm levels of TCNE vapour in ambient atmosphere are found to rapidly decrease the *n*-channel saturation current by at least two orders of magnitude. The effect is only partially reversible on the hydrogen terminated surface, which can be attributed to the accumulation of strongly bound TCNE species on the surface. Covalent passivation of the SOI surface with a decyl monolayer improves the reversibility of the response while only slightly decreasing the sensitivity. On either modification, the current modulation is found to reach a maximum at a substrate temperature around 60 ^{o}C. The strong interaction of TCNE on H-terminated bulk silicon is also studied by HREELS and in-situ STM imaging during dosing of TCNE in UHV (section 6.3). In addition to TCNE, the influence of other electron acceptors on SOI-H pseudo-MOSFETs such as 2,4,6-trinitrotoluene (TNT) is briefly discussed (section 6.4). These observations are

promising for future field-effect applications of silicon in the detection of electron accepting species.

6.2 TCNE

Tetracyanoethylene, C_6N_4 (TCNE) is a prominent electron acceptor with an electron affinity of 3.2 eV [Chowdhury86]. TCNE forms classic charge-transfer complexes with many organic compounds [Merrifield58;Rettig69], and exhibits molecular magnetism in special inorganic metal complexes [Miller98]. There is growing interest to study interactions between TCNE and electronic materials such as graphene [Lu09;Sun10;Coletti10] and single crystal metal surfaces in UHV [Bedwani08;Wegner08;Wegner09]. For instance, Lu and co-authors used DFT calculations to show that TCNE molecules adsorbed on graphene results in a charge transfer of 0.44*e* from graphene to TCNE [Lu09]; based on this strong molecule-substrate interaction the authors predict that the formation of a charge-transfer bond between TCNE and graphene results in *p*-type graphene. Although verification of this interaction has not been tested yet, a recent experiment concluded adsorption of a related electron acceptor, TCNQ (tetracyanoquinodimethane) suppresses the intrinsic *n*-type doping of epitaxial graphene on SiC(0001) [Coletti10] in agreement with the trend predicted by Luo et al.

Single molecules of TCNE have recently been shown to exhibit varying degrees of charge transfer and/or bonding with metal surfaces [Wegner08;Wegner09] depending on the intermolecular versus substrate interactions. In these studies the Crommie group used STM/STS at 4K and complementary DFT calculations [Wegner08]. On Au(111) TCNE molecules form loosely bound randomly oriented islands (easily manipulated by the STM tip) and the dominant interactions are intermolecular quadrupole forces. In contrast isolated flat-lying monomers are formed on Ag(100) due to charge-transfer and Coulomb repulsion between $TCNE^{2-}$ species, whereas tightly bound rectangular structures form compactly on Cu(100) attributed to strong chemical bonding between Cu

atoms and cyano-groups (appearing as four extended-legs in the STM images) in addition to charge transfer. The authors explain the weak interaction between TCNE and gold by noting that atomic Au has the largest electron affinity in the series (2.31 eV) compared to that of silver (1.30 eV) or copper (1.24 eV). The tendency to form chains on Cu(100) rather than isolated islands as on Ag(100) is rationalized by the shorter lattice constant (Cu: 2.55 Å *vs* Ag: 2.89 Å) favouring a substrate mediated self-assembly process. While charge transfer on metals is expected to change electronic properties such as work function and electron affinity, other properties such as electrical conductivity of these structures remains the same. Similar charge transfer effects as observed on TCNE/Ag(100) or TCNE/Cu(100) on a semiconductor such as silicon would be expected to induce a substantial field effect. Selective formation of charge transfer complexes with TCNE and substituted phenylhydrazines (methoxy-, dinitro-) grafted onto H-terminated silicon have been studied recently in our group (unpublished) using surface photovoltage measurements (SPV), in an effort to prepare electronically tailored surfaces. These preliminary studies inspired investigation of the effect of TCNE directly adsorbed onto the bare silicon surface.

6.2.1 Physical properties of TCNE

Table 6.1: Important physical properties of TCNE.

Property	Assignment	Reference
Synthesis	1957	[Cairns57;Cairns58;Heckert57]
Electron affinity	3.17±0.20 eV	[Chowdhury86]
Enthalpy of sublimation	18.65 kcal/mol	[Looney58]
Vapour pressure at 20 ^{o}C	2×10^{-3} Torr	[Boyd63]
Crystal structure	monoclinic and cubic	[Bekoe60]
HOMO-LUMO gap	10.3 eV	[Bélemlilga99]

Noteworthy properties of TCNE and associated studies are listed in Table 6.1. The large electron affinity of TCNE arises from the low electron density around the central alkene, resultant from the four surrounding electronegative cyanide (CN) groups. The basic properties, chemical reactivity and common charge transfer complexes of TCNE can be found in several thorough reviews [Dhar67;Miller06; Bélemlilga99].

In the experiments (section 6.2.2) purum grade (98%) tetracyanoethylene; white crystalline solid; C_6N_4; FW 128.09; mp 198 ^oC, from Sigma-Aldrich was stored at 4 ^oC, then warmed to room temperature for use. ^{13}C NMR confirmed the level of impurities are in the 1% range and can be attributed mostly to water and dicyano- or tricyano- olefin species. The NMR facility was operated by D. Leek. Since TCNE is very toxic caution is advised when working with powders in the lab. TCNE slowly evolves hydrogen cyanide (HCN) in moist air at room temperature [Cairns57]. It should be handled with appropriate protective equipment, including a full-face particle respirator type N100 (US). Consult a material safety data sheet before (MSDS) use.

6.2.2 Adsorption of TCNE on pseudo-MOSFETs

An *n*-channel pseudo-MOSFET [Cristoloveanu92] formed on chemically modified SOI surfaces is used to investigate the interaction of TCNE with oxide-free silicon. TCNE exposure is found to lead to large changes in the output characteristics of the device, reducing the drain current in saturation by at least two orders in magnitude, corresponding to flat-band shifts of ~1 V or higher. Surprisingly, this effect is observed readily in ambient atmosphere by simply exposing a source of solid TCNE in close proximity (<5 mm) to the Si device layer, allowing its room temperature sublimation vapour (2×10^{-3} Torr) [Boyd63] to adsorb onto the surface. While a large response is observed on SOI-H, the current modulation is not completely reversible. Chemical modification of SOI-H to form a decyl monolayer (SOI-**C10**) improves the degree of reversibility in drain current while only reducing the current modulation approximately five-fold. These observations suggest that TCNE behaves as an electron acceptor on

silicon, adsorbing with anionic character, inducing depletion of majority carriers on the *n*-type substrates used here. Figure 6.1 shows a schematic representation of the experiments.

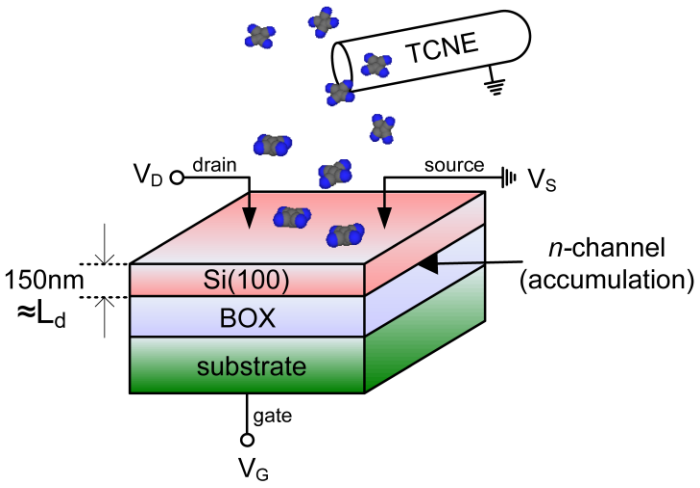

Figure 6.1: Schematic illustration of the experiments (not to scale). Solid TCNE powders are brought in close proximity (<5 mm) to a surface for a controlled duration (3 s), and then retracted. The drain current is monitored and the exposure is repeated at the same conditions. Delivery ampules (glass vial or metallic cap) are grounded to the source contact. The partial TCNE sublimation vapour pressure (2 mTorr) out of ambient (760 Torr) corresponds to a maximum concentration of 3 ppm above the surface.

As described in Ch5 (section 5.2) in the pseudo-MOSFET configuration, the source and drain contacts are formed at the top surface, which serves as the active sensing element. Application of a gate voltage (V_G) on the silicon substrate modulates the current between source and drain. Details of contact formation, H-termination and electrical measurements have been discussed previously in Ch5. The SOI used here is made by the SIMOX method starting from lightly *n*-doped (~1×10^{15} cm^{-2}) Si(100). Application of a positive gate voltage (with respect to the source contact) is used to activate a conductive majority (electron) channel at the device layer/buried oxide(BOX) interface (accumulation mode). The voltage required to induce this channel is termed the flat-band voltage V_{FB}, and is determined from the drain current I_D *vs* drain voltage characteristics (Ch5). To monitor the effect of TCNE exposure, the saturation drain current $I_{D,sat}$ at fixed

V_D and V_G is measured as a function of time as the TCNE source is introduced and then retracted over the sensing area between the top contacts. Current response $I_{D,sat}$(t) of the SOI-H surface to four 3 s exposures of TCNE is shown in Figure 6.2a at V_G=3 V and V_D=5 V.

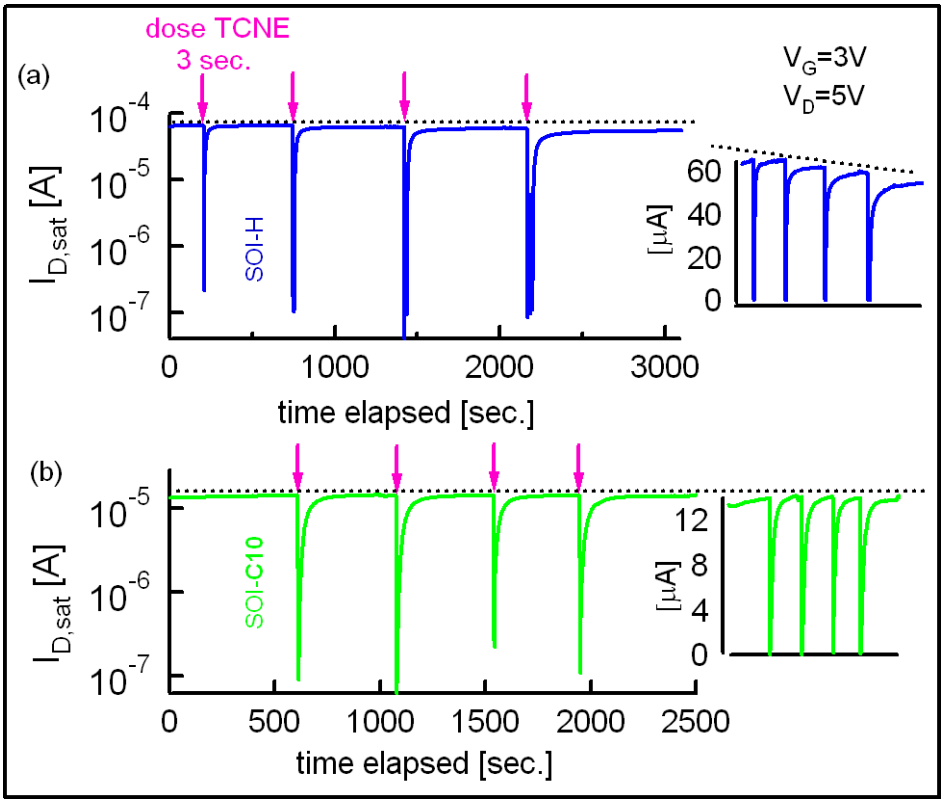

Figure 6.2: Current response *vs* time with successive TCNE doses (marked by arrows) in ambient shown for (a) H-Termination (SOI-H) and (b) Decyl-Modification (SOI-**C10**). The drain current in saturation $I_{D,sat}$(t) is sampled at 1 Hz at a substrate voltage of V_G=3 V and drain voltage of V_D=5 V. The SOI device layer is *n*-type (100) SIMOX operating in accumulation mode and the substrate temperature is set to 60 ^{o}C. Dashed lines mark the baseline current. The current responses on a linear scale are shown in the insets on the right to more clearly show changes in reversibility.

To increase reversibility and reduce recovery times, the substrate was heated to 60 ^{o}C, which was also found to give the highest sensitivity (temperature dependence is discussed below). The source containing TCNE powder was positioned ~5 mm above the surface

for approximately 3 s before it was retracted, to control for the molecular flux at each iteration. This exposure time was chosen based on the minimum duration required to induce a large signal that recovered in a reasonable amount of time. Although longer exposure times/shorter distances produced stronger effects on SOI-H, they were slower to recover and less reversible. Shortly after introducing TCNE, the current drops abruptly by over two orders of magnitude. A control vial with no molecule did not change the drain current. In Figure 6.2a, the current max./min. values from left to right at each dose are 65.4 μA / 220 nA, 64.7 μA / 110 nA, 61.5 μA / 40 nA and 59.1 μA / 86 nA, of which the largest modulation produced on the third dose, is equivalent to an ON/OFF ratio of I_{max}/I_{min}~1.5×10^3. This On/Off ratio I_{max}/I_{min} is somewhat variable, ranging from 3.0×10^2 to 1.5×10^3; since manipulation of the TCNE source was done manually, control over the flux at the surface is likely the largest source of experimental error. The current response is seen to be largely reversible with the current rapidly recovering to close its initial value, presumably due to the TCNE desorbing from the surface. Close examination of the current response shows the recovery of the current upon retracting the source is not complete. This is clearly seen in the inset to the right of Figure 6.2a where the response is plotted on a linear scale and the current is seen to return to a lower value after each successive exposure. By the end of the 4th dose, I_{max} is reduced by ~17% with respect to the initial value. These observations indicate that the effect of TCNE is only partially reversible on SOI-H. This is not too surprising as the H-terminated surface is known to oxidize in ambient, causing shifts in the flat-band voltage as shown previously in section 5.3.3 Figure 5.3. In addition, some TCNE could remain on the surface due to a very strong physical interaction or even reaction with the H-terminated surface (section 6.3).

To improve the stability of the device layer, the SOI-H surface was modified by a gas-phase, photochemically-induced reaction with decene [Eves06] as described in Ch5, to form a decyl monolayer, Si-$(CH_2)_9CH_3$ (SOI-**C10**). The current response of this decyl modified surface to TCNE adsorption (under the same conditions as for SOI-H) is shown in Figure 6.2b. The lower initial current level observed on SOI-**C10** is attributed to interface state formation during the alkylation process (section 5.3.4.2). Exposure of

TCNE on the decyl modified surface still leads to large changes in current, although the On/Off ratios are somewhat reduced (~0.6×10^2-2.3×10^2). In Figure 6.2b, the current max./min. values from left to right at each dose are 13.9 μA / 90 nA, 14.0 μA / 62 nA, 13.9 μA / 220 nA and 14.0 μA / 109 nA of which the largest modulation produced on the second dose, is equivalent to an ON/OFF ratio of I_{max}/I_{min}~2.3×10^2. Decyl modification clearly improves the reversibility of the response with no overall decrease in current observed after the 4th dose as seen in the linear plot to the right of Figure 6.2b. Interestingly, the presence of the dielectric monolayer (with thickness ~1 nm) only moderately reduces the tendency of the adsorbed TCNE molecules to abstract electrons from the surface. A possible mechanism involves adsorption onto the monolayer followed by electron abstraction across the ultra-thin insulating barrier. Partial penetration of TCNE molecules into the monolayer is also conceivable, although less likely since the alkyl chains are densely packed (section 5.3.4.2).

6.2.3 Surface characterization

Surface vibrational spectroscopies were used to further probe the interaction of TCNE with hydrogen and decyl terminated Si(100) surfaces and account for the observations made in the electrical measurements. Attenuated total internal reflection Fourier transform infrared (ATR-FTIR) spectra for both surfaces upon exposure to TCNE are shown in Figure 6.3. On the Si(100)-H surface (Figure 6.3a), successive exposure of TCNE leads to a broad absorbance band from 2180-2260 cm^{-1}, with a distinct peak centered at 2220 cm^{-1} and a weaker shoulder at 2195 cm^{-1}. These features overlap with the range of nitrile group stretch frequencies known for various TCNE complexes [Miller06], thereby suggestive of monolayer level coverage of TCNE that does not desorb effectively at room temperature. Additionally, the weak shoulder at 2195 cm^{-1} is within the acceptable range for an anionic species $TCNE^-$, although assignment of this peak is not definitive. In contrast to the behaviour on Si-H, the same exposure conditions on Si-**C10** did not produce peaks in the CN region as shown in Figure 6.3b. The absence

of persistent TCNE related modes on the decyl surface is consistent with the increased reversibility in the electrical signals observed in Figure 6.2b.

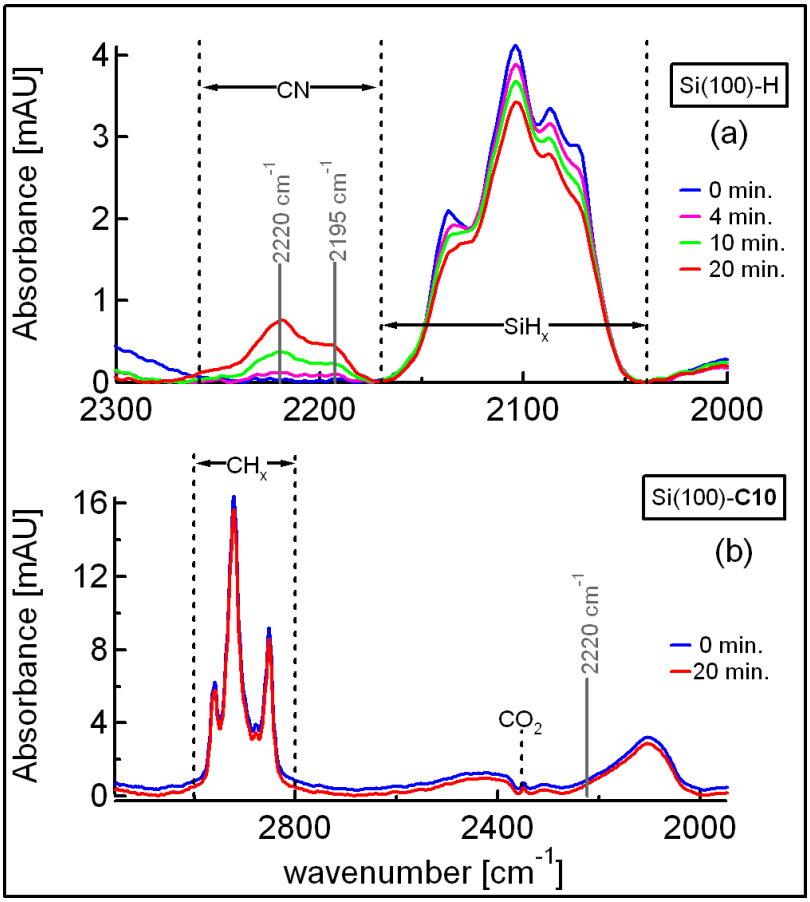

Figure 6.3: ATR-FTIR spectroscopy shows (a) the appearance of the nitrile group stretch at ν_{CN}=2220 cm^{-1} after 10 min exposure of TCNE on Si(100)-H and (b) the absence of the CN stretch on Si(100)-**C10** under the same exposure conditions (spectra have been offset).

Since the exposure was carried out in ambient air the possibility of forming a hydrolyzed species related to TCNE on the surface was also considered; TCNE adsorption on alumina hydrolyzes forming the tricyanoalcoholate ion $C_2(CN)_3OH^-$ [Hipps82;Mazur84] but we did not observe evidence for the expected C-O band around 1580 cm^{-1} (there is broad absorbance in this region before or after exposure). Therefore we cannot conclude

the TVA ion is formed on SOI(100)-H in large amounts or responsible for the irreversible component in the electrical measurements. This is not particularly surprising since H-terminated silicon is hydrophobic with a contact angle 86 degrees, unlike alumina surfaces which are hydrophilic. Since submonolayer levels of water are expected on H-terminated surfaces under ambient conditions (section 3.5.1), the hydrolysis of TCNE to TVA is expected to be considerably slower than on alumina. However, formation of the TVA anion on hydrophilic silicon oxide surfaces (adsorbed water multilayers) is an interesting possibility that has not been reported and could be tested in another study. In the alumina studies, Hipps and Mazur also concluded the TCNE dianion decomposes rapidly in air [Mazur84], but the singly charged TCNE anion was found to be comparatively less air sensitive with a survival time on the order of days under atmospheric conditions. This suggests the irreversible effect observed on SOI(100)-H exposed to TCNE (Figure 6.2a) is likely a result of the strongly adsorbed TCNE anion at least initially. Partial conversion of the TCNE anion to the TVA anion over time could be possible as the surface oxidizes becoming more hydrophilic, as reported previously in solution [Mazur84].

As another explanation for the partial reversibility in the electrical measurements on SOI(100)-H (Figure 6.2a), accelerated oxidation of the H-terminated surface in air was initially suspected in the presence of TCNE since oxidation also leads to irreversible increases in V_{FB} (Ch5), which should cause I_D to decrease under the same bias conditions. Furthermore the Si-H stretch shifts to higher frequency upon oxygen insertion into the backbond gradually exhibiting broad peaks at 2200 cm^{-1} and 2250 cm^{-1} after several hours in ambient, attributed to bonding configurations $SiH_2(O_2)$ and $SiH(O_3)$, respectively [Niwano94]. These oxidation peaks overlap with the CN stretch frequencies observed in Figure 6.3a. To address the possibility these peaks are independent of TCNE exposure and arise normally from native oxidation, the ATR-FTIR spectrum of the H-terminated surface was monitored in ambient atmosphere before exposure to TCNE as shown in Figure 6.4a.

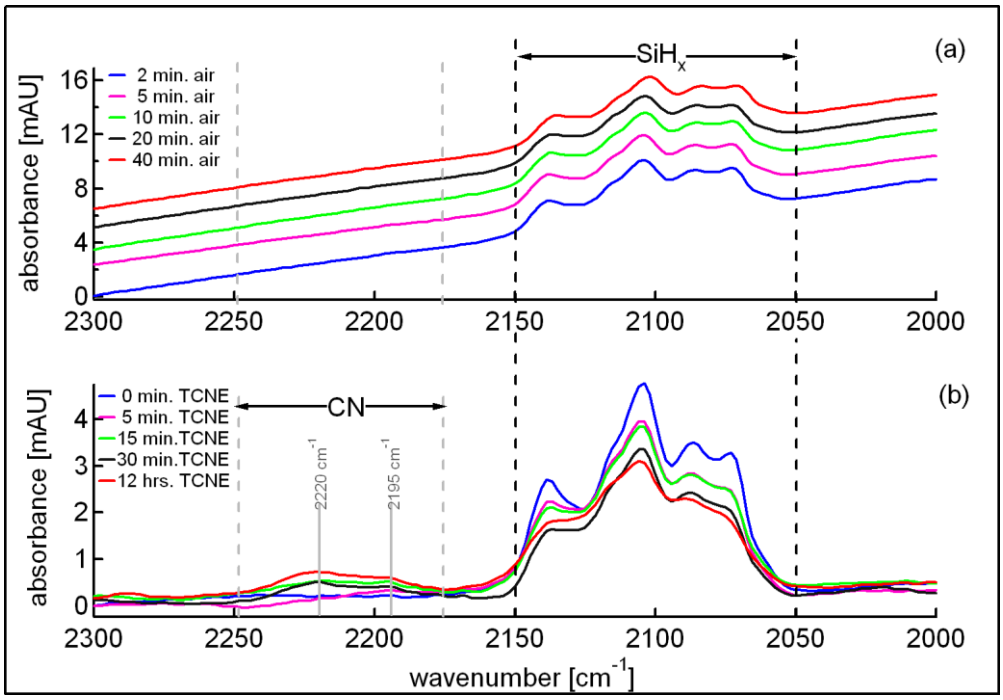

Figure 6.4: ATR-FTIR control experiments comparing spectra in air taken before and after TCNE exposure. (a) The H-Terminated surface, left in air for up to 40 min shows no measurable absorbance attenuation in the SiH_x stretching region, and there are no observable oxidation peaks as reported by Niwano et al. [Niwano94] in this time frame. (b) Upon successive exposure to TCNE the spectra begin to show broad absorbance consistent with the CN stretching modes of TCNE's nitrile groups, with distinct peaks at 2220 cm^{-1} and 2195 cm^{-1}.

The spectra are clearly unchanged after 40 min ambient exposure, with no measurable attenuation or broadening of the SiH_x bands or observation of oxygen in the backbonds based on the peaks reported by Niwano et al. [Niwano94]. Only after exposure to TCNE do the spectra change in Figure 6.4b, revealing growth of broad features and distinct peaks in the CN stretching region at 2220 cm^{-1} and 2195 cm^{-1} (same as in Figure 6.3a), as well as intensity loss in the SiH_x stretching region. These observations support that the ambient vapour phase exposure onto H-terminated silicon leads to a measurable coverage of surface bound TCNE. However it does not reveal the type of bonding to the surface i.e. ionic, covalent, physisorbed, and does not completely preclude the possibility of TCNE induced accelerated oxidation.

High resolution electron energy loss spectroscopy (HREELS) was also carried out to further examine these possibilities and because of the broader spectral range obtained compared to ATR-FTIR. HREELS spectra taken in UHV of the Si(100)-H surface dosed with TCNE vapour in ambient confirm the exposure does not result in appreciable oxidation of the surface as indicated by the absence of Si-O-Si modes. Loss spectra shown in Figure 6.5 were recorded with an LK3000 spectrometer at 60^{o} specular geometry, incident beam energy 6 eV and resolution of 32 cm^{-1}.

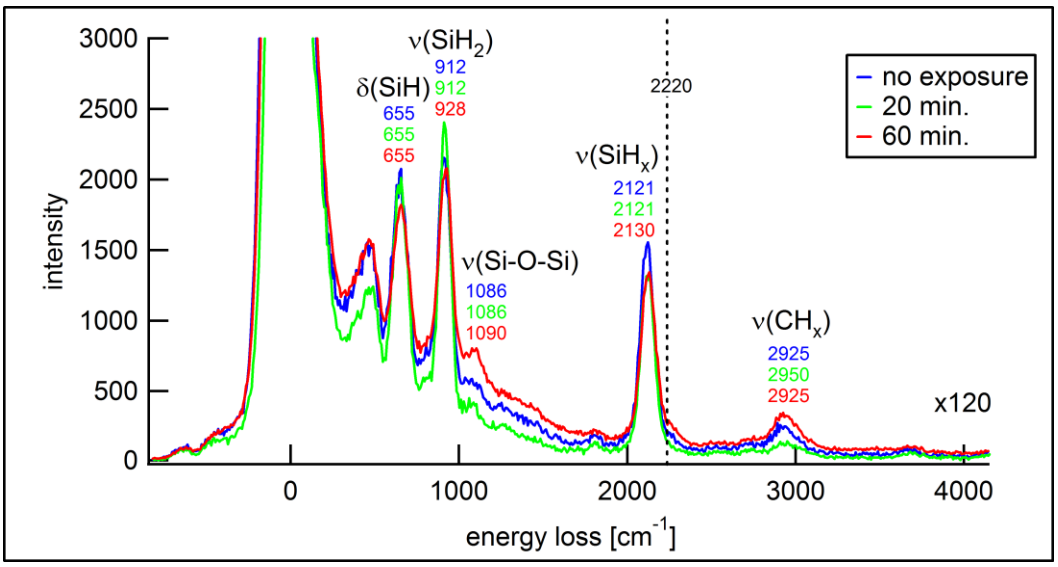

Figure 6.5: HREELS spectra taken in UHV of the freshly etched Si(100)-H surface before and after exposure to TCNE in air for 20 and 60 minutes.

The spectrum of the oxide-free freshly etched Si(100)-H does not change appreciably, even after 60 min exposure to TCNE in ambient. The dominant features labeled in Figure 6.5 are the SiH_x stretch region (2121 cm^{-1}), the SiH_2 dihydride scissor mode (912 cm^{-1}) and the SiH bend mode (655 cm^{-1}). There is a small degree of hydrocarbon around 2925 cm^{-1} and initially very little oxygen adsorbed in Si-O-Si backbonds (1086 cm^{-1}). After 60 min, the Si-O-Si stretch increases only slightly and the SiH stretch shifts to higher frequency, both of which are most likely caused by ambient exposure within this

timeframe. The CN bands which were observed with ambient ATR-FTIR (4 cm^{-1}) in Figure 6.3 and Figure 6.5 are also present but weakly resolved with HREELS (32 cm^{-1}) in Figure 6.5. This observation indicates submonolayer coverage of strongly bound TCNE on Si(100)-H likely results after exposure. Taken together, the HREELS and FTIR spectra strongly suggest that the irreversibility observed in the electrical response of the SOI-H surface is due to the accumulation of strongly bound TCNE species.

6.2.3.1 Liquid phase adsorption of TCNE studied by ATR-FTIR

To more conclusively ascribe the peaks in Figure 6.3 and Figure 6.5 to CN stretching modes TCNE multilayers were adsorbed onto Si surfaces from solution. Intentional deposition of TCNE from solution onto NaBr and various silicon surfaces Si(100)-X, where X={OH (chemical oxide); H; **C10**} was carried out for comparison with the vapour phase IR observations. 135 ppm TCNE dissolved in acetonitrile (MeCN) was drop coated (~20 μL) and allowed to evaporate onto the surfaces to form multilayers, observable by eye as thin film interference regions. Listed below in Table 6.2 are the observed CN stretch positions. The relative intensities are qualitatively assigned in parenthesis according to: (s)-strong, (m)-medium, (w)-weak.

Table 6.2: Comparison of CN stretch modes of TCNE adsorbed on various surfaces by vapour and solution phase adsorption.

	CN stretching vibration(s) [cm^{-1}]	
sample	vapour adsorption	solution deposition
a. NaBr	-	2258(s), 2227(m), 2220 (m), 2189(w)
b. Si(100)/SiO_2	-	2260(s), 2227 (m), 2212(w)
c. Si(100)-H	2220(m), 2195(w)	2258(s), 2220(m), 2212(w)
d. Si(100)-**C10**	none	none

Solid state measurements of uncharged, uncomplexed TCNE $[C_2(CN)_4]^0$ on KBr are commonly reported to have two dominant C≡N infrared stretching vibrations, at approximately 2262 cm^{-1}(s) and 2228 cm^{-1} (m) and a weaker mode at 2214 cm^{-1}(w) [Miller06].

NaBr: As shown in Table 6.2-a spectra on NaBr (transmission geometry) reproduce the two dominant IR modes reported for KBr.

Chemical Oxide: All three CN stretch modes reported for KBr were almost identically reproduced on a piranha cleaned chemical oxide with TCNE physisorbed from solution as shown in Table 6.2-b. After 1 h in air the intensity in this region diminished significantly, suggesting that multilayers formed on the chemical oxide can desorb at room temperature. Upon rinsing in MeCN the CN modes completely disappeared, which is explained by the removal of residual TCNE by the solvent (spectra not shown).

Si(100)-H: Solution phase deposition of TCNE onto Si(100)-H in Table 6.2-c shows a distinct mode at 2220 cm^{-1}, which was also observed in the vapour phase adsorption experiments in Figure 6.3 and Figure 6.4. Note the mode at 2258 cm^{-1} is absent in the vapour phase adsorption spectra in Figure 6.3 and Figure 6.4. This may indicate for submonolayer bound TCNE the mode at 2258 cm^{-1} shifts to lower frequency resulting in the observed mode at 2220 cm^{-1}.The CN absorbance broadens slightly after 2 h in air but does not attenuate in intensity as was observed on the chemical oxide, suggesting TCNE is more strongly bound to the H-terminated surface. Absorbance in this region could only be partially reduced after rinsing in MeCN (completely reduced for chemical oxide) further confirming that TCNE is more strongly bound on Si(100)-H compared to the oxide.

Si-**C10**: TCNE did not absorb at a measurable extent on Si(100)-**C10** (Table 6.2-d) after solution phase deposition. These observations are consistent with the electrical measurements on SOI-**C10** which show increased reversibility and reduced signal (Figure 6.2b) upon exposure to TCNE vapour compared to SOI-H (Figure 6.2a).

6.2.4 Temperature dependent V_{FB} shifts

The temperature dependence of the TCNE charge transfer effect has also been investigated. Figure 6.6 shows the resulting temperature dependence of the TCNE induced flat-band shifts ΔV_{FB} on both SOI-H and SOI-**C10**.

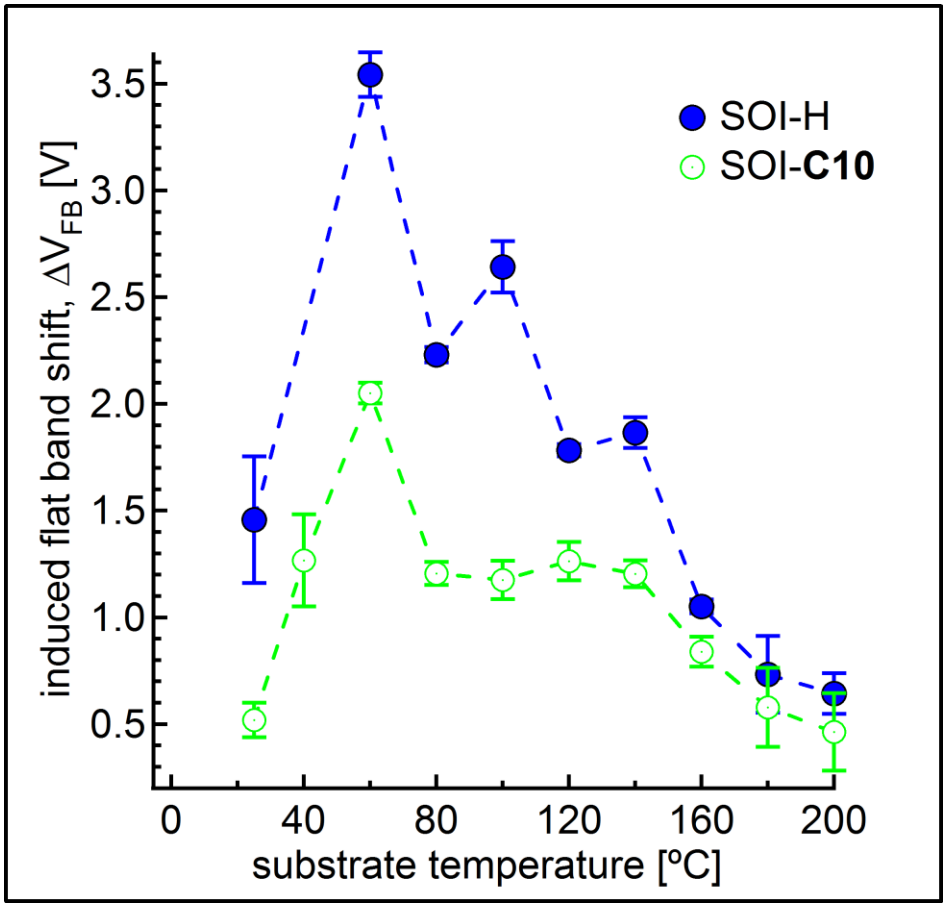

Figure 6.6: TCNE induced flat-band voltage shifts (ΔV_{FB}) corresponding to the current signals observed on SOI-H and SOI-**C10** surfaces as a function of substrate temperature.

The observed current responses over a range of temperatures, from 25°C up to 200°C, are similar to those in Figure 6.2. The large current modulation cycles $I_{max} \leftrightarrow I_{min}$ can be converted to shifts in the flat-band voltage (ΔV_{FB}). These shifts are computed based on

the quadratic model for the saturation current using parameters from the initial I_D-V_D output characteristics as described previously in section 5.3.1. At all temperatures considered the adsorption of TCNE increases V_{FB}, in accordance with decrease in current observed in Figure 6.2. This direction is consistent with negative charge density at the surface causing upward band-bending, thereby depleting the surface of free carriers and raising the (positive) threshold voltage on the substrate required to activate the accumulation channel. The shifts are clearly larger on SOI-H and reduced on SOI-**C10**. In addition, both surfaces exhibit the same trend in ΔV_{FB}, increasing to a maximum near 60 ^{o}C, suggesting that the charge transfer may be thermally activated. The decrease in ΔV_{FB} above this optimal temperature can be explained by faster desorption rates/shorter residence times at the surface.

The degree of charge transfer induced by TCNE adsorption can be estimated from the values of ΔV_{FB} in Figure 6.6 using the expression in Eqn. 5.2 based on the expression given by Hovel [Hovel03]. The changes in surface charge density required to account for the observed shifts at 25 ^{o}C are -8.50×10^{10} cm^{-2} and -3.17×10^{10} cm^{-2} for the SOI-H and SOI-C10 surfaces, respectively. At 60 ^{o}C, the charge transfer increases to -2.07×10^{11} cm^{-2} and -1.25×10^{11} cm^{-2}. Decyl modification therefore is seen to reduce the effective charge transfer by a factor of ~2 to 3. If these charge densities (~10^{11} cm^{-2}) can be ascribed to singly charged $TCNE^{-}$ at the surface, then a lower bound on the coverage required to induce these effects is of the order ~10^{-4} ML.

6.3 TCNE Adsorption in UHV

STM and HREELS studies of TCNE adsorption in UHV on Si(111)-H and Si(100) was carried out to further explore molecule-substrate interactions and possibly reveal insight into the large electrical signals observed in section 6.2.

6.3.1 Experimental Aspects

Si(111)-H: Piranha cleaned silicon cut from Virginia Semiconductor wafers (10 mm×5 mm) with orientation <111>±0.3^{o} toward <11-2>, doped *n*-type (phos.) to 0.5-5 Ω·cm were etched in deoxygenated ammonium fluoride (40% NH_4F), briefly dipped in deoxygenated MilliQ water then transferred to UHV. The samples were gently annealed at 100-200^{o}C for 15 min. to desorb physisorbed contaminants.

Clean 2×1 Si(100): Piranha cleaned silicon cut from Virginia Semiconductor wafers (10 mm×5 mm) with orientation <100>±0.9^{o}, doped *n*-type (phos.) to 1-10 Ω·cm was degassed at 600 ^{o}C for 1 h, then cooled overnight at room temperature at ~3×10^{-10} Torr. The clean 2×1 Si(100) surface was obtained by flashing to 1050 ^{o}C. The temperature of the sample was measured with an infrared pyrometer.

TCNE Exposure: Solid crystals of purum grade TCNE (98%) were loaded into a blank nut onto a valve connected to the main gas-line backed by a turbo-pump. The gas-line was baked initially to remove unwanted impurities. The TCNE compartment was purified by repeated pumping cycles with the turbo pump. The gas-line including TCNE was then heated to a pressure of 1 Torr and the TCNE was dosed in vacuum during the STM measurements through a high precision leak valve. The pressure was measured with an ion-gauge far from the STM setup and away from the line of sight between the incoming molecules and the STM. In-situ topography imaging during dosing was carried out with a commercial STM (Omicron Nanotechnologies STM1), in a UHV chamber (base pressure ~1×10^{-10}) also equipped with a HREELS spectrometer to obtain vibrational spectra of the dosed surface.

6.3.2 Adsorption of TCNE on Si(111)-H at RT

Initially it was not known if in-situ STM dosing experiments would reveal molecular features. This prediction is based on ambient experiments with SOI-H pseudo-MOSFETs (Figure 6.2) since upon removing the TCNE vial the current recovery time constant is ~10 s but the time required to complete a typical STM scan is ~5 min. However molecular features and single molecule binding/desorption events are observable as illustrated in Figure 6.7 in a series of STM images of the same area on a Si(111)-H surfaces during exposure to TCNE.

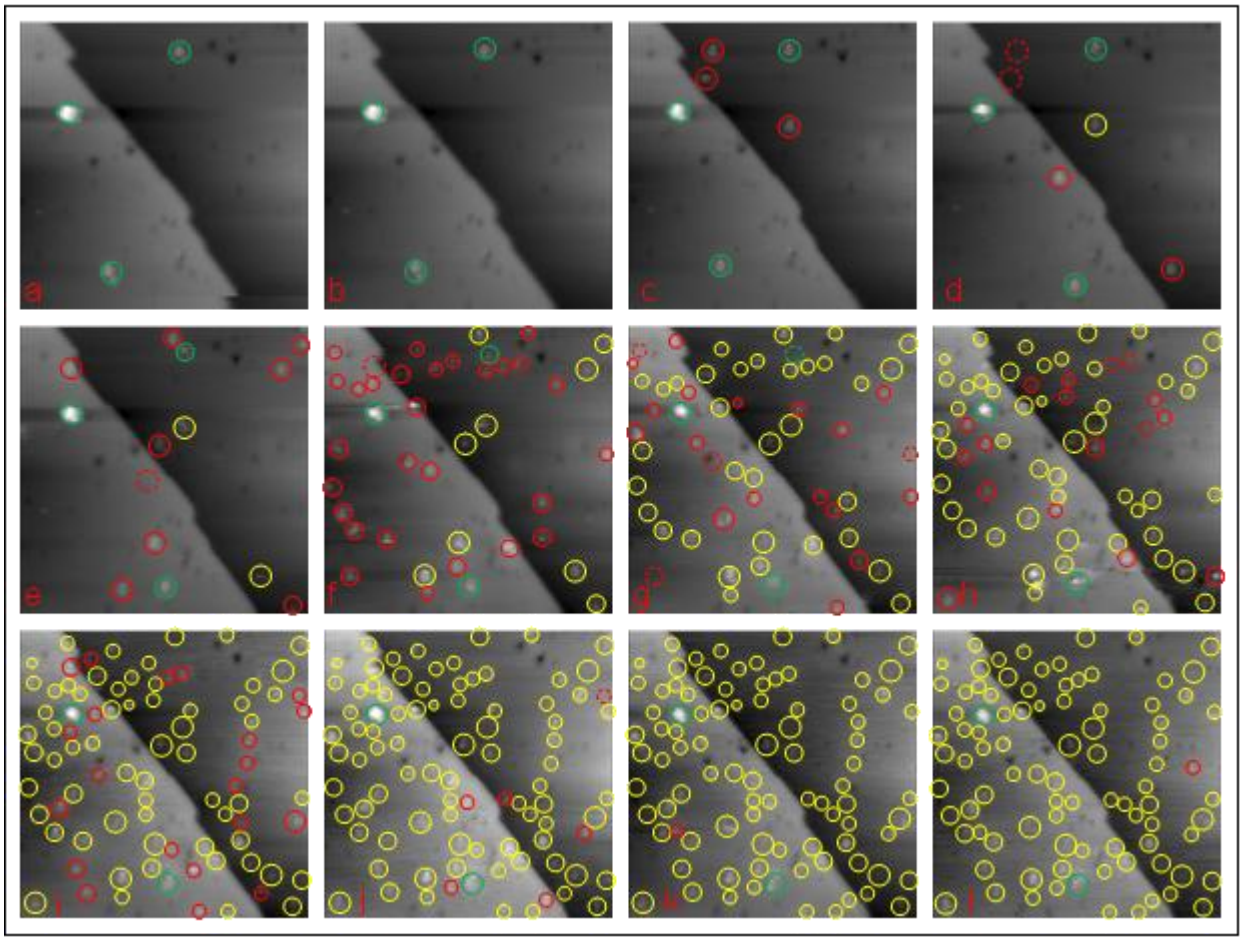

Figure 6.7: Occupied state consecutive STM images of Si(111)-H (51×51 nm^2, -2.05 V, 56 pA) during in-situ exposure to TCNE at RT. Green circles highlight features already present before exposure. Solid red circles represent new features (adsorption), dashed-red represent features which disappeared in the subsequent scan (desorption), and yellow circles represent no change. The scan direction was bottom-to-top and corresponds to initial-final exposure levels of (a) 0-4 L, (b) 5-8 L, (c) 9-109 L, (d) final: 279 L, (e) 449 L, (f) 751 L, (g) 1053 L, (h)-(l) 1350 L.

Subsequent exposure is illustrated in Figure 6.8.

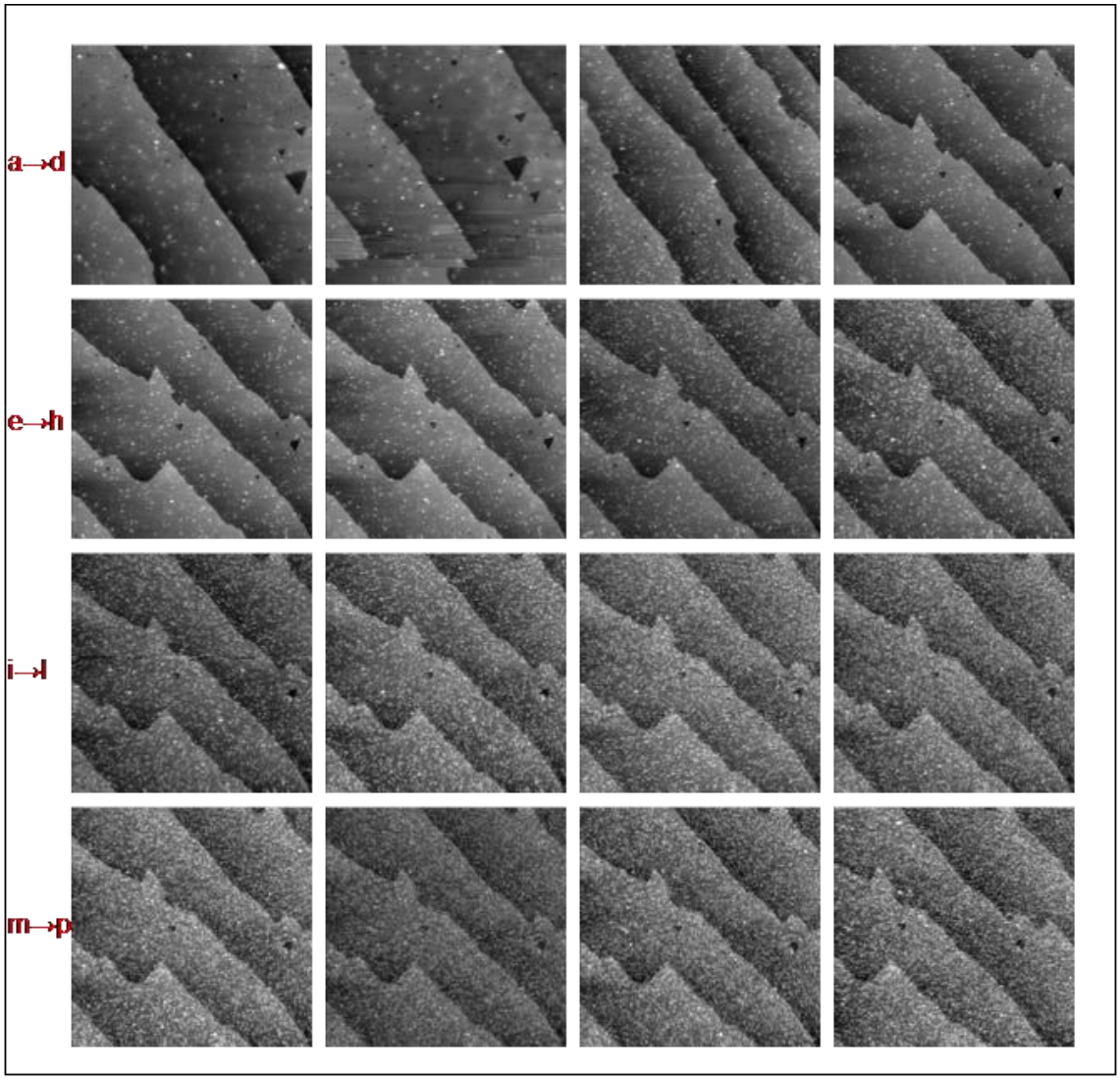

Figure 6.8: Larger area STM images, stability in vacuum, change with annealing and additional exposure to TCNE. (a) 106×106 nm^2, -2.05 V, 83 pA after 1350L exposure to TCNE (continuation from Figure 6.7). (b) The same area (106×106 nm^2, -2.05 V, 83 pA) as in (a) after 12 hrs. (c) a larger area after gentle anneal (<100^oC) for 10 min, (219×219 nm^2, -1.93 V, 13 pA). (d) longer anneal (<100^oC) for 12 hrs, (219×219 nm^2, -2.50 V, 10 pA). (e) Same STM conditions as in (d), additional TCNE exposure (to the already exposed surface with 1350 L TCNE) corresponding to a cumulative final coverage of 1650 L, (f) 1950 L, (g) 2250, (h) 2550 L, (i) 2850 L, (j) 3150 L, (k) 3450 L, (l) 3750 L, (m) 4050 L (n) 4350 L, (o) 4650 L, (p) 4650 L.

Scans in Figure 6.7a and Figure 6.7b are the same at 10^{-8} Torr TCNE. Adsorption events are visible upon increasing the pressure to 10^{-6} Torr (1 L/s) in Figure 6.7c onward. The features in Figure 6.7 correspond to low coverage. There is no evidence that steps are preferred over terraces and the 2*d* distribution of molecules appears spatially uniform. Molecules remain bound to surface even after the dosage is stopped as shown in Figure 6.7l onward.

Figure 6.8 illustrates another series at larger scan area starting with the already exposed surface to 1350 L TCNE from Figure 6.7. The coverage decreases by 15% from 355 molecules/106 nm^2 (3.2×10^{12} cm^{-2}) in Figure 6.8a to 300 molecules/106 nm^2 (2.7×10^{12} cm^{-2}) in Figure 6.8b, after the sample has been held at RT in UHV for 12 h. Upon 10 min annealing to <100 ^{o}C the coverage decreases again by 7% to 1193 molecules/219 nm^2 (2.5×10^{12} cm^{-2}) in Figure 6.8c then after 12 h annealing the coverage decreases an additional 20% to 938 molecules/219 nm^2 (2.0×10^{12} cm^{-2}) in Figure 6.8d. These observations indicate a molecule-surface interaction stronger than simple physisorption such as chemisorption or ionosorption. Additional exposure to TCNE at 1 L/s for ~1 h (Figure 6.8e-p) represents 4650 L of TCNE in total. The corresponding HREELS spectrum is shown in Figure 6.9.

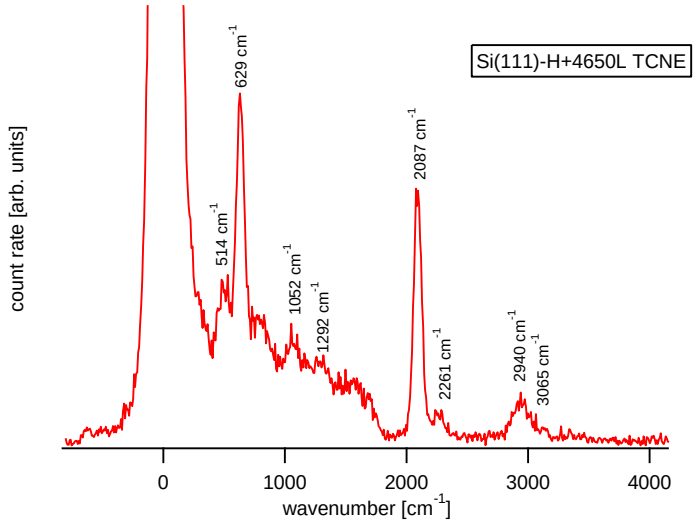

Figure 6.9: HREELS spectrum of Si(111)-H after exposure to 4650L TCNE showing the unshifted Si-H stretch/bend modes, minimal oxidation and features at 2261 cm^{-1}, corresponding to the CN stretch and at 2940 cm^{-1} and 3065 cm^{-1} corresponding to sp^3(alkyl) and sp^2 (alkenyl) CH stretch modes.

Figure 6.9 shows dominant features of the Si(111)-H surface (Figure 3.1), namely the unshifted Si-H stretch and bend modes at 2087 cm^{-1} and 629 cm^{-1} respectively. In addition there is a distinct peak centered at 2261 cm^{-1} which is attributed to the nitrile group stretch frequency of TCNE corresponding to the same mode at 2220 cm^{-1} in ambient ATR-FTIR studies (Figure 6.3) In the C-H stretching region, there are two peaks at 2940 cm^{-1} and 3065 cm^{-1} corresponding to sp^3(alkyl) and sp^2 (alkenyl) C-H stretch modes which may originate from hydrocarbons in the gas line or physisorbed contaminants. Alkenyl modes may arise from reactions of the Si-H surface with TCNE's nitrile groups.

Figure 6.7 through Figure 6.9 show topographically/chemically that TCNE interacts strongly on the H-terminated surface consistent with the partial reversibility in drain current after exposure (Figure 6.2a). To examine if the electron accepting properties of TCNE observable in the electrical measurements on SOI (section 6.2) are visible in STM, molecular features in occupied *vs* unoccupied states are shown adjacently in Figure 6.10. The occupied (Figure 6.10b) *vs* unoccupied (Figure 6.10c) state images of Si(111)-H exposed to 3800 L TCNE are distinct from each other with most bright features in

occupied states dimming in unoccupied states. Representative line scans in Figure 6.10d also confirm the apparent heights are larger in occupied states compared to unoccupied states. The contrast is consistent with reduced tunneling efficiency in unoccupied states which can be explained by a filled TCNE LUMO due to a charge-transfer interaction with the substrate. HREELS spectra corresponding to Figure 6.10a and Figure 6.10bc are shown in Figure 6.11.

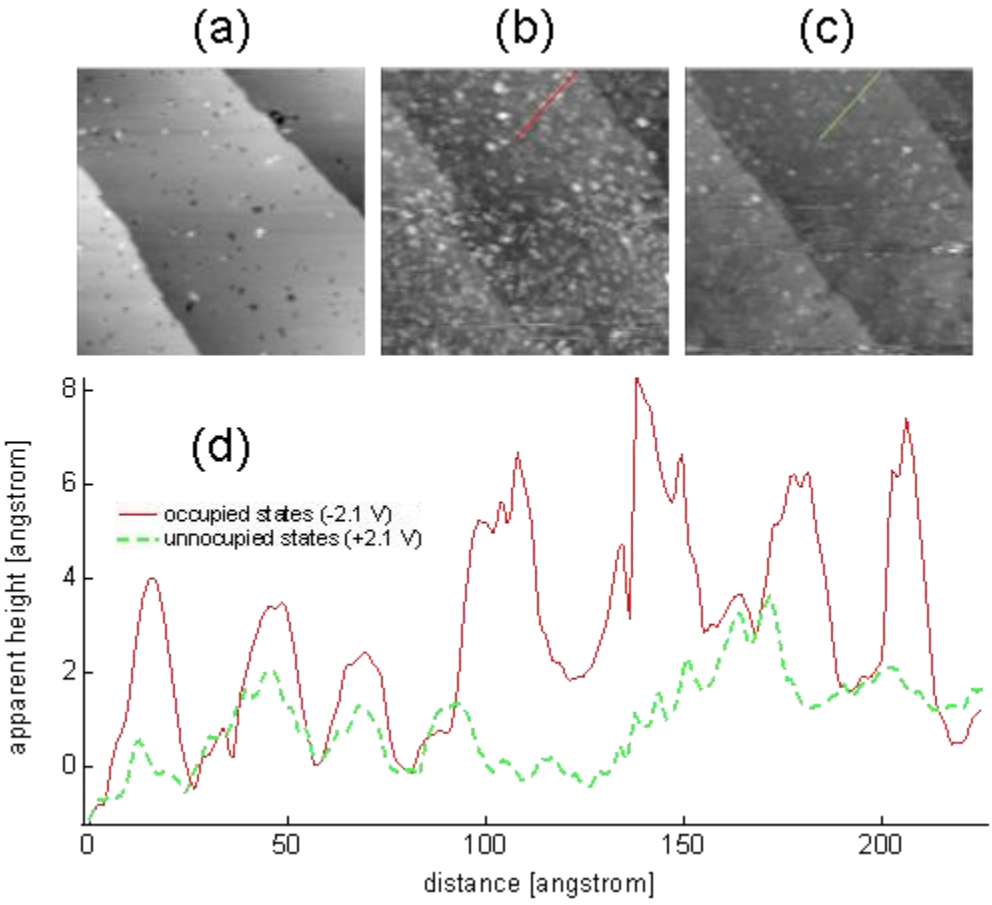

Figure 6.10: STM images of TCNE adsorbed on Si(111)-H; (a) initially 0 L (54×54 nm^2, -2.6 V, 15 pA), (b) occupied state image after 3800 L exposure (70×70 nm^2, -2.1 V, 21 pA), and (c) unoccupied state image of the same area as (b) (70×70 nm^2, +2.1 V, 21 pA). Shown in (d) are representative line scans corresponding to (b) and (c).

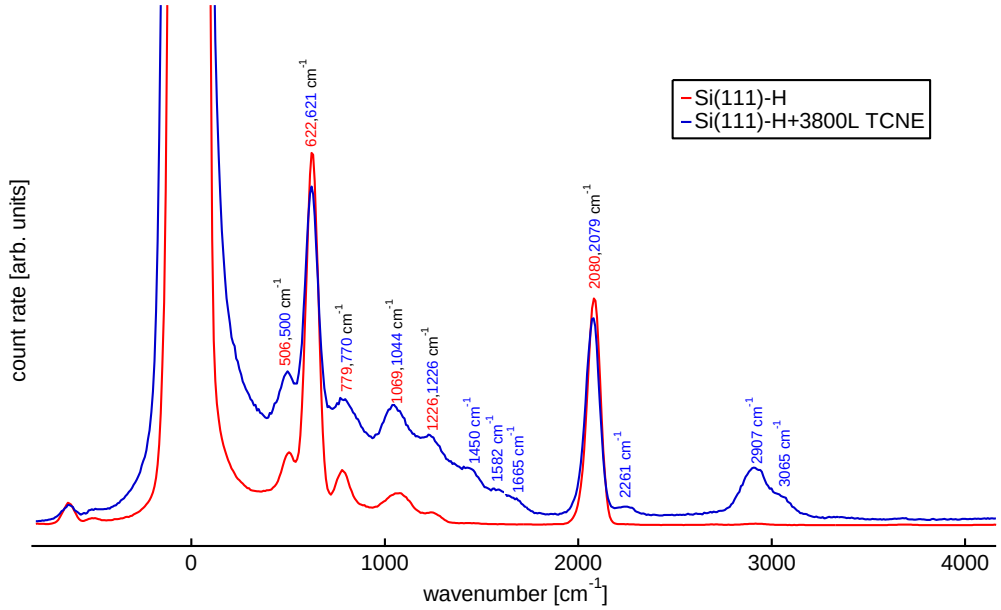

Figure 6.11: HREELS spectra corresponding to STM images in Figure 6.10; initial Si(111)-H surface and after 3800 L exposure to TCNE. The spectra show strong SiH stretch and bend modes, a low degree of oxidation, and evidence for adsorbed TCNE vibrations at 2261 cm^{-1}, 2907 cm^{-1} and 3065 cm^{-1} corresponding to the nitrile group stretch and alkyl/alkenyl C-H groups.

6.3.3 Adsorption of TCNE on Si(100)-2×1 at RT

For comparison with TCNE/Si(111)-H in section 6.3.2 exposure to clean Si(100)-2×1 is informative since chemisorption is expected. Si(100)-2×1 is known to undergo [2+2] reactions with simple alkenes such as ethylene and butene [Wolkow99]. Figure 6.12 illustrates consecutive STM images during *in-situ* dosing of TCNE over the same scan area on Si(100).

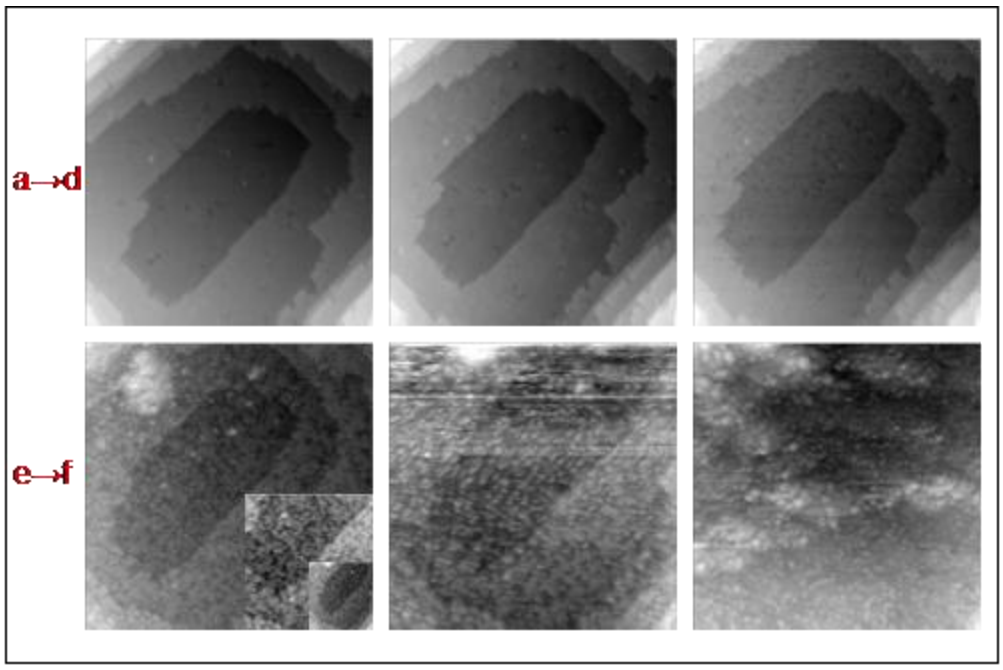

Figure 6.12: Occupied state consecutive STM images of Si(100)- 2×1 (61×61 nm^2, -2.0 V, 21 pA) during in-situ exposure to TCNE at RT. At the end of each scan the final exposure corresponds to (a) initially 0 L, (b) 0.6 L, (c) 3.9 L, (d)7.2 L, (e) 11 L, (f) 15 L.

Dosage at 10^{-9} Torr (Figure 6.12b) does not result in significant changes within the timeframe of one scan. On increasing the pressure to 10^{-8} Torr the images change more quickly with dark depressions appearing uniformly over the surface. At 11-15 L TCNE/Si(100) a complicated mixture of depressions and bright features results, attributed to a combination of unreacted dimers and chemisorbed TCNE. The HREELS spectrum at 15 L is shown in Figure 6.13.

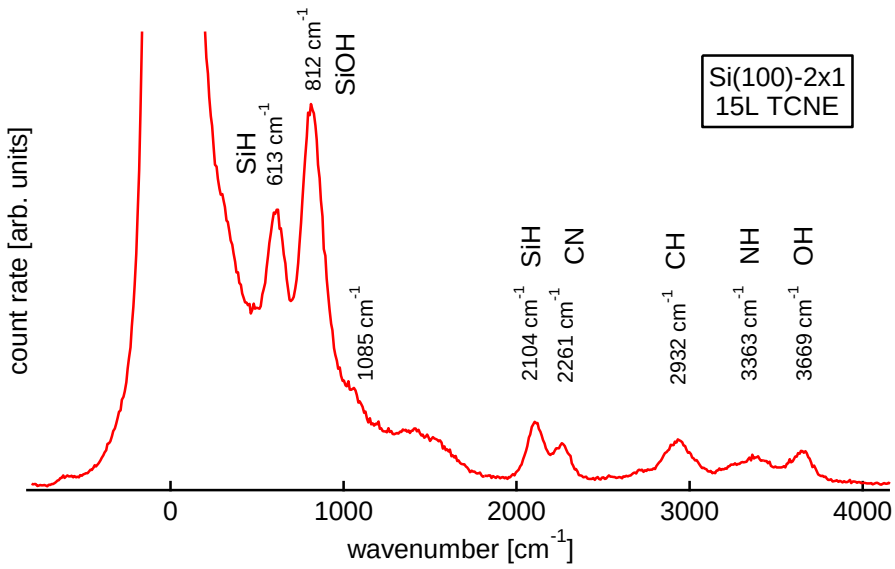

Figure 6.13: Corresponding to Figure 6.12, the HREELS spectrum of Si(100)-2×1 after exposure to 15L TCNE. The spectrum shows several features attributed to reactions with background water at 3669, 2104, 613, and 812 cm^{1} typical for this surface exposure time of a clean surface. Modes attributed to the adsorption (reaction) of TCNE are present at 2261 cm^{-1}, namely the nitrile group stretch, and at 3363 cm^{-1} attributed to the NH stretch.

Several peaks labeled in Figure 6.13 result from background H_2O due to the high reactivity of Si(100)-2×1 with water [Fan10]. Hydroxylation results in OH and SiH stretch and bend modes as indicated. There are multiple reaction pathways by which TCNE could chemisorb onto Si(100)-2×1surface and based on the complexity of the STM series in Figure 6.12 they probably occur in parallel. Losses at 2261 cm^{-1}, 2932 cm^{-1} have been observed on TCNE/Si(111)-H in Figure 6.9 and Figure 6.11 attributed to the CN group vibration and the saturated C-H stretch modes. The NH stretch at 3369 cm^{-1} has observed on TCNE/Si(111)-H only upon annealing to 250 ^{o}C.

The spectral modes of TCNE/Si(100)-2×1 in Figure 6.13 are similar to those observed of TCNE/Si(111)-H. The strongly bound species is likely responsible for the partially irreversible component in the drain current recovery on SOI-H pseudo-MOSFETs (section 6.2). However it is still not conclusive if this irreversible upward-band bending arises from the chemisorption inducing states in the gap or due to the

electron accepting properties of the strongly bound TCNE species (Figure 6.10). The UHV studies have increased knowledge of TCNE adsorption on silicon, but the most direct evidence for a charge transfer interaction still appears in the electrical measurements upon exposure to SOI-H pseudo-MOSFETs in ambient (Figure 6.2 and Figure 6.6).

6.4 Other Acceptors

The large conductivity modulation induced by TCNE on SOI pseudo-MOSFETs described in section 6.2 invites exploration of other electron acceptors. For instance most common explosives have high electron affinities [Huang87;Goodpaster01]. The primary technology for detection of trace explosives is ion mobility spectrometry in which neutral target molecules are ionized by electron attachment; the drift time of the charged molecular fragments is monitored yielding characteristic patterns that can uniquely identify compounds of interest [Ewing01;Oxley08]. Common explosives and their properties are listed in Table 6.3.

Table 6.3: Common explosives, electron affinities and vapour pressures.

Compound	Electron Affinity [eV]	Vapour Pressure [mTorr]
TNT 2,4,6-Trinitrotoluene	2.5 [Song09]	5.8×10^{-3} (7.7 ppb)
RDX 1,3,5-Trinitro-1,3,5-triazacyclohexane	1.40 [Sulzer09]	5.8×10^{-6} (6.0 ppt)
PETN Pentaerythritol tetranitrate	-	2.9 (3.8 ppm)

Patolsky and co-workers have recently reported supersensitive electrical detection of TNT to concentrations below 500 fM using oxidized silicon nanowire arrays functionalized with the silane monolayer APTES [Engel10]. In their fluid delivery system TNT dissolved in water with 0.1% DMSO flown over the SiNW array induces

conductance changes 10%<$\Delta G/G_0$<40% corresponding to analyte concentrations 500 fM<[TNT]<5μM attributed to a charge transfer complex (acid-base pairing) between TNT and the grafted amino ligands on the surface.

Preliminary studies using SOI-H pseudo-MOSFETs demonstrates the feasibility of these substrates for detection of high electron affinity compounds with reasonable sensitivity as illustrated in Figure 6.14 at V_G=-1 V, V_D=5 V. A 1 mL glass ampoule containing 1 mg/mL TNT in CH_3CN was evaporated isolating solid TNT residue. Upon exposure to TNT vapour under similar conditions as in section 6.2, the drain current initially increases and then drops sharply by approximately 50%.

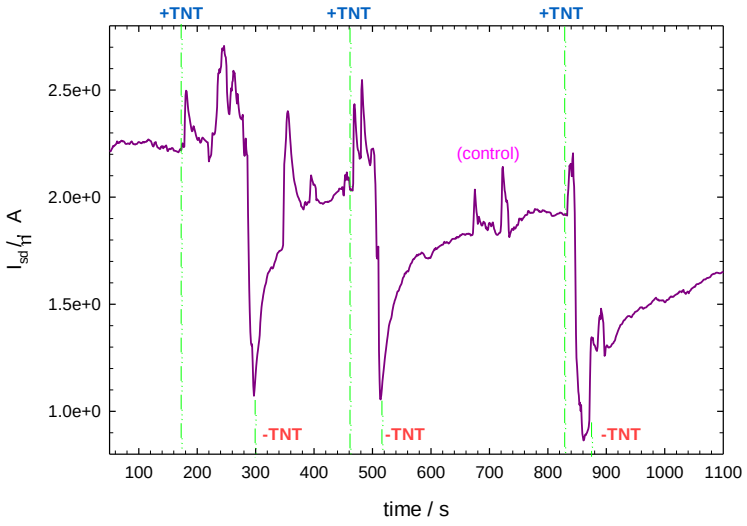

Figure 6.14: I_D monitored at V_G=-1V, V_D=5 V illustrates the sensitivity of SOI-H to TNT vapour. An ampoule containing TNT residue is positioned ~5 mm from the sample at the dashed lines indicated. Upon removal of the vial the current is seen to increase. An empty control ampoule did not lower the drain current.

The response is reversible upon removing the ampoule from the vicinity of the sample and the recovery of I_D is seen to increase by heating the substrate to 40 °C. These observations indicate ppb levels of TNT in ambient atmosphere are feasible on planar oxide-free SOI at signals comparable to Patolsky and co-workers reported on NW's

[Engel10] with no additional efforts to improve the sensitivity. Detection in lab ambient also indicates that the effect is somewhat robust although more tests are required to characterize the sensitivity of SOI-H to well-known interferents such as cleaning solvents. Improvements in selectivity are expected by optimizing the chemical modification. Integration of a miniaturized sampling and pre-concentration system can further improve the sensitivity.

The specificity of an accumulation mode SOI-H pseudo-MOSFET at V_G=2 V, V_D=2 V to a range of explosives is illustrated at right in Figure 6.15. Shown adjacent on the left is the larger response to TCNE (section 6.2) for comparison. In this preliminary run the use of a large TNT prill significantly increases the response in I_D (7-fold) compared to Figure 6.14 (2-fold). Exposure to the plastic explosive Semtex (mixture of RDX and PETN) lowers the current two-fold. Detcord (mostly PETN) results in a 15% response but C-4 (composition 4, mostly RDX) does not induce a measurable change. A plausible explanation for the plastic explosive trends is that RDX is not detectable due to its low vapour pressure of 6 ppt (consistent with the C-4 null signal), and that the PETN present in Semtex and Detcord is largely responsible for the observed responses.

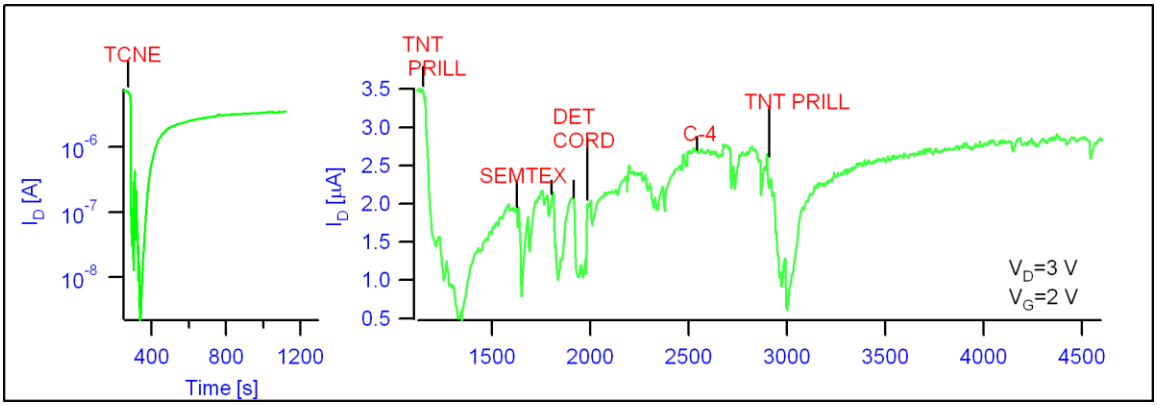

Figure 6.15: Specificity of an SOI-H pseudo-MOSFET operating at V_G=2 V, V_D=2 V exposed to a TNT prill, Semtex, Detcord, and C-4.

The electrical response of SOI-H to the compounds in Figure 6.15 is significantly smaller than that of TCNE likely due to large differences in vapour pressure/electron affinities. The results demonstrate the use of planar oxide free silicon as a detection platform for high electron affinity compounds warrants further study.

6.5 Conclusions

The pseudo-MOSFET technique has been used to demonstrate highly efficient electrical detection of TCNE vapour on oxide-free chemically modified SOI. This effect is attributed to significant charge transfer from the silicon substrate to adsorbed TCNE molecules. Use of a decyl monolayer to passivate the H-terminated surface was found to increase the reversibility of the TCNE induced current modulation, while only slightly decreasing the sensitivity, demonstrating the utility of alkyl monolayers as ultrathin dielectrics in molecular sensing applications. The strong interaction of TCNE on H-terminated bulk silicon is confirmed by HREELS and in-situ STM imaging during dosing of TCNE in UHV. Strongly bound TCNE-species seen in UHV suggests submonolayer chemisorption or ionosorption takes place which likely induces the partially reversible electrical responses observed on SOI-H substrates. Large shifts in device characteristics invite exploration of other high electron affinity species such as explosive compounds. The influence of ppb levels of TNT and other acceptors exposed to SOI-H pseudo-MOSFETs is also found to induce depletion of majority carriers in ambient atmosphere, although the effects are smaller than TCNE due to differences in exposure and electron affinity. These observations are promising for future field-effect applications of silicon in the detection of electron accepting species.

Chapter 7

Conclusions

7.1 Concluding Statements

The recurring theme throughout these studies is that molecular adsorption on silicon strongly influences the surface layer electrical conduction. Increased sensitivity to surface effects on silicon can be achieved using moderately doped SOI wafers whose device layer thickness is comparable to the Debye length in the semiconductor. Surface effects can be monitored with sheet resistance, Hall effect, and pseudo-MOSFET measurements. Oxide-free termination with hydrogen is a useful starting point for investigating the effects of gases on the electrical conductivity in ambient or vacuum, due to its reasonable stability and excellent initial electronic passivation.

The sheet resistance of SOI-H was found to increase significantly with time in ambient air, due to depletion of majority carriers caused by oxidation (Ch3). Physisorbed water was found to further modulate the conductivity, inducing downward band bending and accumulation of majority carriers on *n*-doped films. Adsorption of water in a controlled vacuum system is found to strongly and reversibly increase the conductivity of

both *n*-type and *p*-type SOI-H substrates. These conductivity changes can be attributed to water induced field effects that lead to accumulation of majority carriers on *n*-type and formation of a minority carrier channel (inversion) on *p*-type substrates. The surface charge densities required to account for these effects are on the order of ~10^{11} q·cm^{-2}. This ability of adsorbed water to induce band bending is clearly a significant effect on oxide-free systems and should be accounted for, or at least considered in the interpretation of electrical transport measurements on silicon surfaces in ambient or aqueous solutions

Pyridine adsorption gives rise to similar yet even stronger reversible conductivity modulation effects as compared with water on both *n*-type and *p*-type substrates (Ch4). Adsorption of pyridine in the Torr range gives rise to positive surface charges of 4×10^{11} q·cm^{-2} (*p*-type) and 1×10^{12} q·cm^{-2} (*n*-type), resulting in a surface electric field 3-6 fold higher than that caused by water adsorbed on the same surface. The ability of nitrogen containing molecules such as pyridine, ammonia and triethylamine to reversibly bias *p*-type surfaces into inversion demonstrates a new type of molecular triggered electronic switch where adsorption is used to reversibly gate transport through the silicon substrate.

Accumulation mode pseudo-MOSFETs formed on hydrogen terminated silicon-on-insulator (SOI-H) were also used to probe molecular adsorption and reaction events (Ch5). Current-voltage characteristics of such *n*-channel devices are found to be sensitive to the environment, with the accumulation threshold voltage (V_{FB}), exhibiting large reversible changes upon cycling between ambient atmosphere, high vacuum (<10^{-5} Torr) and exposure to water and pyridine vapour at pressures in the Torr range. The field-effect mobility is found to be comparatively less affected through these transitions. Such large shifts in flat-band voltage caused by donor type molecules is consistent with the surface charge densities measured in Ch3 and Ch4. Oxidation of the H-terminated surface in ambient leads to irreversible shifts in both the flat-band voltage and field-effect mobility. A photochemical gas phase reaction with decene is used to form a decyl monolayer (**C10**) on the SOI(100)-H surface. Formation of this monolayer is found to result in a relatively small shift of threshold voltage and only a slight degradation of the field effect mobility,

suggesting that alkyl monolayer dielectrics formed in this way could function as good passivating dielectrics in field effect sensing applications. These studies demonstrate the utility of the Ψ-MOSFET as a fast and simple approach for probing molecule-surface interactions on chemically modified silicon surfaces.

The pseudo-MOSFET technique was applied to demonstrate highly efficient electrical detection of TCNE vapour on oxide-free chemically modified SOI (Ch6). This effect is attributed to significant charge transfer from the silicon substrate to adsorbed TCNE molecules. Use of a decyl monolayer to passivate the H-terminated surface was found to increase the reversibility of the TCNE induced current modulation, while only slightly decreasing the sensitivity, demonstrating the utility of alkyl monolayers as ultrathin dielectrics in molecular sensing applications. The influence of ppb levels of TNT and other acceptors exposed to SOI-H pseudo-MOSFETs is also found to induce depletion of majority carriers in ambient atmosphere, although the effects are smaller than TCNE due to differences in exposure and electron affinity. These observations are promising for future field-effect applications of silicon in the detection of electron accepting species.

7.2 Opportunities and Prospectives

In the last decade, at least twenty papers have been published on the use of SOI material as an electrically sensitive probe of surface phenomena, mainly from the Weitering, Bausch, Lagally, and Tour groups (Ch1), and work published from this thesis, in broad-readership journals. These contributions have exploited the properties of SOI to study basic processes on clean surfaces, and other processes including chemical and biosensing on oxides and H-terminated silicon. Therefore the feasibility of using SOI for molecular sensing has already been established; however the applications remain illusive. It is expected the next decade will see more applied contributions for chemical and biosensing applications, driven by the need to rapidly and selectively detect molecular species with high sensitivity and low cost.

Project ideas and recommendations for subsequent graduate students continuing in this area at NRC-SIMS/INRS-EMT or other collaboration are provided derived from experiences throughout the years.

7.2.1 Conductivity of SOI in UHV

The electrical response of SOI-H in UHV to gas adsorption through a precision controlled leak valve is an interesting method of correlating surface conductance with exposure and furthermore in terms of molecular coverage assuming the sticking probability and binding energy is known; the coverage could also be estimated separately with a complementary technique such as STM. Empirical relationships between conductivity and exposure/coverage would be a new contribution to the field and potentially useful in determining the underlying mechanisms responsible for charge transfer. The electrical signals would also be sensitive in time to adsorption events during exposure and desorption dynamics in UHV. This project would take a minimum of three years to complete by a Ph.D. student capable of setting up the UHV system and carrying out the measurements. The response of planar SOI could be compared with that of H-terminated SiNW's to conclusively determine the relative sensitivity between these structures at low coverage, which could be published in PRL.

7.2.2 Multiplexed Gas Sensing on SOI

The goal of this project is to monitor multiple terminations in parallel using a single SOI wafer to record the characteristic response of a particular gaseous species, analogous to that of a cross-reactive array. The challenge is to create a simple design that protects the contacts from corrosive chemicals such as HF or piranha so the same sample can be cleaned and H-terminated. The wafer would be patterned into parallel silicon islands sampled sequentially (multiplexed) using a simple switchbox or commercial multiplexer. The distinct real-time response of each island is associated to each gaseous test mixture.

The second part of the project is to design a simple re-usable fluidic applicator from Teflon or PDMS which can be used to control the flow of gaseous mixtures over each island during the sequencing. A mock experiment sketched in Figure 7.1 consists of islands terminated by hydrogen (SOI-H), a decyl monolayer (SOI-**C10)**, a carboxylic acid terminated monolayer (SOI-**COOH**), and an amino-terminated monolayer (SOI-$\mathbf{NH_2}$).

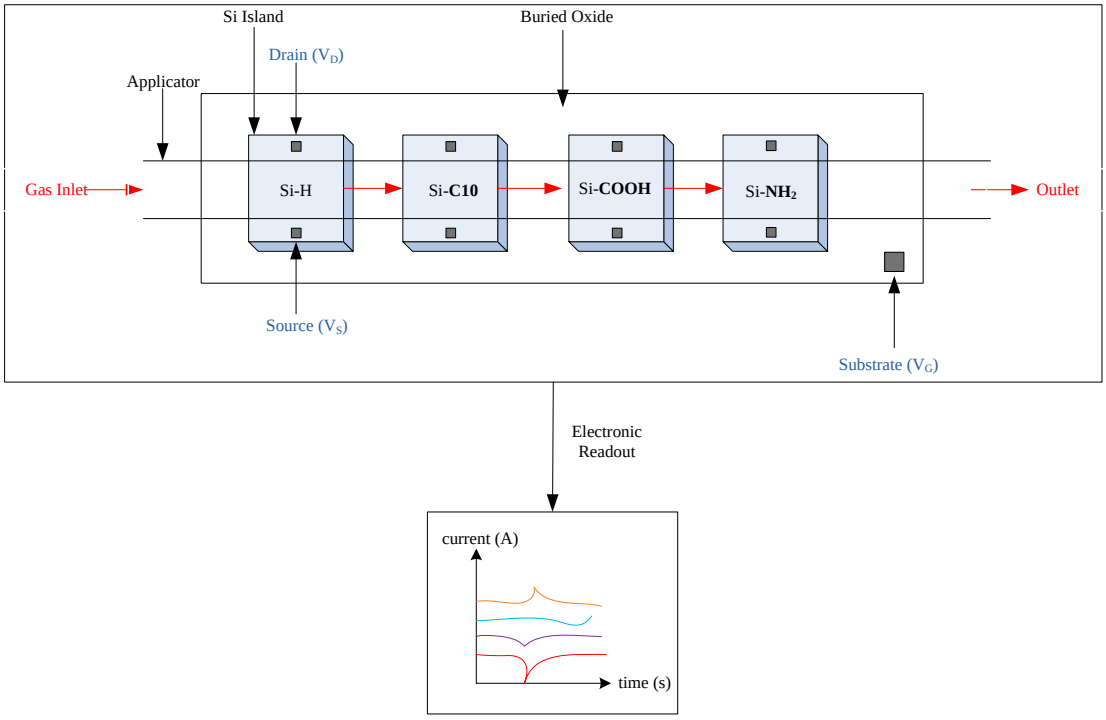

Figure 7.1: Schematic of a multiplexed readout on a multiple-terminated SOI wafer for recording the characteristic response of a gaseous text mixture, analogous to that of a cross reactive array.

Using systematic masking procedures, it should be possible to prepare the alkyl, acid and amino surface terminations in three steps by repeated use of the gas phase approach described in Ch5. This surface termination set would be ideal for comparing the multiplexed response to explosives such as TNT with well known interferents such as household chemicals and aerosols. This project would require a minimum input of five years which could be shared by two graduate students, one M.Sc. and on Ph.D. (primarily

focused on these goals), ideally one with a background in chemical engineering and the other in electrical engineering and both requiring previous training in semiconductor device fabrication as a prerequisite for starting the project. Successful completion of the island array, applicator, chemical patterning and results from an interesting gaseous system (e.g. explosives) could be published in a high profile journal such as lab-on-a-chip or advanced materials.

7.2.3 Overcoming pH dependence in biosensing applications

An unresolved problem on silicon-oxide based field-effect biosensors is the high sensitivity to pH changes due deprotonation of Si-OH groups with increasing pH as described by the site-binding model (Nernstian response 60 mV/pH). The Bausch group showed suppression of this response by 2-5 fold is possible by spincasting a 25 nm PMMA polymer SOI [Nikolaides04], but such a thick layer will inhibit sensitivity for detecting charged biomolecules in electrolyte solution within a Debye length from the surface (1 nm at physiological concentrations).

One solution to this problem is to graft alkyl monolayers on H-terminated SOI (<1 nm) by the simple gas-phase phase technique described in Ch5 and study the subsequent pH dependence in by conductivity/pseudo-MOSFET measurements in the ambient probestation using a Teflon cell and reference electrode in solution. Since alkylation replaces Si-H bonds irreversibly with Si-C bonds (30% coverage), the formation of ionizable Si-OH groups will be suppressed, and hence so is the expected pH response. Should this experiment prove successful, the student could move on to methyl termination (100% Si-C bonds) which is expected to completely suppress the pH dependence. Finally, the student could attempt to functionalize the highly stable methylated at low yield (1%) with carboxylic acid groups using a diazarine compound [Assad08] for subsequent reaction with amine-tagged bio-molecules. This project could be given to a M.Sc. student (primarily focused on these goals) and could be completed in

less than 3 years. Successful demonstration of these targets would constitute the novelty required for a high profile communication or patent.

Bibliography

[Allara et al 95**]** D.L. Allara, A.N. Parikh, F. Rondelez, 'Evidence for a Unique Chain Organization in Long Chain Silane Monolayers Deposited on Two Widely Different Solid Substrates', Langmuir 11 (7), 2357 (1995)

[Allen 62**]** F.G. Allen, G.W. Gobeli, 'Work Function, Photoelectric Threshold, and Surface States of Atomically Clean Silicon', Phys. Rev. 127 (1), 150 (1962)

[Alles 97**]** M.L. Alles, 'Thin Film SOI Emerges', IEEE Spectrum, 37-45, June, (1997)

[Ando 82**]** T. Ando, A. Fowler, F. Stern, 'Electronic properties of two-dimensional systems', Rev. Mod. Phys. 54 (2), 437 (1982)

[Angermann et al 94**]** H. Angermann, T. Dittrich, H. Flietner, 'Investigation of native-oxide growth on HF-treated Si(111) surfaces by measuring the surface-state distribution', Appl. Phys. A 59 (2), 193 (1994)

[Angermann et al 96**]** H. Angermann, K. Kliefoth, H. Flietner, 'Preparation of H-terminated Si surfaces and their characterization by measuring the surface state density', Appl. Surf. Sci. 104, 107 (1996)

[Angermann et al 00**]** H. Angermann, W. Henrion, A. Roseler, M. Rebien, 'Wet-chemical passivation of Si(111)- and Si(100)-substrates', Mater. Sci. Eng. B 73, 178 (2000)

[Angermann et al 04**]** H. Angermann, W. Henrion, M. Rebien, A. Roseler, 'Wet-chemical preparation and spectroscopic characterization of Si interfaces', Appl. Surf. Sci. 235, 322 (2004)

[Angermann et al 08**]** H. Angermann, J. Rappich, I. Sieber, K. Hubener, J. Hauschild, 'Smoothing and passivation of special Si(111) substrates: studied by SPV, PL, AFM and SEM measurements', Anal. Bioanal. Chem. 390, 1463 (2008)

[Angermann et al 09**]** H. Angermann, J. Rappich, C. Klimm, 'Wet-chemical treatment and electronic interface properties of silicon solar cell substrates', Cent. Eur. J. Phys. 7 (2), 363 (2009)

[Anthony et al 08**]** C.J. Anthony, J. Bowen, G. Torricelli, E.L. Carter, M.C.L. Ward, C. Binns, 'AFM characterization of silicon-on-insulator push-in plates for Casimir force measurements', Micro and Nano Lett. 3 (1), 7 (2008)

[Arora et al 82**]** N.D. Arora, J.R. Hauser, D.J. Roulston, 'Electron and hole mobilities in silicon as a function of concentration and temperature', IEEE Trans. Elect. Dev. 29 (2), 292 (1982)

[Ashcroft 76**]** N.W. Ashcroft, 'Solid State Physics', Holt, Rinehart and Winston, New York, 1967

[Assad et al 08**]** O. Assad, S.R Puniredd, T. Stelzner, S. Christiansen, H. Haick, 'Stable Scaffolds for Reacting Si Nanowires with Further Organic Functionalities while Preserving Si-C Passivation of Surface Sites', J. Am. Chem. Soc. 130 (52), 17670 (2008)

[Avasthi et al 10**]** S. Avasthi, Y. Qi, G.K. Vertelov, J. Schwartz, A. Kahn, J.C. Sturm, 'Silicon surface passivation by an organic overlayer of 9,10-phenanthrenequinone', Appl. Phys. Lett. 96 (22), 222109 (2010)

[Awakuni et al 72**]** Y. Awakuni, J.H. Calderwood, 'Water Vapor Adsorption and Surface Conductivity in Solids', J. Phys. D. 5, 1038 (1972)

[Balestra et al 87**]** F. Balestra, S. Cristoloveanu, M. Benachir, J. Brini, T. Elewa, 'Double-Gate SOI Transistor with Volume Inversion: A New Device with Greatly Enhanced Performance', IEEE Elect. Dev. Lett. 8 (9), 410 (1987)

[Bansal et al 96**]** A. Bansal, X. Li, I. Lauermann, N.S. Lewis, S.I. Yi, W.H. Weinberg, 'Alkylation of Si Surfaces Using a Two-Step Halogenation/Grignard Route', J. Am. Chem. Soc. 118 (30), 7225 (1996)

[Bardeen 47**]** J. Bardeen, 'Surface States and Rectification at a Metal Semi-Conductor Contact', Phys. Rev. 71 (10), 717 (1947)

[Bardeen 48**]** J. Bardeen, W.H. Brattain, 'The Transistor, A Semi-Conductor Triode', Phys. Rev.74 (2), 230 (1948)

[Bateman et al 98**]** J.E. Bateman, R.D. Eagling, D.R. Worrall, B.R. Horrocks, A. Houlton, 'Alkylierung von porösem Silicium durch direkte Umsetzung mit Alkenen und Alkinen', Agnew. Chem. Int. Ed. 37 (19), 2683 (1998)

[Batzill et al 06**]** M. Batzill, W. Bergermayer, I. Tanaka, U. Diebold, 'Tuning the chemical functionality of a gas sensitive material: Water adsorption on SnO2(1 0 1)', Surf. Sci. 600 (4), 29 (2006)

[Bedwani et al 08**]** S. Bedwani, D. Wegner, M.F. Crommie, A. Rochefort, 'Strongly Reshaped Organic-Metal Interfaces: Tetracyanoethylene on Cu(100)', Phys. Rev. Lett. 101 (21), 216105 (2008)

[Bekoe et al 60**]** D.A. Bekoe, K.N. Truebold, Zeits. Krist. 113 (1-6), 1 (1960)

[Belemlilga et al 99**]** D. Belemlilga, J.M. Gillet, P.J. Becker, 'Charge and momentum densities of cubic tetracyanoethylene and its insertion compounds', Acta Cryst. B 55, 192 (1999)

[Bin et al 08**]** X. Bin, T.K. Mischki, C. Fan, G.P. Lopinski, D.D.M. Wayner, 'Electrochemical Characterization of Si(111) Modified with Linear and Branched Alkyl Chains', J. Phys. Chem. C 111 (36), 13547 (2008)

[Bloch 28**]** F. Bloch, 'Quantum Mechanics of Electrons in Crystal Lattices', Z. Physik. 52, 555 (1928)

[Blomquist et al 06**]** T. Blomquist, G. Kirczenow, 'Origin of the hole gas at the Si(111):Cl surface: Role of surface electronic structure, impurities, and defects', Phys. Rev. B 73 (19), 195303 (2006)

[Boland et al 92**]** J.J. Boland, 'Role of bond-strain in the chemistry of hydrogen on the Si(100) surface', Surf. Sci. 261, 17 (1992)

[Bollani et al 00**]** M. Bollani, L. Fares, A. Charai, D. Narducci, 'Chemically induced disordering of Si (100) surfaces upon SC1/SC2 etching analyzed by high-resolution transmission electron microscopy', Mater. Sci. Eng. B 73, 240 (2000)

[Bordwell et al 91**]** F.G. Bordwell, H.E. Fried, 'Heterocyclic aromatic anions with 4n + 2 pi.-electrons', J. Org. Chem. 56 (13), 4218 (1991)

[Bose 1904**]** J.C. Bose, 'Detector for electrical disturbances', US Patent 755,840

[Boukherroub et al 99**]** R. Boukherroub, S. Morin, F. Bensebaa, D.D.M. Wayner, 'New Synthetic Routes to Alkyl Monolayers on the Si(111) Surface', Langmuir 15 (11), 3831 (1999)

[Bourland et al 01**]** S. Bourland, J. Denton, A. Ikram, G.W. Neudeck, R. Bashir, 'Silicon-on-insulator processes for the fabrication of novel nanostructures', J. Vac. Sci. Technol. B 19 (5), 1995 (2001)

[Boyd 63**]** R.H. Boyd, 'Thermochemistry of Cyanocarbons', J. Chem. Phys. 38 (10), 2529 (1963)

[Brattain 53**]** W. Brattain, J. Bardeen, 'Surface Properties of Germanium', Bell. Syst. Tech. J. 32, 1 (1953)

[Brown 53**]** W.L. Brown, 'n-Type Surface Conductivity on p-Type Germanium', Phys. Rev. 91 (3), 518 (1953)

[Buck et al 58**]** T.M. Buck, F.S. McKim, 'Effects of Certain Chemical Treatments and Ambient Atmospheres on Surface Properties of Silicon', J. Electrochem. Soc. 105 (12), 709 (1958)

[Bunimovich et al 06**]** Y.L. Bunimovich, Y.S. Shin, W.S. Yeo, M. Amori, G. Kwong, J.R. Heath, 'Quantitative Real-Time Measurements of DNA Hybridization with Alkylated Nonoxidized Silicon Nanowires in Electrolyte Solution', J. Am. Chem. Soc. 128 (50), 16323 (2006)

[Buriak 02**]** J.M. Buriak, 'Organometallic Chemistry on Silicon and Germanium Surfaces', Chem. Rev. 102 (5), 1272 (2002)

[Burrows et al 88**]** V.A. Burrows, Y.J. Chabal, G.S. Higashi, K. Raghavachari, S.B. Christman, 'Infrared spectroscopy of Si(111) surfaces after HF treatment: Hydrogen termination and surface morphology', Appl. Phys. Lett. 53 (11), 998 (1988)

[Cahen et al 05**]** D. Cahen, R. Naaman, Z. Vager, 'The Cooperative Molecular Field Effect', Adv. Funct. Mater. 15, 1571 (2005)

[Cai 02**]** W. Cai, Z. Lin, T. Strother, L.M. Smith, R.J. Hamers, 'Chemical Modification and Patterning of Iodine-Terminated Silicon Surfaces Using Visible Light', J. Phys. Chem. B 106 (10), 2656 (2002)

[Cairns et al 57**]** T.L. Cairns, R.A. Carboni, D.D. Coffman, V.A. Engelhardt, R.E. Heckert, E.L. Little, 'Cyanocarbon Chemistry-Synthesis and Chemistry of Tetracyanoethylene', J. Am. Chem. Soc. 79 (9), 2340 (1957)

[Cairns et al 58**]** T.L. Cairns, R.A. Carboni, D.D. Coffman, V.A. Engelhardt, R.E. Heckert, E.L. Little, E.G. McGeer, B.C. McKusick, W.J. Middleton, R.M. Scribner, C.W. Theobald, H.E. Wineberg, 'Cyanocarbon Chemistry. I. Preparation and Reactions of Tetracyanoethylene', J. Am. Chem. Soc. 80 (11), 2775 (1958)

[Cao 09**]** Q. Cao, J.A. Rogers, 'Ultrathin Films of Single-Walled Carbon Nanotubes for Electronics and Sensors: A Review of Fundamental and Applied Aspects', Adv. Mater. 21, 29 (2009)

[Carrico et al 07**]** B. Carrico, J. Saredy, J.L. Tracy, N.G. Patel, J. Garner, L. Gasparov, 'Measurement of the dc resistance of semiconductor thin film–gas systems: Comparison to several transport models', J. Appl. Phys. 102 (8), 083714 (2007)

[Celler et al 03**]** G.K. Celler, S. Cristoloveanu, 'Frontiers of silicon-on-insulator', J. Appl. Phys. 93 (9), 4955 (2003)

[Cerofolini et al**]** G.F. Cerofolini, D. Mascolo, M.O. Vlad, 'A model for oxidation kinetics in air at room temperature of hydrogen-terminated (100) Si', J. Appl. Phys. 100 (5), 054308 (2006)

[Chabal et al 89**]** Y.J. Chabal, G.S. Higashi, K. Ragavachari, V.A. Burrows, 'Infrared spectroscopy of Si(111) and Si(100) surfaces after HF treatment: Hydrogen termination and surface morphology', J. Vac. Sci. Technol. A 7 (3), 2104 (1989)

[Chen et al 09**]** S. Chen, J.G. Bomer, W.G. Van der Wiel, E.T. Carlen, A. Van den Berg, 'Top-down fabrication of sub-30 nm monocrystalline silicon nanowires using conventional microfabrication', ACS Nano 3 (11), 3485 (2009)

[Chen et al 11**]** K.K. Chen, B.R. Li, Y.T. Chen, 'Silicon nanowire field-effect transistor-based biosensors for biomedical diagnosis and cellular recording investigation', Nano Today 6, 131 (2011)

[Cho et al 03**]** Y.E. Cho, J.Y. Maeng, S. Kim, 'Formation of Highly Ordered Organic Monolayers by Dative Bonding: Pyridine on Ge(100)', J. Am. Chem. Soc. 125 (25), 7514 (2003)

[Chowdhury et al 86**]** S. Chowdhury, P. Kebarle, 'Electron Affinities of Di- and Tetracyanoethylene and Cyanobenzenes Based on Measurements of Gas-Phase Electron-Transfer Equilibria', J. Am. Chem. Soc. 108 (18), 5453 (1986)

[Ciampi et al 10**]** S. Ciampi, J.B. Harper, J.J. Gooding, 'Wet chemical routes to the assembly of organic monolayers on silicon surfaces via the formation of Si–C bonds: surface preparation, passivation and functionalization', Chem. Soc. Rev. 39 (6), 2158 (2010)

[Cicero et al 00**]** R.L. Cicero, M.R. Linford, C.E.D. Chidsey, 'Photoreactivity of Unsaturated Compounds with Hydrogen-Terminated Silicon(111)', Langmuir 16 (13), 5688 (2000)

[Cleland et al 95**]** G. Cleland, B.R. Horrocks, A. Houlton, 'Direct functionalization of silicon via the self-assembly of alcohols', J. Chem. Soc. Faraday Trans 91 (21), 4001 (1995)

[Cohen et al 97**]** R. Cohen, N. Zenou, D. Cahen, S. Yitzchaik, 'Molecular electronic tuning of Si surfaces', Chem. Phys. Lett. 279 (5-6), 270 (1997)

[Cohen et al 99**]** R. Cohen, L. Kronik, A. Shanzer, D. Cahen, A. Liu, Y. Rosenwaks, J.K. Lorenz, A.B. Ellis, 'Molecular Control over Semiconductor Surface Electronic Properties: Dicarboxylic Acids on CdTe, CdSe, GaAs, and InP', J. Am. Chem. Soc. 121 (45), 10545 (1999)

[Colinge et al 87**]** J.P. Colinge, 'A voltage-controlled bipolar-MOS (VCBM) ring oscillator', Electron. Lett. 23 (19), 1023 (1987)

[Colinge et al 88**]** J.P. Colinge, 'Thin-film SOI devices: A perspective', Microelectronic Engineering 8 (3-4), 127 (1988)

[Colinge et al 89**]** J.P. Colinge, 'Thin-film SOI technology: the solution to many submicron CMOS problems', Technical Digest IEDM'89, 817 (1989)

[Colinge et al 98**]** J.P. Colinge, 'Fully-depleted SOI CMOS for analog applications', IEEE Trans. Electron Dev. 45 (5), 1010 (1998)

[Colman et al 69**]** D. Colman, D.L. Kendall, 'Effect of Surface Treatments on Silicon Hall Measurements', J. Appl. Phys. 40 (11), 4662 (1969)

[Comini et al 02**]** E. Comini, G. Faglia, G. Sberveglieri, Z. Pan, Z.L. Wang, 'Stable and highly sensitive gas sensors based on semiconducting oxide nanobelts', Appl. Phys. Lett. 81 (10), 1869 (2002)

[Cooper et al 11**]** A.J. Cooper, K. Keyvanfar, A. Deberardinis, L. Pu, J.C. Bean, 'Dopant passivation and work function tuning through attachment of heterogeneous organic monolayers on silicon in ultrahigh vacuum', Appl. Surf. Sci. 257 (14), 6138 (2011)

[Cristoloveanu 91a**]** S. Cristoloveanu, 'A Review of the Electrical Properties of SIMOX Substrates and Their Impact on Device Performance', J. Electrochem. Soc. 138 (1), 3131 (1991)

[Cristoloveanu 91b**]** S. Cristoloveanu, 'Oxygen-related activity and other specific electrical properties of SIMOX', Vacuum 42 (5), 371 (1991)

[Cristoloveanu et al 92**]** S. Cristoloveanu, S. Williams, 'Point-Contac t Pseudo-MOSFET for In –Situ Characterization of As-Grown Silicon-on-Insulator Wafers', IEEE Electron Dev. Lett. 13 (2), 102 (1992)

[Cristoloveanu et al 95**]** S. Cristoloveanu, S. Li, 'Electrical Characterization of Silicon-On-Insulator Devices', Kluwer, Boston, MA USA 1995

[Cristoloveanu et al 00**]** S. Cristoloveanu, D. Munteanu, M. Liu, 'A Review of the Pseudo-MOS Transistor in SOI Wafers: Operation, Parameter Extraction, and Applications,' IEEE Trans. Electron Dev. 47 (5), 1018 (2000)

[Cristoloveanu et al 01**]** S. Cristoloveanu, 'Silicon on insulator technologies and devices: from present to future', Solid-State Electronics 45 (8), 1403 (2001)

[Coletti et al 10**]** C. Coletti, C. Riedl, D.S. Lee, B. Krauss, L. Patthey, K. von Klitzing, J.H. Smet, U. Starke, 'Charge neutrality and band-gap tuning of epitaxial graphene on SiC by molecular doping', Phys. Rev. B 81 (23), 235401 (2010)

[Coustel et al 11**]** R. Coustel, S. Carniato, G. Boureau, 'Thermodynamic factors limiting the preservation of aromaticity of adsorbed organic compounds on Si(100): Example of the pyridine', J. Chem. Phys. 134 (23), 234708 (2011)

[Cui et al 01**]** Y. Cui, Q. Wei, H. Park, C.M. Lieber, 'Highly Sensitive and Selective Detection of Biological and Chemical Species', Science 293 (5533), 1289 (2001)

[Czochralski 18**]** J. Czochralski, Zeits. F. Phys. Chem. 92, 219 (1918)

[Deal et al 65**]** B.E. Deal, A.S. Grove 'General Relationship for the Thermal Oxidation of Silicon', J. Appl. Phys. 36 (12), 3770 (1965)

[Deutsch et al 07**]** D. Deutsch, A. Natan, Y. Shapira, L. Kronik, 'Electrostatic properties of adsorbed polar molecules: opposite behavior of a single molecule and a molecular monolayer', J. Am. Chem. Soc. 129 (10), 2989 (2007)

[Dhar 67**]** D.N. Dhar, 'The Chemistry of Tetracyanoethylene', Chem. Rev. 67 (6), 611 (1967)

[Dubey et al 07**]** G. Dubey, G.P. Lopinski, F. Rosei, 'Influence of physisorbed water on the conductivity of hydrogen terminated silicon-on-insulator surfaces', Appl. Phys. Lett. 91 (23), 232111 (2007)

[Dubey et al 10**]** G. Dubey, F. Rosei, G.P. Lopinski 'Molecular Modulation of Conductivity on H‐Terminated Silicon‐On‐Insulator Substrates', Small 6 (24), 2892 (2010)

[Dubey et al 11a**]** G. Dubey, F. Rosei, G.P. Lopinski, 'Modulation of flat-band voltage on H-terminated silicon-on-insulator pseudo–metal–oxide–semiconductor field effect transistors by adsorption and reaction events', J. Appl. Phys. 109 (10), 104904 (2011)

[Dubey et al 11b**]** G. Dubey, F. Rosei, G.P. Lopinski, 'Highly sensitive electrical detection of TCNE on chemically passivated silicon-on-insulator', Chem. Comm. 47, 10593 (2011)

[Dumas et al 91**]** P. Dumas, Y.J. Chabal, 'Electron-energy-loss characterization of the H-terminated Si(111) and Si(100) surfaces obtained by etching in NH4F', Chem. Phys. Lett. 181 (6), 537 (1991)

[Dumas et al 92**]** P. Dumas, Y.J. Chabal, P. Jakop, 'Morphology of hydrogen-terminated Si(111) and Si(100) upon etching in HF and buffered-HF solutions', Surf. Sci. 269, 867 (1992)

[Dumin et al 68**]** D.J. Dumin, R.S. Silver, 'Diffused diodes in silicon-on-sapphire', Solid-State Electron. 11 (3), 353 (1968)

[Eng et al 05**]** K. Eng, R.N. McFarland, B.E. Kane, 'High mobility two-dimensional electron system on hydrogen-passivated silicon(111)surfaces', Appl. Phys. Lett. 87 (5), 052106 (2005)

[Eng et al 07**]** K. Eng, R.N. McFarland, B.E. Kane, 'Integer Quantum Hall Effect on a Six-Valley Hydrogen-Passivated Silicon (111) Surface', Phys. Rev. Lett. 99 (1), 016801 (2007)

[Engel et al 10**]** Y. Engel, R. Elnathan, A. Pevzner, G. Davidi, E. Flaxer, F. Patolsky, 'Supersensitive Detection of Explosives by Silicon Nanowire Arrays', Angew. Chem. 49 (38), 6830 (2010)

[Eves et al 05**]** B.J. Eves, G.P. Lopinski, 'Formation and reactivity of high quality halogen terminated Si(111) surfaces', Surf. Sci. Lett. 579 (2-3), 89 (2005)

[Eves et al 06] B.J. Eves, G.P. Lopinski, 'Formation of Organic Monolayers on Silicon via Gas-Phase Photochemical Reactions', Langmuir 22 (7), 3180 (2006)

[Ewing et al 01] R.G. Ewing, D.A. Atkinson, G.A. Eiceman, G.J. Ewing, 'A critical review of ion mobility spectrometry for the detection of explosives and explosive related compounds.', Talanta 54 (3), 5151 (2001)

[Fan 05] Z. Fan, J.G. Lu, 'Gate-refreshable nanowire chemical sensors', Appl. Phys. Lett. 86 (12), 123510 (2005)

[Fan 10] C. Fan, G.P. Lopinski, 'STM and HREELS investigation of gas phase silanization on hydroxylated Si(100)', Surf. Sci. 604 (11-12), 996 (2010)

[Fidelis et al 00] A. Fidelis, F. Ozanam, J.N. Chazalviel, 'Fully methylated, atomically flat (111) silicon surface', Surf. Sci. 444 (1-3), 7 (2000)

[Fischer 68] T.E. Fischer, 'Surface properties of Si from photoelectric emission at room temperature and 80 °K', Surf. Sci. 10 (3), 399 (1968)

[Fraden 96] J. Fraden, 'Handbook of Modern Sensors', Springer-Verlag, New York (1996)

[Fritz 02] J. Fritz, E.B. Cooper, S. Gaudet, P.K. Sorger, S.R. Manalis 'Electronic detection of DNA by its intrinsic molecular charge', PNAS 99 (22), 14142 (2002)

[Gao et al 11] C. Gao, Z.C. Xu, S.R. Deng, J. Wan, Y. Chen, R. Liu, 'Silicon nanowires by combined nanoimprint and angle deposition for gas sensing applications', Microelectron. Eng. 88 (8), 2100 (2011)

[Gerischer et al 88] H. Gerischer, M. Lubke, 'Electrolytic growth and dissolution of oxide layers on silicon in aqueous solutions of fluorides', Ber. Bunsenges Phys. Chem. 92 (5), 573 (1988)

[Gomperz 22] E.V. Gomperz, Zeits. F. Physik. 8, 184 (1922)

[Goodpaster et al 01] J.V. Goodpaster, V.L. McGuffin, 'Fluorescence Quenching as an Indirect Detection Method for Nitrated Explosives', Anal. Chem. 73 (9), 2004 (2001)

[Graf et al 90] D. Graf, M. Grundner, R. Schulz, L. Muhlhoff, 'Oxidation of HF-treated Si wafer surfaces in air', J. Appl. Phys. 68 (10), 5155 (1990)

[Green et al 08**]** J.E. Green, S.J. Wong, J.R. Heath, 'Hall Mobility Measurements and Chemical Stability of Ultrathin, Methylated Si(111)-on-Insulator Films', J. Phys. Chem. C 112 (13), 5185 (2008)

[Grudner et al 86**]** M. Grudner, H. Jacob, 'Investigations on hydrophilic and hydrophobic silicon (100) wafer surfaces by X-ray photoelectron and high-resolution electron energy loss-spectroscopy', Appl. Phys. A 39 (2) 73 (1986)

[Grunthaner et al 86**]** F.J. Grunthaner, P.J. Grunthaner, 'Chemical and electronic structure of the SiO2/Si interface', Mater. Sci. Repts. 1 (2), 65 (1986)

[Grupp et al 98**]** C. Grupp, A.T. Ibrahimi, 'Huge charge transfer from potassium on H:Si(111)-(1×1)', Surf. Sci. 408 (1-3), 160 (1998)

[Gupta et al 88**]** P. Gupta, V.L. Colvin, S.M. George, 'Hydrogen desorption kinetics from monohydride and dihydride species on silicon surfaces', Phys. Rev. B 37 (14), 8234 (1988)

[Hahm et al 04**]** J. Hahm, C.M. Lieber, 'Direct Ultrasensitive Electrical Detection of DNA and DNA Sequence Variations Using Nanowire Nanosensors', Nano Lett. 4 (1), 51 (2004)

[Hasegawa et al 99**]** S. Hasegawaa, X. Tonga, S. Takedaa, N. Satoa, T. Nagaoa, 'Structures and electronic transport on silicon surfaces', Prog. Surf. Sci. 60 (5-8), 89 (1999)

[Hasegawa et al 92**]** S. Hasegawa, S. Ino, 'Surface structures and conductance at epitaxial growths of Ag and Au on the Si(111) surface', Phys. Rev. Lett. 68 (8), 1192 (1992)

[Hayashi et al 97**]** K. Hayashi, S. Yamanaka, H. Watanabe, T. Sekiguchi, H. Okushi, K. Kajimura, 'Investigation of the effect of hydrogen on electrical and optical properties in chemical vapor deposited on homoepitaxial diamond films', J. Appl. Phys. 81 (2), 745 (1997)

[He et al 06**]** T. He, J. He, M. Lu, B. Chen, H. Pang, W.F. Reus, W.M. Nolte, D.P. Nackashi, P.D. Franzon, J.M. Tour, 'Controlled Modulation of Conductance in Silicon Devices by Molecular Monolayers', J. Am. Chem. Soc. 128 (45), 14537 (2006)

[He et al 08**]** T. He, M. Lu, J. Yao, J. He, B. Chen, N.H. Di Spigna, D.P. Nackashi, P.D. Franzon, J.M. Tour, 'Reversible Modulation of Conductance in Silicon Devices via UV/Visible-Light Irradiation', Adv. Mater. 20 (23), 4541 (2008)

[He et al 09**]** T. He, D.A. Corley, M. Lu, N.H. Di Spigna, J. He, D.P. Nackashi, P.D. Franzon, J.M. Tour, 'Controllable Molecular Modulation of Conductivity in Silicon-Based Devices', J. Am. Chem. Soc. 131 (29), 10023 (2009)

[Heckert et al 57**]** R.E. Heckert, E.L. Little. Preparation of Tetracyanoethylene, US patent 2,794,824, June 4 (1957)

[Heiland 59**]** G. Heiland, 'Surface conductivity of semiconductors and its variation by adsorption, transverse electric fields and irradiation', Disc. Faraday Soc. 28, 168 (1959)

[Heilig et al 79**]** K. Heilig, H. Flietner, J. Reineke, 'Investigation of energetic surface state distributions at real surfaces of silicon after treatment with HF and H2O using large-signal photovoltage pulses', J. Phys. D. 12 (6), 927 (1979)

[Heiman et al 66**]** F.P. Heiman, 'Thin-film silicon-on-sapphire deep depletion MOS transistors', IEEE Trans. Electron Dev. 13 (12), 855 (1966)

[Heine et al 65**]** V. Heine, 'Theory of Surface States', Phys. Rev. 138 (6), 1689 (1965)

[Helwig et al 07a**]** A. Helwig, G. Müller, G. Sberveglieri, G. Faglia, 'Gas Sensing Properties of Hydrogenated Amorphous Silicon Films', IEEE Sens. J. 7 (11), 1506 (2007)

[Helwig et al 07b**]** A. Helwig, G. Muller, J.A. Garrido, M. Eickhoff, 'Gas sensing properties of hydrogen-terminated diamond', IEEE Sens. J. 7 (9), 1349 (2007)

[Henrion et al 99**]** W. Henrion, A. Roseler, H. Angermann, M. Rebien, 'Application of UV-VIS and FTIR Spectroscopic Ellipsometry to the Characterization of Wet-Chemically Treated Si Surfaces', Phys. Stat. Sol. A 175 (1), 121 (1999)

[Henrion et al 02**]** W. Henrion, M. Rebien, H. Angermann, A. Roseler, 'Spectroscopic investigations of hydrogen termination, oxide coverage, roughness, and surface state density of silicon during native oxidation in air', Appl. Surf. Sci. 202, 199 (2002)

[Hernandez-Ramirez et al 07**]** F. Hernandez-Ramirez, S. Barth, A. Tarancon, O. Casals, E. Pellicer, J. Rodriguez, J.R. Morante, S. Mathur, 'Water vapor detection with individual tin oxide nanowires', Nanotechnol. 18 (42), 424016 (2007)

[Higashi et al 90**]** G.S. Higashi, Y.J. Chabal, G.W. Trucks, K. Raghavachari, 'Ideal hydrogen termination of the Si(111) surface', Appl. Phys. Lett. 56 (7), 656 (1990)

[Higashi et al 91**]** G.S. Higashi, R.S. Becker, Y.J. Chabal, A.J. Becker, 'Comparison of Si(111) surfaces prepared using aqueous solutions of NH4F versus HF', Appl. Phys. Lett. 58 (15), 1656 (1991)

[Himpsel et al 83**]** F.J. Himpsel, G. Hollinger, R.A. Pollak, 'Determination of the Fermi-level pinning position at Si(111) surfaces', Phys. Rev. B 28 (12), 7014 (1983)

[Hiremath et al 08**]** R.K. Hiremath, M.K. Rabinal, B.G. Mulimani, I.M. Khazi, 'Molecularly Controlled Metal-Semiconductor Junctions on Silicon Surface: A Dipole Effect', Langmuir 24 (19), 11300 (2008)

[Hipps et al 82**]** K.W. Hipps, U. Mazur, 'Tunneling and infrared spectroscopic characterization of surface reaction products. 1. Chemisorption of tetracyanoethylene on partially hydrated alumina', J. Phys. Chem. 86 (26), 5105 (1982)

[Hollt et al 07**]** L. Höllt, M. Born, M. Schlosser, I. Eisele, J. Grabmeier, A. Huber, 'A Modified PseudoMOS Technique to Characterize Interface Quality of SOI Wafers', IEEE Trans. Electron Dev. 54 (10), 2685 (2007)

[Houston et al 95**]** M.R. Houston, R. Maboudian, 'Stability of ammonium fluoride-treated Si(100)', J. Appl. Phys. 78 (6), 3801 (1995)

[Hovel 03**]** H.J. Hovel, 'Si film electrical characterization in SOI substrates by the HgFET technique', Solid-State Electron. 47, 1311 (2003)

[Huang 87**]** S.D. Huang, L. Kolaitis, D.M. Lubman, 'Detection of Explosives Using Laser Desorption in Ion Mobility Spectrometry/Mass Spectrometry', Appl. Spectrosc. 41 (8), 1371 (1987)

[Ibach 74**]** H. Ibach, J.E. Rowe, 'Hydrogen adsorption and surface structures of silicon', Surf. Sci. 43 (2), 481 (1974)

[Ichimura et al 02**]** M. Ichimura, S. Ito, E. Arai, 'Changes in carrier profiles of bonded SOI wafers with thermal annealing measured by the spreading resistance method', Solid-State Electron. 46 (4), 545 (2002)

[Ionescu et al 96**]** A.M. Ionescu, S. Cristoloveanu, D. Munteau, T. Elewa, M. Gri, 'A New Lifetime Characterization Technique Using Drain Current Transients in SOI Material', Solid-State Electron. 39 (12), 1753 (1996)

[Irom et al 02**]** F. Irom, F.F. Farmanesh, A.H. Johnston, G.M. Swift, D.G. Millward, 'Single-Event Upset in Commercial Silicon-on-Insulator PowerPC Microprocessors', IEEE Trans. Nucl. Sci. 49 (6), 3148 (2002)

[Itaya et al 92**]** K. Itaya, R. Sugawara, Y. Morita, H. Tokumoto, 'Atomic resolution images of H‐terminated Si(111) surfaces in aqueous solutions', Appl. Phys. Lett. 60 (20), 2534 (1992)

[Jakop et al 91**]** P. Jakob, Y.J. Chabal, 'Chemical etching of vicinal Si(111): Dependence of the surface structure and the hydrogen termination on the pH of the etching solutions', J. Chem. Phys. 95 (4), 2897 (1991)

[Jiang et al 96**]** C.S. Jiang, S. Hasegawa, S. Ino, 'Surface conductivity for Au or Ag on Si(111)', Phys. Rev. B 54 (15), 10389 (1996)

[Jie et al 08**]** J. Jie, W. Zhang, K. Peng, G. Yuan, C.S. Lee, S.T. Lee, 'Surface-Dominated Transport Properties of Silicon Nanowires', Adv. Func. Mater. 18 (20), 3251 (2008)

[Kern 90**]** W. Kern, 'The Evolution of Silicon Wafer Cleaning Technology', J. Electrochem. Soc. 137 (6), 1887 (1990)

[Kim et al 03**]** W. Kim, A. Javey, O. Vermesh, Q. Wang, Y. Li, H. Dai, 'Hysteresis Caused by Water Molecules in Carbon Nanotube Field-Effect Transistors', Nano Lett. 3 (2), 193 (2003)

[Kingston 54**]** R.H. Kingston, 'Water Vapor and the "Channel" Effect in n-p-n Junction Transistors', Phys. Rev. 93 (2), 346 (1954)

[Kingston 55a**]** R.H. Kingston, S.F. Neustadter, 'Calculation of the Space Charge, Electric Field, and Free Carrier Concentration at the Surface of a Semiconductor', J. Appl. Phys. 26 (6), 718 (1955)

[Kingston 55b**]** R.H. Kingston, 'Water-Vapor-Induced n-Type Surface Conductivity on p-Type Germanium', Phys. Rev. 98 (6), 1766 (1955)

[Kliewer et al 10**]** C.J. Kliewer, G.A. Somorjai, 'Structure Effects on Pyridine Hydrogenation over Pt(111) and Pt(100) Studied with Sum Frequency Generation Vibrational Spectroscopy', Catal. Lett. 137 (3-4), 118 (2010)

[Kobayashi et al 83**]** H. Kobayashi, K. Edamoto, M. Onchi, M. Nishijima, 'Reactions of atomic hydrogen with the Si(111) (7×7) surface by high resolution electron energy loss spectroscopy', J. Chem. Phys. 78 (12), 7429 (1983)

[Kobayashi et al 98**]** K. Kobayashi, H. Yanagigawa, K. Mori, M. Kazuhisa, S. Yamanaka, A. Fujiwara, 'High voltage SOI CMOS IC technology for driving plasma display panels', Proc. ISPSD'98, 141 (1998)

[Kolasinski**]** K.W. Kolasinski, 'Etching of silicon in fluoride solutions', Surf. Sci. 603 (10-12), 1904 (2009)

[Kolmakov 04**]** A. Kolmakov, M. Moskovits, 'Chemical Sensing and Catalysis By One-Dimensional Metal-Oxide Nanostructures', Annu. Rev. Mater. Res. 34, 151 (2004)

[Korec 95**]** J. Korec, 'Silicon-on-insulator technology for high-temperature, smart-power applications', Mater. Sci. Eng. B 29 (1-3), 1 (1995)

[Kovalgin et al 05**]** A.Y. Kovalgin, A.J. Hof, J. Schmitz, 'An approach to modeling of silicon oxidation in a wet ultra-diluted ambient', Microelect. Eng. 80, 432 (2005)

[Kuge et al 96**]** S. Kuge, F. Morishita, T. Tsuruda, S. Tomishima, M. Tsukude, T. Yamaga, K. Arimoto, 'SOI-DRAM Circuit Technologies for Low Power High Speed Multigiga Scale Memories', IEEE J. Solid-State Circ. 31 (4), 586 (1996)

[Landau 57**]** L.D. Landau, 'The theory of a Fermi liquid', Sov. Phys.
JETP 3, 920 (1957)

[Landstrass et al 89**]** M.I. Landstrass, K.V. Ravi, 'Resistivity of chemical vapor deposited diamond films', Appl. Phys. Lett. 55 (10), 975 (1989)

[LaPedus 04**]** M. Lapedus, 'Ibis exits SOI wafer business, terminates MEMC deal', EE Times News and Analysis, (2004)

[LaPedus 10**]** M. Lapedus, 'Analyst: Intel to Endorse SOI at 22 nm', EE Times News and Analysis, (2010)

[Larsson et al 05**]** K. Larsson, J. Ristein, 'Diamond Surface Conductivity under Atmospheric Conditions: Theoretical Approach', J. Phys. Chem. B 109 (20), 10304 (2005)

[Laws et al 02**]** G.M. Laws, T.J. Thornton, J. Yang, L. de la Garza, M. Kozicki, D. Gust, 'Molecular Control of the Drain Current in a Buried Channel MOSFET', Phys. Stat. Sol. B 233 (1), 83 (2002)

[Lee et al 01**]** J.G. Lee, J. Ahner, J.T. Yates, 'The adsorption conformation of chemisorbed pyridine on the Cu(110) surface', J. Chem. Phys. 114 (3), 1414 (2001)

[Levesque et al 11**]** P.L. Levesque, S.S. Sabri, C.M. Aguirre, J. Guillemette, M. Siaj, P. Desjardins, T. Szkopek, R. Martel, 'Probing Charge Transfer at Surfaces Using Graphene Transistors', Nano Lett. 11(1), 132 (2011)

[Li 03**]** J. Li, Y. Lu, Q. Ye, M. Cinke, J. Han, M. Meyyappan, 'Carbon Nanotube Sensors for Gas and Organic Vapor Detection', Nano Lett. 3 (7), 929 (2003)

[Li et al 04] Z. Li, Y. Chen, X. Li, T.I. Kamins, K. Nauka, R.S. Williams, 'Sequence-Specific Label-Free DNA Sensors Based on Silicon Nanowires', Nano Lett. 4 (2), 245 (2004)

[Lien et al 70] E.J. Lien, W.D. Kumler, 'Dipole moment and structure of thiophene derivatives and benzene analogs', J. Pharm. Sci. 59 (11), 1685 (1970)

[Light et al] T.S. Light, S. Licht, A.C. Bevilacqua, K.R. Morash, 'The Fundamental Conductivity and Resistivity of Water', Electrochem. Solid-State Lett. 8 (1), 16 (2005)

[Lin et al 98] K.C. Lin, O.W. Holland, L.C. Feldman, H.H. Weitering, 'Surface characterization of silicon on insulator material', Appl. Phys. Lett. 72 (18), 2313 (1998)

[Linford et al 93] M.R. Linford, C.E.D. Chidsey, 'Alkyl Monolayers Covalently Bonded to Silicon Surfaces', J. Am. Chem. Soc. 115 (26), 12631 (1993)

[Linford et al 95] M.R. Linford, P. Fenter, P.M. Eisenberger, C.E.D. Chidsey, 'Alkyl Monolayers on Silicon Prepared from 1-Alkenes and Hydrogen-Terminated Silicon', J. Am. Chem. Soc. 117 (11), 3145 (1995)

[Looney et al 58] C.E. Looney, J.R. Downing, 'Cyanocarbon Chemistry. XII. Some Physical Characteristics of Cyanocarbon Derivatives', J. Am. Chem. Soc. 80 (11), 2840 (1958)

[Lopinski et al 05] G.P. Lopinski, B.J. Eves, O. Hul'ko, C. Mark, S.N. Patitsas, R. Boukherroub, and T.R. Ward, 'Enhanced conductance of chlorine-terminated Si(111) surfaces: Formation of a two-dimensional hole gas via chemical modification', Phys. Rev. B 71 (12), 125308 (2005)

[Lu et al 09] Y.H. Lu, W. Chen, Y.P. Feng, P.M. He, 'Tuning the Electronic Structure of Graphene by an Organic Molecule', J. Phys. Chem. B 113(1), 2 (2009)

[Lud et al 06] S.Q. Lud, M.G. Nikolaides, I. Haase, M. Fischer, A.R. Bausch,' Field Effect of Screened Charges: Electrical Detection of Peptides and Proteins by a Thin-Film Resistor', ChemPhysChem 7 (2), 379 (2006)

[MacLaren et al 02] D.A. MacLaren, N.J. Curson, P. Atkinson, B. Holst, D.J. Johnson, W. Allison, 'Simple design for the transportation of ex situ prepared hydrogen passivated silicon', J. Vac. Sci. Technol. A 20 (1), 285 (2002)

[Maier et al 00] F. Maier, M. Riedel, B. Mantel, J. Ristein, and L. Ley, 'Origin of Surface Conductivity in Diamond', Phys. Rev. Lett. 85 (16), 3472 (2000)

[Masood et al 10**]** M.N. Masood, S. Chen, E.T. Carlen, A. van den Berg, 'All-(111) surface silicon nanowires: selective functionalization for biosensing applications', ACS Appl. Mater. Interfaces 2 (12), 3422 (2010)

[Mattei et al 02**]** G. Mattei, V. Valentini, V.A. Yakovlev, 'An FTIR study of porous silicon layers exposed to humid air with and without pyridine vapors at room temperature', Surf. Sci. 502, 58 (2002)

[Mazur et al 84**]** U. Mazur, K.W. Hipps, 'Chemisorption of tetracyanoethylene and its mono- and dianions on alumina: an inelastic electron tunneling study', J. Phys. Chem. 88 (8), 1555 (1984)

[McFarland et al 09**]** R.N. McFarland, T.M. Kott, L. Sun, B.E. Kane, 'Temperature-dependent transport in a sixfold degenerate two-dimensional electron system on a H-Si(111) surface', Phys. Rev. B 80 (16), 161310 (2009)

[Merrifield et al 58**]** R.E. Merrifield, W.D. Phillips, 'Cyanocarbon Chemistry. II. Spectroscopic Studies of the Molecular Complexes of Tetracyanoethylene', J. Am. Chem. Soc. 80 (11), 2778 (1958)

[Michalak et al 10**]** D.J. Michalak, S.R. Amy, D. Aureau, M. Dai, A. Esteve, Y.J. Chabal, 'Nanopatterning Si(111) surfaces as a selective surface-chemistry route', Nature Mater. 9, 266 (2010)

[Middleton et al 38**]** B.A. Middleton, J.R. Partington, 'Dipole Moment of Pyridine', Nature 141 (3568), 516 (1938)

[Miller et al 98**]** J.S. Miller, A.J. Epstein, 'Tetracyanoethylene-based organic magnets', Chem. Commun. (13), 1319 (1998)

[Miller 06**]** J.S. Miller, 'Tetracyanoethylene (TCNE): The Characteristic Geometries and Vibrational Absorptions of Its Numerous Structures', Angew. Chem. Int. Ed. 45 (16), 2508 (2006)

[Mischki et al 06**]** T.K. Mischki, R.L. Donkers, B.J. Eves, G.P. Lopinski, D.D.M. Wayner, 'Reaction of Alkenes with Hydrogen-Terminated and Photooxidized Silicon Surfaces. A Comparison of Thermal and Photochemical Processes', Langmuir 22 (20), 8359 (2006)

[Mischki et al 09**]** T.K. Mischki, G.P. Lopinski, D.D.M. Wayner, 'Evidence for Initiation of Thermal Reactions of Alkenes with Hydrogen-Terminated Silicon by Surface-Catalyzed Thermal Decomposition of the Reactant', Langmuir 25 (10), 5626 (2009)

[Mitchell 03**]** S.A. Mitchell, 'Photooxidation of Hydrogen-Terminated Si(111) Surfaces Studied by Optical Second Harmonic Generation', J. Phys. Chem. B 107 (35), 9388 (2003)

[Miwa et al 05**]** J.A. Miwa, B.J. Eves, F. Rosei, G.P. Lopinski, 'Selective Adsorption of Pyridine at Isolated Reactive Sites on Si(100)', J. Phys. Chem. B Lett. 109 (43), 20055 (2005)

[Mönch 70**]** W. Mönch, 'Surface States on Clean and on Cesium-Covered Cleaved Silicon Surfaces', Phys. Stat. Sol. B 40 (1), 257 (1970)

[Mönch 95**]** W. Mönch, Semiconductor surfaces and interfaces Springer Verlag (1995)

[Moore 65**]** G.E. Moore, 'Cramming more components onto integrated circuits', IEEE SSCS Newslett., 38 (8), 114 (1965)

[Morita et al 90**]** M. Morita, T. Ohmi, E. Hasegawa, M. Kawakami, M. Ohwada, 'Growth of native oxide on a silicon surface', J. Appl. Phys. 68 (3), 1272 (1990)

[Morita et al 95**]** M. Morita, T. Ohmi, E. Hasegawa, M. Kawakami, M. Ohwada, 'Growth of native oxide on a silicon surface', Appl. Phys. Lett. 67 (18), 2654 (1995)

[Mott 39**]** N.F. Mott, 'The Theory of Crystal Rectifiers', Proc. R. Soc. Lond. A 171 (944), 27 (1939)

[Na et al 05**]** P.S. Na, H. Kim, H.M. So, K.J. Kong, H. Chang, B.H. Ryu, Y. Choi, J.O. Lee, B.K. Kim, J.J. Kim, J. Kim, 'Investigation of the humidity effect on the electrical properties of single-walled carbon nanotube transistors', Appl. Phys. Lett. 87 (9), 093101 (2005)

[Natan et al 07**]** A. Natan, L. Kronik, H. Haick, R.T. Tung, 'Electrostatic Properties of Ideal and Non-ideal Polar Organic Monolayers: Implications for Electronic Devices', Adv. Mater. 19 (23), 4103 (2007)

[Natarajan et al 98**]** A. Natarajan, G. Oskam, P.C. Searson, 'Characterization of silicon surfaces in HF solution using microwave reflectivity', J. Appl. Phys. 83 (4), 2112 (1998)

[Naumova et al 10**]** O.V. Naumova, B.I. Fomin, D.A. Nasimov, N.V. Dudchenko, S.F. Devyatova, E.D. Zhanaev, V.P. Popov, A.V. Latyshev, A.L. Aseev,Y.D. Ivanov, A.I. Archakov, 'SOI nanowires as sensors for charge detection', Semicond. Sci. Technol. 25 (5), 055004 (2010)

[Neff et al 06a**]** P.A. Neff, A. Naji, C. Ecker, B. Nickel, R. von Klitzing, A.R. Bausch, 'Electrical Detection of Self-Assembled Polyelectrolyte Multilayers by a Thin Film Resistor', Macromolecules 39 (2), 463 (2006)

[Neff et al 06b**]** P.A. Neff, B.K. Wunderlich, S.Q. Lud, A.R. Bausch, 'Silicon-on-insulator based thin film resistors for quantitative biosensing applications', Phys. Stat. Sol. A 203 (14), 3417 (2006)

[Neff et al 07**]** P.A. Neff, A. Serr, B.K. Wunderlich, and A.R. Bausch, 'Label-Free Electrical Determination of Trypsin Activity by a Silicon-on-Insulator Based Thin Film Resistor', ChemPhysChem 8 (14), 2133 (2007)

[Nikolaides et al 03**]** M.G. Nikolaides, S. Rauschenbach, S. Luber, K. Buchholz, M. Tornow, G. Abstreiter, A.R. Bausch, 'Silicon-on-Insulator Based Thin-Film Resistor for Chemical and Biological Sensor Applications', ChemPhysChem 4, 1104 (10) (2003)

[Nikolaides et al 04**]** M.G. Nikolaides, S. Rauschenbach, and A.R. Bausch, 'Characterization of a silicon-on-insulator based thin film resistor in electrolyte solutions for sensor applications', J. Appl. Phys. 95 (7), 3811 (2004)

[Niwano et al 94**]** M. Niwano, J. Kageyama, K. Kinashi, J. Sawahata,
N. Miyamoto, 'Oxidation of hydrogen-terminated Si surfaces studied by infrared spectroscopy', J. Appl. Phys. 76 (4), 2157 (1994)

[Ogawa et al 96**]** H. Ogawa, K. Ishikawa, C. Inomata, S. Fujimura, 'Initial stage of native oxide growth on hydrogen terminated silicon (111) surfaces', J. Appl. Phys. 79 (1), 472 (1996)

[Onclin 05**]** S. Onclin, B.J. Ravoo, D.N. Reinhoudt, 'Engineering Silicon Oxide Surfaces Using Self-Assembled Monolayers', Angew. Chemie. Int. Ed. 44 (39), 6282 (2005)

[Ortiz-Conde et al 07**]** A. Ortiz-Conde, F.J. Garcia-Sanchez, J. Muci, S. Malobabic, J.J. Liou, 'A Review of Core Compact Models for Undoped Double-Gate SOI MOSFETs', IEEE Trans. Elect. Dev. 54 (1), 131 (2007)

[Oskam et al 96a**]** G. Oskam, P.M. Hoffmann, P.C. Searson, 'In Situ Measurements of Interface States at Silicon Surfaces in Fluoride Solutions', Phys. Rev. Lett. 76 (9), 1521 (1996)

[Oskam et al 96b**]** G. Oskam, P.M. Hoffmann, J.C. Schmidt, P.C. Searson, 'Energetics and Kinetics of Surface States at n-Type Silicon Surfaces in Aqueous Fluoride Solutions', J. Phys. Chem. 100(5), 1801 (1996)

[Osminkina et al 05] L.A. Osminkina, A.S. Vorontsov, E.A. Konstantinova, V.Y. Timoshenko, P.K. Kashkarov, 'Influence of Pyridine Molecule Adsorption on Concentrations of Free Carriers and Paramagnetic Centers in Porous Silicon Layers', Semiconductors 39 (4), 458 (2005)

[Oxley et al 08] J.C. Oxley, J.L. Smith, L.J. Kirschenbaum, S. Marimganti, S. Vadlamannati, 'Detection of Explosives in Hair Using Ion Mobility Spectrometry', J. Forens. Sci. 53 (3), 690 (2008)

[Ozdemir 07] S. Ozdemir, J.L. Gole, 'The potential of porous silicon gas sensors', Curr. Opp. Solid-State Mater. Sci. 11 (5), 92 (2007)

[Palmer 61] D.R. Palmer, S.R. Morrison, C.E. Dauenbaugh, 'Surface States on Cleaved Silicon', Phys. Rev. Lett. 6 (4), 170 (1961)

[Pan et al 85] F.M. Pan, J.C. Hemminger, S. Ushioda, 'Adsorption of tetracyanoethylene on a nickel(111) surface studied by Auger electron spectroscopy, thermal desorption spectroscopy, and Raman spectroscopy', J. Phys. Chem. 89 (5), 862 (1985)

[Park et al 07] I. Park, Z. Li, X. Li, A.P. Pisano, S.R. Williams, 'Towards the silicon nanowire-based sensor for intracellular biochemical detection', Bionsens. Bioelectron. 22 (9-10), 2065 (2007)

[Park et al 10] I. Park, Z. Li, A.P. Pisano, S.R. Williams, 'Top-down fabricated silicon nanowire sensors for real-time chemical detection', Nanotech. 21 (1), 015501 (2010)

[Peng et al 11] K.Q. Peng, S.T. Lee, 'Silicon Nanowires for Photovoltaic Solar Energy Conversion', Adv. Mater. 23 (2), 198 (2011)

[Petritz 58] R.L. Petritz, 'Theory of an Experiment for Measuring the Mobility and Density of Carriers in the Space-Charge Region of a Semiconductor Surface', Phys. Rev. 110 (6), 1254 (1958)

[Pettinger et al 78] B. Pettinger, U. Wenning, 'Raman spectra of pyridine adsorbed on silver (100) and (111) electrode surfaces', Chem. Phys. Lett. 56 (2), 253 (1978)

[Pillai et al 07] S. Pillai, K.R. Catchpole, T. Trupke, M.A. Green, 'Surface plasmon enhanced silicon solar cells', J. Appl. Phys. 101 (9), 093105 (2007)

[Popoff et al 10] R.T.W. Popoff, H. Asanuma, H.Z. Yu, 'Long-Term Stability and Electrical Performance of Organic Monolayers on Hydrogen-Terminated Silicon', J. Phys. Chem. C 114 (24), 10866 (2010)

[Porter et al 87**]** M.D. Porter, T.B. Bright, D.L. Allara, C.E.D. Chidsey, 'Spontaneously Organized Molecular Assemblies. Structural Characterization of n-Alkyl Thiol Monolayers on Gold by Optical Ellipsometry, Infrared Spectroscopy, and Electrochemistry', J. Am. Chem. Soc. 109 (12), 3559 (1987)

[Qi 03**]** P. Qi, O. Vermesh, M. Grecu, A. Javey, Q. Wang, H. Dai, 'Toward Large Arrays of Multiplex Functionalized Carbon Nanotube Sensors for Highly Sensitive and Selective Molecular Detection', Nano Lett. 3 (3), 347 (2003)

[Ragmir et al 10**]** N.S. Ramgir, Y. Yang, M. Zacharias, 'Nanowire-Based Sensors', Small 6 (16), 1705 (2010)

[Rao et al 08**]** T.V. Chandrasekhar Rao, J. Antoszewski, L. Faraone, S. Cristoloveanu, T. Nguyen, P. Gentil, N. Bresson, F. Allibert, 'Transport measurements in silicon-on-insulator films: Comparison of Hall effect, mobility spectrum, and pseudo-metal-oxide-semiconductor-field-effect-transistor techniques', J. Appl. Phys. 103 (3), 034503 (2008)

[Rettig et al 69**]** M.F. Rettig, R.M. Wing, 'Tetracyanoethylene anion as a hard σ base. Synthesis and structure of the 1:1 adduct of tetracyanoethylene and bis(π-cyclopentadienyl)vanadium monobromide', J. Inorg. Chem. 8 (12), 2685 (1969)

[Ricca et al 98**]** A. Ricca, C.W. Bauschlicher, 'Accurate Heats of Formation for SiFn and SiFn+, for n=1-4', J. Phys. Chem. A 102 (5), 876 (1998)

[Ritz et al 10**]** C.S. Ritz, H.J. Kim-Lee, D.M. Detert, M.M. Kelly, F.S. Flack, D.E. Savage, Z. Cai, P.G. Evans, K.T. Turner, M.G. Lagally, 'Ordering of nanostressors on free-standing silicon nanomembranes and nanoribbons', New. J. Phys. 12, 103011 (2010)

[Rivillon et al 04**]** S. Rivillon, F. Amy, Y.J. Chabal, M.M. Frank, 'Gas phase chlorination of hydrogen-passivated silicon surfaces', Appl. Phys. Lett. 85 (13), 2583 (2004)

[Sagiv et al 80**]** J. Sagiv, 'Organized monolayers by adsorption. 1. Formation and structure of oleophobic mixed monolayers on solid surfaces', J. Am. Chem. Soc. 102 (1), 92 (1980)

[Sakata et al 00**]** K. Sakata, T. Sato, K. Nakamura, A. Osamura, A. Tachibana, 'Quantum chemical mechanism of oxidation of the hydrogen-terminated Si surface by oxygen anion', Appl. Surf. Sci. 159, 392 (2000)

[Schedin et al 07**]** F. Schedin, A.K. Geim, S.V. Morozov, E.W. Hill, P. Blake, M.I. Katsnelson, K.S. Novoselov, 'Detection of individual gas molecules adsorbed on graphene', Nature Mater. 6, 652 (2007)

[Schlaf et al 99**]** R. Schlaf, R. Hinogami, M. Fujitani, S. Yae, Y. Nakato, 'Fermi level pinning on HF etched silicon surfaces investigated by photoelectron spectroscopy', J. Vac. Sci. Technol. A 17 (1), 164 (1999)

[Schlesier et al 76**]** K.M. Schlesier, J.M. Shaw, C.W. Benyon, 'Al2O3 as a radiation-tolerant CMOS dielectric', RCA Rev. 37, 358 (1976)

[Schlier 59**]** R.E. Schlier, H.E. Farnsworth, 'Structure and Adsorption Characteristics of Clean Surfaces of Germanium and Silicon', J. Chem. Phys. 30 (4), 917 (1959)

[Scott et al 09**]** S.A. Scott, W. Peng, A.M. Kiefer, H. Jiang, I. Knezevic, D.E. Savage, M.A. Eriksson, M.G. Lagally, 'Influence of Surface Chemical Modification on Charge Transport Properties in Ultrathin Silicon Membranes', ACS Nano 3 (7), 1683 (2009)

[Seiffe 11**]** J. Seiffe, M. Hofmann, J. Rentsch, R. Preu, 'Charge carrier trapping at passivated silicon surfaces', J. Appl. Phys. 109 (6), 064505 (2011)

[Shalev et al 09**]** G. Shalev, E. Halpern, A. Doron, A. Cohen, Y. Rosenwaks, I. Levy, 'Surface chemical modification induces nanometer scale electron confinement in field effect device', J. Chem. Phys. 131 (2), 024702 (2009)

[Shaya et al 08**]** O. Shaya, M. Shaked, A. Doron, A. Cohen, I. Levy, Y. Rosenwaks, 'Distinguishing between dipoles and field effects in molecular gated transistors' Appl. Phys. Lett. 93 (4), 043509 (2008)

[Shibata et al 04**]** Y. Shibata, M. Ichimura, E. Arai, 'Conduction type change with annealing in thin silicon-on-insulator wafers', Solid-State Electron. 48 (7), 1249 (2004)

[Sieval et al 99**]** A.B. Sieval, V. Vleeming, H. Zuilhof, E.J.R. Sudholter, 'An Improved Method for the Preparation of Organic Monolayers of 1-Alkenes on Hydrogen-Terminated Silicon Surfaces', Langmuir 15 (23), 8288 (1999)

[Sieval et al 01**]** A.B. Sieval, R. Linke, G. Heij, G. Meijer, H. Zuilhof, E.J.R. Sudholter, 'Amino-Terminated Organic Monolayers on Hydrogen-Terminated Silicon Surfaces', Langmuir 17 (24), 7554 (2001)

[Smits58**]** F.M. Smits, 'Measurement of Sheet Resistivities with the Four-Point Probe', Bell Sys. Tech. J. 711 (1958)

[Sneh et al 96**]** O. Sneh, M.A. Cameron, S.M. George, 'Adsorption and desorption kinetics of H2O on a fully hydroxylated SiO2 surface', Surf. Sci. 364 (1), 61 (1996)

[Song et al 09**]** L. Song, J.E. Bartmess, 'Liquid chromatography/negative ion atmospheric pressure photoionization mass spectrometry: a highly sensitive method for the analysis of organic explosives', Mass Spectrom. 23 (1), 77 (2009)

[Stern 67**]** F. Stern, W.E. Howard, 'Properties of Semiconductor Surface Inversion Layers in the Electric Quantum Limit', Phys. Rev. 163 (3), 816 (1967)

[Stern et al 07**]** E. Stern, J.F. Klemic, D.A. Routenberg, P.N. Wyrembak, D.B. Turner-Evans, A.D. Hamilton, D.A. LaVan, T.M. Fahmy, M.A. Reed, 'Label-free immunodetection with CMOS-compatible semiconducting nanowires', Nature 445, 519 (2007)

[Stern et al 10**]** E. Stern, A. Vacic, N.K. Rajan, J.M. Criscione, J. Park, B.R. Ilic, D.J. Mooney, M.A. Reed, T.M. Fahmy, 'Label-free biomarker detection from whole blood', Nature Nanotech. 5, 138 (2010)

[Sun et al 10**]** J.T. Sun, Y.H. Lu, W. Chen, Y.P. Feng, A.T.S. Wee, 'Linear tuning of charge carriers in graphene by organic molecules and charge-transfer complexes', Phys. Rev. B 81 (15), 155403 (2010)

[Sulzer et al 09**]** P. Sulzer, A. Mauracher, F. Ferreira de Silva, S. Denfil, T.D. Mark, M. Probst, P. Limao-Vieira, P. Scheier, 'Probing royal demolition explosive (1,3,5-trinitro-1,3,5-triazocyclohexane) by low-energy electrons: Strong dissociative electron attachment near 0 eV', J. Chem. Phys. 131 (14), 144304 (2009)

[Sweda et al 06**]** R. Sweda, III-Vs Review: The advanced Semiconductor Magazine 19 (9), December 2006

[Sze 69**]** S. Sze, 'Physics of Semiconductor Devices', New York: Wiley, (1969)

[Takahagi et al 88**]** T. Takahagi, I. Nagai, A. Ishitani, H. Kuroda, Y. Nagasawa, 'The formation of hydrogen passivated silicon single‐crystal surfaces using ultraviolet cleaning and HF etching', J. Appl. Phys. 64 (7), 3516 (1988)

[Takulapalli 10**]** B.R. Takulapalli, 'Molecular sensing using monolayer floating gate, fully depleted SOI MOSFET acting as an exponential transducer', ACS Nano 4 (2), 999 (2010)

[Talin et al 06**]** A.A. Talin, L.L. Hunter, F. Léonard, B. Rokad, 'Large area, dense silicon nanowire array chemical sensors', Appl. Phys. Lett. 89 (15), 153102 (2006)

[Tanielian 78**]** M. Tanielian, H. Fritzsche, C.C. Tsai, E. Symbalisty, 'Effect of adsorbed gases on the conductance of amorphous films of semiconducting silicon - hydrogen alloys', Appl. Phys. Lett. 33 (4), 353 (1978)

[Terry et al 97**]** J. Terry, M.R. Linford, C. Wigren, R. Cao, P. Pianetta, C.E.D. Chidsey, 'Determination of the bonding of alkyl monolayers to the Si(111) surface using chemical-shift, scanned-energy photoelectron diffraction', Appl. Phys. Lett. 71 (8), 1057 (1997)

[Trucks et al 90**]** G.W. Trucks, K. Raghavachari, G.S. Higashi, Y.J. Chabal, 'Mechanism of HF etching of silicon surfaces: A theoretical understanding of hydrogen passivation', Phys. Rev. Lett. 65 (4), 504 (1990)

[Tschitschibabin 24**]** A.E. Tschitschibabin, Ber. Dtsch. Chem. Ges. 57, 1168 (1924)

[Ubara et al 84**]** H. Ubara, T. Imura, A. Hiraki, 'Formation of SiH bonds on the surface of microcrystalline silicon covered with SiOx by HF treatment', Solid-State Comm. 50 (7), 673 (1984)

[Udrea et al 00**]** F. Udrea, D. Garner, K. Sheng, A. Popescu, H.T. Lim, V.I. Milne, 'SOI power devices', Electronics & Communication Engineering Journal, 27-40 February 2000

[Usenko et al 99**]** A.Y. Usenko, W.N. Carr, 'Silicon-on-insulator technology for microelectromechanical applications', SQO 93 (1999)

[Van der Pauw 58**]** L.J. Van der Pauw, 'A Method of Measuring Specific Resistivity and Hall Effect of Discs of Arbitrary Shape', Philips Res. Repts. 13 (1), 1 (1958)

[Van der Pauw 59**]** L.J. Van der Pauw, 'A Method of Measuring the Resistivity and Hall Coefficient on Lamellae of Arbitrary Shape', Philips Tech. Rev. 20 (8), 220 (1959)

[Volokobinskii et al 99**]** M.Y. Volokobinski, A.S. Yastrebov, 'Electric fields of dipole structures', Tech. Phys. 44 (7), 807 (1999)

[Voicu et al 04**]** R. Voicu, R. Boukherroub, V. Bartzoka, T. Ward, J.T. Wojtyk, D.D.M. Wayner, 'Formation, characterization, and chemistry of undecanoic acid-terminated silicon surfaces: patterning and immobilization of DNA', Langmuir 20 (26), 11713 (2004)

[Vu et al 10**]** X.T. Vu, R. GhoshMoulick, J.F. Eschermann, R. Stockmann, A. Offenhausser, S. Ingebrandt, 'Fabrication and application of silicon nanowire transistor arrays for biomolecular detection', Sens. Act. B 144 (2), 354 (2010)

[Wagner et al 72**]** L.F. Wagner, W.E. Spicer, 'Observation of a Band of Silicon Surface States Containing One Electron Per Surface Atom', Phys. Rev. Lett. 28 (21), 1381 (1972)

[Waltenburg et al 95**]** H.N. Waltenburg, J.T. Yates, 'Surface Chemistry of Silicon', Chem. Rev. 95 (5), 1589 (1995)

[Watanabe et al 91**]** S. Watanabe, N. Nakayama, T. Ito, 'Homogeneous hydrogen−terminated Si(111) surface formed using aqueous HF solution and water', Appl. Phys. Lett. 59 (12), 1458 (1991)

[Watanabe et al 95**]** S. Watanabe, S. Sugita, 'Appearance of vertical dihydrides on a silicon surface while dissolving the surface oxide layer in hot water', Appl. Phys. Lett. 66 (14), 1797 (1995)

[Wayner 02**]** D.D.M. Wayner, R.A. Wolkow, 'Organic modification of hydrogen terminated silicon surfaces', J. Chem. Soc. Perkin Trans 2, 23 (2002)

[Wegner et al 08**]** D. Wegner, R. Yamachika, Y. Wang, V.W. Brar, B.M. Bartlett, J.R. Long, M.F. Crommie, 'Single-Molecule Charge Transfer and Bonding at an Organic/Inorganic Interface: Tetracyanoethylene on Noble Metals', Nano Lett. 8 (1), 131 (2008)

[Wegner et al 09**]** D. Wegner, R. Yamachika, X. Zhang, Y. Wang, T. Baruah, M.R. Pederson, B.M. Bartlette, J.R. Long, M.F. Crommie, 'Tuning Molecule-Mediated Spin Coupling in Bottom-Up-Fabricated Vanadium-Tetracyanoethylene Nanostructures', Phys. Rev. Lett. 103 (8), 087205 (2009)

[Wehling et al 08**]** T.O. Wehling, A.I. Lichtenstein, M.I. Katsnelson, 'First-principles studies of water adsorption on graphene: The role of the substrate', Appl. Phys. Lett. 93 (20), 202110 (2008)

[Weldon et al 02**]** M.K. Weldon, K.T. Queeney, J. Eng, K. Raghavachari, Y.J. Chabal, 'The surface science of semiconductor processing: gate oxides in the ever-shrinking transistor', Surf. Sci. 500 (1-3), 859 (2002)

[Weinberger et al 85**]** B.R. Weinberger, H.W. Deckman, E. Yablonovich, T. Gmitter, W. Kobasz, S. Garoff, 'The passivation of electrically active sites on the surface of crystalline silicon by fluorination', J. Vac. Sci. Tech. A 3 (3), 887 (1985)

[Weinberger et al 86**]** B.R. Weinberger, G.G. Peterson, T.C. Eschrich, H.A. Krasinski, 'Surface chemistry of HF passivated silicon: X‐ray photoelectron and ion scattering spectroscopy results', J. Appl. Phys. 60 (9), 3232 (1986)

[Wolkow 99**]** R.A. Wolkow, 'Controlled Molecular Adsorption on Silicon: Laying a Foundation for Molecular Devices', Annu. Rev. Phys. Chem. 50, 413 (1999)

[Xia et al 03**]** Y. Xia, P. Yang, Y. Sun, Y. Wu, B. Mayers, B. Gates, Y. Yin, F. Kim, H. Yan, 'One-Dimensional Nanostructures: Synthesis, Characterization, and Applications', Adv. Mater. 15 (5), 353 (2003)

[Yablonovich et al 86**]** E. Yablonovitch, D.L. Allara, C.C. Chang, T. Gmitter, T.B. Bright, 'Unusually Low Surface-Recombination Velocity on Silicon and Germanium Surfaces', Phys. Rev. Lett. 57 (2), 249 (1986)

[Yau et al 95**]** S.L. Yau, K. Kaji, K. Itaya, 'Electrochemical etching of Si(001) in NH4F solutions: Initial stage and {111} microfacet formation', Appl. Phys. Lett. 66 (6), 766 (1995)

[Yoo et al 01a**]** K. Yoo, H.H. Weitering, 'Surface conductance of Si(100) 2x1 and Si(111) 7x7', Surf. Sci. 482, 482 (2001)

[Yoo et al 01b**]** K. Yoo, H.H. Weitering, 'Surface Conductance near the Order-Disorder Phase Transition on Si(100)', Phys. Rev. Lett. 87 (2), 026802 (2001)

[Yoo et al 02**]** K. Yoo, H.H. Weitering, 'Electrical conductance of reconstructed silicon surfaces', Phys. Rev. B 65 (11), 115424 (2002)

[Zaborovskiy et al 04**]** A.B. Zaborovskiy, D.S. Lutsyk, R.E. Prystansky, V.I. Kopylets, V.I. Timokhin, C. Chatgilialoglu, 'A mechanistic investigation of (Me3Si)3SiH oxidation' J. Org. Chem. 689 (18), 2912 (2004)

[Zhang et al 01**]** X. Zhang, Y.J. Chabal, S.B. Christman, E.E. Chaban, E. Garfunkel, 'Oxidation of H-covered flat and vicinal Si(111)-1×1 surfaces', J. Vac. Sci. Technol. A 19 (4), 1725 (2001)

[Zhang et al 06a**]** P. Zhang, E. Tevaarwerk, B.N. Park, D.E. Savage, G.K. Celler, I. Knezevic, P.G. Evans, M.A. Eriksson, M.G. Lagally, 'Electronic transport in nanometre-scale silicon-on-insulator membranes', Nature Lett. 439, 703 (2006)

[Zhang et al 06b**]** P. Zhang, E.P. Nordberg, B.N. Park, G.K. Celler, I. Knezevic, P.G. Evans, M.A. Eriksson, M.G. Lagally, 'Electrical conductivity in silicon nanomembranes', New J. Phys. 8, 2 (2006)

[Zhao et al 11**]** X. Zhao, S.A. Scott, M. Huang, W. Peng, A.M. Kiefer, F.S. Flack, D.E. Savage, M.G Lagally, 'Influence of surface properties on the electrical conductivity of silicon nanomembranes', Nanoscale Res. Lett. 6(402), 1 (2011)

[Zheng et al 05**]** G. Zheng, F. Patolsky, Y. Cui, W.U. Wang, C.M. Lieber, 'Multiplexed electrical detection of cancer markers with nanowire sensor arrays', Nature Biotech. 23 (10), 1294 (2005)

[Zhou et al 03**]** X.T. Zhou, J.Q. Hu, C.P. Li, D.D.D. Ma, C.S. Lee, S.T. Lee, 'Silicon Nanowires as Chemical Sensors', Chem. Phys. Lett. 369 (1-2), 220 (2003)

Curriculum Vitae

Ph.D. Candidate
Université du Québec, Institut National de la Recherche Scientifique,
Énergie, Matériaux et Télécommunications
1650 Boul. Lionel Boulet, Varennes, J3X 1S2, CANADA

Visiting Worker
National Research Council Canada, Steacie Institute for Molecular Sciences
100 Sussex, Ottawa, K1A 0R6, CANADA

Education

12/2011 **Ph.D. in Materials Science** from INRS-EMT (Defended 5/12/11)
04/2005 **B.Sc. Honours Chemical Physics & Math** from Univ.ofWaterloo

Publications

Journal Articles

[A.5] **G. Dubey**, F. Rosei and G.P. Lopinski, "Highly sensitive detection of TCNE on chemically passivated silicon-on-insulator", *Chem. Commun.* **47**, 10593-95 (2011).

[A.4] **G. Dubey**, F. Rosei and G.P. Lopinski, "Modulation of flat-band voltage on H-terminated silicon-on-insulator pseudo-MOSFETs by adsorption and reaction events", *J. Appl. Phys.* **109**, 104904 (2011).

[A.3] **G. Dubey**, F. Rosei and G.P. Lopinski, "Molecular modulation of conductivity on H-Terminated silicon-on-insulator substrates", *Small* **6**, 2892-99 (2010).

[A.2] R. Anderson, J. Guan, M. Ricard, **G. Dubey**, J. Su, G.P. Lopinski, G. Dorris, O. and B. Simard, "Multifunctional single-walled carbon nanotube-cellulose composite paper", *J. Mater. Chem.* **20**, 2400-07 (2010).

[A.1] **G. Dubey**, F. Rosei and G.P. Lopinski, "Influence of physisorbed water on the conductivity of hydrogen terminated silicon-on-insulator surfaces", *Appl. Phys. Lett.* **91**, 232111 (2007).

Book Chapters

[B.1] D. Landheer, W.R. McKinnon, W.H. Jiang, G.P. Lopinski, **G. Dubey**, N.G. Tarr, M.W. Shinwari, M.J. Deen, "***Bio-Affinity Sensors Based on MOS Field-Effect Transistors***" in: Semiconductor Device-Based Sensors for Gas, Chemical, and Biomedical Applications, Eds. F. Ren and S.J. Pearton, *CRC Press* April 2011.

Awards/Fellowships

2010 NRC-SIMS Annual Award for "*Working above and beyond for the benefit of the institute*".

2008 Trends in NanoTechnonology conference "*Prize to the best poster presented by Ph.D. student*" (Spain).

2006 GSSSP-NRC Graduate Student Scholarship Supplement Program

2005 NSERC CGS M / PGS D-Canada Graduate Scholarship, M.Sc. level (*transferred to Ph.D. in 2006*).

Participation in Conferences/ Symposia/ Workshops

G. Dubey, F. Rosei and G.P. Lopinski Surface "Molecularly Modulated Electrical Transport at Chemically Passivated Silicon Surfaces", *Oral Presentation* at AVS 58: American Vacuum Society's 58th International Meeting, Nashville Convention Center, Nashville, TN, USA Nov 3 2011.

G. Dubey, F. Rosei, and G. P. Lopinski, "Molecularly modulated transport of Si-H surfaces", *Poster* at NRC-SIMS Project Review, Ottawa Canada Dec. 7 2010.

G. Dubey, F. Rosei and G.P. Lopinski Surface "Molecular Gating of SOI surfaces", *Oral Presentation* (Hobson Competition) at Surface Canada 2009, McMaster University, Hamilton Canada Jun 4 2009.

G. Dubey, F. Rosei and G.P. Lopinski Surface "Conductivity of SOI as a probe of adsorption and reaction events", *Poster* at MRS Spring Meeting, Moscone West, San Francisco USA Apr. 16 2009.

G. Dubey, F. Rosei, H. Fritzsche, J. Katsaras and G. P. Lopinski, "Molecularly modulated transport of Si-H surfaces", *Poster* at NRC-SIMS Project Review, Ottawa Canada Dec 17 2009.

G. Dubey, F. Rosei and G.P. Lopinski, "Altering electrical properties of Si films by adsorption" *Oral Presentation* at NRC Colloquium, Ottawa Canada Feb 12th 2008.

G. Dubey B.J. Eves, F. Rosei and G.P. Lopinski, "Electrical transport measurements of modified Si surfaces", *Poster* at CSACS Symposium, McGill University, Montréal Canada May 8 2008.

G. Dubey, F. Rosei and G.P. Lopinski, "Surface conductivity of SOI as a probe of adsorption and reaction events", *Poster* at Trends in Nanotechnology, Oviedo, Spain Sep. 3 2008.

G. Dubey, F. Rosei and G.P. Lopinski, "Using conductivity on silicon-on-insulator to probe molecular adsorption and reaction events", *Poster* at Gordon Research Conference on Chemistry of Electronic Materials, Mount Holyoke College, South Hadley USA Jul. 25 2007.

G. Dubey, F. Rosei and G.P. Lopinski, "Using conductivity on silicon-on-insulator to probe molecular adsorption and reaction events", *Poster* at Nanoforum, Waterloo University, Waterloo Canada Jun. 19 2007.

G. Dubey, B.J. Eves, F. Rosei and G.P. Lopinski, "Influence of molecular adsorbates on the surface conductance of SOI(100)", *Poster* at CSACS Symposium, Concordia University, Montréal Canada May 3 2007.

G. Dubey, F. Rosei and G.P. Lopinski, "Electronic transport at modified SOI surfaces", *Poster* at Surface Canada 2006, Queen's University, (selected for CSC/CAP Division of Surface Science website), Kingston Canada May 16 2006.

G. Dubey, F. Rosei and G.P. Lopinski, "Electrical properties at thin silicon surfaces", *Oral Presentation* at NRC Colloquium, Ottawa Canada May 25 2006.

G. Dubey and G.P. Lopinski, "Electrical Properties at Organically Modified Surfaces", *Poster* at NRC-Colloquium Ottawa Canada Aug.15 2005.

Resume

L'adsorption des espèces polaires ou chargés sur des surfaces semi-conducteur peut moduler les propriétés électriques. Transport électrique dans les semiconducteurs est généralement insensible aux processus de surface en raison des chemins de conduction en parallèle à travers le substrat, à l'exception de cas particuliers, tels que des états de surface de conduction ou de la bande-flexion (“band-bending”) grande [Landsrass89; Jiang96; Lopinski05]. Une méthode simple qui élimine la conduction à travers le substrat et améliore la sensibilité à la «région de charge d'espace (SCR)" est d'utiliser un film mince (épaisseur d) avec une épaisseur similaire à la longueur de Debye (L_D) dans le film.

Une approche émergente utilise chimiquement passivé substrats de silicium-sur-isolant (“Silicon-on-insulator”: SOI) pour étudier d'adsorption moléculaire et des événements de réaction.Cette approche permet l'étude des semi-conducteurs-molécule interactions, mais permet également l'étude de capteurs chimiques utilisant des surfaces de silicium. Substrats SOI sont composées d'un film mince de silicium (30<d<3000 nm) séparée du substrat par un oxyde (“buried-oxide”: BOX). La BOX isole électriquement la surface (distincte du substrat), ce qui augmente la sensibilité aux processus de surface. Étant donné un niveau de dopage de ~10^{15} cm^{-3}, L_D~100 nm et donc la conductivité électrique d'un film ayant une épaisseur similaire à L_D devrait être très sensible à la charge de surface. Une tension appliquée sur le substrat (qui agit comme une porte de la conductivité du film), peut être utilisé pour activer majorité / minorité canaux dans le 'retour' Si / SiO_2 interface, qui forme un dispositif simple appelé un pseudo-MOSFET [Cristoloveanu92].Oxydé SOI dans des solutions d'électrolytes a été explorée pour la bio-détection [Nikolaides04;Lud06;Neff07]. Récemment, le développement de matériaux semiconducteurs nanostructurés a conduit à un regain d'intérêt dans les effets induits par adsorption. Par exemple, la conductivité de nanofils de silicium (SiNW) a été montré pour être sensibles à l'adsorption de petites molécules en phase gazeuse [Zhou03;Talin06] et des molécules biologiques (DNA,protéines) en solution

[Cui01;Hahm04;Bunimovich06;Stern07]. L'utilisation du SOI est plus simple que l'utilisation de nanofils, et permet également l'application des techniques “surface-science” pour la caractérisation de l'interface active [Lin98].

Ce travail vise à explorer et de comprendre les propriétés électriques des "sans-oxyde" de silicium modifiées chimiquement, à l'aide de SOI pour augmenter la sensibilité à la conductivité de surface. Quatre-sonde méthodes, (“four-probe”) sont utilisés pour mesurer l'effet feuille de résistance (“sheet resistance”: R_s) et de Hall tension (“Hall voltage”: V_H ; “Hall coefficient”: R_H) pour déterminer le type de porteur de charge et de la mobilité. Un deux-sonde (“two-probe”) pseudo- MOSFET géométrie est utilisé pour mesurer les caractéristiques $I_D(V_D,V_G)$, tension “flatband” (V_{FB}) et de courant de drain (I_D). Le thème de nos observations est que l'environnement chimique influe fortement sur la conduction électrique de surface. Bien que ces surfaces sont très sensibles aux espèces moléculaires et des réactions, le développement de capteurs et est trop avancées pour ce travail, mais les perspectives et les perspectives pour des applications potentielles sont envisagées.

Chapitre 3: Influence de l'adsorption de l'eau

La feuille de résistance (R_s) dans l'air ambiant a été mesuré dans le «van der Pauw-géométrie" en utilisant des Keithley 2400 mètres. Le contact électrique a été faite en utilisant eutectique (Gallium-Indium). Figure 3.2a montre la feuille de résistance des deux échantillons, n-type SOI (111)-H comme une fonction du temps. L'augmentation de la résistance est provoquée par des états de surface. Les états de surface occupent des électrons. Cela provoque une charge de surface négative et une augmentation de la bande-flexion (épuisement, “depletion”, “upward band-bending”).

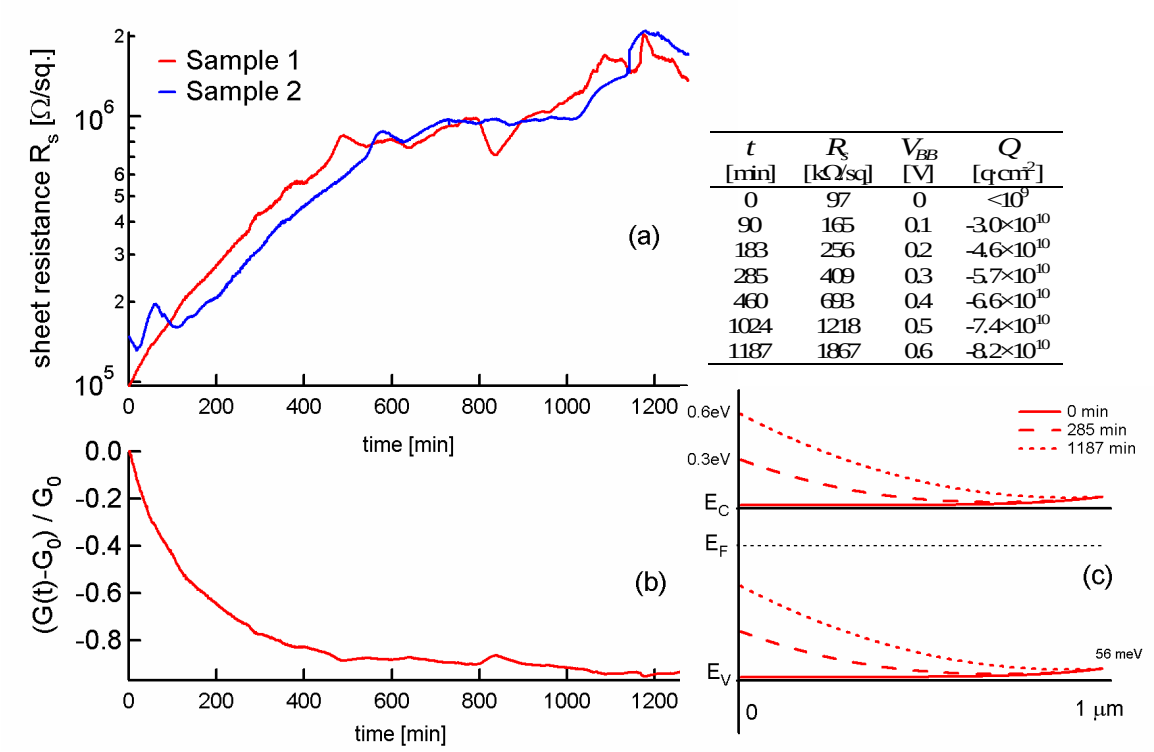

t [min]	R_s [kΩ/sq]	V_{BB} [V]	Q [q·cm^{-2}]
0	97	0	$<10^{9}$
90	165	0.1	-3.0×10^{10}
183	256	0.2	-4.6×10^{10}
285	409	0.3	-5.7×10^{10}
460	693	0.4	-6.6×10^{10}
1024	1218	0.5	-7.4×10^{10}
1187	1867	0.6	-8.2×10^{10}

Figure 3.2: (a) Air-oxydation du n-type (d=1 μm) SOI(111)-H observé par la résistance augmente. (B) variation relative de la conductance de la surface. (C) correspondant bande-flexion.

Afin de réduire le taux d'oxydation, 1 micron SOI (111)-H échantillons ont été purgés avec un gaz inerte (Ar ou N_2). Bien que le taux d'oxydation diminue en raison de la purge, l'observation surprenante est que l'ouverture de la purge provoque une forte augmentation de la résistance comme dans la Figure 3.6.

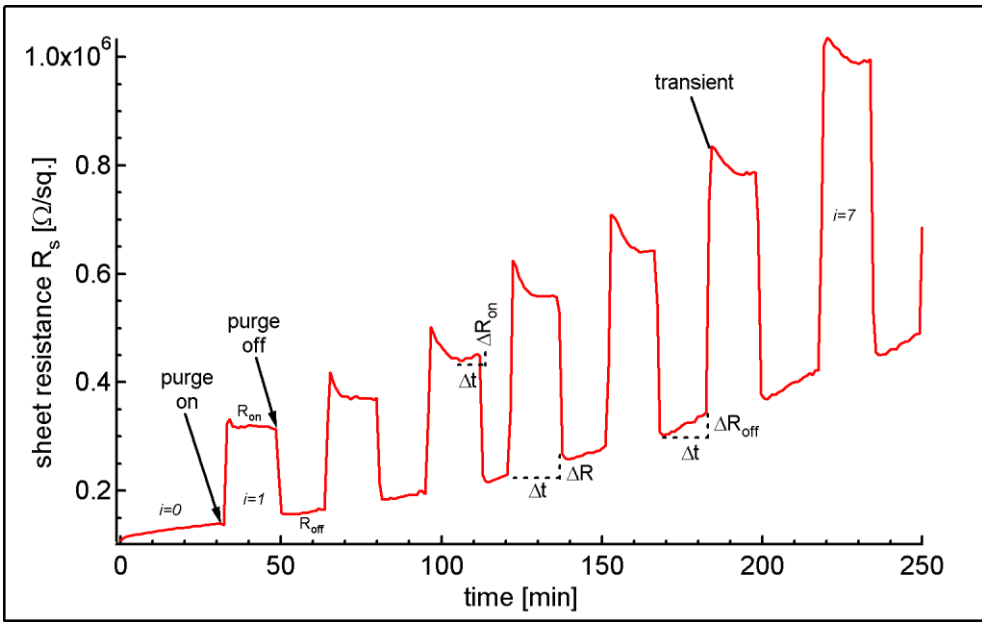

Figure 3.6: Air-oxydation du n-type 1 SOI(111)-H (d=1 µm) observée en augmentant feuille de résistance. Purge avec Ar gaz résultats dans des changements réversibles dans la résistance.

Depuis la purge réduit l'humidité au-dessus de l'échantillon, la figure 3.6 suggère qu'il ya une couche d'eau adsorbée qui augmente la conductivité.

Pour prouver cela, des expériences ont été réalisées dans un environnement contrôlé en utilisant un système de vide. En combinant quatre-sonde-résistance (R_s) et les mesures de tension de Hall (V_H), les changements de conductivité peuvent être corrélées avec des changements dans la densité des porteurs. La figure 3.9 montre la réponse d'un SIMOX SOI(100)-H substrat (d=150 nm, type n) dans la vapeur d'eau pure dans des conditions de vide.

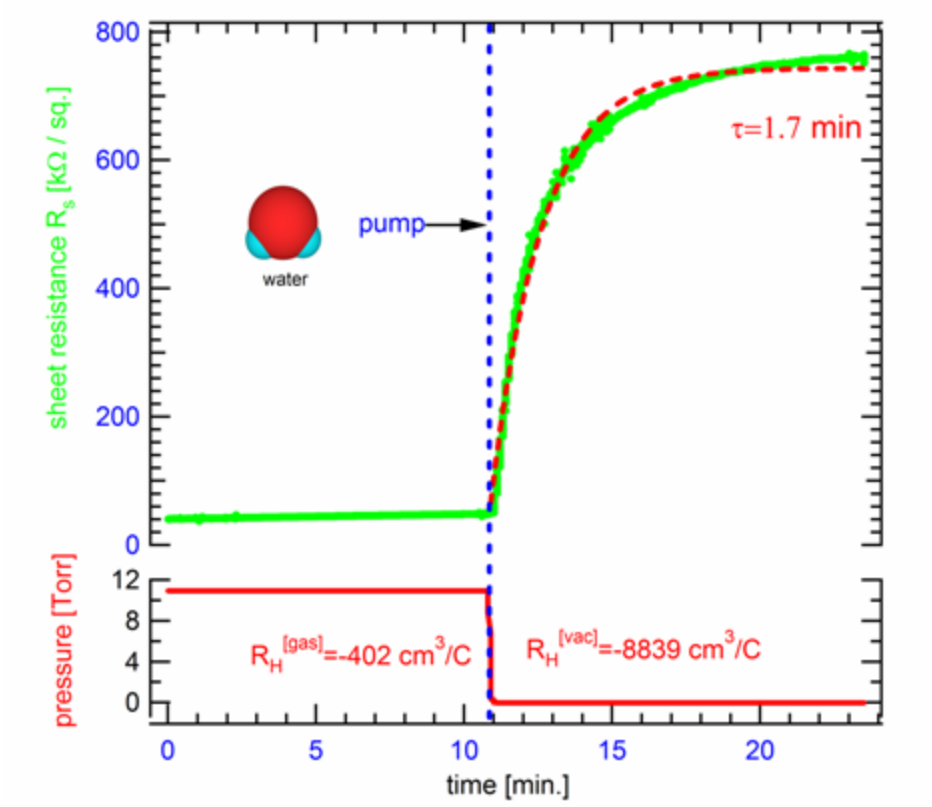

Figure 3.9: La feuille de résistance du matériau SOI (100)-H augmente lorsque l'eau (11 Torr) est pompée loin du système de vide. L'augmentation du coefficient de Hall (R_H) et augmenter la résistance d'un facteur 20 dans le vide, ce qui indique que la variation de conductivité est due à des changements dans la densité de porteurs de charge.

Sous une pression de 11 Torr de l'eau, la feuille de résistance se trouve être stable à 40 kΩ. Après le pompage pour éliminer la vapeur d'eau, la feuille de résistance est augmentée par un facteur de 20 à 762 kΩ. L'augmentation de coefficient de Hall est proportionnelle à l'augmentation de la feuille de résistance. L'augmentation de la résistivité et la tension de Hall comme l'eau désorbés de la surface indique que la présence d'eau sur la surface agit pour augmenter la densité de porteurs (par exemple, induisent une accumulation de porteurs majoritaires).

Les observations dans la figure 3.9 nécessite une charge de surface de 2.2 x 10^{11}cm^{-2}.

L'effet de l'eau sur le p-type SOI (111)-H est montré dans la figure 3.11 (d=3 µm). Lorsque 11 Torr de l'eau est introduite dans la chambre, la résistance diminue. Après le pompage de suite l'eau, la résistance est rétablie. Cependant, contrairement à l'exemple précédent (n-type SOI), cette fois-ci il ya un changement de signe de V_H. Ce changement

de signe de la tension de Hall implique que l'augmentation de la conductivité de surface est due à la formation d'un canal d'électrons (type-n), aussi connu comme “inversion”. Une autre différence avec le comportement des substrats de type-p est que le changement dans la résistance à l'exposition à l'eau n'est pas monotone. Ce changement initial est agrandi dans l'encart de la figure 3.11.

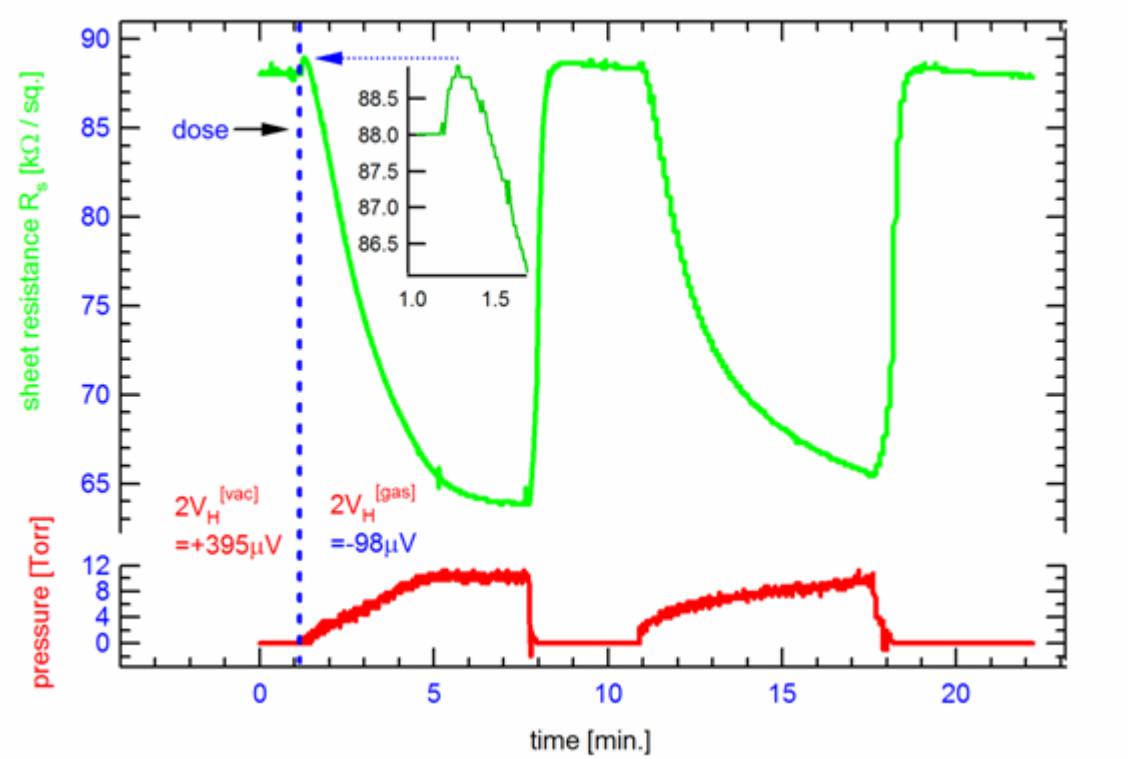

Figure 3.11: Adsorption et désorption d'eau sur le p-type SOI (111)-H (d=3µm). La surface devient inversé (type-n) dans 11 Torr de l'eau, indiquée par un changement de signe de la tension de Hall. Le passage de l'épuisement de l'inversion est visible dans l'encart. Le coefficient de Hall dans le vide reste le même avant et après.

Nous attribuons ce comportement à l'épuisement initial des porteurs majoritaires (“holes”) qui augmente la résistance avant d'adsorption supplémentaires conduit à l'inversion. Une charge de surface positive de ~ 1 10^{11} q cm^{-2} est suffisant pour rendre compte des observations de la figure 3.11.

Une possibilité est que l'eau est un donneur d'électrons. Comme un donneur d'électrons, il ya un transfert de charge avec le substrat. Un transfert de charge électrochimique impliquant le transfert d'un électron (H_3O^+) d'une couche d'eau faiblement acide avait été proposé auparavant pour tenir compte de l'observation de l'eau

induite par de type p de surface conductivité de l'hydrogène résilié surfaces diamant [Maier00; Larsson05]. Cependant, ce mécanisme n'explique pas les observations actuelles. Le transfert de charge peut être intrinsèque à l'interface silicium-eau ou facilitée par un état de surface. Les calculs théoriques de l'interaction de l'eau sur Si-H sont nécessaires pour faire avancer ces possibilités.

Chapitre 4: gaz autres

La forte influence de l'eau physisorbé sur la conductivité du SOI-H (Ch3) suggère d'explorer les effets d'autres espèces moléculaires. Pyridine (azine, Azabenzene) C_5H_5N est un candidat attractif en tant que molécule polaire avec un moment dipolaire de 2.2 D [Middleton 38] et une active d'électrons isolés paire [Pettinger78]. Pyridine s'agit d'une base bien connue faible [Johnson65], en faisant un donneur d'électrons bon.

Figure 4.1a montre le résultat de l'exposition de la pyridine sur SIMOX (type n; d= 150 nm). Lorsque la pyridine est exposée, la conductivité de l'échantillon augmente de près de deux ordres de grandeur que la pression est autorisé à augmenter de façon continue jusqu'à 13 Torr. Mesures de tension Hall avant et après adsorption sont trouvés à l'échelle avec des changements dans la résistance.

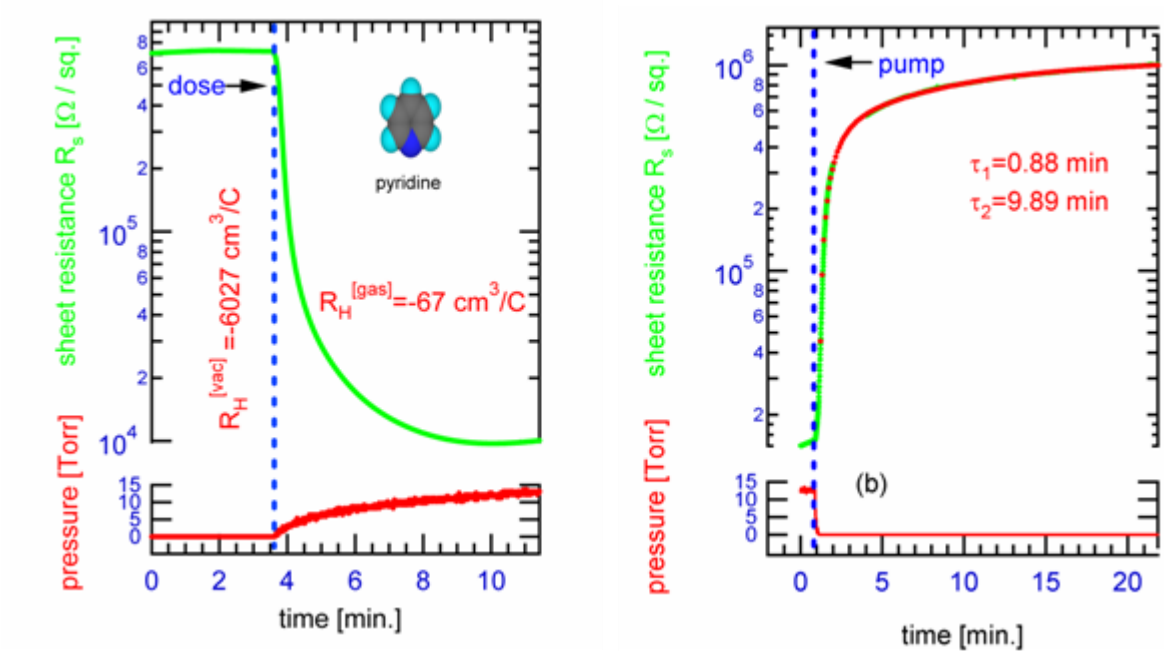

Figure 4.1 (a): L'adsorption de pyridine-vapeur sur un substrat SOI(100)-H de type n. (B) la désorption de la pyridine a un effet réversible sur la conductivité. Évacuation de pyridine élimine la couche d'accumulation et le retour coefficient de résistance et de Hall pour des valeurs comparables à ce qui était initialement mesurée.

La corrélation entre R_s et V_H indique que les changements de conductivité sont principalement associés aux changements dans la densité porteuse induite par un effet de champ plutôt que des changements dans la mobilité. Comme avec de l'eau d'adsorption sur n-type SOI, cette observation montre que la pyridine conduit à l'accumulation de porteurs majoritaires (électrons). Des simulations indiquent que ~ 172 mV de la bande-flexion est nécessaire de tenir compte des changements observés, ce qui nécessite la charge de surface de q ~ 10^{12} qcm^{-2}, soit presque six fois supérieure à celle induite par l'eau. Evacuation de la pyridine confirme l'effet est réversible comme dans la figure 4.1b.

L'exposition de la pyridine sur le p-type SOI (d=3 µm) est montré dans la figure 4.4a.

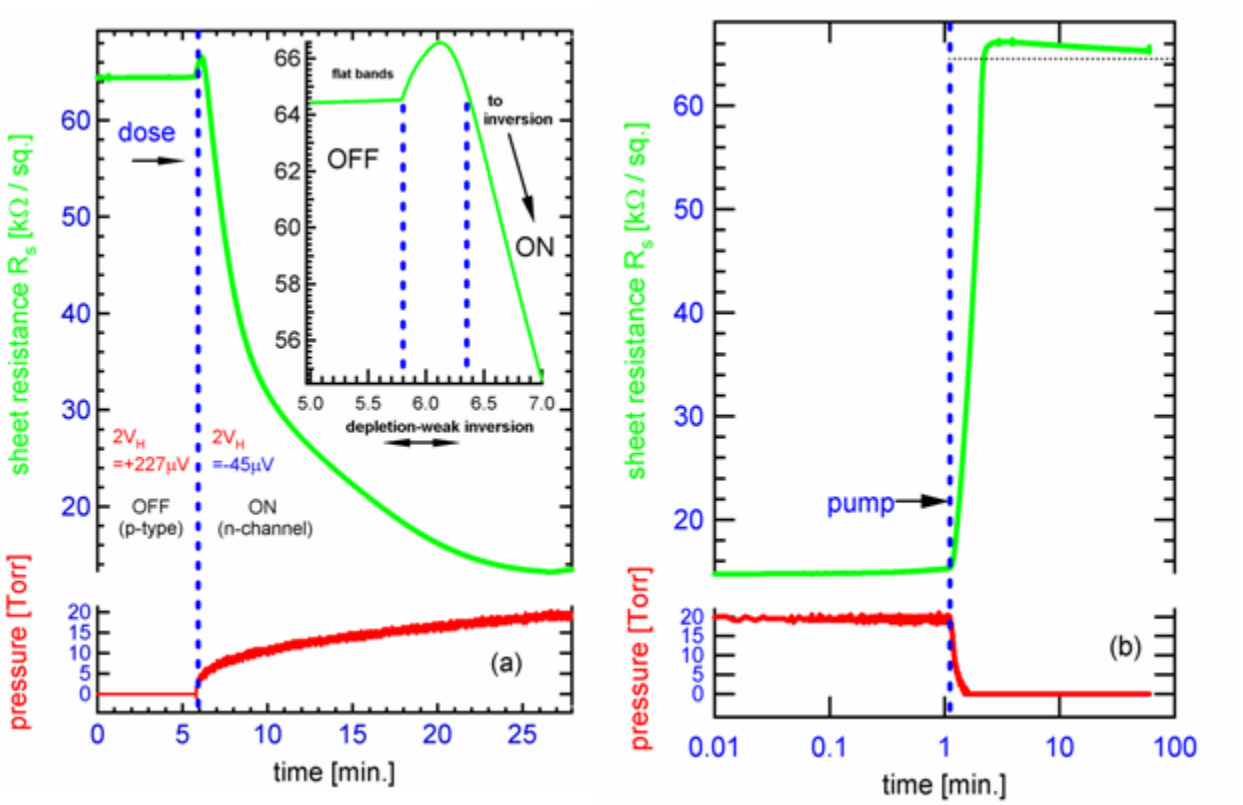

Figure 4.4: (a) L'exposition de la pyridine sur le p-type SOI SOI (111)-H ce qui provoque une diminution de la feuille de résistance. Un changement de signe de la tension de Hall montre que la surface devient inversée. (B) Les correspondants désorption isothermes montre cet effet est réversible.

La charge de surface nécessaire de tenir compte des changements observés dans la figure 4.4 est ~ 3×10^{11} q cm^{-2}, plus d'un facteur de 3 fois supérieure à celle induite par la présence d'eau. Ceci peut être attribué à la nature de pyridine qui est un donneur d'électrons bonne.

La réponse du matériau SOI (111)-H pour certaines classes de molécules est montré dans la figure 4.6. Un substrat de type p est exposé au toluène, thiopene, et la pyridine. Afin de minimiser la contamination croisée entre les doses, la ligne de gaz commun est chauffé doucement. La résistance dans le vide est de 65.7 kΩ tandis que la tension de Hall est de 224 mV (@ 1 uA et 560 G). Il ya un changement négligeable lorsque 15 Torr de toluène ($C_6H_5CH^3$) est exposée. Encore une fois il ya un changement négligeable (<1%) quand 20 Torr de thiophène (C_5H_4S) est exposée. Lorsque~10 Torr de pyridine est introduite, il ya une forte réponse, similaire à ce qui a été observé avant.

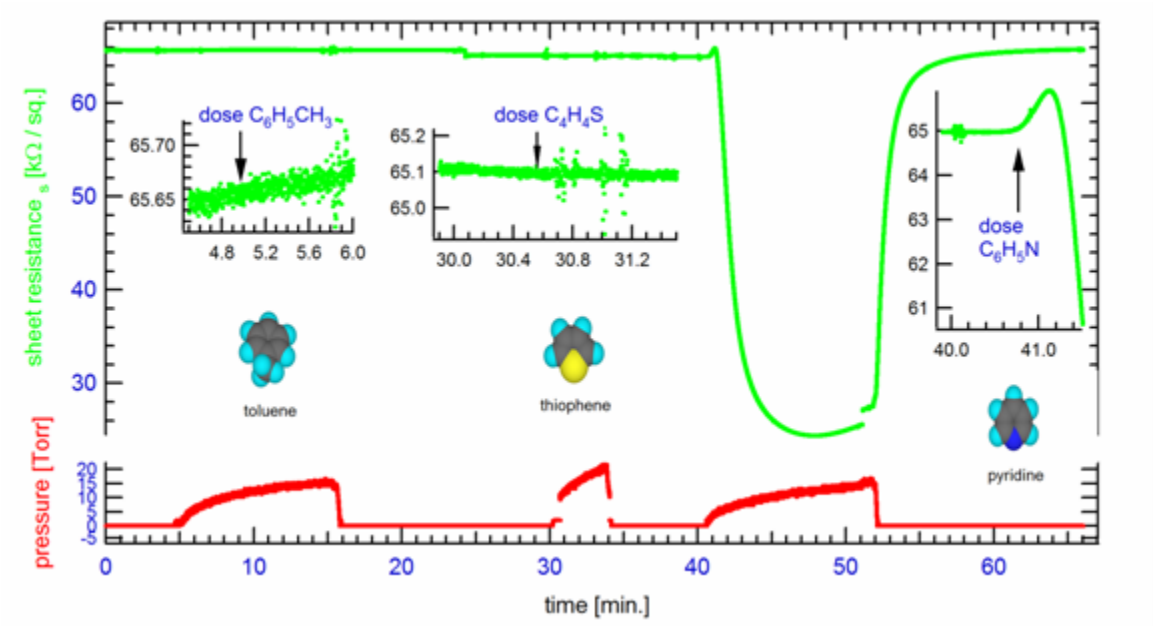

Figure 4.6: Feuille de résistance des changements après l'exposition au toluène, le thiophène et la pyridine, sur SOI(111)-H de type p. La conductivité est inchangé pendant l'exposition au toluène ou thiophie.

La capacité de certains autres gaz à moduler la conductivité du SOI-H a été étudiée sur type p SOI(111)-H (d=3µm). Les résultats sont résumés dans le tableau 4.3. D'oxygène ou d'azote n'a pas provoqué de changement significatif sur 1 Torr <P<1000 Torr. Toutefois, les amines induisent une forte modulation de la conductivité. L'ammoniac (NH_3) et de triéthylamine ($N(C_2H_5)_3$) a induit des effets similaires que la pyridine. Ces effets sont aussi réversibles. Analogue à la pyridine, l'ammoniaque et la triéthylamine sont polaires et ont une seule paire de bases qui peuvent abstrait des“holes”.

GAZ	P [Torr]	(R [gaz]-R [vac]) / R [vac]
Pyridine	19	0,4
Triéthylamine	20	0,4
D'ammoniac	85	0,4
Ethanol	10	0,4
L'oxygène	9	0,4
L' azote	1000	0,4

Tableau 4.3: Résumé de la conductivité de modulation induite par l'exposition à d'autres gaz.

Nous avons montré que SOI-H substrats sont des plateformes modèle intéressant qui permet l'utilisation de mesures de conductivité de la sonde moléculaire d'adsorption / désorption d'événements. Molécules contenant de l'azote, tel que la pyridine, l'ammoniaque et de la triéthylamine modifier la conductivité de type p à type n.

Chapitre 5: Les pseudo-MOSFET mesures

L'architecture de substrats SOI facilite l'e formation d'un transistor pseudo-MOS (Ψ-MOSFET) simplement en faisant des contacts dans la couche de silicium et en utilisant le substrat de silicium comme une porte. Il a d'abord été décrit par Williams et Cristoloveanu [Cristoloveanu92] comme une méthode de caractérisation in-situ des plaquettes SIMOX. L'application de cette approche pour contrôler les processus de

surface est encore à ses premiers stades. SIMOX substrats ont été utilisés. L'épaisseur du film était de 150 nm. Le contact électrique a été faite en utilisant eutectique (Gallium-Indium). Une tension de drain (V_D) et porte-tension (V_G) ont été appliqués, et le courant de drain (I_D) a été mesurée.

Les caractéristiques $I_D(V_D,V_G)$ du canal-n (“n-channel”) de le SOI-H Ψ-MOSFET en mode d'accumulation sont présentés dans la figure 5.1 a Les mesures ont eu lieu sous vide et pendant l'exposition à la vapeur d'eau.

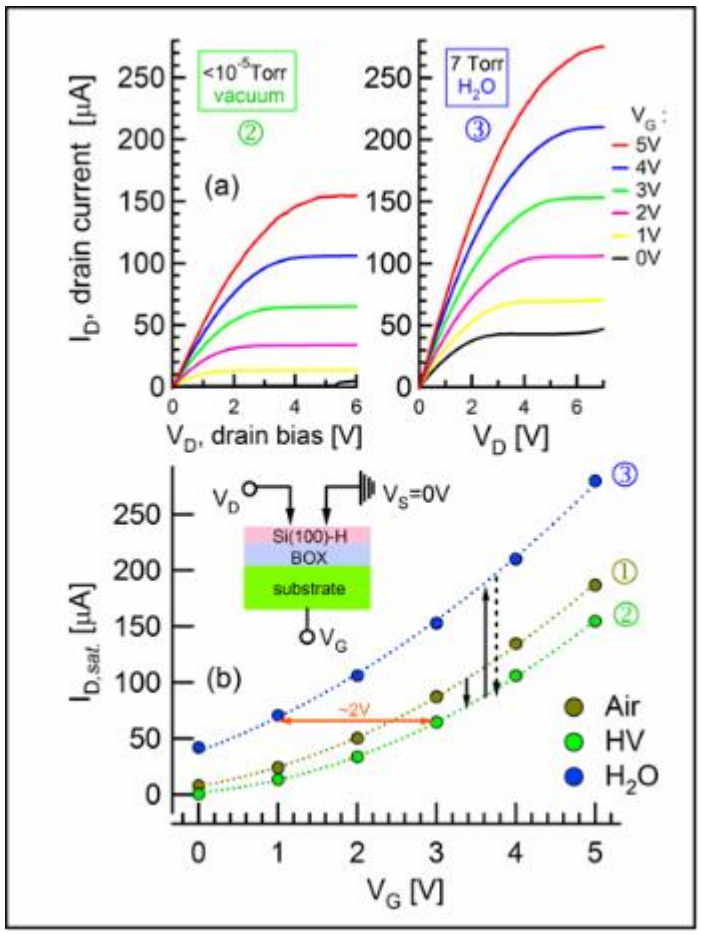

Figure 5.1 (a) Caractéristiques de la pseudo-MOSFET dans le vide et après l'exposition à la vapeur d'eau. (B) régime quadratique pour l'extraction de paramètres.

L'exposition à la vapeur d'eau est démontré qu'ils ont un effet significatif sur les caractéristiques de le FET. Analytiquement, les caractéristiques Ψ-MOSFET en mode saturation et linéaire (mode triode) sont similaires à un MOS-transistor

[Cristoloveanu00]. Dans le régime de saturation $V_D>V_G-V_{FB}$ le drain est correctement décrite par $I_D,sat=½\beta_{sat}(V_G-V_{FB})^2$ tel que tracé dans la figure 5.1b. La valeur de β_{sat} est égale à un produit de la mobilité μ_{sat} et la capacité capacitance $C_{BOX}=9.2$ nF / cm^2. Les facteurs dans les trois environnements sont $\beta_{sat}(1)=9.6\pm0.2$ $\mu A/V^2$, $\beta_{sat.}(2)=9.7\pm0.2$ $\mu A/V^2$ et $\beta_{sat.}(3)=8.7\pm0.3$ $\mu A/V^2$, correspondant à une moyenne $<\beta_{sat.}>= 9.3\pm0.6$ $\mu A/V^2$. Cela indique que la mobilité est essentiellement constante tout au long de ces transitions. La mobilité apparente est estimée à $<\mu_{sat.}>\approx1360\pm80$ cm^2/V s.

Contrairement à la mobilité (ne pas changer), le V_{FB} est très sensible à l'environnement chimique: $V_{FB}(1)=-1.3$ ±0.05 V, V_{FB} $(2)=-0.7\pm0.04$ V et $V_{FB}(3)=-3.0\pm0.1$ V. Ces transitions sont réversibles ; cela indique que l'adsorption de l'eau sur la surface est un processus réversible qui ne dégrade pas les propriétés électroniques, compatibles avec des études en Ch3.

La surface peut être passivée par des monocouches moléculaires (“molecular monolayers”) composés de chaînes alkyle, liée de manière covalente. Ces monocouches peut protéger la surface de l'oxydation. Les méthodes les plus courantes utilisent des réactions thermique ou photochimique des alcènes (liquid) avec Si-H [Linford95; Boukherroub99; Popoff10]. Nous avons choisi d'utiliser un développé récemment en phase gazeuse procédé d'alkylation photochimique [Eves06]. Dans ce processus, 185 nm photons exposés à la vapeur d'alcène (decene) sont utilisés pour créer des espèces actives (radicaux). Les radicaux forment des sites réactifs à la surface (“dangling-bonds”). Les alcènes réagissent directement avec les dangling-bonds et commencer une réaction en chaîne, ce qui conduit à la formation d'une monocouche alkyle. Cette approche se révèle être parfaitement adapté à la forme des monocouches sur notre SOI(100)-H pseudo-MOSFET.

Il était nécessaire de caractériser la formation monocouche en utilisant la procédure en phase gazeuse. ATR-FTIR spectres de Si(100)-H avant et après réaction en phase gazeuse avec décène sont démontrées dans la Figure 5.4.

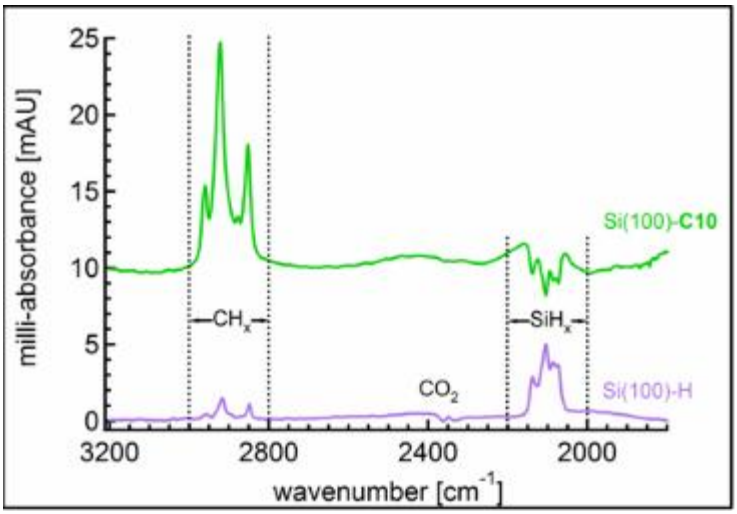

Figure 5.4: ATR-FTIR caractérisation de la formation de monocouches en utilisant la méthode en phase gazeuse photochimique [Eves06]. Spectra correspondent aux initiales Si(100)-H de surface (en bas) et de Si- C10 surface (en haut) formé par une réaction en chaîne des radicaux à 185 nm avec 1-décène.

Effets de la formation d'une monocouche sur la surface de SOI ont été étudiées en utilisant le pseudo-MOSFET comme le montre dans la figure 5.5. Bonnes $I_D(V_D,V_G)$ caractéristiques de FET sont obtenues pour la surface SOI-C10. Bien que le courant à la même tension est significativement réduite par rapport à la surface SOI-H. Dans la figure 5.5b, la V_{FB} est augmenté de 1.9 V et $\beta_{sat.}$ baisse de 15%. La mobilité initiale du SOI-H a été sat.μ= 1020 ± 60 cm^2/V s.

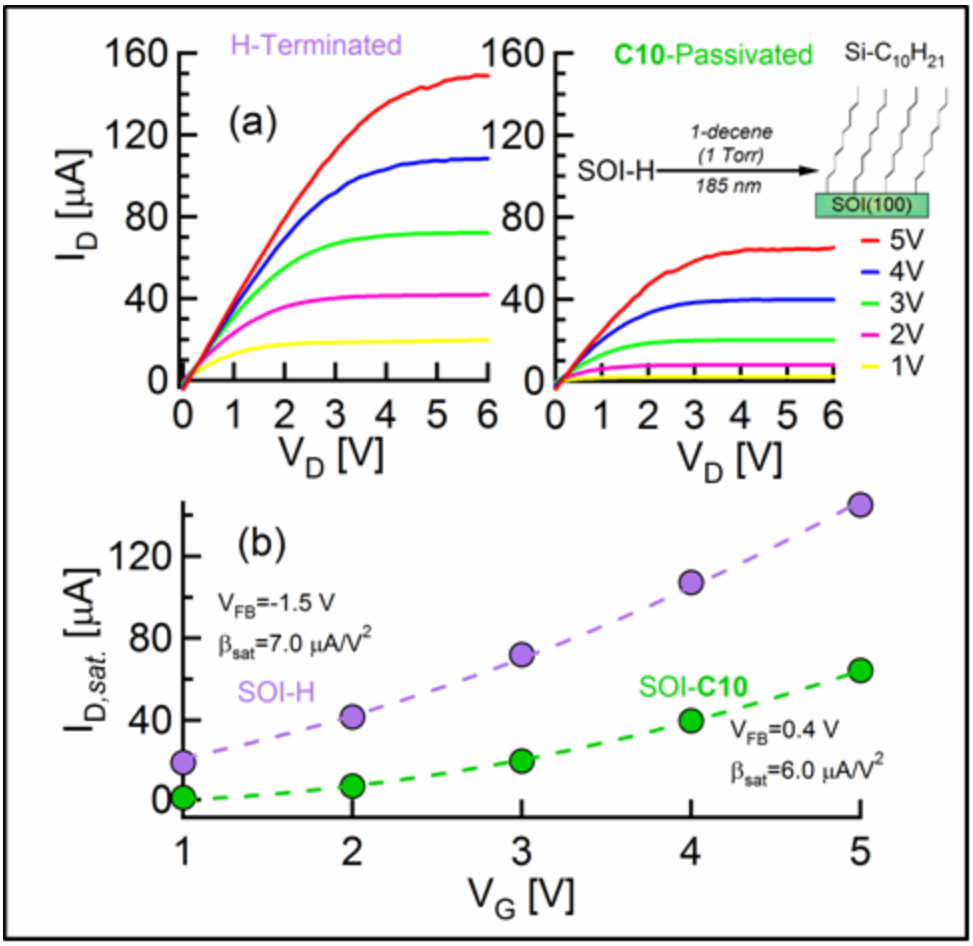

Figure 5.5: Effet de la modification covalente de 150 nm SOI(100)-H sur les caractéristiques de la Ψ-MOSFET.

Partie de l'augmentation de V_{FB} peuvent être attribuer à la création d'états de surface électriquement actifs associés à la réaction. Cependant, la formation de la monocouche hydrophobe est également prévu de réduire la couverture de H_2O adsorbés à l'interface à SOI-H, qui a été montré pour avoir un impact significatif sur les caractéristiques. Donc, une partie de l'augmentation de V_{FB} est probablement causée par (partielle) de déplacement de l'eau. La cause et la nature de la formation de l'état de l'interface lors de la phase gazeuse ne sont pas caractérisés. Ceux-ci peuvent être liés à des impuretés dans le décène solution ou la pression d'oxygène dans le fond de la chambre, auquel cas le processus pourrait être optimisée. Ils peuvent également provenir de la nouvelle génération d'une faible densité de dangling bonds (“mid-gap” états) dans la réaction en chaîne.

En résumé, les caractéristiques de la SOI-H Ψ-MOSFET a été montré pour être très sensible à adsorption moléculaire et de la réaction d'événements, et peut être utilisée pour distinguer entre l'adsorption réversible de modulation induite par opposition à des changements irréversibles induits par les réactions.

Chapitre 6: Sensibilité aux accepteurs d'électrons

Le pseudo- MOSFET [Cristoloveanu92] est utilisée pour étudier l'interaction des TCNE avec SOI-H. La figure 6.1 montre une représentation schématique des expériences.

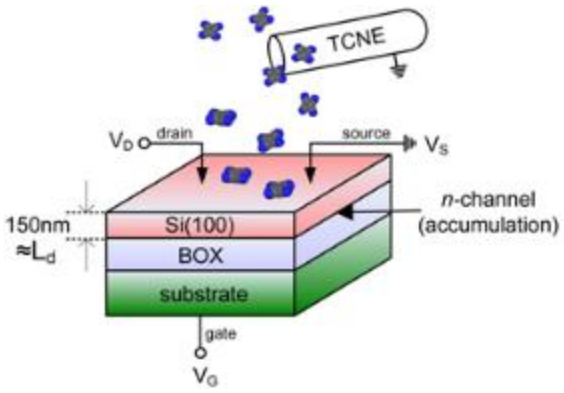

Figure 6.1: Schématique de l'expérience. Poudre TCNE solides est amené à proximité (<5 mm) sur une surface pendant un temps contrôlé (3 s), et ensuite rétracté. Le courant de drain est surveillé et l'exposition est répétée dans les mêmes conditions.

La réponse actuelle est montré dans la figure 6.2a à V_G =3 V et V_D=5 V. Pour augmenter la réversibilité et de réduire les temps de récupération, le substrat est chauffé à 60 ^oC, qui a également été trouvé pour donner la plus haute sensibilité (dépendance de la température est discuté ci-dessous). Peu après l'introduction de TCNE, le courant diminue de plus de deux ordres de grandeur.

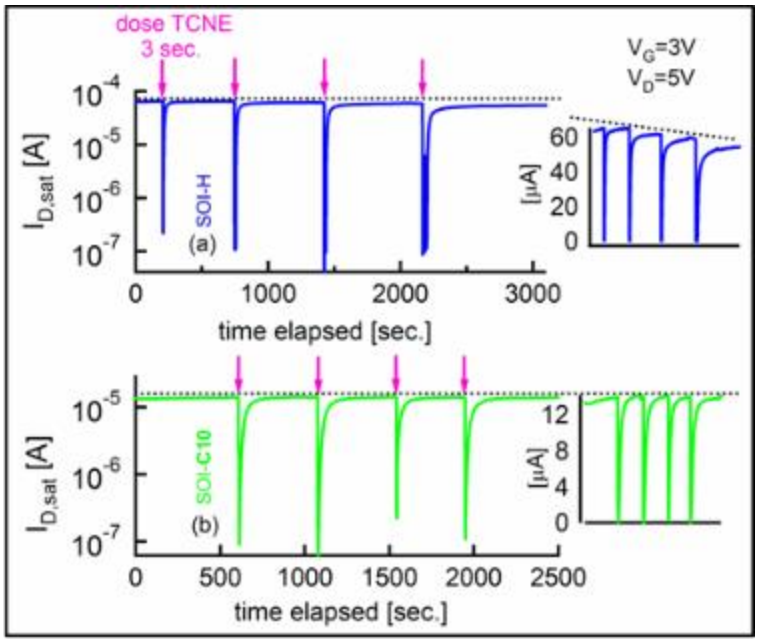

Figure 6.2: Réponse en courant en fonction du temps avec TCNE doses successives (marqués par des flèches) dans l'air ambiant montre pour (a) SOI-H et (b) Modification de décyle-SOI-C10. Les réponses actuelles sur une échelle linéaire sont présentés dans les encarts sur le droit de montrer plus clairement la réversibilité.

Dans la figure 6.2a, les valeurs de gauche à droite à chaque dose est de I_{max}/I_{min} sont 65 µA / 220 nA, 64.7 µA / 110 nA, 61.5 µA / 40 nA et 59.1 µA / 86 nA, avec une modulation maximale produite sur la troisième dose est équivalente à un ratio ON/OFF de~1.5×10^3. Le repose est quelque peu variable, allant de, car la manipulation de la source de TCNE a été fait manuellement, le flux de contrôle à la surface est probablement la principale source de l'erreur expérimentale. Un examen attentif de la réponse actuelle montre la récupération de I_D n'est pas entièrement réversible. Ceci est clairement visible dans la boîte à droite dans la figure 6.2a où la réponse est tracée sur une échelle linéaire et le courant est vu pour revenir à une valeur inférieure après chaque exposition successive. Ces observations indiquent que l'effet de TCNE est seulement partiellement réversibles sur SOI-H. Cela montre qu'il ya une interaction très forte entre TCNE et la surface.

Pour améliorer la stabilité, une réaction en phase gazeuse avec décène a été utilisé pour former une monocouche moléculaire (SOI-C10). La réponse actuelle de la surface modifiée pour TCNE adsorption (de la même manière que dans SOI-H) est montré dans

la figure 6.2b. L'exposition de la TCNE sur SOI-C10 provoque le courant de diminuer, bien que les ratios On/Off, sont légèrement réduit (~ 0.6×10^2 -2.3×10^2). Dans la figure 6.2b, les valeurs de gauche à droite à chaque dose est de I_{max}/I_{min} sont 13.9 µA / 90 nA, 14.0 µA / 62 nA, 13.9 µA / 220 nA et 14.0 µA / 109 nA avec une modulation maximale produite sur la deuxième dose est équivalente à un ON/OFF ratio de ~2.3×10^2. Décylique modification améliore clairement la réversibilité de la réaction comme on le voit dans le tracé linéaire à la droite de la figure 6.2b. Fait intéressant, la présence d'un film mince (d'une épaisseur de ~1 nm) que légèrement réduit la tendance du TCNE pour arracher des électrons à la surface. Pénétration partielle des molécules (de TCNE) dans la monocouche est possible, quoique moins probable, car les chaînes alkyle sont très denses.

Spectroscopie vibrationnelle de surface a été utilisée pour étudier l'interaction de TCNE avec SOI-H et SOI-C10. ATR-FTIR spectres pour les deux surfaces avec une exposition à TCNE sont présentés dans la figure 6.3. L'exposition de TCNE à Si(100)-H (figure 6.3a), conduit à une absorption large de 2180 cm^{-1} à 2260 cm^{-1}, avec un pic distinct centré à 2220 cm^{-1} et un petit épaulement au 2195 cm^{-1}. Ces caractéristiques sont typiques des groupe nitrile, connue pour des complexes de TCNE [Miller06]. Cela suggère qu'il est toujours présent TCNE sur la surface qui est lié fortement. En contraste avec le surface de Si-H, les mêmes conditions d'exposition sur le Si-C10 ne produit pas de pics dans la région du CN comme dans la figure 6.3b. Le manque de modes TCNE associée à la surface est cohérent avec les mesures réversibles observés dans la figure 6.2b.

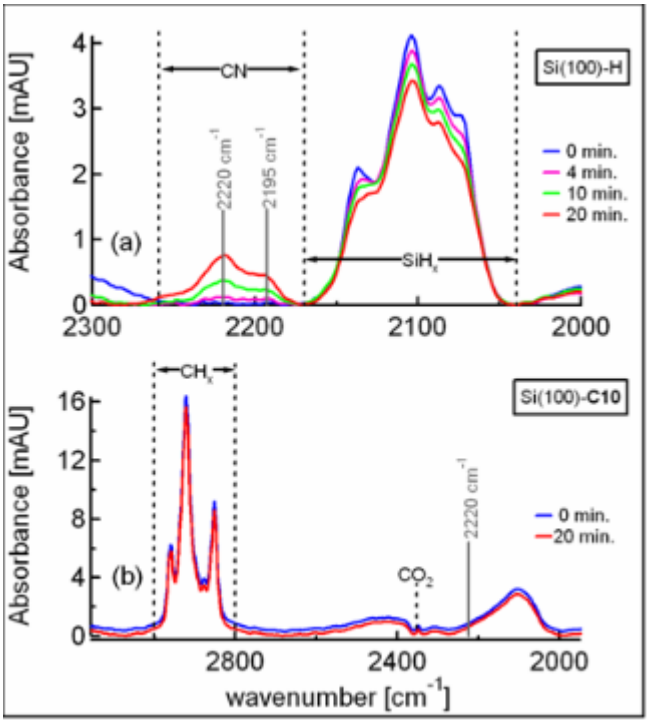

Figure 6.3: ATR-FTIR spectroscopie (a) d'observation de le groupe nitrile à 2220 cm^{-1} après 10 min. d'exposition de TCNE sur Si(100)-H et (b) l'absence de le groupe CN sur Si(100)-C10 sous les mêmes conditions d'exposition (spectres ont été compensés).

La dépendance de la température de la charge-transfert avec TCNE a été étudiée. Figure 6.6 montre le change de V_{FB} en fonction de la température pour SOI-H et SOI-C10.

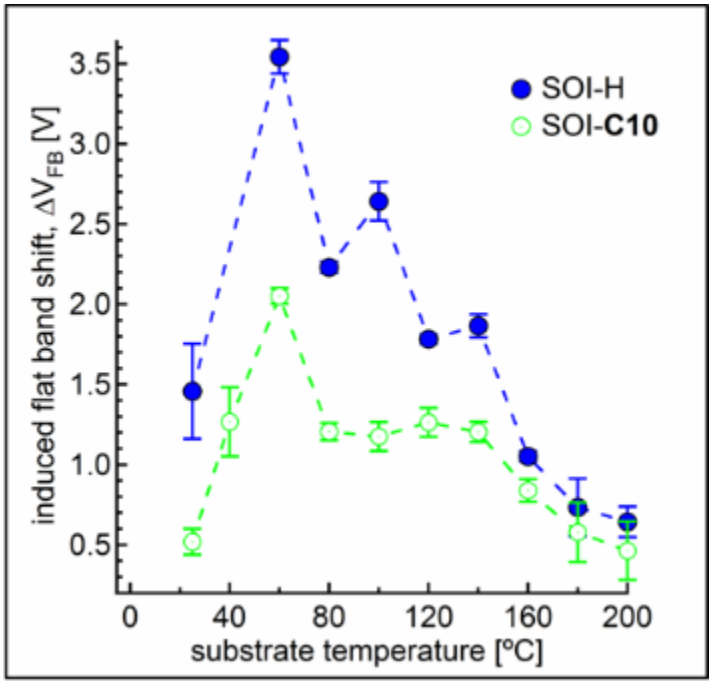

Figure 6.6: Effet de TCNE sur le V_{FB} en fonction de la température pour les deux surface, SOI-C10 et SOI-H.

Les cycles de modulation de courant $I_{max} \leftrightarrow I_{min}$ peuvent être convertis à l'évolution de tension-flatband. Ces changements sont calculés sur la base du modèle quadratique pour le courant de saturation en utilisant les paramètres initiaux de la $I_D(V_D,V_G)$ caractéristiques tel que décrit dans Ch5. A toutes les températures considérées, l'adsorption de TCNE augmente V_{FB} en conformité avec la diminution du courant observé dans la figure 6.2. Cette observation est cohérente avec la densité de charge négative sur la surface. Les changements sont beaucoup plus grandes sur SOI-H et réduit sure SOI-C10. En outre, les deux surfaces d'exposition de la même tendance en ΔV_{FB}, augmentant à un maximum d'environ 60 ^{o}C, ce qui suggère que le transfert de charge peut être activé thermiquement.

Le degré de transfert de charge induite par la TCNE adsorption peut être estimée à partir des valeurs de ΔV_{FB} dans la figure 6.6 en utilisant l'expression dans l'équation 5.2 basé sur l'expression donnée par Hovel [Hovel03]. Les changements dans la densité de charge de surface nécessaire pour tenir compte de la tendance observée à 25 ° C est -8.50×10^{10} cm^{-2} et -3.17×10^{10} cm^{-2} pour la SOI-H et SOI-C10 surfaces, respectivement. A 60 ^{o}C, le transfert de charge augmente à -2.07×10^{11} cm^{-2} et -1.25×10^{11} cm^{-2}. Décylique

modification est envisagée afin de diminuer la charge effective d'un facteur ~2-3. Si ces densités de charge (~10^{11} cm^{-2}) peut être attribuée à une seule charge $TCNE^-$ à la surface, puis une limite inférieure sur la couverture nécessaire pour provoquer ces effets est d'environ ~10^{-4} ML.

La technique de pseudo-MOSFET a été utilisée pour démontrer la détection très efficace de TCNE sur SOI modifiés chimiquement. Cet effet est attribué à transfert de charge significative du substrat de silicium a les molécules TCNE. L'utilisation d'une monocouche SOI-C10 de passiver la surface a été trouvée pour augmenter la réversibilité de la modulation de courant Ces observations démontrent que les monocouches moléculaires sont des diélectriques bon pour les applications de détection.